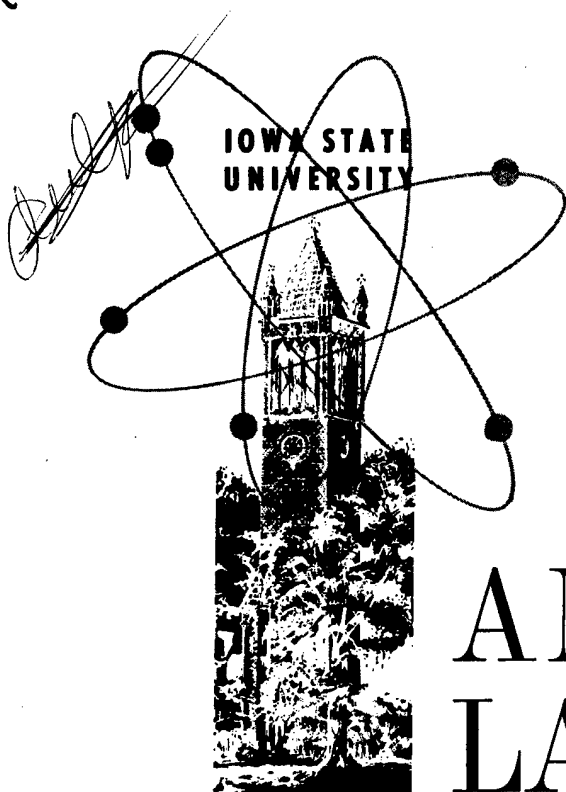


WF 767
Un3.1isu
no. 500
IS-500
contin.
file

ANNUAL SUMMARY REPORT

July 1961 June 1962

B052101



dr

AMPTIAC

AMES LABORATORY

U.S. A.E.C.

DISTRIBUTION STATEMENT A
Approved for Public Release
Distribution Unlimited

research and development
report in

- chemistry
- engineering
- metallurgy
- physics

Reproduced From
Best Available Copy

20010920 222

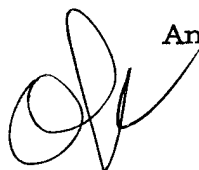
General, Miscellaneous, and Progress Reports (UC-2)
TID-4500, December 15, 1961

UNITED STATES ATOMIC ENERGY COMMISSION
Research and Development Report

ANNUAL SUMMARY RESEARCH REPORT
IN CHEMISTRY, ENGINEERING, METALLURGY AND PHYSICS

July 1, 1961 - June 30, 1962

by

A stylized, handwritten signature in black ink, consisting of several loops and a long horizontal stroke extending to the right.

Ames Laboratory Staff

September 1962

Ames Laboratory
at
Iowa State University of Science and Technology
F. H. Spedding, Director
Contract W-7405 eng-82

Legal Notice

This report was prepared as an account of Government sponsored work. Neither the United States, nor the Commission, nor any person acting on behalf of the Commission:

- A. Makes any warranty of representation, express or implied, with respect to the accuracy, completeness, or usefulness of the information contained in this report, or that the use of any information, apparatus, method or process disclosed in this report may not infringe privately owned rights; or
- B. Assumes any liabilities with respect to the use of, or for damages resulting from the use of any information, apparatus, method or process disclosed in this report.

As used in the above, "person acting on behalf of the Commission" includes any employee or contractor of the Commission, or employee of such contractor, to the extent that such employee or contractor of the Commission, or employee of such contractor prepares, disseminates, or provides access to, any information pursuant to his employment or contract with the Commission, or his employment with such contractor.

Printed in USA. Price \$4.00. Available from the

Office of Technical Services
U. S. Department of Commerce
Washington 25, D.C.

TABLE OF CONTENTS

CHEMISTRY

ENGINEERING

METALLURGY

PHYSICS

REACTOR

APPENDICES

I. Educational Services

II. List of Shipments

CHEMISTRY
DIVISION

IS-500

ANNUAL SUMMARY RESEARCH REPORT IN CHEMISTRY

by

AMES LABORATORY CHEMISTRY STAFF

F. H. Spedding, Director, C. A. Goetz, C. V. Banks, L. S. Bartell,
J. D. Corbett, A. H. Daane, F. R. Duke, V. A. Fassel,
J. S. Fritz, B. C. Gerstein, R. S. Hansen, C. Heitsch,
D. S. Martin, J. E. Powell, R. E. Rundle,
H. J. Svec and A. F. Voigt

IS-500

ANNUAL SUMMARY RESEARCH REPORT IN CHEMISTRY

For the period July 1, 1961 - June 30, 1962

This report is prepared from material
submitted by the group leaders
of this Laboratory

Previous research reports in this series are:

ISC-35	ISC-421
ISC-41	ISC-450
ISC-56	ISC-484
ISC-69	ISC-505
ISC-74	ISC-530
ISC-76	ISC-574
ISC-113	ISC-606
ISC-130	ISC-643
ISC-133	ISC-706
ISC-137	ISC-757
ISC-171	ISC-834
ISC-193	ISC-902
ISC-220	ISC-976
ISC-245	ISC-1049
ISC-285	ISC-1116
ISC-299	IS-15
ISC-321	IS-192
ISC-337	IS-350
ISC-394	

IS-500

CONTENTS

CHEMISTRY

	<u>Physical and Inorganic Chemistry</u>	Page
1.	The Separation of Rare Earths by Ion Exchange (F. H. Spedding and J. E. Powell).....	1
2.	Stability Constants of the Rare-Earth Chelates (J. E. Powell)..	1
3.	The Hydration and Solubilities of Yttrium and Rare-Earth Chelates Formed with Anions of α -Hydroxy Acids (J. E. Powell).....	4
4.	Separation of Lithium Isotopes	6
5.	Preparation of Rare-Earth Metals (F. H. Spedding and A. H. Daane).....	6
	5.1 Purification of Rare-Earth Metals by Filtering	6
	5.2 Vacuum Distillation.....	8
	5.3 Electron Beam Melting.....	8
6.	Properties of Rare-Earth Metals	8
	6.1 High Temperature Allotropes	8
	6.2 Vapor Pressure Studies.....	9
	6.3 Electrical Resistivity.....	10
	6.4 High Temperature Calorimetry	10
	6.5 Extrusion of Europium	11
7.	Rare-Earth Alloys (F. H. Spedding and A. H. Daane).....	11
	7.1 Equilibrium Studies.....	11
	7.1.1 Sc-V System.....	11
	7.1.2 Y-Mn System	12
	7.1.3 Y-Ho System	12
	7.1.4 Nd-Y System	13
	7.2 Magnetic Studies.....	13
8.	Bonding in Borides(A. H. Daane).....	14
9.	Heat Content of Silicon (A. H. Daane).....	15
10.	Heat Capacity Measurements (B. C. Gerstein and F. H. Spedding).....	15
	10.1 Terbium.....	15
	10.2 Erbium.....	16
	10.3 Thulium	16
	10.4 Ytterbium	17
	10.5 Europium	18
11.	Thermal Investigation of Crystal Field Splittings in Rare-Earth Ethylsulfates (B. C. Gerstein)	18
12.	Low Field Magnetic Studies of Thermal Hysteresis in Rare- Earth Metals in the Range 1.3 - 300°K (B. C. Gerstein)	19
13.	Magnetic Properties of Stable Free Radicals (B. C. Gerstein).....	20
14.	Surface Chemistry (R. S. Hansen).....	20
15.	Capillary Ripples (R. S. Hansen).....	24

	Page
16. Fused Salt Research (F. R. Duke).....	25
16.1 Mechanism of Electrical Conductivity	25
16.2 Reactions in Fused Salts	25
17. Solution of Metals in Their Molten Salts (J. D. Corbett)	27
17.1 Metal-Metal Salt Phase Studies	27
17.1.1 Praseodymium Chlorides	27
17.1.2 Rare-Earth Metal Bromides	27
17.1.3 Yttrium and Gadolinium Halides	28
17.1.4 The Antimony Sulfide System.....	30
17.2 Resistivity Measurements on Solutions of Metals in Their Molten Salts	30
17.3 Raman Spectra of Molten Salts.....	31
17.4 Metal-Metal Halide Reactions in the Vapor Phase.....	32
18. Solid Subhalides	32
18.1 The Structure of Bismuth Monochloride.....	33
18.2 Magnetic Susceptibilities of Neodymium Chlorides and Iodides.....	33
18.3 Physical Properties of the Metallic Diiodides	33
19. Solutions of Gallium(I) Salts in Aqueous Base (J. D. Corbett)...	34
20. Mass Spectra of Volatile Inorganic Compounds (H. J. Svec)....	34
20.1 Heats of Formation of VOF_3 , CrO_2F_2 , CrO_2Cl_2 and AsF_3	34
20.2 Heats of Formation of the Hydrides of Groups IVB and VB (H. J. Svec).....	36
20.3 The Mass Spectra of Aluminum Hydride-Methyl Amine Complexes.....	38
21. The Mass Spectra of the Amino Acids (H. J. Svec).....	38
22. The Absolute Isotopic Abundance of Cr, V, Li and O in Some Minerals (H. J. Svec).....	39
22.1 Natural Abundance of the Cr Isotope in Secondary Minerals.....	39
22.2 Natural Abundance of the Vanadium Isotopes in Ores and Minerals	39
22.3 Natural Abundance of the Oxygen Isotopes in the Boron Minerals Found in the Kramer Ore Body at Boron, California	40
22.4 Natural Abundance of the Li Isotopes in Some Minerals and Ores	42
23. The Vibrational Frequencies and Structure of $\text{AlH}_3 \cdot 2\text{N}(\text{CH}_3)_3$ (C. W. Heitsch).....	44
24. The Vapor Phase Dissociation of $\text{AlH}_3 \cdot 2\text{N}(\text{CH}_3)_3$ (C. W. Heitsch).....	45
25. The Compound $\text{AlH}_3 \cdot \text{N}(\text{CH}_3)_3$, Its Dipole Moment and Structure (C. W. Heitsch).....	45
26. The Structure of the Trimethyl-Amine Adduct of Aluminum- borohydride (C. W. Heitsch).....	47
27. Study of Thin Films (L. S. Bartell).....	49
28. Secondary Isotope Effects (L. S. Bartell)	50
29. Electron Diffraction Studies (L. S. Bartell)	51

30.	Nature of Chemical Binding (K. Ruedenberg).....	52
31.	Electronic Structure and Ultraviolet Spectra.....	53
	31.1 Aromatic Hydrocarbons (K. Ruedenberg).....	53
	31.2 Platinum Complexes (K. Ruedenberg and D. S. Martin ..	53
32.	Two-, Three-, and Four-Atom Energy Interactions in Molecules (K. Ruedenberg).....	54

Pyrometallurgy

1.	Distribution of Fission Products and Plutonium between Alloy Phases (A. F. Voigt).....	54
2.	Extraction of Plutonium from Uranium by Silver, Lanthanum and Cerium (A. F. Voigt).....	57
3.	Dew-Point Determination of Vapor Pressures of Zinc over Its Alloys (A. F. Voigt).....	58
4.	Fused Salt Separations of Uranium and Thorium (A. F. Voigt)	59

Analytical Chemistry

1.	Solvent Extraction (C. V. Banks).....	60
2.	Reversed Phase Partition Chromatography (C. V. Banks)....	61
3.	Determination of Phosphine Oxides (C. V. Banks).....	63
4.	Indium (C. V. Banks)	64
5.	1,10-Phenanthroline Complexes (C. V. Banks).....	64
6.	Absorption Spectra of the Rare Earths (C. V. Banks).....	65
7.	Nickel-Nickel Bond in Nickel Dimethylglyoxime	65
8.	Nickel(II) Complexes in Alkaline Media	66
9.	Nickel(II)-Vic-Dioxime Complexes (C. V. Banks)	67
10.	Nickel and Copper Dimethylglyoximes (C. V. Banks and R. E. Rundle).....	68
11.	Oxygen in Metals by Inert Gas Fusion Technique (C. V. Banks)	68
12.	Service Analyses (C. V. Banks).....	69
13.	Analytical Ion-Exchange Separations (J. S. Fritz).....	69
14.	Analytical Separations using Solvent Extraction.....	71
	14.1 Iron.....	71
	14.2 Thorium and Uranium.....	71
15.	Nonaqueous Acid-Base Titrations.....	72

Spectrochemistry

1.	Interstitial Oxygen, Nitrogen and Hydrogen Content of Metals (V. A. Fassel).....	73
	1.1 D-C Carbon Arc-Gas Chromatographic Simultaneous Determination of the Oxygen and Nitrogen Content of Steels	73

	Page
1.2 Determination of Oxygen in Vanadium Metal.....	75
2. Analytical Emission Spectroscopy (V. A. Fassel).....	75
2.1 Excitation of Line Spectra in Fuel-Rich Oxy-Acetylene Flames	75
2.2 Quantitative Determination of Sodium and Tungsten in Tungsten Bronzes.....	77
2.3 Vacuum Ultraviolet Spectroscopy	79
2.4 Electrical Discharges in Noble Gas Atmospheres - Theory and Analytical Applications.....	81
3. Infrared Spectra of Nitrogen Containing Compounds (V. A. Fassel).....	82
4. Spectroscopic and Other Service Analyses (V. A. Fassel).....	85

Radiochemistry

1. Activation Analysis for Sodium in the Sodium Tungsten Bronzes (A. F. Voigt).....	85
2. Recoil Reactions with Carbon-11 (A. F. Voigt).....	86
3. Production and Study of Radioactive Species (A. F. Voigt).....	89
4. Photoproduction Cross Sections (A. F. Voigt).....	90
5. Exchange Reactions in Cyclopentadienyl Cobalt Complexes (A. F. Voigt)	90
6. Szilard-Chalmers Processes (D. S. Martin, Jr.).....	91
7. Isotopic Exchange and Substitution Reactions for Platinum(II) Complexes (D. S. Martin, Jr.).....	93
8. Ligand Field Theory of Square Platinum Complexes (D. S. Martin, Jr.).....	97

Structural Chemistry

1. Strong Hydrogen Bonding (R. E. Rundle).....	100
1.1 β -Diketones	100
1.2 2,4-Furandicarboxylic Acid (R. E. Rundle).....	102
2. Transition Metal Complexes (R. E. Rundle).....	102
2.1 Structure of Dimanganese Decacarbonyl	102
2.2 The Structure of $C_{12}H_{12}V$	104
2.3 Magnetic Properties of Transition Metal Halides	104
3. Coordination Number and Valence (R. E. Rundle).....	105

List of Reports and Publications

1. Reports for Cooperating Laboratories	107
2. Publications.....	108

PHYSICAL AND INORGANIC CHEMISTRY

1. THE SEPARATION OF RARE EARTHS BY ION EXCHANGE (F. H. Spedding* and J. E. Powell)

The investigation of ion-exchange elution processes for separating rare-earth mixtures was continued. A pilot-plant run, designed to demonstrate the feasibility of recycling eluant solution when HEDTA is used in conjunction with H^+ -state ion-exchange resin, was completed. In this experiment, 1150 lb. of Er_2O_3 , 150 lb. of Yb_2O_3 and 130 lb. of Tm_2O_3 (thulium is one of the least abundant rare-earth elements) were prepared in purities exceeding 99.9% from a concentrate containing 80% Er, 10% Tm, 10% Yb. It was demonstrated that more than 90% of the dilute HEDTA eluant required in such a separation can be recovered routinely and recycled without adversely affecting the quality of the product rare earths.

2. STABILITY CONSTANTS OF THE RARE-EARTH CHELATES (J. E. Powell)

It is the difference in stabilities of chelate or complex species formed by association of the rare-earth cations with various anions that affords the means of separation in ion-exchange systems. For this reason work on the determination of stability constants was continued.

The stabilities of the 1:1 and 1:2 rare-earth nitrilotriacetate species were measured by the polarographic method at 10, 20, 30 and 40°C. The data can be found in Report IS-421 by Samuel C. Levy and J. E. Powell and agree well with other values reported by Schwarzenbach and Gut,¹

*First name listed indicates group leader in charge of work.

¹G. Schwarzenbach and R. Gut, *Helv. Chim. Acta* 39, 1589 (1956).

Anderegg,¹ Noddack and Oertel,² and Moeller and Ferrus.³ Solubilities of the hydrated 1:1 rare-earth nitrilotriacetate species were also determined.

The formation constants of some hydroxocomplexes of the type $RChOH^-$, formed by combination of OH^- with neutral 1:1 rare-earth chelates of the type RCh , have been determined. The constants are tabulated in Table I.

In connection with an investigation of some weak rare-earth complexes, the stabilities of some of the individual rare-earth propionate complexes were determined. Although the list is incomplete, the available constants are given in Table II (due to the low concentrations of reactants, b_3 and β_3 could not be determined). They are quite similar to the corresponding constants for the rare-earth acetate complexes.

Work on stability constants during this report period is summarized in the following papers: "Formation Constants of the Complex Species Formed by Interaction of Rare Earth N^1 -Hydroxyethylethylenediamine- N,N,N^1 -Triacetate Complexes with an Equivalent Amount of Base" by A. K. Gupta and J. E. Powell has been accepted by Inorganic Chemistry; "Formation Constants of the Complex Species Formed by Interaction of Rare Earth Nitrilotriacetate Complexes with an Equivalent Amount of Base" by A. K. Gupta and J. E. Powell was submitted to Inorganic Chemistry. The following papers were published: "Acetate Complexes of the Rare-Earths and Several Transition-Metal Ions" by R. S. Kolat and J. E. Powell, Inorg. Chem. 1, 293 (1962); "Determination of the

¹G. Anderegg, Helv. Chim. Acta 43, 825 (1960).

²W. Noddack and G. Oertel, Z. Electrochem. 61, 1216 (1957).

³T. Moeller and R. Ferrus, submitted for publication ca. 1962.

Table I

The Stability Constants of the Hydroxo-Complexes Formed by Interaction of Rare-Earth HEDTA and NTA Chelates with Hydroxyl Ion

(25°C; $\mu = 0.1$ (KNO₃))

Rare Earth	Atomic Number	$\log K'_R(\text{HEDTA})\text{OH}$	$\log K'_R(\text{NTA})\text{OH}$
Y	39	4.76±.05	6.39±.04
La	57	3.46±.03	5.89±.11
Ce	58	-	-
Pr	59	3.69±.07	5.72±.05
Nd	60	3.59±.06	5.86±.05
Pm	61	-	-
Sm	62	3.70±.06	6.59±.05
Eu	63	4.03±.03	6.84±.08
Gd	64	3.98±.07	6.54±.05
Tb	65	4.52±.07	6.67±.05
Dy	66	4.88±.04	6.84±.10
Ho	67	5.12±.04	6.66±.09
Er	68	5.14±.05	6.56±.05
Tm	69	5.11±.04	6.24±.11
Yb	70	5.21±.06	6.29±.12
Lu	71	5.13±.09	6.30±.10

Table II

Formation Constants of Some of the Individual Rare-Earth Propionate Complex Species

(25°C; $\mu = 0.1$ (NaClO₄))

Rare Earth	Atomic Number	$b_1 = \beta_1$	b_2	β_2
Y	39	75	15	1120
La	57	78	15	1130
Ce	58	112	17	1910
Pr	59	132	22	2910
Nd	60	157	21	3250
Pm	61	-	--	--
Sm	62	161	31	4950
Eu	63	168	33	5550
Gd	64	122	30	3610
Tb	65	99	39	3900
Dy	66	85	33	2830

Table II (Continued)
(25°C; $\mu = 0.1$ (NaClO₄))

Rare Earth	Atomic Number	$b_1 = \beta_1$	b_2	β_2
Ho	67	90	32	2840
Er	68	87	35	3030
Tm	69	81	33	2630
Yb	70	85	28	2370
Lu	71	100	34	3380

Rare-Earth--HEDTA Stability Constants by the Mercury-Electrode Method" by J. E. Powell and J. L. Mackey, Inorg. Chem. 1, 418-421 (1962); and "A Calorimetric Study of the Reaction of Rare-Earth Ions with EDTA in Aqueous Solution" by J. L. Mackey, J. E. Powell and F. H. Spedding, J. Am. Chem. Soc. 84, 2047-2050 (1962).

3. THE HYDRATION AND SOLUBILITIES OF YTTRIUM AND RARE-EARTH CHELATES FORMED WITH ANIONS OF α -HYDROXY ACIDS (J. E. Powell)

The crystalline 1:3 chelates formed between trivalent rare-earth cations and the glycolate and lactate anions have been prepared and studied, and an investigation of the corresponding rare-earth α -hydroxyisobutyrate has been initiated. There is a progressive increase in hydration and a decrease in solubility with increasing molecular weight of the ligand acid. Except in the case of the glycolates, part of which separate in anhydrous form, there is a regular decrease in solubility with increasing atomic number of the metal ion. The data for rare-earth glycolates and lactates are given in Table III.

Thermal decomposition of the dihydrated rare-earth glycolates proceeds through the anhydrous stage by initial loss of two moles of water per

Table III

The Hydration and Solubilities of Rare-Earth Glycolates and Lactates in Water at Several Temperatures

Compound	Solubility (g cmpd/100 g H ₂ O)		Compound	Solubility (g cmpd/100 g H ₂ O)	
	20°	60°		20°	60°
La(gly) ₃	0.38	0.46	La(lac) ₃ · 3H ₂ O*	--	--
Ce(gly) ₃	0.38	0.49	Ce(lac) ₃ · 3H ₂ O*	--	--
Pr(gly) ₃	0.42	0.46	Pr(lac) ₃ · 3H ₂ O*	--	--
Nd(gly) ₃	0.45	0.45	Nd(lac) ₃ · 3H ₂ O*	--	--
Pm(gly) ₃	--	--	Pm(lac) ₃ · 3H ₂ O	--	--
Sm(gly) ₃	0.82	0.67	Sm(lac) ₃ · 3H ₂ O	1.25	1.87
Eu(gly) ₃	0.84	0.81	Eu(lac) ₃ · 3H ₂ O	0.65	1.08
Gd(gly) ₃ · 2H ₂ O	1.02	--	Gd(lac) ₃ · 3H ₂ O	0.41	0.75
Tb(gly) ₃ · 2H ₂ O	0.55	1.13	Tb(lac) ₃ · 3H ₂ O	0.24	0.59
Dy(gly) ₃ · 2H ₂ O	0.32	0.69	Dy(lac) ₃ · 3H ₂ O	0.17	0.36
Ho(gly) ₃ · 2H ₂ O	0.23	0.52	Ho(lac) ₃ · 3H ₂ O	0.13	0.30
Er(gly) ₃ · 2H ₂ O	0.17	0.37	Er(lac) ₃ · 3H ₂ O	0.11	0.22
Tm(gly) ₃ · 2H ₂ O	0.14	0.32	Tm(lac) ₃ · 3H ₂ O	0.09	0.19
Yb(gly) ₃ · 2H ₂ O	0.11	0.23	Yb(lac) ₃ · 3H ₂ O	0.07	0.15
Lu(gly) ₃ · 2H ₂ O	0.09	0.22	Lu(lac) ₃ · 3H ₂ O	0.06	0.13
Y(gly) ₃ · 2H ₂ O	0.22	0.46	Y(lac) ₃ · 3H ₂ O	0.13	0.27

* These materials cannot be prepared readily from water solutions. They are hygroscopic and apparently extremely soluble in water.

mole of compound at temperatures between 170 - 210°C. Very little hydrolysis or degradation is apparent at this stage. At 320 - 350°C an inflection, corresponding approximately to Ln(gly)CO₃, is noted, except in the case of Ce(gly)₃ which decomposes directly to the dioxide.

Thermal decomposition of the trihydrated lactates studied proceeds with the loss of one mole of water at 90 - 110° and two moles of water between 120 - 160°. A composition approximating Ln(lac)CO₃ is observed at about 290°C in each case.

Preliminary results show that the rare-earth α -hydroxyisobutyrate, in general, separate from water as hexahydrates in the form of minute silky needles. Thermal studies indicate that dehydration proceeds in two distinct steps with the loss of four moles and two moles of water per mole of compound, respectively. A marked decrease in solubility from the light to the heavy end of the series was noted in the preparation of the hydrated rare-earth α -hydroxyisobutyrate. It appears that they are more soluble in cold water than in hot water, although precise data are not yet available. Note that the lesser hydrated rare-earth glycolates and lactates behave differently, being more soluble hot than cold.

4. SEPARATION OF LITHIUM ISOTOPES

A paper entitled "The Separation of Lithium Isotopes by Ion Exchange", by J. E. Powell, was published in J. Inorg. Nuclear Chem. 24, 183-186 (1962).

Abstract--The single-stage separation factor for the separation of ^6Li and ^7Li by distribution between a solution of lithium acetate and the lithium form of a sulphonated styrene-divinylbenzene copolymer (Dowex 50 X 24) has been measured by a method of frontal analysis. The value obtained was 1.0026 ± 0.0003 . The comparative merits of elution and displacement chromatography as means of resolving lithium isotopes are discussed.

5. PREPARATION OF RARE-EARTH METALS (F. H. Spedding and A. H. Daane)

5.1 Purification of Rare-Earth Metals by Filtering

The previous report from this group indicated that in attempts to purify yttrium by various techniques some metallic impurities could not

be eliminated by vacuum distillation but could be removed by filtering the molten yttrium through a porous tungsten crucible. This work has been extended in some experiments in which samples of yttrium containing added impurities were filtered through a porous tungsten filter in the same manner as the previous experiments. The results of these experiments are given in Table IV. It will be noted that the degree of removal in some cases is related to the solid solubility of the particular impurity in tungsten as in the case of Nb, Cr and Mo.

Table IV

Element	Content before Filtering	Content after Filtering	% Removal	Approx. Solid Solubility of Element in Tungsten
O	160 ppm	400 ppm	--	negligible
C	153	165	--	"
N	125	193	--	"
F*	2500	25	99	-----
Si	100	200	--	0.8 wt%
Ti†	3200	500	84	5 wt%
Fe†	334	120	64	0.8 wt%
Zr†	8275	7310	14	1 wt%
Mn†	3815	450	90	-----
Al†	60000	58000	--	2 wt%
V	6820	890	87	-----
Co	440	290	34	1 wt%
Ni	5200	3900	25	1 wt%
Nb	5020	86	98	complete
Cr	4660	70	98	complete
Hf	6850	5300	23	-----
Mo	4560	80	98	complete
Pt	575	390	32	2 wt%

*Present as YF_3 or YOF.

†Average over several runs.

5.2 Vacuum Distillation

In a series of experiments to observe the purification of gadolinium by modification of a vacuum distillation technique, small amounts of tungsten powder were added to the gadolinium metal to be purified. This was done to see if the scavenging of some of these elements by tungsten in the filtering process described above would be observed in this type of process. The gadolinium was distilled at a temperature of 1950°C in a vacuum of 5×10^{-6} mm Hg. The distillate from this experiment was found to have a generally higher purity than the starting material and the most notable effect observed was the decrease in the iron concentration from 200 ppm to less than 50 ppm. This same technique has been found to give similar results with other heavy rare-earth metals.

5.3 Electron Beam Melting

A sample of cerium was electron beam melted and it was found that this treatment decreased the oxygen content from 1900 ppm to 300 ppm; the hardness of this metal was 20 on the Rockwell-L scale. This is the lowest oxygen content observed in this Laboratory for a sample of cerium.

6. PROPERTIES OF RARE-EARTH METALS

6.1 High Temperature Allotropes

Previous work from this Laboratory has shown that the light earth metals, yttrium and possibly gadolinium, exist in a body-centered cubic form at high temperatures. In a study of some yttrium-magnesium alloys, Gibson and Carlson¹ showed that the body-centered cubic form of yttrium could be retained by quenching to room temperature. Alloys of some heavy rare-earth metals with magnesium in the 0 to 50 at. % range have

¹E. D. Gibson and O. N. Carlson, Trans. ASM 52, 1084 (1960).

been examined by thermal, microscopic and x-ray methods. The x-ray and thermal data obtained in this study are given in Table V. This work has shown the existence of a body-centered cubic form of Gd, Tb, Dy, Ho, Er, Tm and Lu. On cooling slowly the high temperature body-centered cubic solid solution decomposes eutectoidally into a hexagonal rare-earth-magnesium solid solution plus a simple cubic peritectic AB type compound.

Table V

Rare-Earth Metal	Lattice Parameter, Å		Eutectoid Temp. -5°C	Peritectic Temp. -5°C
	bcc Allotrope ± 0.02 Å	Simple Cubic REMg ± 0.02 Å		
Gd	4.05	3.824	679	865
Tb	4.02	3.796	695	857
Dy	3.98	3.786	706	857
Ho	3.96	3.776	710	851
Er	3.94	3.758	699	822
Tm	3.92	3.749	671	761
Lu	3.90	3.727	593	671

6.2 Vapor Pressure Studies

The vapor pressure of terbium and gadolinium has been measured by the Knudsen method employing a quartz fiber microbalance. While the analysis of the data is not complete, the approximate heats of vaporization for gadolinium and terbium were found to be 89.5 and 86.1 kcal per mole respectively. As an indication of the approximate vapor pressures observed in these studies, that of terbium is 10^{-1} mm at 2000°K and 10^{-3} mm at 1650°K; for gadolinium the vapor pressure is 10^{-2} mm at 1875°K, 10^{-4} mm at 1650°K.

6.3 Electrical Resistivity

A study of the nature of the electrical resistivity of some rare-earth alloys has been completed and the work is described in a paper, 'Mechanisms of the Electrical Resistivity of Rare-Earth Alloys', by F. A. Smidt, Jr. and A. H. Daane, submitted for publication in the Journal of the Physics and Chemistry of Solids.

Abstract--The electrical resistivity of Gd-Lu, Tb-Lu and Gd-Er alloys at low temperatures has been measured, and the contributions to the electrical resistivity have been evaluated. The residual resistivities follow Nordheim's rule. Some relation between the resistivity and the structure of these alloys was observed.

6.4 High Temperature Calorimetry

The high temperature heat constant of Sc and some heavy rare-earth metals has been measured utilizing the Bunsen ice calorimeter described in previous reports from this Laboratory. The data obtained are given in Table VI. We intend to extend these measurements to above the melting points of each of these metals.

Table VI

Temp. °C	Gd	Er	$\Delta H_o^{t^\circ C}$ cal/g		Ho	Sc
			Tb	Dy		
100	837	661	662	642	629	616
200	1538	1344	1324	1272	1296	1215
300	2239	2045	2038	1946	1974	1885
400	2955	2742	2774	2653	2660	2564
500	3665	3440	3518	3373	3369	3219
600	4412	4196	4363	4097	4070	3938
700	5171	4934	5205	4820	4833	4681

Table VI (Continued)

Temp. °C	$\Delta H_o^{t^\circ C}$ cal/g					
	Gd	Er	Tb	Dy	Ho	Sc
800	5948	5715	6000	5608	5603	5425
900	6711	6521	6885	6405	6396	6216
1000		7328	2868	7282	7215	6980
1100		8186	8819	8196	8143	7812

6.5 Extrusion of Europium

Because of the extreme softness observed for europium metal it was felt that extrusion would be a satisfactory process for the preparation of some small samples of this metal. It was found that the metal would, indeed, extrude readily at room temperature; a pressure of only 16,000 psi on a one-inch diameter billet was sufficient to extrude 1/8-in. wire.

7. RARE-EARTH ALLOYS (F. H. Spedding and A. H. Daane)

7.1 Equilibrium Studies

7.1.1 Sc-V System

A cursory examination of the scandium-vanadium system has been made using metallographic and x-ray diffraction techniques. As was expected, no intermediate phase was observed in this system. The solid solubility of scandium in vanadium was found to be less than 0.2 at. % at 1100°C. A paper, "Sc-Ti System and the Allotropy of Scandium", by B. J. Beaudry and A. H. Daane, has been accepted for publication in the Transactions of the Metallurgical Society of AIME.

Abstract--The scandium-titanium system was studied by thermal, metallographic and x-ray methods. Scandium was found to transform at 1334°C from α (hexagonal) to β which was concluded to be center cubic since a continuous series of solid solutions is formed between β scandium and β titanium at elevated temperatures.

There is a minimum in the solidus at 51 wt% Ti and 1300°C; a monotectoid at 1050°C and 49 wt% Ti and a eutectoid at 875°C and 91.5 wt% Ti. The maximum solubility of Ti in α Sc is 13.5 wt% at the monotectoid horizontal while the maximum solubility of Sc in α Ti is 6.5 wt% at 875°C.

7.1.2 Y-Mn System

The study of the Y-Mn System has been completed and has been published in Trans. AIME 224, 354-357 (1962).

Abstract--The yttrium-manganese system has been investigated by thermal, metallographic and x-ray diffraction methods. There are three intermetallic compounds present: YMn_2 which melts congruently, YMn_4 which undergoes syntectic decomposition, and YMn_{12} which undergoes peritectic decomposition. The compound YMn_4 is ferromagnetic at room temperature with a Curie temperature of 214°C. There are eutectics at 25.2, 60.9 and 82.0 wt% Mn which melt at 878°, 1100° and 1075°C, respectively. Crystallographic data are given for YMn_4 and YMn_{12} . The terminal solid solubilities are low.

7.1.3 Y-Ho System

The yttrium-holmium system has been investigated, using arc melted specimens of the metals. X-ray diffraction data obtained are given in Table VII, which indicates the nearly ideal nature of the alloys in this system. Thermal analyses, while not complete, have not indicated the presence of a high temperature form of holmium.

Table VII

% Y in Ho	a_0 in Å	c_0 in Å	$\frac{c}{a}$
00.00	3.5790	5.6232	1.571
16.19	3.5913	5.6425	1.571
33.29	3.6012	5.6600	1.572
48.05	3.6146	5.6800	1.571
65.10	3.6241	5.7048	1.574
83.34	3.6382	5.7246	1.574
100.00	3.6505	5.7451	1.573

7.1.4 Nd-Y System

Work has begun on the neodymium-yttrium system. X-ray diffraction studies have shown that neodymium is soluble in alpha yttrium at room temperature to at least 53 at.%. An intermediate phase has been observed in this system at higher neodymium concentrations with the same "samarium structure" previously reported by Spedding, et al.¹

7.2 Magnetic Studies

In order to examine the nature of the "samarium structure" that has been observed in several light rare-earth-heavy rare-earth alloys, a magnetic study of some of the samarium structure phases has been started. Data obtained in measurements made on several of these samarium structure alloys below room temperature are given in Table VIII. It should be noted that the three alloys given in Table VIII are of three distinct types. In La-Gd, the light metal is diamagnetic while the heavy metal is paramagnetic; in Nd-Y, the light metal is paramagnetic and the heavy metal is diamagnetic; in Nd-Tm, both metals are paramagnetic. These three samples show different behavior in $1/X$ vs T plots.

¹F. H. Spedding, R. M. Vailletta and A. H. Daane, Trans. ASM (September 1962).

Table VIII

Alloy	Temp. °K	$g \cdot 10^6$ (obs.)	$g \cdot 10^6$ (theo.)
La-Gd	300.4	166.8	121.5
	251.6	210.2	145.8
	199.1	265.0	182.2
	150.1	384.5	243.0
	98.22	514.0	364.3
	78.82	534.2	468.0
Nd-Y	301.1	31.49	30.37
	255.1	35.78	36.38
	198.0	45.26	45.35
	146.8	58.82	60.34
	106.9	77.15	90.29
	77.73	97.99	116.0
Nd-Tm	300.3	71.08	77.70
	250.9	85.16	93.24
	203.1	107.2	116.5
	149.3	141.8	155.4
	100.6	217.6	233.1
	78.25	268.5	297.9

8. BONDING IN BORIDES (A. H. Daane)

The nature of the bonding in metallic borides has been investigated using single crystal measurements on several samples of yttrium borides. The results of this study are given in two papers, the abstracts of which appear below:

"Electron Requirements of Bonds in Metal Borides", R. W. Johnson and A. H. Daane, submitted to The Journal of Chemical Physics.

Abstract--Electrical resistivity measurements on samples of borides of yttrium, strontium, calcium and barium together with Hall coefficient measurements on single crystals of YB_2 , YB_6 and YB_{12} have been used to evaluate proposed bonding systems in these borides. The models for these systems have been derived from a LCAO treatment of the boron-boron bonds, such as has been proposed by Lipscomb and others. The agreement between the experimental data and the proposed models appears satisfactory.

"Floating Zone Method of Preparing Single Crystals of Refractory Borides", R. W. Johnson, submitted to Journal of Applied Physics.

Abstract--A floating zone technique for the preparation of single crystals of samples of borides of yttrium has been devised. An eddy-current concentrator in an induction furnace provides the means of achieving temperatures above 2500°C in this work.

9. HEAT CONTENT OF SILICON (A. H. Daane)

To aid in resolving the discrepancy in the literature on the heat capacity of silicon, the heat content on silicon was measured from room temperature to 1100°C. The data are given in Table IX.

Table IX

	Temp. °C	$H_o^{t^\circ C}$ cal/g
Si:	100	490
	200	1028
	300	1592
	400	2168
	500	2748
	600	3350
	700	3956
	800	4579
	900	5210
	950	5514
	1000	5841
	1050	6153
	1100	6491

10. HEAT CAPACITY MEASUREMENTS (B. C. Gerstein and F. H. Spedding)

10.1 Terbium

A paper, "Correlation between Heat Capacity Anomaly in Tb and Magnetic Transition in Tb_2O_3 ", by B. C. Gerstein, F. J. Jelinek and F. H. Spedding, was published in Phys. Rev. Letters 8, 425 (1962).

Abstract--Terbium metal exhibits a heat capacity anomaly at 2.4°K. Because of the entropy associated with the anomaly, the anomaly has been attributed to an impurity oxide phase. The magnetic susceptibility of Tb_2O_3 was measured in the range 1.3 - 250°K to determine if a correlation exists between the heat capacity bump in the metal and a magnetic transition in the oxide. The susceptibility of the oxide exhibits a sharp peak at 2.42°K.

10.2 Erbium

A paper, "Thermal Study of Crystal Field Splittings in Erbium Ethylsulfate", by B. C. Gerstein, C. J. Penney and F. H. Spedding, was submitted for publication in The Journal of Chemical Physics.

Abstract--The heat capacities of erbium ethylsulfate and yttrium ethylsulfate have been measured in the range 12 - 300°K. The magnetic contribution of the erbium ion has been evaluated with the help of an assumption concerning the difference in lattice contributions between the erbium and yttrium salts. This contribution agrees, to within experimental error, with the experimental energy level scheme for the $^4I_{15/2}$ state of the tripositive erbium ion, published by Erath.¹

10.3 Thulium

"Thermal and Magnetic Study of Crystal Field Splittings in Thulium Ethylsulfate", by B. C. Gerstein, L. Jennings and F. H. Spedding, has been accepted for publication in The Journal of Chemical Physics.

¹E. H. Erath, J. Chem. Phys. 34, 1985 (1961).

Abstract--The heat capacity and principal susceptibilities of thulium ethylsulfate have been measured in the range 15 - 300°K and 1.3 - 200°K respectively. The heat capacity of lutetium ethylsulfate has been measured in the range 15 - 300°K. The contribution of the 4f electrons in the tripositive Tm ion to the heat capacity of thulium ethylsulfate has been evaluated experimentally by making an assumption concerning the difference in the lattice heat capacities of Tm and Lu ethylsulfates. The contribution of the 4f electrons in the tripositive Tm ion to the heat capacity and principal susceptibilities has been calculated using the angular part of the crystal field matrix elements calculated by Stevens and Elliott,¹⁻⁴ and two sets of crystal field parameters currently available in the literature.^{5,6} The experimental results indicate that the crystal field parameters of Wong and Richman⁵ are more nearly correct than those of Gruber and Conway.⁶

10.4 Ytterbium

The heat capacity of ytterbium has been re-measured in the range 15 - 350°K. The results are essentially the same as those obtained in previous measurements. Recent data on Yb below 4°K obtained from O. V. Lounasmaa⁷ at Argonne National Laboratory yielded a Debye temperature of 118.1°K, and a conduction electron term of 0.0029 joules

¹K. W. H. Stevens, Proc. Phys. Soc. (London) A65, 209 (1952).

²R. J. Elliott, Rev. Mod. Phys. 25, 167 (1953).

³R. J. Elliott and K. W. H. Stevens, Proc. Roy. Soc. (London) A219, 387 (1953).

⁴R. J. Elliott and K. W. H. Stevens, Ibid. A218, 553 (1953).

⁵E. Y. Wong and I. Richman, J. Chem. Phys. 34, 1182 (1960).

⁶J. B. Gruber and J. G. Conway, J. Chem. Phys. 32, 1531 (1960).

⁷O. V. Lounasmaa, private communication.

(g at. wt deg)⁻¹. These values, together with compressibility and thermal expansion data of Bridgman¹ and Hanak,² yield a magnetic contribution to the heat capacity of Yb which is inconsistent with the magnetic data of Lock.³ The heat capacity of a redistilled block of Yb will be measured in the range 15 - 350°K in order to determine if the seemingly anomalous magnetic contribution of the first sample was caused by the method of sample preparation and associated oxygen and nitrogen impurities. The first sample was prepared by lanthanum reduction of YbF₃. It has been found that this method can lead to oxygen impurity as high as 0.3% by weight.

10.5 Europium

The heat capacity of europium has been measured in the range 12 - 350°K. A lambda type anomaly has been found at 88.5°K. The height of the anomaly appears to increase with decreasing temperature increment in the individual heat capacity points. An antiferromagnetic transition has been found in Eu through magnetic measurements by Bozorth and Van Vleck.⁴ The temperature of the transition determined by magnetic measurements is 89°K.

11. THERMAL INVESTIGATION OF CRYSTAL FIELD SPLITTINGS IN RARE-EARTH ETHYLSULFATES (B. C. Gerstein)

The heat capacity of erbium ethylsulfate has been measured in the range 12 - 300°K. The magnetic contribution of the tripositive erbium

¹P. T. Bridgman, Proc. Am. Acad. Arts. Sci. 83, 1 (1954).

²F. H. Spedding, J. J. Hanak and A. H. Daane, J. Less Common Metals 3, 110 (1961).

³J. M. Lock, Proc. Phys. Soc. (London) 70B, 476 (1957).

⁴R. M. Bozorth and J. H. Van Vleck, Phys. Rev. 118, 1493 (1960).

ion to the heat capacity of the salt has been evaluated. This contribution agrees, to within experimental error, with the results calculated using the energy level scheme for the $^4I_{15/2}$ state of tripositive Er published by Erath.¹

The heat capacities of holmium ethylsulfate and dysprosium ethylsulfate have been measured in the range 13 - 300°K. The magnetic contributions to the respective heat capacities have not yet been evaluated.

12. LOW FIELD MAGNETIC STUDIES OF THERMAL HYSTERESIS IN RARE-EARTH METALS IN THE RANGE 1.3 - 300°K (B. C. Gerstein)

Initial susceptibilities of Ho and Dy metals have been measured from 1.3 - 200°K using an ac mutual inductance technique. The magnitudes

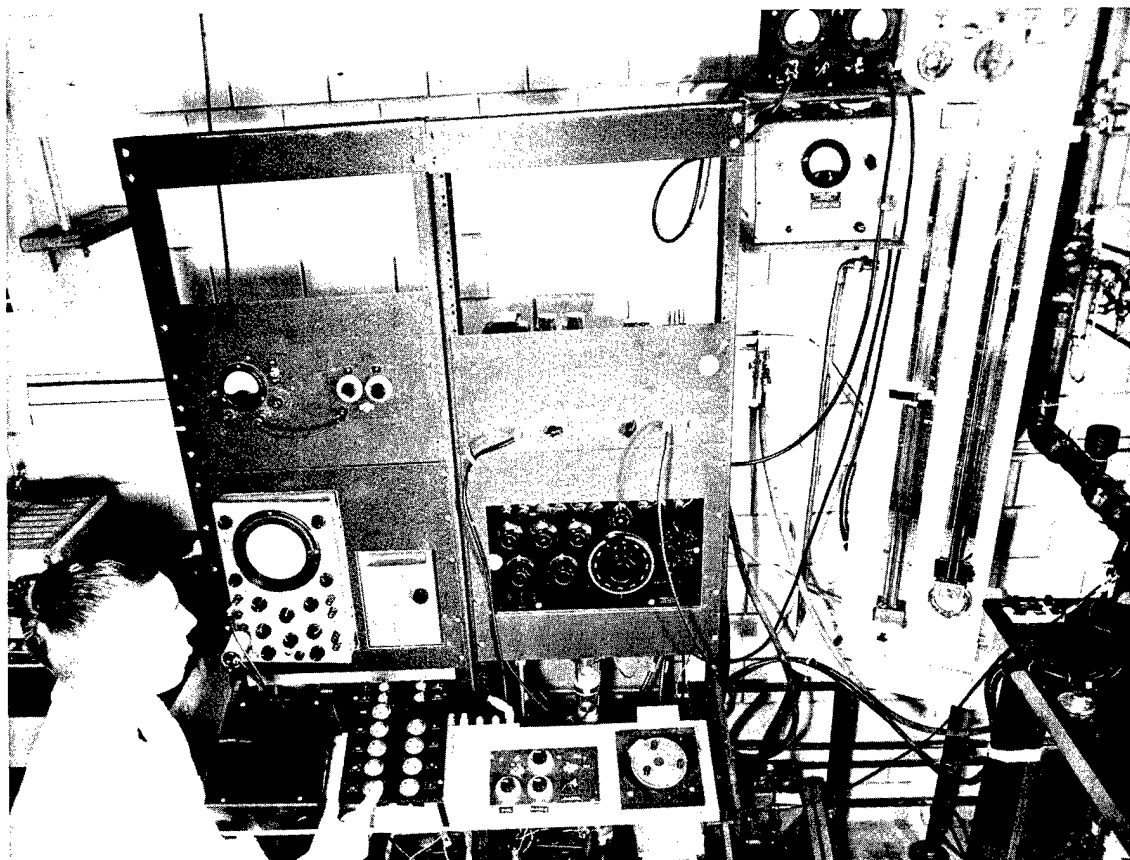


Fig. 1. Mutual Inductance Initial Susceptibility Apparatus

¹E. H. Erath, J. Chem. Phys. 34, 1985 (1961).

of the real compared to the imaginary susceptibilities indicate that the form of the susceptibility below the Curie points for both Ho and Dy may be attributed to a relaxation process. Thermal hysteresis was detected in the region of the Curie point for the measurements on Dy. Such hysteresis was also observed in the heat capacity of Dy. No hysteresis was observed in the magnetic measurements on Ho, although thermal hysteresis was observed in the heat capacity measurements on Ho in the region of the Curie point.

13. MAGNETIC PROPERTIES OF STABLE FREE RADICALS (B. C. Gerstein)

The initial susceptibility of diphenyl picryl hydrazyl has been measured in the range 1.3 - 200°K. The susceptibility exhibits a peak at 3.8°K. The form of the peak, together with the broad maximum¹ in the heat capacity in the range 1 - 4°K suggests that the cooperative interaction between unpaired spins is either one or two dimensional.

14. SURFACE CHEMISTRY (R. S. Hansen)

A paper, "Thermodynamics of Interfaces between Condensed Phases", by Robert S. Hansen, was published, J. Phys. Chem. 66, 410-415 (1962).

Abstract--Measurements of properties of plane interfaces between condensed phases generally are conducted at constant pressure. The Gibbs surface excess convention, which eliminates pressure as an independent variable, is not the natural convention for such measurements. A convention eliminating chemical potentials of two components is discussed and shown to be particularly appropriate for condensed phase interfaces. The physical interpretation of this convention and formulas for evaluation of thermodynamic quantities from experimental data are presented. An approach to the evaluation of statistical theories of adsorption from solution in terms of experimental thermodynamic information is illustrated.

¹J. P. Goldsborough, M. Mandel and G. E. Pake, "Proceedings of the Seventh International Conference on Low Temperature Physics", Graham and Hollis-Hallett, Ed., University of Toronto Press, Toronto, Canada, pp. 702-705, 1961.

A paper, "Trends in Colloid and Surface Chemistry in the Mainstream of Modern Chemistry", by Robert S. Hansen and C. A. Smolders, was published, J. Chem. Ed. 39, 167-178 (1962).

Abstract--This article was based on an invited lecture presented by the senior author at the Symposium on Education in Colloid and Surface Chemistry held by the American Chemical Society at its September, 1961 meeting (Chicago, Illinois). The article surveys recent trends in colloid and surface chemistry, discussing major problems of thirty years ago that are now solved in principle (the nature of interaction of gases with solids at distances greater than one molecular diameter, the nature of lyophilic colloids, and the nature of lyophobic colloids), major areas receiving active and productive current study (the nature of the first adsorbed layer, especially in chemisorption, the mechanism of electrochemical reactions, and the nature of the wetting process) and unsolved problems needing new research approaches (the nature of physical adsorption from solution in the monolayer region, the nature of mechanical properties of surface films, and the nature of foams and emulsions).

A paper by John R. Arthur, Jr. and Robert S. Hansen, "A Study of the Adsorption of Hydrogen, Ethane, Ethylene and Acetylene on Iridium by Field Emission Electron Microscopy", was published, J. Chem. Phys. 36, 2062-2071 (1962).

Abstract--A field emission microscope permitting precise control of iridium emitter temperature from 4 to 1700°K was used to study changes in emission patterns and work functions resulting from time and temperature dependent surface reactions in the adsorption of hydrogen, ethane, ethylene and acetylene on iridium.

The qualitative character of the emission patterns indicates a rather uniform covering of the high index faces of iridium by all species studied in the temperature range 70–300°K. Hydrocarbon species, once chemisorbed, are substantially immobile at temperatures below 700°K; above 700°K an intensification of emission pattern, probably due to carbonization, occurs around the edges of the III planes.

Iridium surfaces containing adsorbed species were flashed for controlled periods of time to controlled temperatures; characteristic changes in work function resulted which were both time and temperature dependent. These experiments indicate that hydrogen is readily desorbed by iridium above 400°K, and that a large portion of adsorbed ethane is readily desorbed at 100°K, but a residue from adsorbed ethane is not desorbed below 1000°K. For a given flash time, curves representing work function as a function of flash temperature for adsorbed ethylene and acetylene show characteristic differences below 450°K but are very similar above 450°K. Results are interpreted as indicating chemisorption of ethylene, dehydrogenation of chemisorbed ethylene to form chemisorbed acetylene and chemisorbed hydrogen, desorption of chemisorbed hydrogen, dehydrogenation of chemisorbed acetylene and finally crystallization of carbon residue.

A further paper by John R. Arthur, Jr. and Robert S. Hansen, "The Adsorption and Surface Reactions of Hydrocarbons on Clean Iridium", covering our work on catalytic reactions by field emission microscopy, was presented at the meeting of the New York Academy of Science, April 7, 1962, and will appear in the annals of the New York Academy of Science.

Abstract--The adsorption of ethane, ethylene and acetylene on clean iridium in a field emission microscope has been found to cause characteristic changes in the work function of the iridium surface. Further changes, which are time and temperature dependent, result when such

surfaces are heated. Flash filament experiments have shown that the changes in work function on heating are due to desorption reactions and that the desorbed product consists principally of hydrogen. By assuming a linear relationship between surface coverage and work function, it has been possible to determine the desorption kinetics from the observed rates of work function change at various temperatures. The results are consistent with a mechanism involving stepwise surface dehydrogenation in which a pair of hydrogen atoms is removed from the hydrocarbon molecule in each step, followed by the desorption of the adsorbed hydrogen. At very high temperatures the remaining carbon atoms are removed, presumably by evaporation.

Thus far we have been able to establish the kinetic mechanism and kinetic parameters (activation enthalpy and frequency factor) for the desorption of hydrogen and the dehydrogenation of acetylene adsorbed on iridium with considerable precision. The kinetic mechanism of the dehydrogenation of ethylene appears clearly indicated but more data are needed to establish the kinetic parameters with satisfactory precision. An Omegatron mass spectrometer has been installed as part of the flash filament desorption spectrometer, and with the help of this instrument we were able to confirm that hydrogen was the sole desorption product from the decomposition of chemisorbed ethylene and acetylene above 300°K; we were further able to establish the presence of an ethane desorption peak from chemisorbed ethylene on flashing to 100°K and presume this to result from the disproportionation of chemisorbed ethylene.

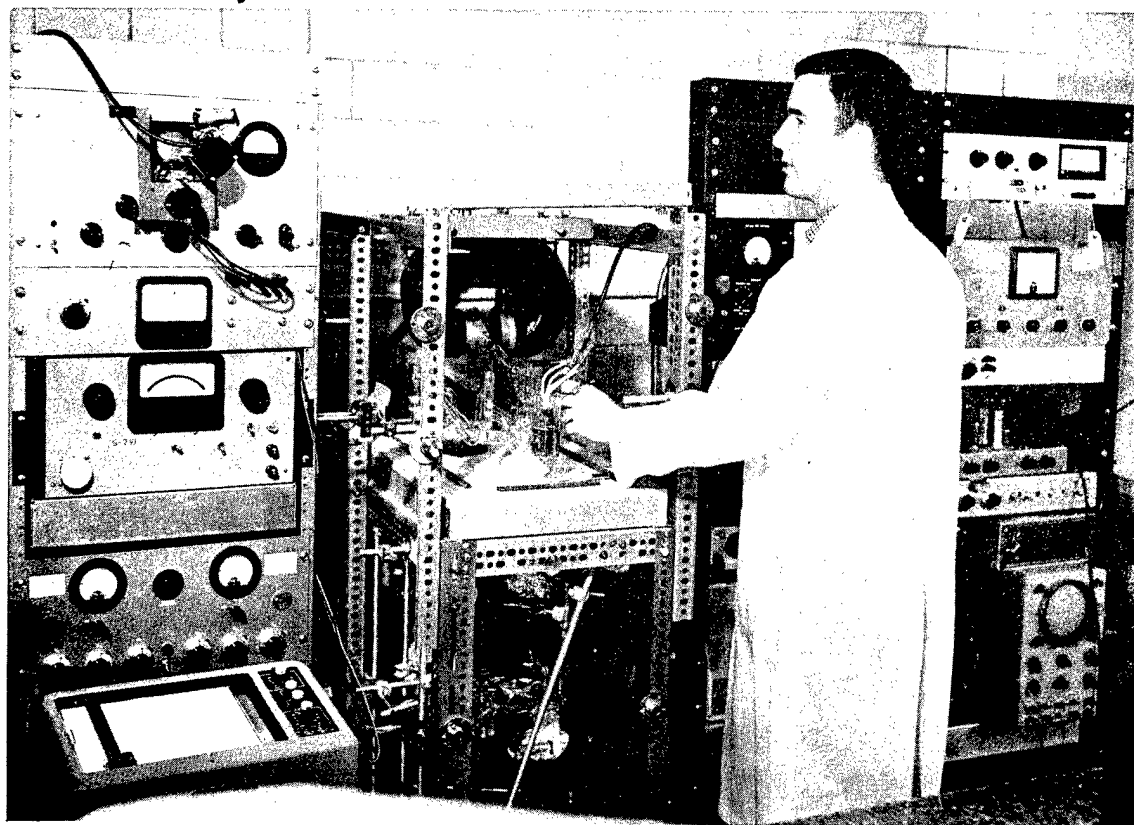


Fig. 2. Flash Filament Desorption Spectrometer

15. CAPILLARY RIPPLES (R. S. Hansen)

The first phase of a study of the dispersion in velocity of propagation of capillary ripples and of their amplitude attenuation has been completed. A hydrodynamic theory of velocity dispersion and amplitude attenuation was developed, and includes effects of surface viscoelasticity and diffusion. According to this theory, limiting forms for the dependence of velocity and amplitude attenuation on frequency are reached at high and low viscoelasticity in the surface films which are such that parameters of viscoelasticity do not appear. Precise instrumentation for measuring velocity

of propagation and amplitude attenuation of capillary ripples was devised; the instrumentation is electronic rather than optical in principle. Dependence of these properties on frequency was measured for pure water, heptanoic acid solutions of various concentrations, stearic acid monolayers at various film pressures, and for films of various other materials on water. Experimental results agreed with limiting forms of the hydrodynamic theory developed, within experimental error in all cases. (It should be noted that the limiting forms contained no adjustable parameters at all.) The theory was therefore quantitatively verified at least in its limiting forms.

16. FUSED SALT RESEARCH (F. R. Duke)

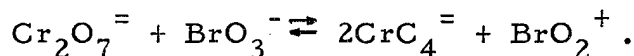
16.1 Mechanism of Electrical Conductivity

It has been found that in a mixture of KNO_3 and LiNO_3 , the two cations move at the same rates regardless of composition; when potassium is the major cation, the lithium assumes the mobility of potassium in pure KNO_3 . The converse is true also.¹ The interpretation we give to these results is that the ions do not move as individuals, but rather that they move in groups. Further experiments are now under way in which cesium ion is being used in mixtures with alkaline earth ions to attempt to determine the manner of motion of bivalent cations. The transport numbers of pure salts: KNO_2 , NaNO_2 , TlNO_3 , RbNO_3 and CsNO_3 have been determined.

16.2 Reactions in Fused Salts

The chemistry of BrO_2^+ , ClO_2^+ and IO_2^+ ions in fused alkali nitrates has been studied. These ions are prepared by the reaction exemplified below:

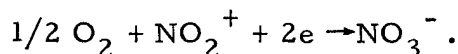
¹F. R. Duke and G. Victor, J. Am. Chem. Soc. 83, 3337 (1961).



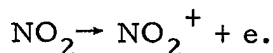
Fused alkali nitrates are the solvents. The equilibrium proceeds furthest in the case of IO_3^{-} and to the least extent with ClO_3^{-} .

Work on the catalytic decomposition of BrO_3^{-} (catalyzed by Br^{-}) to Br^{-} and O_2 was completed and has been accepted for publication in Journal of Physical Chemistry.

A primary cell has been developed whose potential depends upon the concentration of NO_2^{+} in the fused nitrate. It consists of a standard reference electrode in conjunction with platinum over which either O_2 or NO_2 is flowing. In the first case the electrode reaction is:



The second is:



The first electrode system (O_2) appears to operate the best and will in the future allow much more rapid progress in studying the chemistry of NO_2^{+} , BrO_2^{+} , ClO_2^{+} and similar ions.

A paper by F. R. Duke and E. R. Shute, "The Catalytic Decomposition of Bromate in Fused Alkali Nitrates", has been accepted for publication in Journal of Physical Chemistry.

Abstract--The catalytic decomposition reaction: $\text{BrO}_3^{-} + \text{Br}^{-} \rightarrow \text{Br}^{-} + \text{O}_2$ proceeds at a measurable rate in fused NaNO_3 , KNO_3 or $\text{NaNO}_3 - \text{KNO}_3$ mixtures in the temperature range 340 to 370°C. A kinetic study of the reaction shows that the decomposition proceeds by a slow rate-controlling step: $\text{BrO}_3^{-} + \text{Br}^{-} \rightarrow \text{BrO}_2^{-} + \text{BrO}^{-}$ followed by rapid reactions of the intermediates to give the final products. The activation energy for the reaction in molten NaNO_3 is determined and the effect of the alkali cation on the reaction rate demonstrated. This effect is interpreted on the basis of the polarizing power of the cation.

A paper, "Transference Numbers and Ion Association in Pure Fused Alkaline Earth Chlorides", by E. D. Wolf and F. R. Duke, has been submitted for publication in the Journal of the Electrochemical Society.

Abstract--The transference number of the chloride ion was determined in pure fused MgCl_2 , CaCl_2 , SrCl_2 , and BaCl_2 utilizing radioactive chloride ions in a porous quartz membrane cell. On the basis of a two-step dissociation for these salts, $\text{MCl}_2 \rightarrow \text{MCl}^+ + \text{Cl}^- \rightarrow \text{M}^{++} + 2\text{Cl}^-$, the extent of the second dissociation was qualitatively predicted from a consideration of the relative mobilities of the ions.

17. SOLUTION OF METALS IN THEIR MOLTEN SALTS (J. D. Corbett)

The study of solution of metals in their salts is being directed to (1) the exploration of new systems for evidence of this sort of interaction and (2) the investigation of properties relating to the nature of the dissolved product.

17.1 Metal-Metal Salt Phase Studies

17.1.1 Praseodymium Chlorides

Further evidence on the $\text{Pr}-\text{PrCl}_3$ system has been obtained through addition of small amounts of neodymium to the system. In this case the $\text{PrCl}_{2.3}$ phase, which normally disproportionates back into Pr and PrCl_3 only 70° below its melting point,¹ is stabilized by substitution of as little as 3 mole % neodymium into the solid phase. The result is structurally very similar to the known $\text{NdCl}_{2.37 \pm .03}$.

17.1.2 Rare-Earth Metal Bromides

Liquid lanthanum and cerium bromides show only a moderate interaction with the respective metals and do not form intermediate solid

¹Report IS-350, Annual Summary Research Report in Chemistry, 1960-61.

phases (Table X). Their behavior is thus similar to that of the corresponding chloride systems where about 9 mole % metal dissolves in the melt. The Pr-PrBr₃ system exhibits the formation of the stable phase PrBr_{2.4}; in this case the brassy-colored intermediate appears to be related to the metallic diiodides of these elements $[M^{3+}_e(I^-)_2]^2$ and PrI_{2.5} as it shows a definite electronic conductivity in the solid state. A cryoscopic number very close to three, as also found with the corresponding chlorides, is obtained from the experimental liquidus curves for these bromide systems using entropies of fusion interpolated between the known chloride and iodide values.

17.1.3 Yttrium and Gadolinium Halides

The system Y-YI₃ shows only a simple eutectic, whereas molten gadolinium chloride and iodide yield lower phases on reaction with the metal, as shown in Table X. Equilibrations with excess gadolinium metal have established the lower iodide as GdI₂; in order to have at least one liquid phase present in these so that an appreciable rate of formation of the lower phase takes place, it is necessary to hold the system in the 6° range between the eutectic and peritectic temperatures. Low resistivities of the brassy-colored GdI₂ suggest it, too, is related to the metallic diiodides found with the lighter rare-earth metals.

Gadolinium chloride reacts with metal to form an unusual, reduced phase near GdCl_{1.6} in composition. Thermal analysis data for the eutectic point and powder patterns of the quenched mixtures clearly show that the new phase is not a more conventional dichloride but that it has a

¹J. D. Corbett, L. F. Druding, W. H. Burkhard and C. B. Lindahl, Disc. Farad. Soc. 32, 79 (1961).

Table X

Selected Phase Data for Some Rare-Earth Metal-Metal Halide Systems

System M-MX ₃	Mp.MX ₃ °C	Phase Data Mole % M	Temp.	Intermediate Solid Phase
La-LaBr ₃	786	14.2 14.9	728° eu. 800	none
Ce-CeBr ₃	730	12.2 13.4	685 eu. 800	none
Pr-PrBr ₃	693	15.6 16.2 17	578 eu. 601 mp. 700	PrBr _{2.4}
Y-YI ₃	997 (978 tr.)	11.7 14.2	948 eu. 1100	none
Gd-GdCl ₃	605	1 4 5	601 eu. 732 mp. 950	GdCl _{1.6}
Gd-GdI ₃	931 (740 tr.)	14.2 14.3 14.3	825 eu. 831 mp. 920	GdI _{2.0}

eu. - eutectic; mp. - melting (peritectic); tr. - transition points

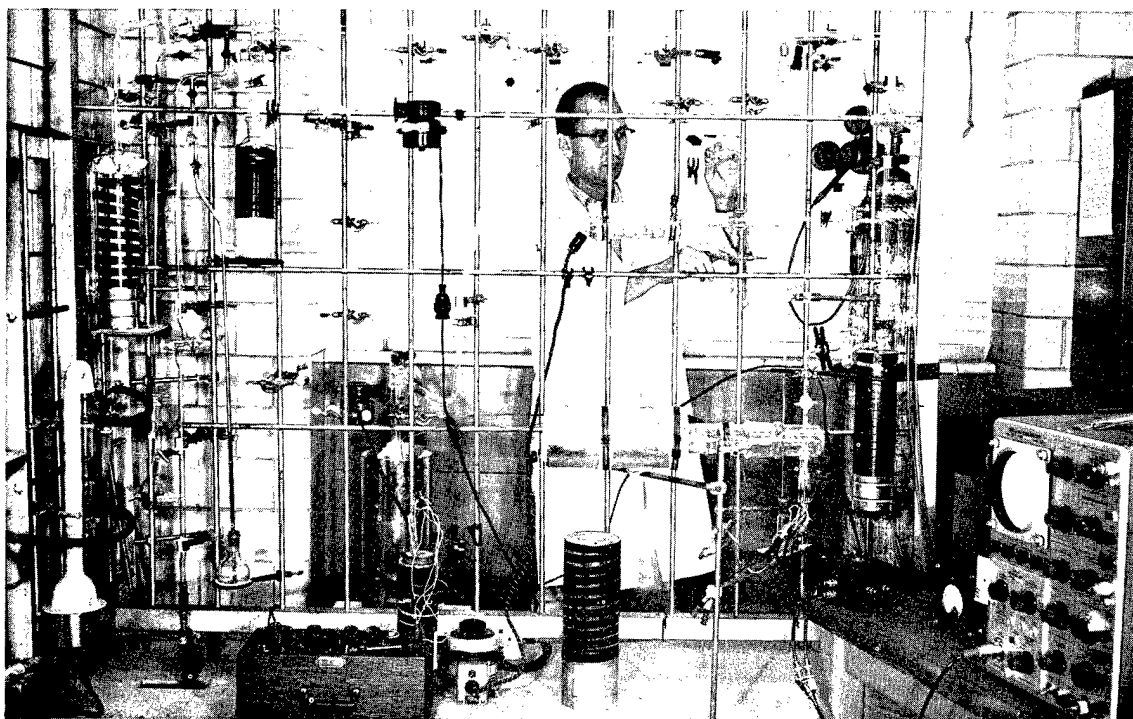


Fig. 3. Measuring Resistivity of Metallic Diiodides

chloride to gadolinium molar ratio between about 1.55 and 1.65. Resistivity measurements on the fibrous needles of $\text{GdCl}_{1.6}$ give no hint of electronic conduction, so that the valence electrons must be presumed to be localized on ions in true, lower oxidation states.

17.1.4 The Antimony Sulfide System

Metal-metal salt systems involving sulfide as the anion quite generally show larger metal solubilities and greater electronic conductivities than the corresponding chloride melts. The relatively small electronic contribution to the total conductivity reported¹ for solutions containing large amounts of Sb in molten Sb_2S_3 has therefore prompted some re-examination of this system. High purity Sb_2S_3 prepared from the elements and vacuum sublimed has been found to melt at 559° , 9° higher than reported, while thermal analysis studies show that the eutectic in the system is at 524° and $17.8 \pm 0.5\%$ Sb rather than at 520° and 25% Sb, and the solubility at 780° , $42 \pm .5$ instead of 48.2%. The effect on the conductivity results of the impurities that were thus evidently present in the earlier work remains to be determined. Uncertainties as to the behavior of solutes in this melt make any possible inference of their nature from the Sb_2S_3 liquidus curve too equivocal to be significant.

17.2 Resistivity Measurements on Solutions of Metals in Their Molten Salts

The lighter rare-earth metal-metal iodide melts present an interesting problem as to the character of the conduction and in the nature of the dissolved metal since the first three metals form solid, metallic diiodides $\text{M}^{3+}\text{e}(\text{I}^-)_2$ and the fourth, the salt-like but unconventional solid $\text{NdI}_{1.95}$.

¹T. Yanagase and G. Derge, J. Electrochem. Soc. 103, 303 (1956).

The specific conductivities of the corresponding MI_3 - MI_2 melts have been determined as a function of composition up to conductivities of $20 \text{ ohm}^{-1} \text{ cm}^{-1}$ in cooperation with M. A. Bredig, A. S. Dworkin and H. R. Bronstein at Oak Ridge National Laboratory. The results, somewhat similar to those for the corresponding chloride melts^{1,2,3} within the more limited composition range accessible in the latter, show an increasing large electronic contribution to the total conductance with increasing metal content, reaching the limit of the apparatus¹ ($20 \text{ ohm}^{-1} \text{ cm}^{-1}$) at about 14% lanthanum or cerium and 26% praseodymium, considerably less than the 33.3% composition corresponding to the diiodides. The neodymium iodide system shows substantially only ionic conductance, as also found with the neodymium chloride melts.² Of particular interest is the observation that solutions of 8.5% La in LaI_3 and 16% Pr in PrI_3 have positive temperature coefficients of conductivity equal to and 35% of that liquid MI_3 , respectively, even though the electronic contributions to the total conductivity are approximately 7.4 and 4.1 times that by ions. It is thus necessary that electrons from the dissolved metal be considered as localized or trapped, either as such or as distinct M^{2+} ions.

17.3 Raman Spectra of Molten Salts

A paper, "The Cadmium (I) Ion Cd_2^{2+} . Raman Spectrum and Relationship to Hg_2^{2+} ", by John D. Corbett, has been accepted for publication in Inorganic Chemistry.

¹A. S. Dworkin, H. R. Bronstein and M. A. Bredig, Disc. Farad. Soc. 32, in press (1961).

²H. R. Bronstein, A. S. Dworkin and M. A. Bredig, J. Phys. Chem. 66, 44 (1962).

³A. S. Dworkin, H. R. Bronstein and M. A. Bredig, Ibid. 66, 1201 (1962).

Abstract--The Raman spectrum is reported for the system $0.67 \text{ Cd}_2(\text{AlCl}_4)_2 - 0.33 \text{ Cd}(\text{AlCl}_4)_2$ in the molten state at 250° and, incompletely, as the solid mixture at 70° . In addition to the known transitions of AlCl_4^- , the melt exhibits a strong shift of $183 \pm 3 \text{ cm}^{-1}$ due to the Cd_2^{2+} ion. The weakness of the bonding in the diatomic cadmium(I) ion is indicated both by the 10 cm^{-1} line width observed with the melt and by the smallness of the calculated force constant (1.11 mdyne/\AA). The properties of the Cd_2^{2+} ion and related species are contrasted to those of the more stable mercury analogues, and an interpretation is advanced for the anomalous stability of the mercury(I) ion.

17.4 Metal-Metal Halide Reactions in the Vapor Phase

The generally accepted interpretation of solutions of cadmium in liquid CdCl_2 is in terms of the formation of the diamagnetic solute Cd_2Cl_2 . Heretofore the only identification of an intermediate in the gaseous $\text{Cd}-\text{CdCl}_2$ system has been the observation of the CdCl monomer in arc spectra. It has now been established that the vapor in equilibrium with the metal-saturated melt at 580 to 680° contains significant amounts of the CdCl monomer, as identified by its characteristic adsorption peaks at 307 and $317 \text{ m}\mu$, and that any dimer or higher polymer must either be relatively unimportant or have no absorption between 280 and $1000 \text{ m}\mu$.

18. SOLID SUBHALIDES

A number of new and unusual solids have been discovered in the course of the above investigations. These compounds are furnishing new information regarding lower oxidation states, structures, non-stoichiometric compositions, and electrical and magnetic properties in the solid state.

18.1 The Structure of Bismuth Monochloride

A paper with this title, by Alex Hershaft and John D. Corbett, was published as a Letter to the Editor in J. Chem. Phys. **36**, 551 (1962). This is a preliminary report of the unusual structure reported previously for $\text{BiCl}_{1.167}$.

18.2 Magnetic Susceptibilities of Neodymium Chlorides and Iodides

The effective magnetic moments determined for the tri- and di-chlorides and iodides of neodymium are given in Table XI. The agreement with the theoretical values given by Van Vleck for an f^4 configuration is satisfactory for salts of this type, although the data offer no significant explanation for the iodide deficiency found in $\text{NdI}_{1.95}$.

Table XI

Salt	Applicable Range	$\mu_{\text{eff. exp.}}$	B.M. theory	°K
NdCl_3	78 - 575°K	$3.8 \pm .03$	3.62	31
NdI_3	78 - 575	$3.7 \pm .03$	3.62	9
$\text{NdCl}_{2.04}$	78 - 220	$2.9 \pm .03$	2.68	9
$\text{NdI}_{1.95}$	78 - 220	$2.9 \pm .03$	2.68	12

18.3 Physical Properties of the Metallic Diiodides

Physical properties of the isomorphous compounds LaI_2 , CeI_2 and PrI_2 have been found to support their formulation as $[\text{M}^{3+}(\text{I}^-)_2]$. An apparatus has been constructed that enables the resistivities of cast, polycrystalline rods of these to be determined in vacuum by ac potentiometric methods. Preliminary results for LaI_2 indicate a specific resistivity close to that of the metal, increasing with increasing temperature. In agreement with this behavior, LaI_2 shows a small

paramagnetism appropriate to a metal, although the temperature dependence at lower temperatures is greater than that of an ideal metal. The diiodides appear to have an orthorhombic structure so that anisotropy in metallic properties is to be expected.

19. SOLUTIONS OF GALLIUM(I) SALTS IN AQUEOUS BASE (J. D. Corbett)

Although the gallium(I) ion is commonly thought to react rapidly with water under all conditions, it has been discovered that solution of salts such as $\text{Ga}(\text{GaCl}_4)$ in aqueous base are quite stable (half life of 5.2 hr in 1 M NaOH). The kinetics of the homogeneous reduction of water in this system have been studied together with some of the characteristic reducing reactions with added ions and E° estimates for the Ga(I)-Ga(III) couple in base and in acid. An attractive alternate for the production of these solutions has been found in the anodic oxidation of gallium metal into aqueous base.

20. MASS SPECTRA OF VOLATILE INORGANIC COMPOUNDS (H. J. Svec)

20.1 Heats of Formation of VOF_3 , CrO_2F_2 , CrO_2Cl_2 and AsF_3

Values for ΔH_f° of the neutral parent molecules as well as the ion fragments of these compounds have been calculated from appearance potential measurements. In the calculations it was assumed that the kinetic energy of the fragments was negligible and hence the values listed in Table XII are maximum values.

In the course of the study of the mass spectra of VOF_3 observations were made of a dielemental species corresponding to $\text{V}_2\text{O}_2\text{F}_5^+$. A study of the variation of the intensity of this ion with the pressure of VOF_3 in the sample system showed a linear increase. However, this linear

Table XII

Heats of Formation of VOF_3 , CrO_2F_2 , CrO_2Cl_2 and AsF_3
and Their Ion Fragments in kcal/mole

	V	Cr		As
	F	F	Cl	F
MOX_3	-393±2			
MO_2X_2		-291±2	-202±2	
MX_3				-221±3
MO_2X_2^+		31±2	88±2	
MO_2X^+		53±2	89±2	
MOX_3^+	- 31±2			
MX_3^+	- 53±2			96±4
MX_2^+	12±2	32±2	100±2	90±2
MX^+	118±2	59±2	140±2	207±2
MOX_2^+	- 35±2	37±2	103±2	
MOX^+	11±2	110±3	102±3	
MO_2^+		102±2	90±2	
MO^+	83±2	148±3	174±3	
M^+	(275)*	(237)*	(237)*	(304)*

*Taken from W. M. Latimer, "Oxidation Potentials", Prentice Hall Inc., 1952, second edition.

increase had a slope different from that of VOF_3^+ ; thus, the formation of $\text{V}_2\text{O}_2\text{F}_5^+$ takes place in the ion source, probably by some surface reaction involving a surface-saturated adsorbed species. Previously, similar dielemental ion species of Cr had been observed¹ corresponding to $\text{Cr}_2\text{O}_4\text{F}_4^+$, $\text{Cr}_2\text{O}_4\text{Cl}_3^+$, $\text{Cr}_2\text{O}_4\text{F}_2\text{Cl}^+$ and $\text{Cr}_2\text{O}_4\text{FCl}_2^+$. No pressure studies were made at the time of this work but a similar explanation for these species is probable.

¹G. D. Flesch and H. J. Svec, J. Am. Chem. Soc. 81, 1787 (1959).

20.2 Heats of Formation of the Hydrides of Groups IVB and VB (H. J. Svec)

Values for the heats of formation of silane, germane, stannane, plumbane, phosphine, arsine, stibine and bismuthine have been obtained from appearance potential measurements. Excess kinetic energy effects have been shown to be negligible and the agreement of the mass spectrometer derived values are in good agreement with calorimetric values where they exist. A summary of these data is given in Table XIII.

Table XIII
Heats of Formation of the Group IVB and VB
Hydrides in kcals/mole

	This Work	Calorimetric Value
SiH_4	8.5	7.3
GeH_4	21.6	21.6
SnH_4	38.9	23.0
PbH_4	59.9	
PH_3	1.3	1.4
AsH_3	15.9	15.0
SbH_3	34.7	34.6
BiH_3	66.8	

Average bond energies obtained from the appearance potential data are compared in Table XIV with theoretical and calorimetric values. Fragmentation patterns for the positive ions of PbH_4 and BiH_3 from 70 volt electrons are given in Table XV. These patterns follow the same trends observed for the other hydrides of the Group IVB and VB hydrides.

A paper, "The Mass Spectra of Some Volatile Hydrides", by F. E. Saalfeld and H. J. Svec, was accepted for publication in Inorganic Chemistry. A more detailed report of this work (IS-386) was distributed.

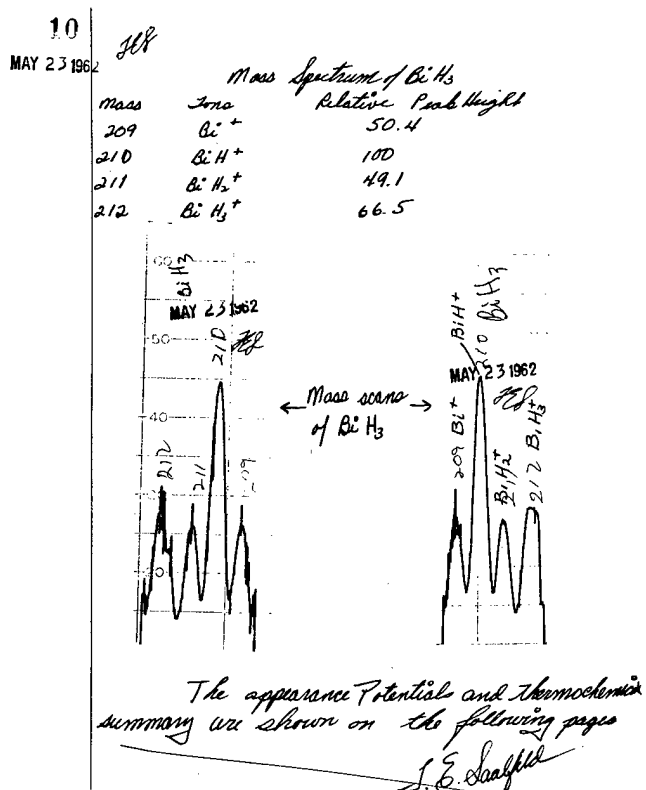


Fig. 4. Page from the Research Notebook Describing the First Positive Characterization of Bismuthine

Table XIV

Average M-H Bond Energies for the IVB and VB Hydrides in kcals/mole

	This Work	Theoretical*	Calorimetric†
Si-H	72.2	79	76.5
Ge-H	68.3	74	69.0
Sn-H	70.3	71	60.4
Pb-H	48.4		
P-H	76.4	77	76.8
As-H	72.9	71	66.8
Sb-H	61.1	70	60.9
Bi-H	46.1		

*M. L. Huggins, J. Am. Chem. Soc. 75, 4123 (1953).

†S. R. Gunn and L. G. Green, J. Phys. Chem. 65, 779 (1961).

Table XV
Fragmentation Patterns of PbH_4 and BiH_3 *

	Pb	Bi
MH_4^+	0.1	
MH_3^+	60.4	66.5
MH_2^+	100.0	49.1
MH^+	5.0	100.0
M^+	25.0	50.4

* These patterns are based on a value of 100.0 for the most abundant ion fragment.

Work on the dihydrides of P, As, Sb, Si, Ge and Sn is underway. Some appearance potential measurements have been made but no thermochemical quantities have yet been calculated. An interesting extension of this work has been the observation of the fragment Sb_3^+ in the mass spectrum of Sb_2H_4 .

20.3 The Mass Spectra of Aluminum Hydride-Methyl Amine Complexes

Fragmentation patterns of $\text{AlH}_3 \cdot \text{N}(\text{CH}_3)_3$, $\text{AlH}_3 \cdot 2\text{N}(\text{CH}_3)_3$, AlD_3 , $2\text{N}(\text{CH}_3)_3$ and $(\text{AlH}_3 \cdot \text{N}(\text{CH}_3)_2\text{C}_2\text{H}_4\text{N}(\text{CH}_3)_3)_2$ have been studied. The spectra are principally those of the amine adducts although small ion currents due to AlH_3^+ , AlH_2^+ , AlH^+ and Al^+ are observed.

From the appearance potentials of the parent ion, $\text{AlH}_3 \cdot \text{N}(\text{CH}_3)_3^+$, the $\text{N}(\text{CH}_3)_3^+$ ion and the $\text{N}(\text{CH}_3)_2^+$ ion, a value for the dissociation energy of Al-N in $\text{AlH}_3 \cdot \text{N}(\text{CH}_3)_3$ has been computed to be 21 ± 2 Kcals/mole.

21. THE MASS SPECTRA OF THE AMINO ACIDS (H. J. Svec)

The mass spectra of 25 natural and related α amino acids have been obtained by means of a mass spectrometer equipped with a crucible ion

source. Correlations of these data have been made with the ion fragments and mechanisms leading to these fragments have been proposed. Comparisons have been made with the mass spectra of the ethyl esters of the amino acids and with other carboxylic acid and their esters. A paper, "The Mass Spectra of the α Amino-acids", by Gregor Junk and Harry J. Svec, was submitted for publication in The Journal of the American Chemical Society.

22. THE ABSOLUTE ISOTOPIC ABUNDANCE OF Cr, V, Li AND O IN SOME MINERALS (H. J. Svec)

22.1 Natural Abundance of the Cr Isotope in Secondary Minerals

A study of the variation of the Cr isotopes in chrom micas, chlorites, garnets, diopsides, clays, crystallites and two meteorites has been made. Slight variations from values previously obtained for chromites were observed in the chrom-bearing clay-like minerals. A large variation was seen for the Cr isotopes in the Holbrook meteorite. However, the latter data may contain uncertainties due to unknown interfering impurities in the CrO_2F_2 used to introduce the element into the mass spectrometer. A paper, "The Absolute Abundance of the Chromium Isotopes in Some Secondary Minerals", by H. J. Svec and G. D. Flesch and J. Capellen, has been accepted for publication in Geochemica Et Cosmochimica Acta.

22.2 Natural Abundance of the Vanadium Isotopes in Ores and Minerals

In the minerals and ores studied to date no real differences in the isotopic composition of vanadium in eleven high content minerals have been observed. These data are compared with other published values in Table XVI.

Table XVI

Abundance of the Vanadium Isotopes

Research	Ion Source	Material	Ion	V^{50}/V^{51}	Deviation
Hess, Ingraham (1949)	Electron Bombardment	$VOCl_3$	V^+	0.00256	0.00004
			V^{++}	0.00274	0.00004
			VCl^+	0.00254	0.00005
Hess, Ingraham (1949)	Surface Ions	V_2O_5	V^+	0.00268	0.00026
			VO^+	0.00271	0.00027
Leland (1949)	Evap. of V from W filament	V	V^+	0.00231	0.0001
This Work (Flesch and Svec)	Electron Bombardment	VOF_3	VOF_3^+	0.002522	0.000004 (rms)

22.3 Natural Abundance of the Oxygen Isotopes in the Boron Minerals Found in the Kramer Ore Body at Boron, California

In the hydrated borates from the Kramer Ore Body a knowledge of the distribution of the oxygen isotopes in both the water of crystallization and the "borate" ions can contribute information about the changing climatic conditions under which the various deposits were laid down. Seven samples covering a range of approximately 25 ft of the ore body and found in distinct layers were subjected to oxygen release by heating with $KBrF_4$. Both the dehydrated minerals and the water of crystallization were examined. In all cases the distribution of the oxygen isotopes in the water of crystallization was identical with that of the associated boron mineral. Isotopic assays were made on the O_2 evolved from the reaction mixtures. The results are listed in Table XVII.

Table XVII

Distribution of Oxygen Isotopes in Boron Minerals from the
Kramer Ore Body

Layer	Minerals	O_2^{34}/O_2^{32}	Comments
1	Ulexite	0.004022 ± 4	Mixed with realgar
2	Lesserite	0.004052 ± 6	Sodium borates leached out
3	Inderite	0.004020 ± 20	Layer just above borax
4	Borax	0.004050 ± 5	Interstitial shales in bed
5	Kernite	0.004115 ± 6	Cleavage fragment
6	Kernite-borax	0.004091 ± 5	Primary
7	Probertite	0.004010 ± 6	Vein in shale below ore body
	Atmospheric water	$0.00393 \pm 1^*$	
	Atmospheric O_2	0.004090 ± 5	

*This uncertainty represents the variation in rain waters collected in different places and at different times during a storm. It is not the measurement uncertainty.

The results listed in the table start at the top of the ore body and continue to just below it. Laboratory tests with water enriched in O^{18} indicate rapid equilibration of the oxygen atoms in borate ions with those of water. Thus, one can assume that the oxygen in the minerals examined were in isotopic equilibrium with that of the water in the lake at the time of the mineral precipitation. Three relatively wet periods are evident from the data. During these times the rate of influx of fresh water into the lake was great enough to dilute the enriched water so as to approach the value for the oxygen isotopes in fresh water as indicated by the value for rain water given in the table. During ensuing dry periods, evaporation

resulted in a concentration of the O^{18} content of the lake water and hence the enrichment of the borate minerals. It is noteworthy that O^{18} content in sample 5 exceeds that in atmospheric O_2 .

22.4 Natural Abundance of the Li Isotopes in Some Minerals and Ores

Twenty minerals and ores have been studied in a special mass spectrometer designed to assay Li for its isotopic composition. The assay uncertainties in this instrument are 1 part in 1000 or less, a factor of 2 to 3 better than previously reported for this measurement. All observations were made by comparing the samples with two mixtures of Li^6 and Li^7 made with carefully purified and characterized compounds by standard gravimetric procedures. The mixtures were made up to approximate the expected natural distribution of the Li isotopes. Some samples previously assayed by A. E. Cameron of the Oak Ridge National Laboratory were included in this study. Results of the study are given in Table XVIII. Two features stand out in the data. One concerns a 4.5% variation in the 6/7 ratio from the sample with the lowest ratio to that with the highest ratio. The other involves a systematic difference between the results of this work and that of A. E. Cameron, all the results of our work being 2.6 to 2.8% higher. No attempt was made by Cameron to determine the extent of discriminations in his mass spectrometers in contrast with the measurements here. He observed some chemical fractionation in his preparations as is indicated by the double values for some samples. We have followed his ion exchange procedures and have made certain of our exchange column cuts by flame spectra tests on all fractions to insure quantitative combination of all cuts containing lithium.

Table XVIII

Abundance of the Li Isotopes in Some Ores and Minerals

Mineral or Ore	Origin Concentrates	6/7 ratio	
		This Work	A. E. Cameron
Spodumene	King's Mtn., N. C.	0.08233	
Spodumene	King's Mtn., N. C.	0.08220	0.08019-0.07974
Spodumene	Bernic Lake, Ont., Canada	0.08120	
Spodumene	Black Hills, S. Dak.	0.08123	
Spodumene	Belgian Congo	0.08166	
Spodumene	Helen Beryl Mine, Black Hills, S. Dak.	0.08205	
Spodumene	Quetico Park, Ont., Canada	0.08284	
Spodumene	Rhodesia, S. Africa	0.08200	
Spodumene	Quebec concentrates	0.08177	
Spodumene	Valdor, Quebec	0.08168	
Spodumene	Quebec Lithium Corp.	0.08168	
Spodumene	Lithium Corp. Amer. Bessemer City, N. C.	0.08194	
Spodumene (Kunzite-gem quality)	Pala, San Diego County, Calif.	0.08130	
Li_2NaPO_4	Searles Lake, Calif.	0.07948	0.07745 ion exchg. 0.07662 phosphate
Lepidolite	Foote Mineral Co., Colo.	0.08140	0.07930 prep A 0.07949 prep B
Lepidolite	Ingersoll Mine, S. Dak.	0.08110	0.07880 prep A 0.07867 prep B
Lepidolite	Bernic Lake, Ont., Canada	0.08003	
Amblygonite	Bernic Lake, Ont., Canada	0.08062	
Eucryptite		0.08119	
Li_2CO_3 Laboratory Standard	A. E. Cameron	0.07921	0.07733

23. THE VIBRATIONAL FREQUENCIES AND STRUCTURE OF $\text{AlH}_3 \cdot 2\text{N}(\text{CH}_3)_3$

(C. W. Heitsch)

In an attempt to gain information relative to the structure of the compound, $\text{AlH}_3 \cdot 2\text{N}(\text{CH}_3)_3$, the infrared spectrum has been scanned in the gas phase from 330 cm^{-1} to 5000 cm^{-1} . Through the assistance of Dr. John F. Ferraro of the Argonne National Laboratory, the Raman spectrum in liquid trimethyl amine was scanned on a Cary #81 spectrometer from 50 to 3500 cm^{-1} . With the assistance of Richard Kniseley of this Laboratory, these data have been assigned on the basis of a D_{3h} symmetry for the molecule.

For simplicity, the bands attributable to the $\text{N}(\text{CH}_3)_3$ moiety have been omitted. It is apparent that there is very little difference between these bands in the complex and in the free amine. The observed frequencies and their assignments are shown in Table XIX.

Table XIX

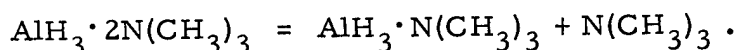
Absorption Spectra of $\text{AlH}_3 \cdot 2\text{N}(\text{CH}_3)_3$

Frequency (cm^{-1})		Activity	Class	Assignment	Mode
$\text{AlH}_3 \cdot 2\text{N}(\text{CH}_3)_3$	$\text{AlD}_3 \cdot 2\text{N}(\text{CH}_3)_3$				
1725	$\left\{ \begin{array}{l} \text{R} \\ \text{R} \end{array} \right\}$	A_1'	ν_1 Sym. Al. H st.	
			E'	ν_5 Asym. Al. H st.	
1711	1250	IR			
895	649	IR	A_2''	ν_4 Al. H OP def.	
795	607	$\left\{ \begin{array}{l} \text{IR} \\ \text{R} \end{array} \right\}$	E'	ν_6 Al. H IP def.	
768				
729	538	$\left\{ \begin{array}{l} \text{IR} \\ \text{R} \end{array} \right\}$	E''	ν_8 AlH_3 rock	
726				
466	R	A_1'	ν_2 Sym. Al-N st.	
460	IR	A_2''	ν_3 Asym. Al-N st.	
----	$\left\{ \begin{array}{l} \text{IR} \\ \text{R} \end{array} \right\}$	E'	ν_7 Al-N def.	
198				

The spectra constitute a strong support for a trigonal bipyramidal structure of D_{3h} symmetry. A square pyramid of C_{2v} symmetry would involve splitting several of the degeneracies as would most other probable models.

24. THE VAPOR PHASE DISSOCIATION OF $AlH_3 \cdot 2N(CH_3)_3$ (C. W. Heitsch)

The vapor density of the compound, $AlH_3 \cdot 2N(CH_3)_3$, was studied over the range from 65 to 135°C with pressures ranging from 17 to 55 mm of mercury. Below 90° with pressures of the order of 20 mm, the data suggest the reaction:



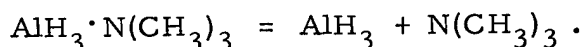
The equilibrium constants evaluated for the above reaction are expressed by the equation:

$$\text{Log}_{10} K_{\text{pmm}} = 11.971 - 3937.0 T .$$

From this, the enthalpy for the reaction in this temperature range can be estimated:

$$\Delta H = -18.0 \pm 0.1 \text{ kcal/mole.}$$

Above 90°, a second reaction is appreciable which involves a multiplication of the number of molecules in the gas phase. Since the reaction appears to be thermally reversible, the most logical reaction would be:



An effort to obtain data of sufficient accuracy to characterize this second reaction is underway.

25. THE COMPOUND $AlH_3 \cdot N(CH_3)_3$, ITS DIPOLE MOMENT AND STRUCTURE

(C. W. Heitsch)

A reliable procedure for the synthesis of the compound $AlH_3 \cdot N(CH_3)_3$ has been developed along the lines reported by Ruff and

Hawthorne.¹ Preliminary results of a dipole moment determination place the moment in the vicinity of 5.2 D. This is significantly larger than that for the analogous boron compound, $\text{BH}_3 \cdot \text{N}(\text{CH}_3)_3$, for which the value of 4.62 D has been reported.² One would anticipate an increase of this order of magnitude in going from the boron compound to the more polarizable aluminum compound. The non-polar dimer, $(\text{CH}_3)_3\text{N}(\text{AlH}_2)=\text{H}_2=(\text{AlH}_2)\text{N}(\text{CH}_3)_3$, has been proposed by Wiberg³ and by Ruff and Hawthorne to account for the anomalous cryoscopic molecular weights observed in benzene. It is apparent from the large value of the dipole moment that such a species must be present in a very low concentration.

Four vibrational frequencies have been observed for the AlH_3 modes in the gas phase infrared spectrum of the complex. Two of these, 1845 and 1792 cm^{-1} have been assigned to the symmetric and asymmetric Al-H stretching modes respectively. This inversion of the usual order of asymmetric and symmetric modes is supported by their relative intensities and by comparison with the assignments made for the compound, $\text{GaH}_3 \cdot \text{N}(\text{CH}_3)_3$.⁴ The Al-H deformation modes are very close to being degenerate, 775, and 767 cm^{-1} respectively.

¹J. K. Ruff and M. F. Hawthorne, J. Am. Chem. Soc. 82, 2141 (1960).

²J. R. Weaver and C. W. Heitsch, "The Chemistry of Boron Hydrides and Related Hydrides", R. W. Parry, R. C. Taylor, and C. E. Nordman, Ed., WADC Tech. Rept. 59-207, May 1959, University of Michigan.

³E. Wiberg, H. Graf, M. Schmidt and R. W. Lacal, Z. Naturforsch. 7b, 578 (1952).

⁴D. F. Shriner, R. H. Amster and R. C. Taylor, J. Am. Chem. Soc. 84, 1321 (1962).

These data are most easily assigned to a monomeric model of C_{3v} symmetry. The absence of any bands not attributable to the $N(CH_3)_3$ moiety in the 1200 to 1700 cm^{-1} region implies the absence of a significant concentration of any hydrogen-bridged dimer.

26. THE STRUCTURE OF THE TRIMETHYL-AMINE ADDUCT OF ALUMINUMBORO-HYDRIDE (C. W. Heitsch)

The compound $Al(BH_4)_3 \cdot N(CH_3)_3$ was first reported by Schlesinger, Sanders and Burg.¹

The cryoscopic molecular weight was determined to be 113, which is within 15% of the calculated value for the monomer, 130. Thus a dimeric species is thought to be unlikely. Nor is it probable that the material is a stoichiometric mixture of two or more products.

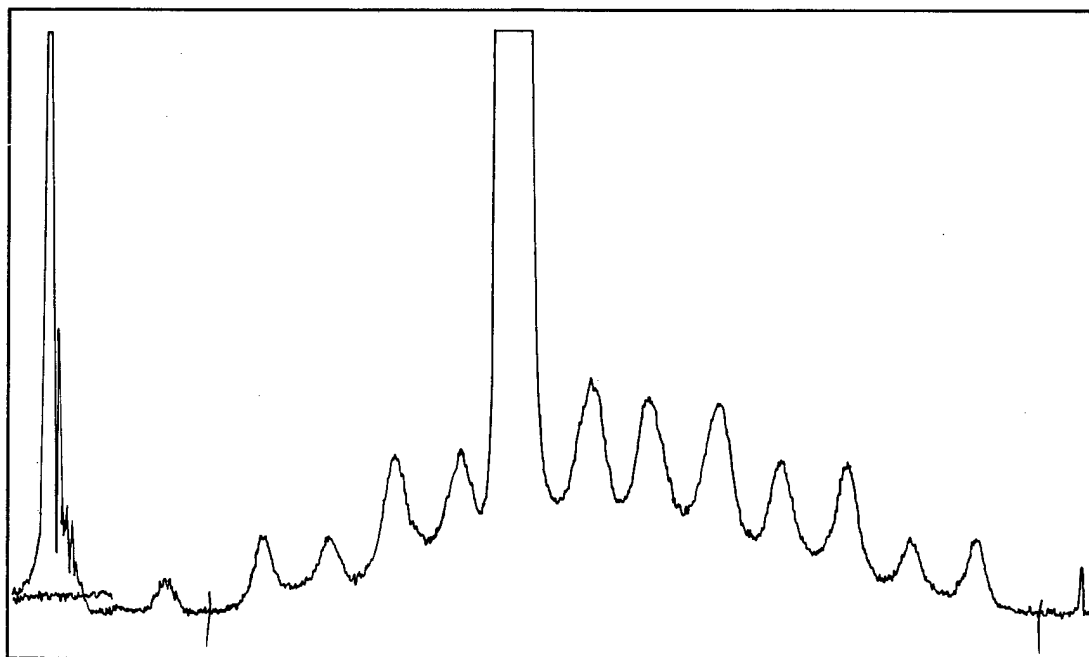


Fig. 5. NMR Spectrum of $Al(BH_4)_3 \cdot N(CH_3)_3$
60 Mc, 10% in C_6H_6

¹H. I. Schlesinger, R. T. Sanderson and A. B. Burg, J. Am. Chem. Soc. 62, 3421 (1940).

The proton nuclear magnetic resonance spectrum was observed in benzene solution at 60 Mc and is shown in Fig. 5. Intensities, from left to right, in terms of one proton units, are 0.5, 0.5, 1.0, 1.0, 10.5, 1.5, 1.5, 1.5, 1.0, 1.0, 0.5 and 0.5. If one mentally subtracts the nine methyl protons from the fifth peak, the remainder corresponds to 1.5 protons. Thus the twelve hydridic protons are accounted for in the twelve peak multiplet. Such a multiplet can arise from a set of identical protons, coupled simultaneously to a nucleus of $3/2$ spin, like the B^{11} nucleus, and another of $5/2$ spin, like the Al^{27} nucleus. The corresponding experimental coupling constants are 89.1 cps for $J_{H^{11}-B^{11}}$ and 46.4 cps for $J_{H^{11}-Al^{27}}$. The chemical shift, relative to $Si(CH_3)_4$ is -0.74 ppm. All of these data are in good agreement with a structure of twelve identical protons, coupled to both boron and the aluminum.

Verification for this interpretation was supplied by P. C. Lauterhur of Mellon Institute who very generously scanned a sample of this compound with a 40 Mc machine. The fact that the spectra supplied by Mr. Lauterhur from a 40 Mc instrument are essentially the same as those procured with our 60 Mc machine eliminates the possibility of this very complicated spectrum arising from several chemically different hydrogens.

The infrared spectrum of the compound has been scanned from 5000 to 230 cm^{-1} in both the gas phase as well as in benzene and cyclohexane solutions. Above 1000 cm^{-1} the spectrum is remarkably similar to the sum of the spectra of $Al(BH_4)_3$ and $N(CH_3)_3$ with some modest shifts with respect to the BH modes. A detailed analysis of this spectrum

is in process but it can now be stated that the mode of binding the BH_4 groups to the aluminum is very similar to that in $\text{Al}(\text{BH}_4)_3$.

The picture that can be constructed from the above data is one in which the nitrogen and the three boron atoms are arranged in an axially distorted tetrahedral arrangement. The three borons are bound to the aluminum by double hydrogen bridge links, bringing the coordination number of aluminum to seven.

27. STUDY OF THIN FILMS (L. S. Bartell)

A paper, "Polarimetric Determination of Absorption Spectra of Thin Films on Metal. I. Interpretation of Optical Data", by L. S. Bartell and D. Churchill, was published in J. Phys. Chem. 65, 2242 (1961).

Abstract--A polarimetric method for the determination of electronic absorption spectra of films of molecular thickness adsorbed on polished metal surfaces is described. Schemes for finding the thickness, refractive index, and absorption coefficient of adsorbed films are discussed. The practicability of the method is demonstrated by a determination of the absorption spectrum of a 1 molar dispersion of tetraphenylporphine in a film of collodion 31 Å thick, on chromium. The spectrum of the 31 Å dispersion was found to be similar to the spectrum of a bulk solution of the compound in benzene. It is shown also that direct photometric measurements of reflectivities from surfaces may yield useful spectral information about films.

A paper, "Structure and Molecular Orientation in Multimolecular Films of Long-Chain n-Hydrocarbon Derivatives", by C. L. Sutula and L. S. Bartell, was published in J. Phys. Chem. 66, 1010 (1962).

Abstract--An electron diffraction study has been made on the structure and molecular orientation in multimolecular films of a variety of long-chain molecules. Films were prepared several ways, but principally by evaporating dilute solutions on metal slides. Most of the films studied were 30 to 40 molecules thick, although films considerably thinner and thicker were examined. The films were found to consist of microcrystals with 00 ℓ planes parallel to the surface of the substrate, in agreement with previous studies. Careful measurements of the lattice parameters and crystal form were made. These showed, contrary to several previous studies involving some of the same compounds, that the molecular packing in the colloidal films is characteristic of that and indistinguishable from that occurring in the bulk crystals. Evidence is presented which indicates that the exceptional packing found in the earlier studies of thin films was the result of impurities rather than the extreme thinness.

Two new methods are reported for preparing thin films with molecules aligned in a designated direction.

28. SECONDARY ISOTOPE EFFECTS (L. S. Bartell)

A paper, "On Secondary Isotope Effects in Molecular Structure", by L. S. Bartell, has been accepted for publication in The Journal of Chemical Physics.

Abstract--The causes of primary isotope effects in structure and kinetics and of secondary isotope effects in kinetics are briefly reviewed. It is concluded that secondary isotope effects should occur in molecular structure as well as in kinetics. Preliminary data supporting this conclusion are presented and conjectures are made about types of molecules which should exhibit the greatest effects.

29. ELECTRON DIFFRACTION STUDIES (L. S. Bartell)

A paper, "Significance of Bond Lengths Determined by Electron Diffraction", by L. S. Bartell and Kozo Kuchitsu, has been accepted for publication in the Journal of the Physical Society of Japan.

Abstract--The derivation of structural parameters of known absolute significance, as mean and equilibrium bond lengths, from experimental electron diffraction patterns is discussed. A series of diatomic molecules has been investigated to test the theoretical interpretation of diffraction patterns, and, at the same time, to test the precision of the latest techniques of electron diffraction. Preliminary least-squares results for bond lengths and amplitudes of vibration for the molecules O_2 , NO , N_2 , and Cl_2 , analyzed as Morse anharmonic oscillators, are reported. Standard errors range from 0.0008Å to 0.003Å. The results, when corrected for vibrational effects, are found to agree with spectroscopic results to within experimental error. A brief discussion is given of the possible utility of the accuracy now attainable in structure determination.

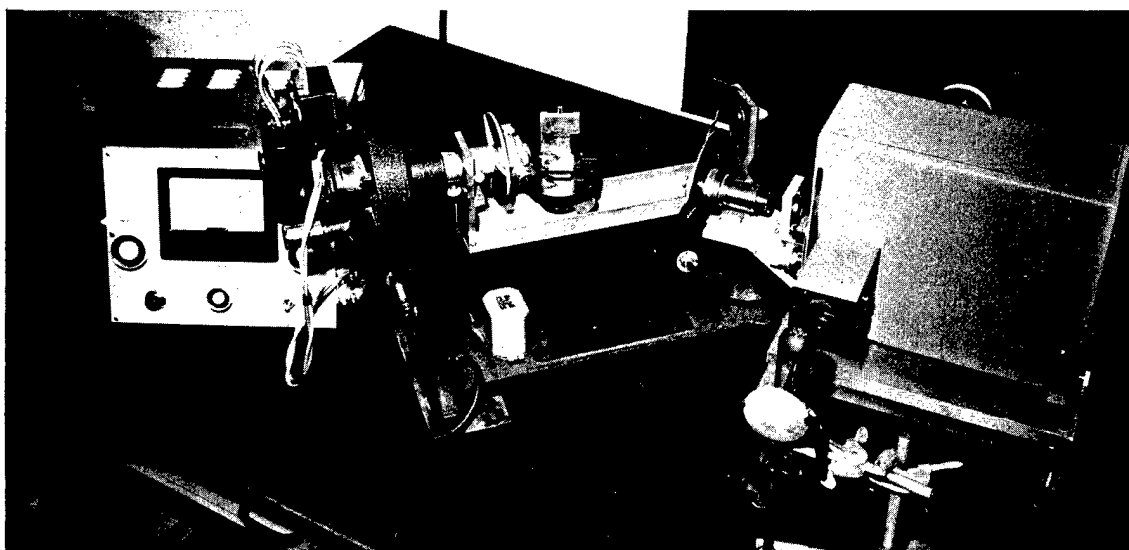


Fig. 6. Electron Diffraction Unit

30. NATURE OF CHEMICAL BINDING (K. Ruedenberg)

Research in this group over the last years has led to the first known rigorous partitioning, on purely quantum mechanical premises, of the molecular binding energy in terms of fragments which can be interpreted in terms of physical and chemical concepts. This theory was published during the current year in the April 1962 issue of the Reviews of Modern Physics.

Four applications of this approach were completed during the current year. A careful examination of the simplest molecule, H_2^+ , has shown that the generally accepted opinions regarding the origin of chemical binding need revision. Whereas some opinions, based on the free-electron model, consider chemical binding as a purely kinetic effect, the majority consensus believes it to originate from purely electrostatic interactions which take place in the bond region. Our investigation demonstrates that binding, in actuality, results from a rather subtle interplay between the kinetic consequences of the uncertainty principle in the bond region and the electrostatic potential interactions near the nuclei.

An application to the water molecule has confirmed these conclusions and, moreover, led to a detailed understanding of the many factors involved in the binding process in such a molecule.

The third application was a study of the hydrides LiH, BH, NH, FH. This comparative analysis led to a determination of the trends which are shown by the various contributing factors in a series of analogous molecules.

A similar comparative objective was pursued in the fourth application, an analysis of the homonuclear diatomics Li_2 , Be_2 , C_2 , N_2 , F_2 .

The results of this work, which will be published later this year, have given new insights in the binding mechanism in these molecules and will be useful for the understanding of chemical binding in general.

31. ELECTRONIC STRUCTURE AND ULTRAVIOLET SPECTRA

31.1 Aromatic Hydrocarbons (K. Ruedenberg)

A theoretical investigation into the structure of aromatic hydrocarbons on the basis of the theory of pi-electrons, was completed and has resulted in the successful calculation of the optical and ultraviolet spectra of 33 of these molecules. The number of carbon atoms per molecule varied between six and thirty. For many of these, in particular the large peri-condensed systems, these have been the first theoretical calculations of such properties ever carried out. The results will be published in the December 1962 issue of the Journal of Physical Chemistry.

31.2 Platinum Complexes (K. Ruedenberg and D. S. Martin)

In cooperation with members of the Radiochemistry Group II, an investigation on the ultraviolet spectra of the square-planar complexes of the Pt(II) ion, such as PtCl_4 , $\text{Pt}(\text{Cl}_{4-n})(\text{NH}_3)_n$, $\text{Pt}(\text{Cl}_{4-n})(\text{H}_2\text{O})_n$, $\text{Pt}(\text{Cl}_{4-n})(\text{OH})_n$ etc. was completed with the help of the methods of ligand field theory. The spectra of ten complexes were calculated in gratifying agreement with experiment. A previously existing controversy was settled concerning the proper interpretation of one of the observed absorption bands in these molecules. The results will be published in the June 1962 issue of Inorganic Chemistry.

32. TWO-, THREE-, AND FOUR-ATOM ENERGY INTERACTIONS IN MOLECULES

(K. Ruedenberg)

Progress was made in the work on the calculation of interelectronic interaction energies arising from electrons distributed over two, three, and four atoms, the most general interactions occurring in molecules and solids. Completed were computer programs for overlap integrals and for Coulomb integrals. It was discovered that Coulomb integrals and overlap integrals are related to each other by Poisson's differential equation, and that overlap integrals are related to confluent hypergeometric functions.

Useful expansions have been found by which the three- and four-center integrals can be expressed in terms of Coulomb and overlap integrals. Three- and four-center energy integrals have been evaluated.

PYROMETALLURGY

1. DISTRIBUTION OF FISSION PRODUCTS AND PLUTONIUM BETWEEN ALLOY PHASES (A. F. Voigt)

The investigation of the distribution of plutonium and various fission products between molten alloy phases has been completed. In this program irradiated U-5% Cr eutectic was treated with Mg-Ag alloys of varying composition to determine the distribution of products between these two immiscible alloy phases. The extractions were made with roughly equal volumes of the two phases at 1000°C in a rocking furnace. The extraction time of 60 min was followed by 10 min in a static vertical position before quenching.

The data summarized in Table XX supplement those given in the previous annual report (IS-350) and complete our study of the effect of composition on the extraction. The distribution coefficients, K_d , are defined as the activity of the component per gram of extractant phase divided by its activity per gram of the uranium phase. The results are also shown as percentage extracted and percentage removed. The latter includes removal by processes such as volatilization and slagging as well as by extraction.

It can be seen from Table XX that the effect of composition on the extraction is quite pronounced. With alloys of low and intermediate silver content, the extraction of plutonium is small, and it is only with essentially pure silver that the extraction coefficient becomes large. On the other hand, the extraction coefficients for the rare earths are much higher for magnesium or alloys of intermediate composition than for high silver compositions.

A part of this study has been concerned with the interphase solubility of the four metals, U, Cr, Ag and Mg, which constitute the two phases. Equilibrations have been made between the U-Cr eutectic with a fixed composition of 5% Cr and Mg-Ag alloys over the total range of composition. Results were determined for uranium dissolved in the Mg-Ag phase and for silver dissolved in the U-Cr. In both cases the solubility is strongly dependent on the composition of the Mg-Ag alloy. The solubility of uranium in silver is about 4 wt% but it decreased to 0.03% in magnesium. It would be expected that less silver would pass into the U-Cr phase from dilute alloys than from a pure silver phase but the change is probably greater

Table XX

Extraction of Irradiated U-Cr Alloy with Mg-Ag Alloys

Element	Extractant Alloy Composition (wt% Mg)				
	33.5	26.4	5.4	2.5	0.114
Pu					
	1.10	1.12	19.9	48.9	123.
	K _d Removed	18.5	91.9	96.7	98.7
	% Extracted	19.9	79.7	91.1	97.4
Sr					
	110.	26.7	30.5	37.2	22.2
	K _d Removed	93.0	96.7	98.1	96.3
	% Extracted	56.2	38.7	50.1	48.8
Ba					
		61.7	22.6	22.4	15.0
	K _d Removed	97.2	96.5	97.1	95.7
	% Extracted		38.6	36.7	38.9
Y					
	1024.	181.	26.8	93.9	11.4
	K _d Removed	99.7	99.6	99.6	96.0
	% Extracted	69.9	4.6	20.6	27.8
Ce					
	1028.	308.	82.7	654.	73.3
	K _d Removed	99.7	99.5	99.9	99.1
	% Extracted	81.8	20.3	42.1	49.5
Zr					
	0.079	0.087	0.15	0.25	0.44
	K _d Removed	38.7	23.1	33.5	58.7
	% Extracted	1.5	5.8	9.2	10.9

than expected, from 3×10^{-2} wt% from silver to 4×10^{-4} wt% from a Mg-6% Ag alloy. The other interphase solubilities, namely, magnesium in the U-Cr eutectic and chromium in the Mg-Ag phases, were very small.

2. EXTRACTION OF PLUTONIUM FROM URANIUM BY SILVER, LANTHANUM AND CERIUM (A. F. Voigt)

A report (IS-470) entitled "Removal of Plutonium from Uranium by Molten Metal Extraction", by A. F. Voigt, R. G. Clark, J. E. Gonser, D. L. Haes, G. L. Lutz and K. L. Malaby, was distributed.

Abstract--The extraction of plutonium from molten uranium with immiscible molten metals, silver, lanthanum and cerium, has been investigated. A facility is described in which these experiments on uranium containing 0.2% plutonium were conducted safely. The distribution coefficients and efficiency of removal from uranium were determined for silver and lanthanum at several temperatures in the range 1175-1375°C and for cerium at 1225°C.

In order to permit a statistical analysis of the results, 20-30 g of metal were used for each phase and, after cooling, the phases were sectioned and the sections analyzed individually. It was found that the extraction into silver was accompanied by slagging reactions which removed variable quantities of the plutonium and led to poor agreement among runs. Hence, the distribution coefficient and its temperature dependence could not be determined with accuracy. An average value of 14 ± 1 was obtained for the coefficient, defined on a molar basis. The lanthanum and cerium extractions were much more reproducible since slagging of plutonium is not as likely in the presence of these more active metals. They extract much less of the plutonium, with a distribution coefficient of 0.4 for lanthanum and 0.5 for cerium.

Comparison is made with the results of McKenzie et al.¹ on the same system but under greatly different experimental conditions.

¹D. E. McKenzie, W. M. Jenkinson, and A. S. Denovan, Can. J. of Chem. 34, 1176 (1956).

3. DEW-POINT DETERMINATION OF VAPOR PRESSURES OF ZINC OVER ITS ALLOYS (A. F. Voigt)

The knowledge of the vapor pressure of a component metal above its alloy with another metal is of considerable use in understanding the nature of the alloy. From this information thermodynamic activity coefficients, enthalpies, free energies of formation and other important properties of the system can be obtained. One method of determining partial vapor pressures is the dew-point technique in which a closed evacuated system containing the alloy is heated to a fixed temperature except for a single point such as a finger in the system which is cooled below this temperature. If the vapor pressure of one component is greater than that of the other, it will vaporize from the alloy and condense on this cold finger when the temperature of the finger reaches the dew point for the metal. The vapor pressure of the metal at the dew point is the equilibrium value for the pure metal and is known from a separate determination.

In the present modification of the method, zinc was the volatile metal and Zn^{65} tracer was added to it. The 1.1 Mev gamma radiation from Zn^{65} was detected with a scintillation probe aimed at the point of condensation through a narrow collimator. An increase in the counting rate indicated when the dew point was reached and the temperature of the cold finger at that moment, measured and recorded with a thermocouple circuit, was used with the known vapor pressure temperature curve of pure zinc to determine the vapor pressure. For an alloy of a given composition the vapor pressures can be determined over a 150-200° temperature range.

Three systems involving zinc have been studied, namely, Zn-Al, Zn-Th and Zn-Y. The Zn-Al system is a simple eutectic with no inter-metallic phases, and the data were used to calculate the activity coefficients of the zinc directly and of the aluminum using the Gibbs-Duhem equation. The Zn-Th and Zn-Y systems each contain a number of inter-metallic compound phases. The vapor pressure data were used to calculate the enthalpies, free energies and entropies of formation of these compounds.

4. FUSED SALT SEPARATIONS OF URANIUM AND THORIUM (A. F. Voigt)

The development of methods for separating uranium and thorium is of considerable importance for the future use of the Th- U^{233} fuel cycle. Several pyrometallurgical procedures for this separation are being studied. Because of the size of the cross sections of U^{233} for fission and Th^{232} for capture, the steady state concentration of U^{233} in a Th blanket will not exceed $\sim 1\%$. A satisfactory separation method should obtain a fairly quantitative removal of this 1% with simple chemical processing, while leaving the thorium itself unchanged. Since thorium has a very high melting point, pyroprocessing methods generally use one of its low melting alloys as the phase from which the uranium is separated.

Various fused salt mixtures are being examined to find one which will preferentially oxidize and extract one of the components in an alloy containing 75% Al, 25% Th and 0.25% U. In one series, mixtures of LiCl and $ThCl_4$ are being examined to determine if the uranium can be oxidized to UCl_3 and extracted from the molten alloy. The use of mixtures with low $ThCl_4$ content, approximately equivalent to the uranium

present in the alloy, led to extraction of only a few percent of the uranium. A ten-fold increase in the ThCl_4 increased the extraction to $\sim 10\%$ of the uranium. Further studies are in progress to see if a useful process can be built on this system.

It has been reported that a pronounced effect on the behavior of uranium and thorium exists in the system $\text{KCl-AlCl}_3\text{-Al}$ when the KCl/AlCl_3 ratio is nearly unity. Attempts are underway to apply this phenomenon to the separation of these Th-1% U mixtures.

ANALYTICAL CHEMISTRY

1. SOLVENT EXTRACTION (C. V. Banks)

An investigation of the solvent extraction properties of bis(di-n-hexylphosphinyl) methane, HDPM, and related organophosphorus compounds was continued. Many metals, especially from perchloric acid media, are almost completely extracted into an organic phase containing HDPM in some solvent such as 1,2-dichlorobenzene. The distribution coefficients, D , observed for the extraction of uranium from hydrochloric and perchloric acid media are given in Table XXI.

Table XXI

Extraction of Uranium(VI) from Mineral Acid Media
into a 0.05 M Solution of HDPM in 1,2-Dichlorobenzene

Molarity of Acid	log D	
	HCl	HClO_4
0.037	-	1.41
0.089	-	3.00
0.140	-	3.15
0.244	-	3.40
0.346	-	3.68
0.5	0.96	-
0.557	-	3.57

Table XXI (Continued)

Molarity of Acid	log D	
	HCl	HClO ₄
1.0	1.51	-
1.07	-	3.64
2.0	2.30	-
2.11	-	3.58
3.0	3.06	-
3.12	-	3.68
5.0	3.62	-
5.19	-	3.85
6.5	3.59	-
7.26	-	3.79
8.0	3.43	-
9.33	-	3.54

2. REVERSED PHASE PARTITION CHROMATOGRAPHY (C. V. Banks)

The use of bis(di-n-hexylphosphinyl)methane, HDPM, as a stationary phase for paper and column chromatography of various cations was studied. Sharp separations of a number of metal perchlorates such as lithium from sodium and the alkaline earths from one another were obtained by merely spotting the neutral perchlorates on paper impregnated with HDPM and eluting with water. The movement of the mineral acids on HDPM treated papers was also studied. An especially sharp separation of barium and strontium from the lighter alkaline earths was obtained since only the former two elements were displaced by perchloric acid.

The relative movement of various metal perchlorates on paper impregnated with HDPM can be seen from their R_F and R_R values in Tables XXII and XXIII. The papers were prepared by immersing the paper in a 0.1 M solution and HDPM in carbon tetrachloride and allowing the carbon tetrachloride to evaporate. The R_F or R_R values are a function of the

Table XXII

R_F Values for Metal Perchlorates by Ascending Chromatography
on Papers Impregnated with HDPM

Metal	R_F	
	H_2O	0.1 M $HClO_4$
Li	1	1
Na	1	1
K	1	1
Mg	0.14	0.24
Ca	0.07	0.04
Sr	0.29	0.85
Ba	0.32	0.85
($HClO_4$)	-	0.85
Mn	0.03	0
Co	0.11	0.11
Ni	0.20	0.54
Cu	0.12	0.14
Zn	0.11	0.07
Pb	0.05	0
Hg	0.04	0.01
UO_2^{++}	0	0
Ce^{+3}	0	0

Table XXIII

R_R Values for Alkali and Alkaline Earth Perchlorates on Papers
Impregnated with HDPM

Metal	R_R (H_2O as eluent)
Li	0.55
Na	0.78
Be	0.26
Mg	0.30
Ca	0.23
Sr	0.44
Ba	0.47

amount of HDPM on the paper but the relative order of these values remains the same. This is illustrated by the movement of calcium and magnesium perchlorates in Table XXIV.

Table XXIV

Movement of Calcium and Magnesium as a Function of HDPM
Concentration on Paper (Eluent - 0.1 M HClO_4)

Substance	R_R	
	1.0×10^{-6} moles HDPM $\frac{\text{cm}^2}{\text{cm}^2}$	3.8×10^{-6} moles HDPM $\frac{\text{cm}^2}{\text{cm}^2}$
HClO_4 (acid front)	0.62	0.46
Mg	0.43	0.28
Ca	0.23	0.11

The column separation of various cations on columns packed with various materials impregnated with HDPM was also investigated.

Elution curves were obtained for the alkali and alkaline earth perchlorates on columns packed with a fluorocarbon polymer molding powder, impregnated with HDPM. Separations which appear particularly promising are the separation of magnesium from yttrium; barium and strontium from calcium and magnesium; and sodium and potassium from lithium and the alkaline earths. The order of elution was generally the same as that indicated by the R_F and R_R values on paper.

3. DETERMINATION OF PHOSPHINE OXIDES (C. V. Banks)

Paper chromatography was used to check the purity of various phosphine oxides using ethanol-water mixtures as eluting agents. The location of the phosphine oxides was determined by spraying with a reagent containing hydrochloric acid, titanium(IV) and potassium thiocyanate. Most phosphine oxides, phosphonic and phosphinic acids and phosphate esters showed up as bright yellow spots.

A modification of Young and White's procedure for the determination of titanium(IV) trioctylphosphine oxide¹ was found to be generally useful for the determination of trace amounts of phosphine oxides. In this case, an excess of titanium(IV) is added to the aqueous phase and the yellow color formed in the presence of a phosphine oxide and thiocyanate is extracted into chloroform. The method is simple and sensitive with a molar absorptivity for HDPM of 14,600 liter mole⁻¹cm⁻¹. The method is particularly useful in studies of the solubility of these organophosphorus compounds in water.

4. INDIUM (C. V. Banks)

A new method has been developed for the polarographic determination of small amounts of indium in lead-2% zinc and zinc-2% lead alloys. The published methods for the determination of small amounts of indium either did not produce satisfactory results in samples of this type or else required long and difficult separations. In this method the lead is separated by precipitation as lead sulfate but is allowed to remain with the solution. The supporting electrolyte is 10% tartaric acid. The effect of pH has been studied. No evidence of zinc interference or co-precipitation of indium with the lead could be found.

5. 1,10-PHENANTHROLINE COMPLEXES (C. V. Banks)

1,10-Phenanthroline is a common analytical reagent and a better knowledge of its reactions with various ions is quite desirable. We recently measured the stability constant, K_1 , for the formation of the AgP^+ and the over-all stability constant, K_2 , for AgP_2^+ . Preliminary

¹ J. P. Young and J. C. White, Anal. Chem. 31, 393 (1959).

results indicate that K_1 and K_2 are approximately 2.1×10^5 and 1.7×10^{12} , respectively. It has also been observed that 1,10-phenanthroline, 5-methyl-1,10-phenanthroline, 5-chloro-1,10-phenanthroline, and 5-phenyl-1,10-phenanthroline all react with hydrogen ion to form a monoprotinated complex of the type PH^+ , while 5-nitro-1,10-phenanthroline forms a diprotinated complex of the type PH_2^{++} .

6. ABSORPTION SPECTRA OF THE RARE EARTHS (C. V. Banks)

A paper by Charles V. Banks, Merlyn R. Heusinkveld and Jerome W. O'Laughlin, "Absorption Spectra of the Lanthanides in Fused Salt Media", was published in Anal. Chem. 33, 1235-1240 (1961).

Abstract--Spectra are presented for solutions of praseodymium, neodymium, samarium, europium, gadolinium, terbium, dysprosium, holmium, erbium, thulium, and ytterbium fluorides in fused LiCl-KCl eutectic at 400°C. These spectra are discussed and compared with similar results which have been obtained in the same and other fused salt media and in aqueous solutions. Molar absorptivities for selected absorption bands of the rare-earth spectra which might be useful in quantitative analytical determinations are also given. The spectra were obtained with the Cary Model 12 spectrophotometer using an electrically heated cell block furnace as the cell holder.

7. NICKEL-NICKEL BOND IN NICKEL DIMETHYLGLYOXIME

A paper with the above title, by Charles V. Banks and Samuel Anderson, was published in J. Am. Chem. Soc. 84, 1486 (1962).

Abstract--Godycki and Rundle have shown that in nickel dimethylglyoxime the square planar molecules are stacked one above another, 3.42 \AA , so that the nickel atoms lie in a straight row that extends throughout the length of the crystal. They proposed that weak intermolecular nickel-nickel bonds exist and could contribute to the crystal

energy. Frasson and Panattoni have shown that in nickel ethylmethylglyoxime the packing system is completely different from that in nickel dimethylglyoxime. In fact, the nickel-nickel direction is not perpendicular to the plane of the molecule and the nickel-nickel distance (4.75 \AA) is so great that nickel-nickel bonding is not possible.

This suggests that a study of the heats of solution of nickel dimethylglyoxime and nickel ethylmethylglyoxime in non-coordinating solvents such as *n*-heptane and carbon tetrachloride would give a measure of the relative stabilities of these two crystals and, in fact, might give a good measure of the strength of the nickel-nickel bond in nickel dimethylglyoxime.

The ΔH° values show that the crystal energy of nickel dimethylglyoxime is about 9 to 11 kcal more stable than that of nickel ethylmethylglyoxime. In view of the x-ray crystal structure studies and the observations that such properties of these complexes as the "abnormal" dichroism, solubility product, and metal-metal distances in these complexes, it seems reasonable to attribute a large part of this great difference in the crystal energies to the presence of nickel-nickel bonding.

8. NICKEL(II) COMPLEXES IN ALKALINE MEDIA

A paper by Charles V. Banks and J. P. LaPlante, '4-Carboxy-1,2-cyclohexanedionedioxime Complexes of Nickel(II) in Alkaline Media', has been accepted for publication in Analytica Chimica Acta.

Abstract--The reactions of 4-carboxy-1,2-cyclohexanedionedioxime and nickel(II) were studied in alkaline media. Spectrophotometric studies indicate the presence of a 1:1 complex ion, NiD^- . Magnetic susceptibility measurements on a series of solutions of varying ratios of vic-dioxime and nickel(II) showed that the 1:1 complex ion was diamagnetic and that two paramagnetic complexes, probably NiD_2^{-4} and NiD_3^{-7} , are present in solution. The stability constants for the three complexes were calculated from spectrophotometric and magnetic susceptibility data. The log *k* values were found to be $\log k_1 = 28.74$, $\log k_2 = 0.76$, and $\log k_3 = 3.67$, respectively.

A paper by Charles V. Banks and J. P. LaPlante, "The Oxidized Complex of Nickel with 4-Carboxy-1,2-cyclohexanedionedioxime in Alkaline Media", has been accepted for publication in Analytica Chimica Acta.

Abstract--The reaction of oxygen with a nickel(II) complex of 4-carboxy-1,2-cyclohexanedionedioxime in alkaline media was studied spectrophotometrically, polarographically, and by spectrophotometric titrations with tin(II) chloride. The rate of formation of the oxidized complex was found to be first order at 25° and 50°C. The values obtained for the rate constants are $k'_1 = 2.71 \times 10^{-2} \text{ hrs.}^{-1}$ (25°C.) and $5.35 \times 10^{-2} \text{ hrs.}^{-1}$ (50°C.).

The effect of reducing agents on the formation of the oxidizing complex was studied. It was found that tin(II) chloride, hydrazine sulfate, and hydroxylammonium chloride prevented the formation of the oxidized complex.

The magnetic susceptibility data was interpreted by the valency bond theory. A reaction mechanism for the formation and decomposition of the oxidized complex is proposed.

9. NICKEL(II)-VIC-DIOXIME COMPLEXES (C. V. Banks)

A paper by Charles V. Banks and Samuel Anderson, "Stability Constants and Intrinsic Solubility of Several Nickel(II)-vic-Dioxime Complexes", has been accepted for publication in Inorganic Chemistry.

Abstract--In order to better understand the factors which affect the solubility of the nickel(II)-vic-dioxime complexes, the intrinsic solubility constant, K_s , was measured and correlated with the nickel-nickel bond distances in several complexes. The acid dissociation constants of the vic-dioximes in water were determined by measurements in several concentrations of dioxime. The pK_{a1} values were obtained by extrapolation to zero concentration of dioxime. Values of the over-all stability constants in water, K_1 and K_2 , were determined by calculating from the corresponding values in 75% dioxane-25% water mixtures. The solubility product

constants, K_{sp} , were determined from pH measurements by the method of Banks and Barnum. The intrinsic solubility constants, K_s , were calculated from K_{sp} and $K_2 = K_{sp} \cdot K_2$.

Excluding nickel dimethylglyoxime and nickel(II) 4-methylnioxime, there appears to be a smooth relationship between the intrinsic solubility constant and nickel-nickel bond distance in the crystals of the nickel(II) complexes of nioxime, 4-isopropylnioxime, 3-methylnioxime, and heptoxime.

10. NICKEL AND COPPER DIMETHYLGLYOXIMES (C. V. Banks and R. E. Rundle)

A paper by R. E. Rundle and C. V. Banks, "On Solubilities and Structures of Nickel and Copper Dimethylglyoximes", was submitted for publication in Journal of Physical Chemistry.

Abstract--It is shown that the solubility and enthalpy data of Fleischer and Freiser for $Ni(DMG)_2$ and $Cu(DMG)_2$ are consistent with ~ 10 kcal/mole for Ni-Ni bonds in $Ni(DMG)_2$, if proper recognition of the crystal structures of the two compounds is made. In the crystal, each monomer of $Cu(DMG)_2$ has two hydrogen bonds of 2.70 and 2.53 Å, while there are two hydrogen bonds of 2.40 Å in $Ni(DMG)_2$. The enthalpy involved in the rearrangement of the hydrogen bonds in $Cu(DMG)_2$ upon solution has been estimated to be about -33 kcal/mole. The Cu-O bond energy in $Cu(DMG)_2$ has been estimated to be about 44 kcal/mole. It is noteworthy that this Cu-O bond energy is so large that $Cu(DMG)_2$ could not dissolve as monomers in non-complexing solvents without a large gain in the energy of hydrogen bonding in going from the dimer to the monomer.

11. OXYGEN IN METALS BY INERT GAS FUSION TECHNIQUE (C. V. Banks)

A paper by George J. Kamin, Jerome W. O'Laughlin and Charles V. Banks, "The Determination of Oxygen in Vanadium, Niobium, and Tantalum by the Inert Gas Fusion Technique", was submitted for publication in Analytical Chemistry.

Abstract--The inert gas fusion technique has been applied to the determination of oxygen in the Group V-A metals: vanadium, niobium, and tantalum. Commercially available instrumentation was used. A platinum flux technique was found to be satisfactory for the determination of oxygen in vanadium, but results on niobium and tantalum by this method were erratic. Reproducible results were obtained on niobium and tantalum samples when a mixed nickel-platinum bath, containing 60-80 weight per cent nickel, was employed with the platinum flux. Oxygen contents from 100 to 1000 ppm. were determined on standard samples with a standard deviation of 3% for vanadium and 5% for niobium and tantalum.

12. SERVICE ANALYSES (C. V. Banks)

A total of 8754 service analyses were completed during the period of this report.

13. ANALYTICAL ION-EXCHANGE SEPARATIONS (J. S. Fritz)

Work was completed on a selective ion-exchange separation of vanadium and a paper entitled "Cation Exchange Separation of Vanadium from Metal Ions", by J. S. Fritz and J. E. Abbink, has been accepted for publication in Analytical Chemistry.

Abstract--Vanadium(IV) or (V) can be separated from other metal ions by elution from a cation exchange column with dilute acid containing 1% or less hydrogen peroxide. Vanadium is quantitatively removed as a vanadium(V)-hydrogen peroxide complex; the other metal ions are eluted later with stronger acids. Separations of vanadium(IV) or (V) from 25 metal ions are reported. Varying ratios of vanadium(V) to iron(III) up to 1:100 are separated.

A paper entitled "Anion Exchange Separation of Thorium Using Nitric Acid", by James S. Fritz and Barbara B. Garralda, has been accepted for publication in Analytical Chemistry.

Abstract--Thorium is quantitatively retained by an anion exchange column from aqueous 6M nitric acid solution. Most other metal ions are completely eluted from the column with 75 to 100 ml. of 6M nitric acid. Following the separation, thorium is stripped from the column with 0.5M nitric acid and titrated with EDTA.

The elution of certain cations from a cation exchange column with aqueous nitric and hydrochloric acids was studied. It was found that 1.5 M nitric acid will quantitatively elute calcium(II), strontium(II), magnesium(II) and nickel(II) from a 1.2 x 16 cm cation exchange column in the hydrogen form. Rare earths and yttrium(III) are quantitatively retained by the column.

Chromium interferes with many ion-exchange separations and analytical determinations of other metallic elements. Separation of chromium as chromium(VI) on a conventional cation- or anion-exchange column is unsatisfactory because of partial reduction of chromium(VI) by the resin. This problem is obviated by using a column containing zirconium dioxide anion exchanger. Quantitative separation of chromium from several other metal ions has been achieved.

Lead(II) can be separated from many other metal cations by elution from a cation exchange column with 0.6 M hydrobromic acid. The column and eluting agent are warmed to about 60°C to avoid the formation of a lead bromide precipitate on the column. Bismuth(III) and cadmium(II) are eluted before the lead with warm, dilute hydrochloric acid; tin(IV) is eluted with dilute hydrofluoric acid.

Barium(II) can be separated from strontium(II) and calcium(II) by adsorption of the barium(II) on a nitrate-form anion exchange column from a solution containing 90% methyl alcohol and 10% aqueous 5 M nitric acid. The more difficult separation of strontium(II) from calcium(II)

is accomplished with the same column using 80% isopropyl alcohol and 20% of an aqueous nitric acid solution.

A manuscript entitled "Cation Exchange in Acetone-Water-Hydrochloric Acid", by James S. Fritz and Thomas A. Rettig, was submitted to Analytical Chemistry for publication.

Abstract--Distribution coefficients have been measured for the partition of metal ions between cation exchange resin and acetone-water-hydrochloric acid solutions. The differences in distribution coefficients of metal ions are greater in acetone-water media than in aqueous media of the same hydrochloric acid concentration. Using distribution coefficient data, conditions for column separations of mixtures can be selected. Column separations of metal ion mixtures can be effected by eluting with acetone-water-hydrochloric acid solutions of different compositions. Successful separations of a number of mixtures are reported.

14. ANALYTICAL SEPARATIONS USING SOLVENT EXTRACTION

14.1 Iron

A paper entitled "Separation of Iron by Liquid-Liquid Column Extraction", by J. S. Fritz and C. E. Hedrick, was submitted to Analytical Chemistry for publication.

Abstract--Iron(III) can be separated from many elements by extraction from 6 to 8M hydrochloric acid. The extraction is carried out by passing the aqueous hydrochloric acid solution through a column packed with 2-octanone adsorbed onto a polyfluorocarbon resin. Fluoride, phosphate, sulfate or citrate cause no interference. Traces of iron(III) can be separated quantitatively from large amounts of copper(II) or zinc(II); traces of titanium(IV) can be separated from large amounts of iron(III).

14.2 Thorium and Uranium

Thorium(IV) and uranium(VI) can be extracted quantitatively from 5 to 6 M nitric acid by tributylphosphate without any added salting-out agent. This will be useful for mixtures requiring additional separations before analysis.

15. NONAQUEOUS ACID-BASE TITRATIONS

A paper entitled "Potentiometric Studies of the Titration of Weak Acids with Tetrabutylammonium Hydroxide", by L. W. Marple and J. S. Fritz, was published in Anal. Chem. 34, 796-800 (1962).

Abstract--The sources of amine, carbonate and silver impurities in tetrabutylammonium hydroxide have been investigated and techniques for their removal have been evaluated. The stability of the base in water, isopropanol, tert-butanol and pyridine was determined. Salt bridge systems of the type



have been devised for acetone, isopropanol, tert-butanol and pyridine.

Titration of weak and very weak acids using the glass indicating electrode were reproducible to within two to five millivolts.

A paper entitled "Potentiometric Titration of Acids in Tertiary Butanol", by J. S. Fritz and L. W. Marple, has been accepted for publication in Analytical Chemistry.

Abstract--The use of tertiary butyl alcohol as a solvent for the titration of acids has been evaluated. Potentiometric titrations of mineral acids, carboxylic acids, dicarboxylic acids and phenols were performed using the glass indicating electrode and calomel reference electrode. The solvent was found to be particularly suited to differentiating titrations because the slopes of the titration curves of individual acids are very flat in the buffer region. Other advantages of this solvent are that it can be commercially obtained in pure form, and that it shows little leveling tendency for strong acids.

The fundamental equilibria of acids dissolved in tertiary butyl alcohol are being studied by potentiometric, spectrophotometric and conductometric means. Perchloric acid was the strongest acid observed in tertiary

butyl alcohol, but it is incompletely ionized. The ionization constant of perchloric acid is approximately 10^{-3} . Approximate ionization constants of other mineral acids, carboxylic acids and phenols were measured by potentiometric means. The effect of adding the acid anion as the tetrabutylammonium salt has been investigated, as has the effect on the ionization of weak acids of adding a salt such as tetrabutylammonium perchlorate.

SPECTROCHEMISTRY

1. INTERSTITIAL OXYGEN, NITROGEN AND HYDROGEN CONTENT OF METALS

(V. A. Fassel)

1.1 D-C Carbon Arc-Gas Chromatographic Simultaneous Determination of the Oxygen and Nitrogen Content of Steels

Our spectroscopic studies have shown that the interstitial oxygen, nitrogen and hydrogen contents of metals can be extracted quantitatively and rapidly in high-current, dc carbon arc discharges in noble gas atmospheres. The extracted gases (CO , N_2 and H_2) can, in principle, be detected and determined by non-spectroscopic techniques. During the past year a gas chromatographic technique has been successfully applied to this problem. Following the dc carbon arc extraction, a small portion of the resulting gas mixture is transferred to a commercial gas chromatograph. A molecular sieve column serves to separate the individual components and a sensitive thermal conductivity cell detects the CO and N_2 in the effluent stream. Recorded peak heights corresponding to changes in thermal conductivity of the effluent stream are related to the impurity concentrations. The sensitivity is about 5 ppm. Quantitative determinations



Fig. 7. Determination of O_2 and N_2 in Metals

in nitrogen and oxygen have been made in the concentration range 30 to 1000 ppm in low and high alloy steels, with a relative standard deviation ranging from 2 to 5% of the amount present. Approximately 5 min are required for the complete analysis. Preliminary results indicate that this technique is also applicable to other metals.

1.2 Determination of Oxygen in Vanadium Metal

A comparative study on the determination of oxygen in vanadium metal by the vacuum fusion-manometric, the inert gas fusion-capillary trap, and the dc carbon arc, emission spectroscopic technique has demonstrated that concordant analytical results can be obtained by the three methods. Synthetic standards were employed to validate the absolute accuracy. The experimental conditions under which accurate determinations can be made are delineated in a paper which has been submitted to Analytical Chemistry for publication.

2. ANALYTICAL EMISSION SPECTROSCOPY (V. A. Fassel)

2.1 Excitation of Line Spectra in Fuel-Rich Oxy-Acetylene Flames

A paper entitled "Flame Spectra of the Rare-Earth Elements", by V. A. Fassel, R. H. Curry and R. N. Kniseley, has been accepted for publication in Spectrochimica Acta.

Abstract--The rare-earth elements, including scandium and yttrium emit intense line spectra when absolute ethanol solutions of rare-earth halide or perchlorate salts are aspirated into fuel-rich, oxy-acetylene flames. In contrast, in the hotter stoichiometric flames, only a few very weak lines are detectable. Recordings of the spectra are given, along with the exact wavelengths of about 1200 of the strongest lines. A discussion of the analytical utility of the stronger lines and excitation processes which may account for the striking enhancement of line intensities is included. All of the experimental evidence collected thus far suggests that these fuel-rich flames provide a more favorable environment for the existence of rare-earth atoms in the flame gases.

The recordings shown in Fig. 8 illustrate the striking simplicity of these flame spectra as compared to the lines emitted in arc or spark

discharges. This simplicity is a fortuitous consequence of the low energy distribution prevailing in the fuel-rich flames. The effective rotational (OH band components) and electronic temperature (iron lines) in these flames have been measured, the values obtained ranging from 2970 to 3080°K. At these temperatures only the lowest excited states are significantly populated, and the degree of ionization is so low that lines originating in the low excited states of the ion are rarely observed. In contrast, arc or spark discharges produce an almost fully developed first and second spectrum of these elements.

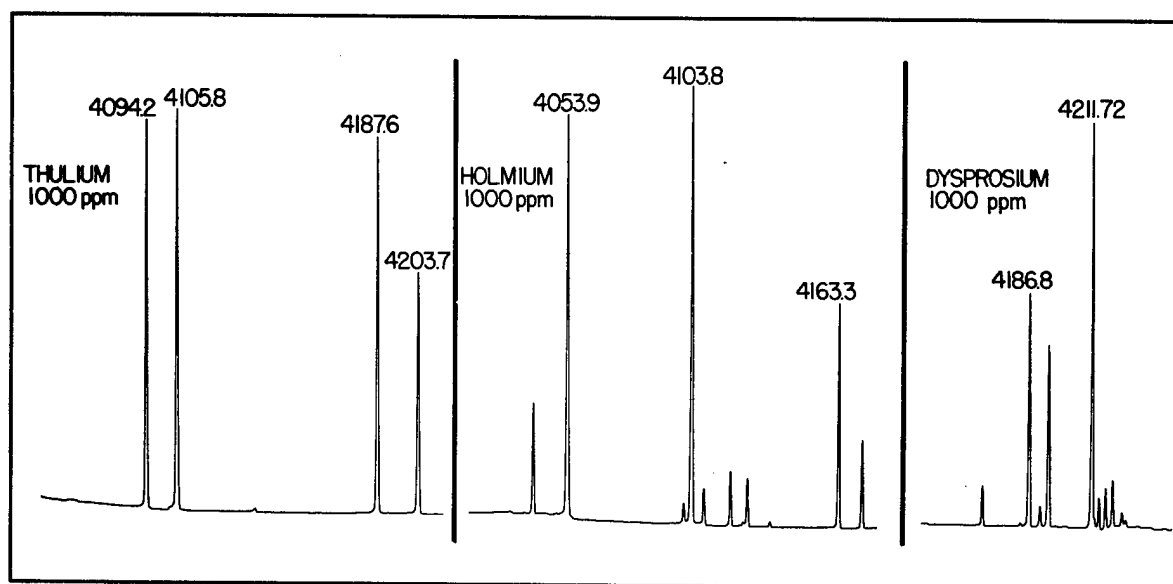


Fig. 8. Line Spectra of Rare-Earth Elements Excited in Fuel-Rich Oxy-Acetylene Flames

The fuel-rich oxy-acetylene flame spectra are simple enough so that a small table model (0.5 meter) grating spectrometer can be utilized for the analysis of rare-earth mixtures. The application of these spectra to the quantitative determination of Sc, Dy, Ho, Er, Tm and Lu in complex rare-earth mixtures has been demonstrated. The determination of the other members of the series is now being explored. The sensitivities of detection of the strongest lines have been assessed and are summarized in Table XXV.

Analytically useful spectra of the elements vanadium, niobium, titanium and rhenium can also be observed in these flames. Heretofore, lines of these elements were not detected in the hotter stoichiometric flames, suggesting that the enhancement mechanism is the same as for the rare earths.

Table XXV
Sensitivities of Detection

Element	Wavelength (Å)	Sensitivity (ppm in solution)
La	4187.3	40
Pr	4951.4	15
Nd	4924.5	5
Sm	4783.1	5
Gd	4401.9	25
Tb	4318.9	10
Dy	4211.7	0.5
Ho	4103.8	0.5
Er	4007.9	2
Tm	4094.2	0.5
Lu	3359.6	3
Sc	3907.5	1
Y	4102.4	3

2.2 Quantitative Determination of Sodium and Tungsten in Tungsten Bronzes

The tungsten bronzes, specifically Na_xWO_3 and Li_xWO_3 are non-stoichiometric compounds which exhibit unusual electrical and mechanical

properties. These properties appear to be sensitively dependent on the value of "x", consequently an accurate knowledge of their sodium or lithium content is of interest. Because of the chemical stability of these compounds, the quantitative determination of the alkali metal content by chemical methods is a singularly difficult task. To perform these analyses, an emission spectrometric technique has been developed. The procedure is based on the dc carbon arc excitation of the following blends:

<u>For Na</u>	<u>For Li</u>
1 part sample	1 part sample
3.3 parts GeO_2	220 parts GeO_2
1.6 parts powdered graphite	110 parts powdered graphite
0.1 part RbCl	22 parts RbCl

All of the ingredients in these blends serve a useful function. The GeO_2 serves as a fusing agent in the electrode receptacle. This fusion action destroys differences in physical or chemical constitution between actual sample crystals and the synthetic standards. The latter are mechanical blends of WO_3 and pure sodium or lithium tungstates. The germanium in the fused melt also aids in the smooth and reproducible volatilization and excitation of the alkali metals. The powdered graphite reacts with the tungsten to form the very refractory carbide, thus suppressing the spectrum of tungsten. The RbCl serves as an internal standard, since its behavior during the volatilization and excitation process is very similar to the sodium and lithium constituents in the sample. The intensity ratios of the following line pairs are related to concentration in the usual manner:

$\frac{\text{Na } 6154\text{\AA}}{\text{Rb } 6298\text{\AA}}$, $\frac{\text{Na } 6160\text{\AA}}{\text{Rb } 6298\text{\AA}}$, $\frac{\text{Li } 6013\text{\AA}}{\text{Rb } 6206\text{\AA}}$, $\frac{\text{Li } 6103\text{\AA}}{\text{Rb } 6159\text{\AA}}$, and $\frac{\text{Li } 6103\text{\AA}}{\text{Rb } 6298\text{\AA}}$. The concentration range corresponding to "x" values from 0.04 to 0.6 can be determined with a relative standard deviation of 3 to 4% of the amount present.

2.3 Vacuum Ultraviolet Spectroscopy

The wide scope and utility of emission spectrometric techniques as applied to the metallic elements is due in great measure to the fact that the sensitive spectral lines of these elements lie in the easily accessible visible and ultraviolet spectral regions. There is every reason to believe that the same scope and utility can be extended to the non-metallic and metalloidal elements by working in the vacuum ultraviolet region where the sensitive lines of these latter elements lie. Hence, the vacuum ultraviolet region offers one of the most promising avenues for detecting and determining trace impurities of the elements or compounds of O, N, H, S and the halogens.

Of the possible types of light sources available for the excitation of gases in this spectral region, the microwave-driven electrode-less discharge was selected because (1) it eliminates the problem of contamination of the source by the electrode material, (2) the problems of electrical insulation, heat dissipation, and elevated-temperature vacuum seals are avoided and (3) this source is remarkably stable and convenient to operate.

The vacuum ultraviolet facility has been applied to the problem of determining the oxygen and nitrogen content of the noble gases, especially helium. This technique will be applicable not only to the direct analysis

of gaseous mixtures, but also to the determination of these elements in a wide variety of solid materials by mating this analytical procedure with an appropriate gas extraction technique. Thus far, this investigation has yielded the following observations:

- (1) The microwave-driven electrode-less discharge channels an amount of light energy into the VUV region far exceeding the expectations of a 125-watt source. It is believed that this high excitation efficiency is directly related to the high ion/electron ratio in this source, an investigation of which might prove helpful to the understanding of excitation phenomena in gas discharges.
- (2) Band spectra are profusely emitted from the microwave-driven discharge, more so than from dc discharges between electrodes under the same conditions. This is believed also to be a manifestation of a high degree of ion excitation in this source.
- (3) Chemical reactions between gaseous species exert considerable influence on the spectra emitted from this source. For this reason, the use of this discharge for analytical purposes necessitates a high degree of control not only of pressure, but also of the flowrate of gas passing through the discharge zone.
- (4) The necessity of controlling gas flowrate has led to the design and construction of an automatic device capable of maintaining gas pressure constant to within ± 0.10 Torr, and gas flowrate constant to within ± 0.6 ml STP per minute.
- (5) The detection limit for nitrogen in helium using the N 1743 \AA line has been extended down to 0.05 vpm, and the detection limit

for oxygen is estimated to be 1 vpm using the CO 1730Å band component.

(6) The use of a mixed adsorption bed of charcoal and molecular sieve cooled to liquid nitrogen temperatures has proved capable of purifying helium to the extreme degree required for analytical work at these low concentrations.

2.4 Electrical Discharges in Noble Gas Atmospheres - Theory and Analytical Applications

The excitation of emission spectra in various electrical discharges is the heart of any emission spectrometric analytical procedure. The various processes occurring in the discharge plasma and at the electrode surfaces are greatly simplified by studying discharges in rare gas atmospheres. This avoids the obscuring effects of compound formation between molecular constituents in the air or reaction with the electrodes. A knowledge of the maximum excitation temperature attained in these discharges should lead to a better understanding of excitation processes. The determination of the maximum excitation temperatures is complicated by the fact that there is a spatial temperature distribution as well as a concentration distribution of atomic or molecular species whose spectral radiation serves as a thermometric species. Our approach to this problem is to employ chemical equilibria for calculating the concentration profile of the thermometric species (CN), when N₂ is introduced into the carbon-arc column. Toward this end, the equilibrium constants for the reactions $N_2 \rightleftharpoons 2N$, $CN \rightleftharpoons C+N$, and $C_2 \rightleftharpoons 2C$ have been calculated at 250° intervals from 250 - 15,000°K.

The solution of the simultaneous equilibria for the concentrations of the atomic and molecular species as a function of temperature has been determined by means of an IBM 704 computer. The cases studied were 1%, 0.1%, 0.05% and 0.01% N_2 originally present in one atmosphere of an inert gas. The resulting concentrations of CN were used in calculating the intensities of several CN rotational lines as a function of temperature. The integrated intensity ratios of these lines were then obtained for various maximum discharge temperatures and compared with the corresponding experimental intensity ratios.

Preliminary results indicated two unexpected phenomena. First, the maximum temperatures were much lower than expected, being of the order of 6000°K in helium and less than 5000°K in argon. Secondly, the intensity ratios of CN lines to one another vary with the concentration of CN present in the discharge. This was confirmed both theoretically and experimentally and pointed out the serious errors that would be obtained in temperature measurements by the two line method where this effect is not considered. With proper consideration of this concentration effect it appears that the same maximum temperature is obtained regardless of the CN concentration for a given inert atmosphere discharge.

3. INFRARED SPECTRA OF NITROGEN CONTAINING COMPOUNDS (V. A. Fassel)

Investigations of the vibrational spectra of nitrogen-containing organic compounds have been continued. Observation of the $^{15}N/^{14}N$ and D/H isotopic shifts are extensively employed in these studies to identify those vibrations involving appreciable motion of the N and H atoms. The magnitude of the isotope shifts provides insight into the nature of the vibration

A detailed study of the amide functional group in benzamide has been completed. A paper, "Infrared Spectra of Nitrogen Containing Compounds. I. Benzamide", by R. N. Kniseley, V. A. Fassel, E. L. Farquhar and L. S. Gray, describing the results of this study, has been accepted for publication by Spectrochimica Acta.

Abstract--A study of the infrared spectra of benzamide, benzamide- ^{15}N , and benzamide- d_2 has shown that the frequencies of the Amide I and Amide II bonds appear to invert in going from solution to solid state. Other frequencies which are useful in characterizing the primary amide group are also identified.

Further studies on the spectra of halogen, nitro, amino and methyl ring-substituted benzamides have provided the following information:

1. Evidence has been obtained to indicate that the $\text{C}_{\text{ar}}-\text{C}-\text{N}$ system acts as a vibrational unit giving rise to a symmetrical and an asymmetrical stretching vibration. The NH_2 deformation couples with the higher frequency $\text{C}-\text{C}-\text{N}$ stretch, giving rise to the Amide II band and the Amide III band. Thus, these two bands are coupled vibrations of the δ_{NH_2} and $\nu_{\text{C}-\text{C}-\text{N}}$ modes. The other $\nu_{\text{C}-\text{C}-\text{N}}$ absorption lies near 1150 cm^{-1} . The Amide I band is essentially a pure $\text{C}=\text{O}$ stretching mode although slight nitrogen movement may be involved in some of the compounds.
2. The Amide and amino NH_2 stretching and bending absorptions have been differentiated in the amino benzamides.
3. In m-nitrobenzamide, the association in the solid apparently occurs through hydrogen bonding between the NH_2 and NO_2 groups, probably forming a cyclic dimer. The $\text{C}=\text{O}$ is apparently only weakly bonded.

4. In p-nitrobenzamide association occurs through hydrogen bonding of the NH_2 group to both the NO_2 and C=O groups.

5. The frequencies of the Amide I and II bands are apparently inverted in the solid state spectra of most of these compounds, the exceptions being m- and p-nitrobenzamide and p-aminobenzamide.

Progress has also been made in interpreting the spectra of acetanilide and its ortho ring substituted derivatives. Some of the more significant findings are summarized below.

1. The origin of the Amide I, II and III bands appears to be the same as in benzamide, except that the vibrational unit is the C-N-C_{ar} system in the acetanilide compounds.

2. The Amide II band is at a lower frequency in ortho substituted acetanilides as compared with the corresponding meta and para derivatives. This is apparently a steric effect.

3. The principal NH stretching vibration in ortho substituted acetanilides is $\sim 50 \text{ cm}^{-1}$ lower than in the corresponding meta and para derivatives.

4. The NH group forms an intermolecular hydrogen bond to the NO_2 group in o-nitroacetanilide.

5. Ortho hydroxyacetanilide forms hydrogen bonds intermolecularly through the OH group. The NH stretching frequency is essentially the same in both dilute solution and solid state spectra, corresponding to an unbonded NH group.

A systematic investigation of the spectra of aliphatic and aromatic thiocyanates, isothiocyanates and isocyanates was initiated. Complete vibrational assignments have been made for some of the simpler molecules

and several interesting examples of isomerism have been found in the branched systems. Extensive studies of the $^{15}\text{N}/^{14}\text{N}$ isotope shifts are anticipated for these compounds.

4. SPECTROSCOPIC AND OTHER SERVICE ANALYSES (V. A. Fassel)

During the period covered by this report, 3390 samples submitted by other groups in the Laboratory were analyzed or examined by optical emission, infrared absorption, and vacuum fusion or inert gas fusion techniques. Multiple analyses were made on many of the samples.

RADIOCHEMISTRY

1. ACTIVATION ANALYSIS FOR SODIUM IN THE SODIUM TUNGSTEN BRONZES (A. F. Voigt)

The sodium-tungsten bronzes, which have the composition Na_xWO_3 with x varying from 0 to 0.9, are of great interest as subjects of study in solid state physics since their properties can be changed in a regular manner by changing the value of x . Of importance in understanding these properties is knowledge of the exact value of x , which is difficult to determine by standard chemical or spectroscopic techniques. Activation analysis by neutron activation of sodium to ^{24}Na is being applied to the problem.

The large activity produced in tungsten (W^{187}) in neutron irradiations makes it necessary to perform a chemical separation after the activation in order to prepare a pure sample of Na^{24} for counting. Several separation schemes have been tried in which the tungsten is converted to a volatile halide leaving the sodium behind. The use of nitrosyl chloride is safe

and convenient, but a small amount of the sodium is apparently lost from the apparatus along with the tungsten. Bromide trifluoride, which converts the tungsten to a volatile fluoride leaving the sodium behind as NaF, operates at a lower temperature and leads to less loss of sodium. However, the handling of this reagent is more difficult.

A number of successful analyses have been made on samples of several compositions using the Iowa State University UTR-10 Training Reactor as the neutron source. The method appears to be capable of greater accuracy than is currently being obtained by the spectrographic or chemical methods. Errors in the value of x have been reduced to a few per cent. Experiments are in progress to determine how accurate the method can be made. Since the substance used for comparison in the analysis is a compound of known stoichiometry, sodium tungstate, Na_2WO_4 , it should be possible to establish this method for an absolute determination of x , and it could then be used to calibrate standards for the spectrographic methods, if these are more convenient for routine application.

2. RECOIL REACTIONS WITH CARBON-11 (A. F. Voigt)

A continuing program of study is underway on the recoil chemistry of C^{11} as produced in the synchrotron from C^{12} in organic compounds. The goal of this work is an understanding of the mechanism of the reactions of highly energetic carbon atoms as they are produced in an organic system. To date only the gaseous products have been studied since they can be separated by gas chromatography and detected in a flow counter in the time available before the C^{11} has all decayed ($T_{1/2} = 20.4 \text{ min}$).

With the development of an internal probe for the synchrotron, techniques are available for producing much greater activities than were possible in earlier work. A greater variety of products can be observed and shorter radiation times can be used. The internal probe, however, introduces a complication in that the radiation level is much higher in this location since the electrons themselves as well as the bremsstrahlung pass through the sample. The observed reactions of the C^{11} are the result not only of the recoil but also of radiation damage to the molecules in the system.

A study has been made of the effects of total radiation dose and of dissolved iodine as a radical scavenger on the yields of gaseous products resulting from the irradiation of cyclohexane. Acetylene was found to be the most prominent gaseous product; its yield was not affected by changes in the radiation time or dose or by the presence of iodine in the system. Methane, ethylene, propylene and ethane were the other products observed in order of decreasing yield. For these compounds increasing dose produced a considerable increase in yield up to a point beyond which larger doses had no effect. The presence of iodine during radiation brought the yields at high doses down to the values obtained by extrapolating the results for the iodine-free system to zero dose. Results are not sufficiently complete for a full explanation of these phenomena. However, it can be concluded that acetylene is formed by reactions which occur while the recoiling fragment containing C^{11} still has energy above that of its surroundings, i. e., by a "hot" reaction mechanism. The work discussed above has been described in a paper, "Radiation Dose and

Iodine Scavenger Effects on Recoil C¹¹ Reactions in Cyclohexane", by E. P. Rack and A. F. Voigt, which has been submitted for publication in the Journal of Physical Chemistry.

Other hydrocarbons are receiving similar study as targets for the x-ray beam. Benzene and the various straight and branched chain hexanes have been irradiated. In all the cases the most abundant product is acetylene. The yields of gaseous products from benzene are considerably less than those from non-aromatic hydrocarbons. These also increased with increased branching of the hydrocarbon chain.

The effect of dissolved oxygen on the yield of the gaseous products is also being studied since even small quantities of oxygen lead to the production of some CO and CO₂. The relative yields of these compounds compared to the hydrocarbons are being measured as functions of the amount of oxygen in the system in order to obtain information on the method of their formation.

Thus far we have restricted the study to the gaseous products because there are difficult problems in adapting the gas chromatograph method to less volatile compounds. Other counting techniques are being developed and apparatus redesigned to permit operation of the chromatograph at higher temperatures so that the non-volatile products can also be examined.

Because the yields are affected by the intensity of electron and gamma radiation passing through the sample, a knowledge of the magnitude of the radiation level is important. Work is in progress on the adaptation of

standard techniques for determining radiation intensity, such as the Fricke dosimeter, to the small volumes of these irradiated samples.

3. PRODUCTION AND STUDY OF RADIOACTIVE SPECIES (A. F. Voigt)

Certain radioactive species which are difficult to produce in any other way can be made by photoexcitation reactions. Some of these, particularly among the rare-earth elements, are being studied with the Iowa State University 45 Mev synchrotron as the x-ray source.

Work on thulium isotopes produced by (γ, p) reactions on ytterbium has essentially been completed. Some new information was obtained on a 62 hr Tm^{172} produced by irradiating enriched Yb^{173} . However, its decay scheme is very complicated and the sources produced were not of sufficient strength to add much to the data already available. The next heavier isotope, Tm^{173} , was similarly produced by the irradiation of normal ytterbium and enriched Yb^{174} . Thulium-173 was found to have a half-life of 8.0 ± 0.5 days. The β -decay which has an energy of ~ 1 Mev leads to excited states in Yb^{173} which have been reported from studies of the electron capture decay of Lu^{173} and from Coulomb excitation. Gamma-gamma coincidence studies were carried on the transition from these states to the ground state of Yb^{173} . Progress was made toward an understanding of the decay and its correlation with the level assignments expected for this isotope.

Similar work is in progress on Lu^{179} produced by the irradiation of Hf^{180} . A half-life of 4.6 hr was obtained for the decay of this nuclide. Studies with a scintillation spectrometer and employing coincidence techniques have been used to obtain a tentative decay scheme. According to this scheme, the total energy of the decay is 1.33 Mev and 88% of the

transitions occur via a beta ray of this energy. The other 12% of the beta decays have an energy of 1.1 Mev and are followed in prompt coincidence by a 0.212 Mev gamma ray.

4. PHOTOPRODUCTION CROSS SECTIONS (A. F. Voigt)

A paper, "Photoproduction of Beryllium-7", by M. S. Foster and A. F. Voigt, has been accepted for publication in The Journal of Inorganic and Nuclear Chemistry.

Abstract--The nuclide Be^7 has been produced by photoactivation of Be^9 , B and C^{12} using the bremsstrahlung beam of an electron synchrotron operated at 45 Mev. Integrated cross sections for the formation of Be^7 have been estimated by comparison with the $\text{Ta}^{181}(\gamma, n)\text{Ta}^{180m}$ reaction. The reaction $\text{C}^{12}(\gamma, 2p3n)\text{Be}^7$ has also been observed in irradiations at 30, 35 and 40 Mev maximum energy. Its yield has been compared with that of the $\text{C}^{12}(\gamma, n)$ reaction at 45 Mev. The reaction $\text{Al}^{27}(\gamma, 2p3n)\text{Na}^{22}$ was observed at 45 Mev.

5. EXCHANGE REACTIONS IN CYCLOPENTADIENYL COBALT COMPLEXES

(A. F. Voigt)

A paper, "Exchange Reactions of Cyclopentadienyl Cobalt Compounds", by J. F. Weiher, S. Katz and A. F. Voigt, has been accepted for publication in Inorganic Chemistry.

Abstract--Exchange reactions have been studied between bis(cyclopentadienyl) cobalt compounds in anhydrous acetone solution. No exchange occurs between $[\text{Co}^{\text{III}}(\pi\text{-C}_5\text{H}_5)_2]^+$ and Co^{++} . Exchange between $\text{Co}^{\text{II}}(\pi\text{-C}_5\text{H}_5)_2$ and $[\text{Co}^{\text{III}}(\pi\text{-C}_5\text{H}_5)_2]^+$ is instantaneous. Minute traces of oxygen cause oxidation of the former to a derivative with two molecules of $\text{Co}(\text{C}_5\text{H}_5)_2$ per oxygen atom which undergoes slow exchange with $[\text{Co}^{\text{III}}(\pi\text{-C}_5\text{H}_5)_2]^+$ probably by an ionization mechanism. A trichloromethyl derivative formed by reaction between $\text{Co}^{\text{II}}(\text{C}_5\text{H}_5)_2$ and CCl_4 does not exchange Co with $[\text{Co}^{\text{III}}(\pi\text{-C}_5\text{H}_5)_2]^+$ or Cl^- with LiCl .

6. SZILARD-CHALMERS PROCESSES (D. S. Martin, Jr.)

Preliminary studies of the "hot atom reactions" in solid tris-(ethylenediamine) cobalt(III) nitrate have been conducted in which the fate of the radioactive cobalt, prepared by (γ, n) processes in synchrotron irradiations, has been determined. Initial work has used the $\text{Co}^{58\text{m}}$ which can be obtained with good intensities, but which has an inconveniently short half-life of 9.2 hr. The principal radiations from $\text{Co}^{58\text{m}}$ are conversion electrons from a 25 kev γ -transition and the Co-K x-rays. The latter have been counted with a plastic-bonded, paper-wall proportional counter in conjunction with a 128 channel analyzer. The 7.9 kev x-ray peak is well-resolved with this equipment. The cobalt samples are plated as metal on platinum discs and a careful evaluation of the

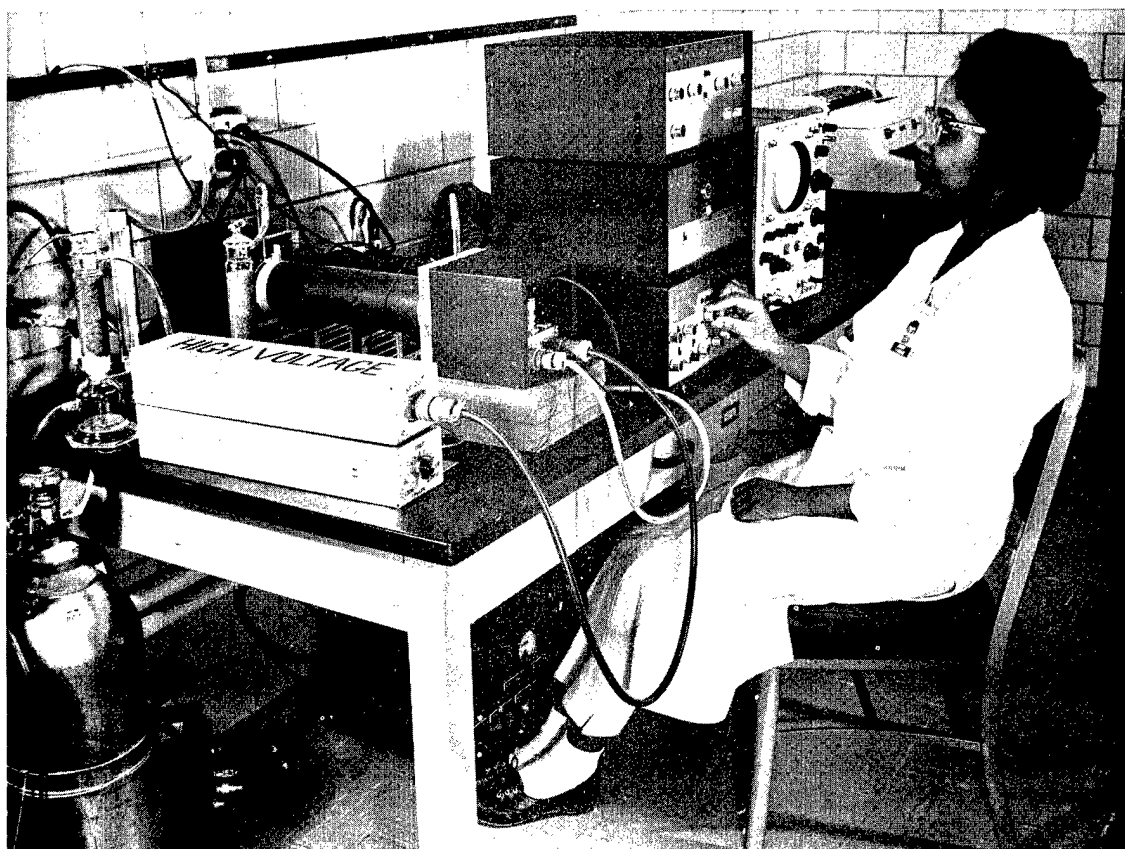


Fig. 9. Paper-Walled Proportional Counter for the X-ray Region

self-absorption correction is in progress. This correction has been found to be approximately linear with thickness and amounts to 30% for 10 mg/cm^2 .

Results of a Szilard-Chalmers experiment for a sample inside the synchrotron donut are included in Table XXVI where they are compared with an earlier experiment with an external target. Apparently, the high radiation flux causes the $\text{Co}^{58\text{m}}$, which had undergone the Szilard-Chalmers recoil process, to reform the target complex. Since one of the purposes of the investigation is to evaluate the reforming of the target complex by thermal processes, it appears that it will be necessary to employ external irradiations with their lower intensities.

Table XXVI

Fraction of $\text{Co}^{58\text{m}}$ Activity Found in Various Fractions of a Sample of $[\text{Co}(\text{en})_3](\text{NO}_3)_3$ Following the (γ, n) Process

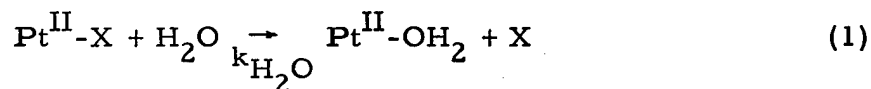
Fraction	Internal Target	External Target
$\text{Co}^{\text{II}}[\text{Pptd. as Co}^+(\text{OH})_2]$	11%	51%
$[\text{Co}(\text{en})_3]^{+++}$	67%	21%
Other	$18 \pm 5\%$	27%

Recently, it has been found that the Co^{58} activity can be counted with a newly acquired 3-in. well-crystal. Although the intensities are much lower, the long half-life of 72 days permits counting of the 0.80 Mev γ -ray with statistics comparable to that for the $\text{Co}^{58\text{m}}$. In this case the counting samples can be prepared more readily and self-absorption is not a serious factor.

7. ISOTOPIC EXCHANGE AND SUBSTITUTION REACTIONS FOR PLATINUM(II) COMPLEXES (D. S. Martin, Jr.)

A careful and thorough study of the kinetics and equilibria for the substitution reactions of chloride ligands in the chloride-ammonia complexes of platinum(II), which has extended during the past several years, is continuing. These complexes possess the interesting square planar configuration for ligands and their reactions are exceptionally slow. The use of isotopic tracers has made it possible to determine the rate of halide replacement by itself, and it has also been possible to assess the very important role of hydrolysis in the substitution reactions. The series of complexes is extensive enough that the systematics demonstrating the effect of structural parameters are now appearing. In particular, the results have indicated some interesting consequences upon the widely discussed trans-effect. The synthesis of a number of the compounds is difficult; and even though many of them were originally reported in the nineteenth century, the attainment of sufficient purity and the establishment of criteria for purity have been continuing problems.

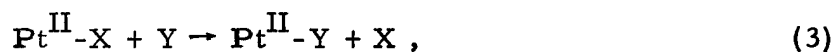
For the acid hydrolysis reaction of these complexes,



the rate is generally given by the expression:

$$\text{Rate} = k_{\text{H}_2\text{O}}[\text{Pt}^{\text{II}}\text{-X}]. \quad (2)$$

In many instances for a general substitution reaction,



the rate expression applies,

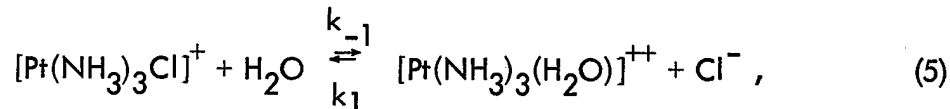
$$\text{Rate} = k_1[\text{Pt}^{\text{II}}\text{-X}] + k_y[\text{Pt}^{\text{II}}\text{-X}]\text{Y}. \quad (4)$$

The rate contains a term which is independent of the concentration of the entering ligand as well as the expected second order term. In a number of cases the rate constant of acid hydrolysis has been measurable and generally k_1 has equaled k_{H_2O} within the accuracy of measurements. The first term in Eq. (4) occurs because an initial acid hydrolysis is followed by a rapid replacement of H_2O by Y.

From recent results it is clear that OH^- is a very weak nucleophilic agent for these complexes and the replacement of Cl^- by OH^- involves first the attack by H_2O . It is possible for NH_3 to compete with H_2O for the replacement of chloride, and at moderate concentrations of NH_3 it appears the two reactions have comparable rates. Once an H_2O has replaced a chloride, the resulting acidic proton of the H_2O ligand is neutralized by OH^- to yield the hydroxo-complex. NH_3 is ineffective in the replacement of OH^- . In sufficiently acid solutions to permit the presence of appreciable aquo-ligands the NH_3 concentration has been reduced by the formation of NH_4^+ , so there is no first term for the NH_3 substitution reactions. Chloride ion as a nucleophilic agent competes effectively with H_2O only in neutral molecules and positive ions.

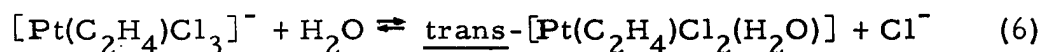
A manuscript, "Chlorotriammineplatinum(II) Ion. Acid Hydrolysis and Isotopic Exchange of Chloride Ligand", by F. Aprile and D. S. Martin, Jr., has been accepted for publication in Inorganic Chemistry. This paper was also presented at the National American Chemical Society Meeting in Chicago in September 1961.

Abstract--The acid hydrolysis of $Pt(NH_3)_3Cl^+$ has been shown to occur to a measurable extent. For this reaction:



the equilibrium quotient was measured at 25°C and 35°C. At 25°C the quotient was 8.4×10^{-5} at $\mu(\text{ionic strength}) = 0$ and 27×10^{-5} at $\mu = .318 \text{ M}$. This variation is consistent with the expected changes in activity coefficients. ΔH° for the reaction was found to be approximately 0. The rate constant, k_1 , was $2.6 \times 10^{-5} \text{ sec}^{-1}$ at 25°C, and it was nearly independent of ionic strength. The acid hydrolysis provides a mechanism for the exchange of the chloride ligand and Cl^- . Exchange experiments with Cl^{36} showed that in addition to the acid hydrolysis, a process, first order in both $[\text{Pt}(\text{NH}_3)_3\text{Cl}]^+$ and Cl^- , with a rate constant of $7 \times 10^{-5} \text{ sec}^{-1} \text{ M}^{-1}$ contributes to the exchange. The behavior of the entire series of chloroammines of platinum(II) toward acid hydrolysis and chloride exchange has been summarized, and a likely mechanism for the processes has been discussed.

An investigation of the kinetics of the isotopic exchange of the chloride ligands in trichloro(ethylene)platinate(II) with chloride ion has recently been concluded. This complex is of special interest since the ethylene, with its unusual situation in which the π -electrons form the bond to platinum, is so strongly "trans-directing" that the chloride trans to it is in labile equilibrium with respect to replacement by H_2O according to reaction (6).



However, the exchange of the chloride cis to ethylene occurs slowly; and the complex rate law was found to apply,

$$\begin{aligned} \text{Rate Exchange} = & k_1[\text{Pt}(\text{C}_2\text{H}_4)\text{Cl}_3^-] + k'_1[\text{Pt}(\text{C}_2\text{H}_4)\text{Cl}_2(\text{H}_2\text{O})] \\ & + k_2[\text{Pt}(\text{C}_2\text{H}_4)\text{Cl}_3^-][\text{Pt}(\text{C}_2\text{H}_4)\text{Cl}_2(\text{H}_2\text{O})]. \end{aligned} \quad (7)$$

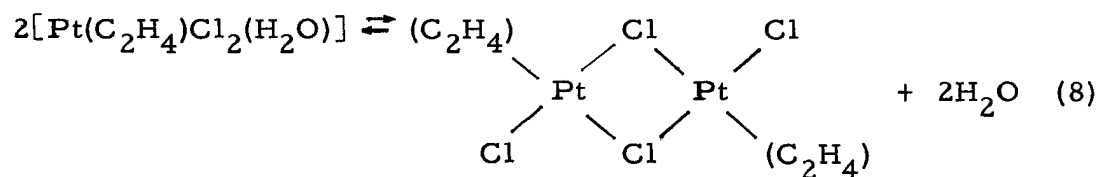
The observed rate constants are included in Table XXVII together with the indicated enthalpies and entropies of activation.

Table XXVII

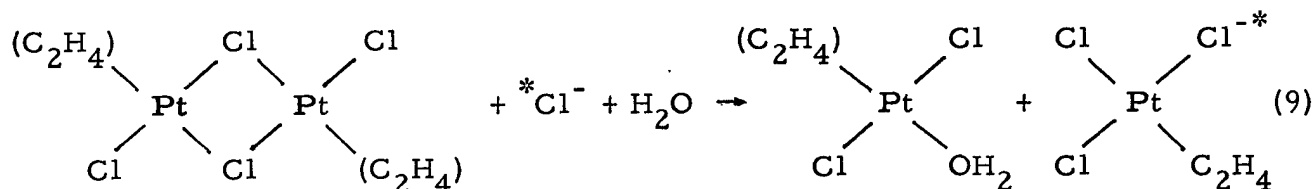
Rate Constants for the Exchange of the Cis-Chloride Ligands
with $\text{Cl}^- [\text{H}^+] = 0.142$ and $\mu = 0.318$

Temp.	k_1 $\times 10^5 \text{ sec}^{-1}$	k_1' $\times 10^5 \text{ sec}^{-1}$	k_2 $\times 10^5 \text{ sec}^{-1} \text{ M}^{-1}$
15°C	0.083	0.69	280
25°C	0.29	2.8	860
35°C	0.97	9.2	2600
ΔH^\ddagger kcal	21	22	19
ΔS^\ddagger e.u.	-13	- 4.5	- 2.3

The first two terms of (7) can be attributed to acid hydrolysis processes of the respective species. The magnitude of k_1 however is an order of magnitude smaller than the constants for the acid hydrolysis of eight other complexes, which have shown remarkably small variations. No term such as the third one in Eq. (7) has previously been found in this series, and it must correspond to a very unusual process. This term dominates under the majority of conditions tested. It indicates the formation of a dimer in the transition state. Thus as a first step the equilibrium could be rapidly established.



A second rate determining step could be,



The dimeric species proposed is the one which is formed readily in alcohol solutions of $\text{t-}[\text{Pt}(\text{C}_2\text{H}_4)\text{Cl}_2(\text{H}_2\text{O})]$ and which is well characterized. Apparently, the unique structure of the ethylene-platinum bond, which leads to its strong trans-directing effect, also promotes the formation and stability of the chloride-bridge dimers which undergo the ligand exchange. Some exploratory spectrophotometric experiments have indicated the equilibrium constant for reaction (8), is small, which would be required for the mechanism.

8. LIGAND FIELD THEORY OF SQUARE PLATINUM COMPLEXES (D. S. Martin, Jr.)

Report IS-342, "Energy Levels of Platinum II. Complexes on the Basis of Ligand Field Theory", by R. F. Fenske and D. S. Martin, was distributed. A manuscript, "Ligand Field Theory of Square Platinum(II) Complexes", by R. F. Fenske, D. S. Martin, Jr. and K. Ruedenberg, has been accepted for publication in Inorganic Chemistry.

Abstract--The energy spectrum resulting from the $5d^8$ configuration in a square-planar ligand field is calculated, using the point-dipole approximation, on the basis of a complete inner-configurational interaction, including spin-orbit coupling. The transition energies calculated for nine Pt(II) complexes are in good agreement with the observed spectra.

The ordering of the d-orbitals is found to be as follows: $d_{xz} = d_{yz} < d_z^2 < d_{xy} < d_x^2 - y^2$. The disagreement between this result and a previous proposal is discussed in detail. Tables for the weak-field and strong-field matrix elements are given.

A plot of the energy levels in terms of the ligand field parameter, the effect dipole moment, is shown in Fig. 10 for the case of zero spin-orbit coupling. The final treatment includes spin-orbit coupling. The comparison of the calculated and observed transition energies from the ultraviolet spectrum of platinum(II) complexes is shown in Table XXVIII.

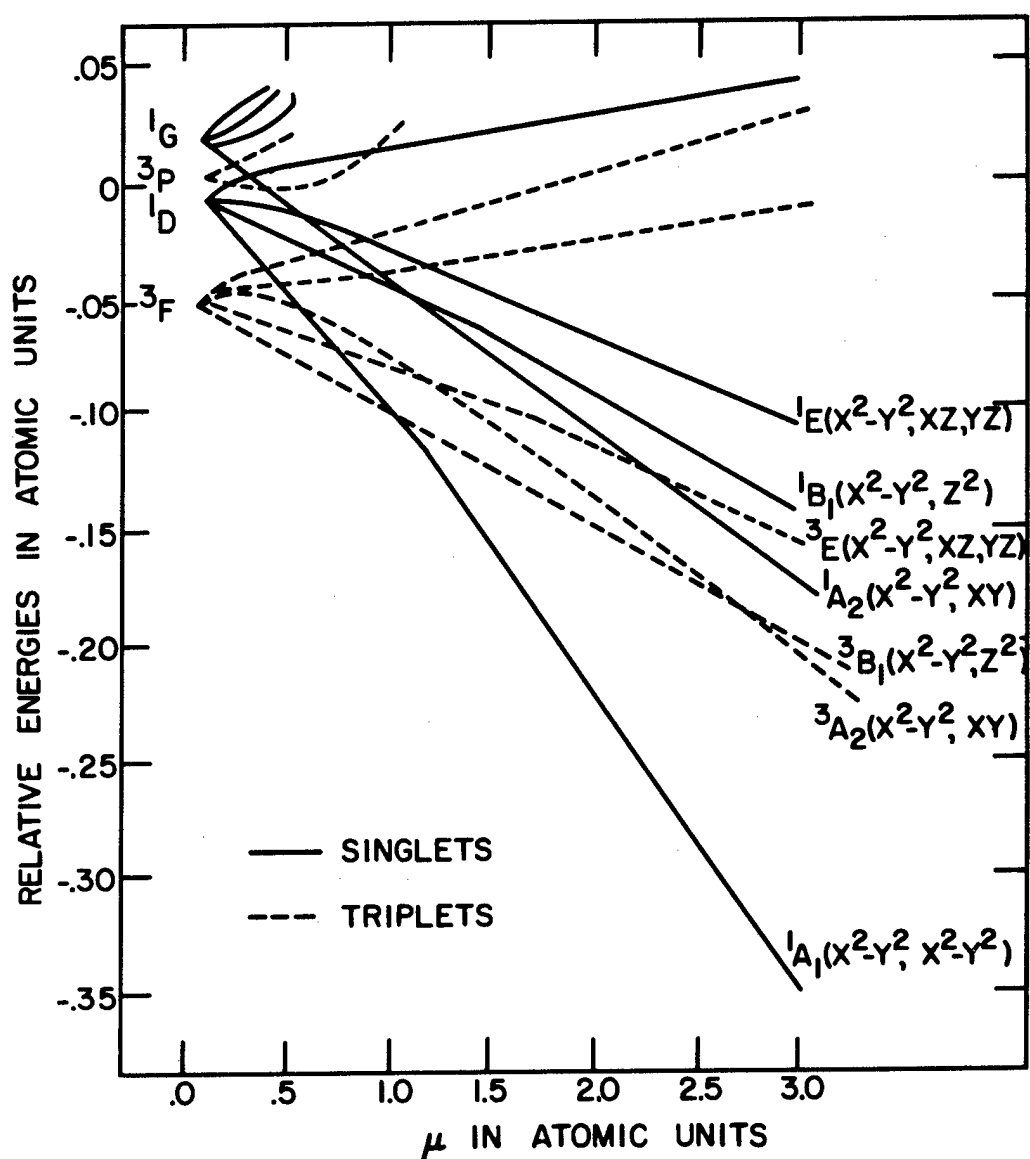


Fig. 10. Energy Levels of Pt(II)

Table XXVIII

Comparison of Final Transition Energies with Observed Spectral Maxima*

** Cmpd.	Peak 2 std. $1A_1 \rightarrow 1A_2$	Dipole moment (a.u.)	Peak 1 Obsd. $1A_1 \rightarrow 1B_1$	Calc. $1A_1 \rightarrow 1B_1$	Obsd. $1A_1 \rightarrow 3A_2$	Peak 3 Calc. $1A_1 \rightarrow 3B_1$
First Calculation†						
1	2.55	2.89	3.02	2.92	2.10	2.16
2	2.89	3.24	3.33	3.28	2.41	2.50
3	3.17	3.38	3.67	3.61	2.68	2.83
4	3.12	3.34	3.71	3.53	2.64	2.76
5	3.33	3.51	3.72	3.81	2.73	3.00
6	2.64	2.96	3.14	3.02	††	2.26
7	2.72	3.02	3.18	3.11	††	2.34
8	2.90	3.16	3.33	3.31	††	2.51
9	3.60	3.70	3.92	4.10	3.10	3.25
Second Calculation+						
5	3.33	2.74	3.72	3.68	2.73	2.80
9	3.60	2.92	3.92	3.99	3.10	3.16

* All results are in wave numbers $\times 10^{-4}(\text{cm}^{-1})$.

** The complexes are as follows:

1. $[\text{PtCl}_4]^{-2}$
2. $[\text{Pt}(\text{NH}_3)\text{Cl}_3]^{-1}$
3. t - $[\text{Pt}(\text{NH}_3)_2\text{Cl}_2]$
4. t - $[\text{Pt}\{(n\text{-C}_5\text{H}_{11})_2\text{NH}\}_2\text{Cl}_2]$
5. c - $[\text{Pt}(\text{NH}_3)_2\text{Cl}_2]$
6. $[\text{Pt}(\text{H}_2\text{O})\text{Cl}_3]^{-1}$
7. $[\text{Pt}(\text{OH})\text{Cl}_3]^{-2}$
8. $[\text{Pt}(\text{OH})_2\text{Cl}_2]^{-2}$
9. $[\text{Pt}(\text{NH}_3)_3\text{Cl}]^{+1}$

† Values for the parameters for Group I complexes are: $R = 2.34 \text{ \AA}$, $F_2 = 0.005488 \text{ a.u.}$, $F_4 = 0.000392 \text{ a.u.}$, $\alpha = 0.00942$.

†† Experimental values unknown.

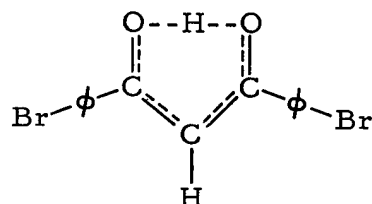
† Values for the parameters for Group II complexes are: $R = 2.20 \text{ \AA}$, $F_2 = 0.005488 \text{ a.u.}$, $F_4 = 0.000392 \text{ a.u.}$, $\alpha = 0.00942 \text{ a.u.}$

STRUCTURAL CHEMISTRY

1. STRONG HYDROGEN BONDING (R. E. Rundle)

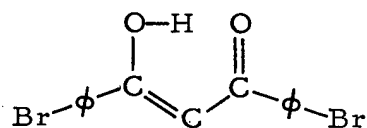
1.1 β -Diketones

Many β -diketones exist exclusively as enols in the solid state. As reported previously¹ bis(m-bromobenzoyl) methane is such an enol and the structure found for it provides strong evidence that in the enol ring there is complete resonance



so that the ring is symmetrical; the hydrogen bond is symmetrical and very short (2.47Å).

In this compound the molecule lies on a two-fold axis, and it is possible that an asymmetric structure



is being averaged over two orientations. Consequently, we have determined the structure of the bis(chlorobenzoyl)methane which is not isomorphous, but crystallizes in the general positions of the space group Pbc. No molecular symmetry is required in this space group and the chance of disorder averaging is remote. Nevertheless, the final structure is also symmetric with a short hydrogen bond. Bond distance comparisons of the two structures are shown in Table XXIX.

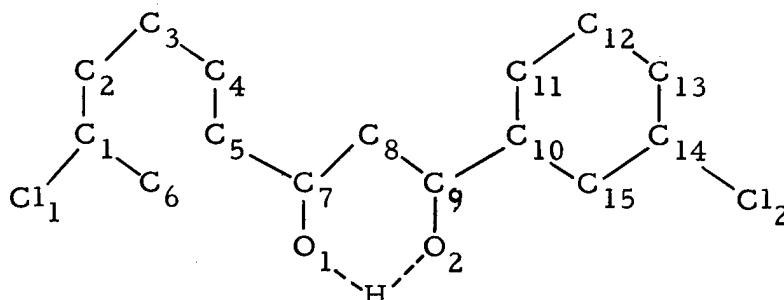
¹IS-350, Annual Summary Research Report in Chemistry, Ames Laboratory, 1960-61.

Table XXIX

Bond Distances in Bis(meta-chlorobenzoyl)methane from 3-D Data and Bromo

Atom Pair	Cl Compound Distance (Å)	Br Compound Distance (Å)
Br or Cl ₁ -C ₁	1.7389±.009	1.901±.007
C ₁ -O ₂	2.4674±.009	2.464±.015
C ₁ -C ₂	1.3937±.013	1.392±.009
C ₂ -C ₃	1.4253±.013	1.400±.009
C ₃ -C ₄	1.4134±.012	1.410±.008
C ₄ -C ₅	1.3972±.012	1.389±.010
C ₅ -C ₆	1.4041±.012	1.397±.010
C ₆ -C ₁	1.392 ±.011	1.375±.009
C ₅ -C ₇	1.4970±.012	1.457±.009
C ₇ -O ₁	1.2951±.011	1.306±.008
C ₇ -C ₈	1.4094±.011	1.393±.008
C ₈ -C ₉	1.3988±.010	
C ₉ -O ₂	1.3194±.010	
C ₉ -C ₁₀	1.4959±.011	
C ₁₀ -C ₁₅	1.359 ±.011	
C ₁₀ -C ₁₁	1.3635±.012	
C ₁₁ -C ₁₂	1.4233±.011	
C ₁₂ -C ₁₃	1.4293±.013	
C ₁₃ -C ₁₄	1.3485±.015	
C ₁₄ -C ₁₅	1.4123±.011	
C ₁₄ -Cl ₂	1.7297±.009	

Numbering of the molecule

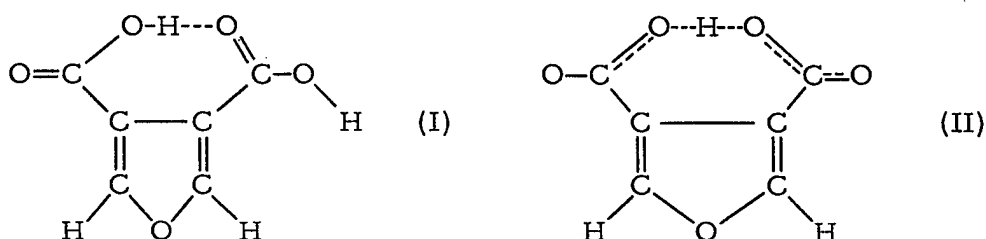


In the bromo compound the molecule is symmetric about C₈. Errors are standard errors.

Both structures are highly refined structures using scintillation counter data, full matrix least squares refinement with asymmetric thermal parameters for each atom. Standard deviations in bond distances reach a maximum of about 0.01 Å for both. Comparable distances in the two molecules agree surprisingly well; all differences are insignificant.

1.2 2,4-FURANDICARBOXYLIC ACID (R. E. Rundle)

Structural work has started on 2,4-Furandicarboxylic acid(I) and will be extended to the acid ion (II) where a strong and possibly symmetric hydrogen bond may be found. The acid, (I), crystallizes in space group P^2_1/m or $P2_1$, and a partially completed structure suggests that the crystal is held together in planes by a network of hydrogen bonds.



Compound II has been prepared as the sodium salt and will be studied during the coming year.

2. TRANSITION METAL COMPLEXES (R. E. Rundle)

2.1 Structure of Dimanganese Decacarbonyl

A paper, "The Crystal Structure of Dimanganese Decacarbonyl, $\text{Mn}_2(\text{CO})_{10}$ ", by Lawrence F. Dahl and Robert E. Rundle, has been submitted for publication in Acta Crystallographica.

Abstract-- $\text{Mn}_2(\text{CO})_{10}$ crystallizes with four molecules per unit cell in space group $I2/a$ with $\underline{a} = 14.16 \pm 0.02 \text{ \AA}$, $\underline{b} = 7.11 \pm 0.02 \text{ \AA}$, $\underline{c} = 14.67 \pm 0.02 \text{ \AA}$, $\beta = 105^\circ \pm 0.5^\circ$. The approximate structure was determined from two-dimensional data by a combination of the heavy atom and isomorphous-replacement techniques ($\text{Re}_2(\text{CO})_{10}$) (Dahl, et al., 1957). The structure has been refined to an R_1 value of 7.0% by the application of an anisotropic least-squares method to the three-dimensional data.

$\text{Mn}_2(\text{CO})_{10}$ consists of discrete molecules of approximately D_{4d} symmetry. Each manganese atom is octahedrally coordinated to five carbonyl groups and the other manganese atom in such a way that the equatorial carbonyl groups are arranged in a staggered configuration. The refined distance for the direct Mn-Mn bond is 2.923 \AA .

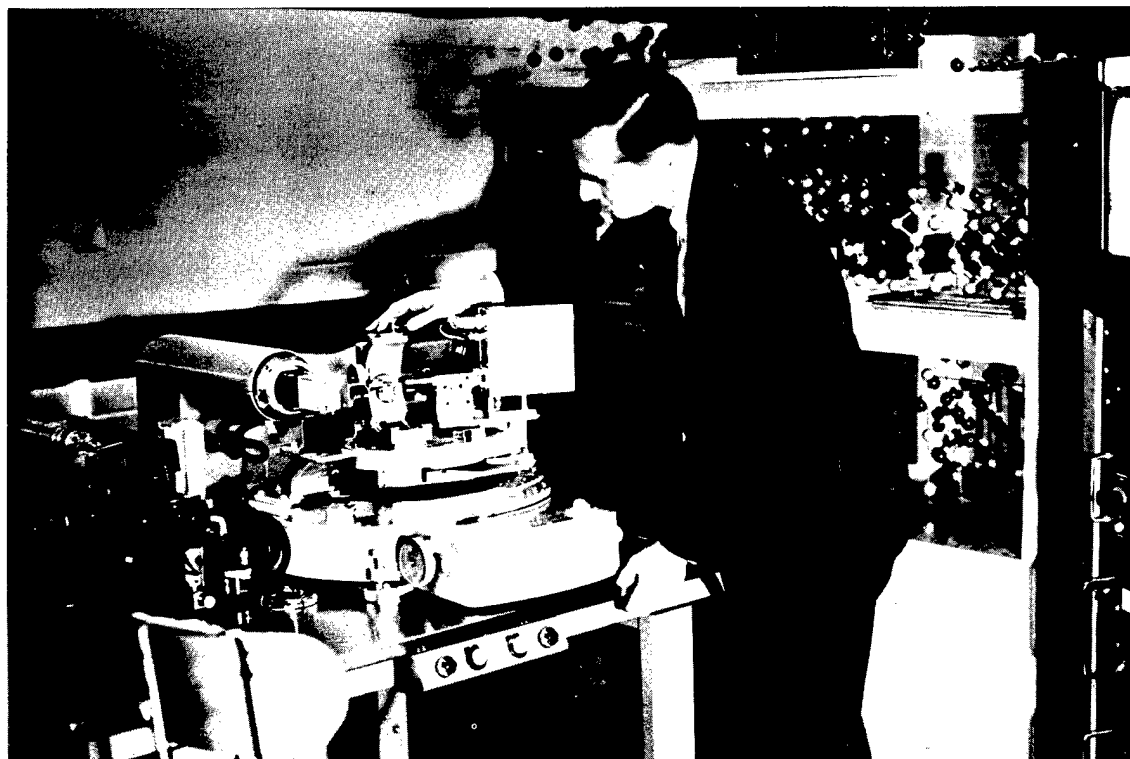


Fig. 11. X-ray Laboratory

2.2 The Structure of $C_{12}H_{12}V$

This compound was prepared by F. G. A. Stone at Harvard, and the method of preparation leaves the structural formula unknown. A preliminary structure has now been determined by x-ray diffraction.

$C_{12}H_{12}V$ forms orthorhombic, violet colored crystals. The space group is Pnma or Pn2a with lattice constants

$$a = 11.058 \quad b = 10.845 \quad c = 7.929 \text{ \AA}; \quad Z = 4.$$

Intensity data and Patterson projections suggest that Pnma is the correct space group, so that the molecules lie on mirror planes.

Tentative V and C positions have been obtained from Patterson projections and Fourier projections. The molecules seem to be $C_5H_5VC_7H_7$, with the vanadium atoms between planar or nearly planar five- and seven-membered rings. The compound is paramagnetic. Refinement is now underway on intensities from 1539 reflections collected by a G. E. counter spectrometer adapted for single crystals.

2.3 Magnetic Properties of Transition Metal Halides

The magnetic susceptibilities of $CuCl_2(s)$, $CrCl_2(s)$ and $KCuCl_3(s)$ have been examined to $\sim 1^\circ K$ by means of a mutual inductance bridge method. In all cases these apparently antiferromagnetic halides showed a rise in χ at very low temperatures, quite an unexpected result. In this very low temperature range, well below the apparent Néel temperature, $1/\chi$ vs T again becomes linear, approaching zero for a temperature very close to $T = 0^\circ K$.

We have noted that in all cases where we have seen this phenomenon, the metal atom is located at positions of no symmetry in the crystal,

and we suspect that a net moment arises in the otherwise antiferromagnetic crystal due to the influence of the interior magnetic field of the crystal which would generally destroy the perfect antiferromagnetic alignment if the metal atoms are not at points of symmetry.

3. COORDINATION NUMBER AND VALENCE (R. E. Rundle)

A paper, "Coordination Number and Valence in Modern Structural Chemistry", has been prepared for publication in "Record of Chemical Progress". In this paper structural work from the x-ray group in Ames and elsewhere has been taken to show that steric factors play an important role in determining coordination number, but that the final configurations found always obey the Lewis rare-gas rule except for transition metal complexes where valence orbitals are very well shielded sterically so that they are not available for bond formation.

The importance of using symmetry as a guide to the understanding of the bonding in molecules is pointed out. Some advantages of molecular orbital theory to valence bond theory depend upon the ready adaptability of the former to symmetry arguments.

LIST OF REPORTS AND PUBLICATIONS

1. REPORTS FOR COOPERATING LABORATORIES

- IS-214 Hiller, M. A. and J. E. Powell, Some Physical and Chemical Properties of Scandium and the Rare Earths.
- IS-215 Johnson, K. E. and G. S. Hammond, Kinetics of the Alkylation and Acylation of Nickel Dipivaloylmethide.
- IS-216 Saalfeld, F. and H. J. Svec, The Mass Spectrum of Stannane.
- IS-217 Valletta, Robert and A. H. Daane, Structures and Phase Equilibria of Binary Rare-Earth Metal Systems.
- IS-218 Matson, L. K. and F. H. Spedding, Further Studies in the Elution of Copper and Neodymium from a Cation-Exchange Resin with Ammonia-Ethylenediaminetetraacetic Acid Solutions.
- IS-219 Nelson, R. A. and F. H. Spedding, Some Thermodynamic Properties of Aqueous Solutions of Terbium.
- IS-220 Sellers, Irvin and F. H. Spedding, Temperature and Flow Rate Effects on the Ion-Exchange Separation of Erbium and Thulium.
- IS-262 Livingston, H. L. and D. E. Williams, Arc Melting in the Tungsten Electrode Furnace.
- IS-329 James, D. B. and J. E. Powell, Ion Exchange Elution Sequences with Chelating Eluants.
- IS-350 Ames Laboratory Staff, Annual Summary Research Report in Chemistry for July 1, 1960-June 30, 1961.
- IS-376 Wong, Kai Mow and A. F. Voigt, Activation Analysis for Rare Earths.
- IS-386 Saalfeld, F. E. and H. J. Svec, The Mass Spectra of Some Volatile Hydrides.
- IS-417 Csejka, D. A. and F. H. Spedding, Some Thermodynamic Properties of Aqueous Rare-Earth Chloride Solutions.
- IS-421 Levy, S. C., Some Properties of Rare-Earth Nitrilotriacetate Complexes.
- IS-470 Voigt, A. F., R. G. Clark, J. E. Gonser, G. J. Lutz and K. L. Malaby, Removal of Plutonium from Uranium by Molten Metal Extraction.

- IS-504 Conzemius, Robert Joseph and H. J. Svec, Analysis of Carbon Monoxide-Nitrogen Mixtures by High Resolution Mass Spectrometry.
- IS-510 Fellows, Wm. Dean and J. S. Fritz, Analysis of Mixtures of Alcohols by Acylation.

2. PUBLICATIONS

- Arthur, J. R., Jr. and R. S. Hansen, A Study of the Adsorption of Hydrogen, Ethane, Ethylene, and Acetylene on Iridium by Field Emission Microscopy. *J. Chem. Phys.* 36, 2062-2071 (1962).
- Banks, C. V. and S. Anderson, Nickel-Nickel Bond in Nickel Dimethylglyoxime. *J. Am. Chem. Soc.* 84, 1486 (1962).
- Banks, C. V., M. R. Heusinkveld and J. W. O'Laughlin, Absorption Spectra of the Lanthanides in Fused Lithium Chloride-Potassium Chloride Eutectic. *Anal. Chem.* 33, 1235-1240 (1961).
- Bartell, L. S. and D. Churchill, Polarimetric Determination of Absorption Spectra of Thin Films on Metal. I. Interpretation of Optical Data. *J. Phys. Chem.* 65, 2242-2247 (1961).
- Bartell, L. S., Kozo Kuchitsu and R. J. DeNeui, Mean and Equilibrium Molecular Structures of Methane and Deuteromethane as Determined by Electron Diffraction. *J. Chem. Phys.* 35, 1211-1218 (1961).
- Bruner, B. L. and J. D. Corbett, A Vapour-Pressure Study of the Solution of Antimony in Liquid Antimony (III) Iodide-The Formation of Sb_2I_4 . *J. Inorg. Nucl. Chem.* 20, 62-65 (1961).
- Duke, F. R., Acid-Base Reactions in Fused Alkali Nitrates. *J. Chem. Educ.* 39, 57-58 (1962).
- Duke, F. R., Complex Ions in Fused Salts. *Advances in the Chemistry of the Coordination Compounds*, 227-229 (1961).
- Duke, F. R. and H. M. Garfinkel, Complex Ions in Fused Salts. Cadmium and Lead Bromides. *J. Phys. Chem.* 65, 1627-1629 (1961).
- Duke, F. R. and G. Victor, Mechanism of Electrical Conductivity in Fused Salts. *J. Am. Chem. Soc.* 83, 3337 (1961).
- Evens, F. Monte and Velmer A. Fassel, Emission Spectrometric Determination of Oxygen in Niobium Metal. *Anal. Chem.* 33, 1056-1059 (1961).
- Fitzwater, D. R., Anisotropic Structure Factor Calculations. *Acta Cryst.* 14, 1242-1244 (1961).
- Foster, M. S., D. L. Weaver and A. F. Voigt, Photoproduction of Calcium-47. *Intern. J. Appl. Rad. Iso.* 12, 60-62 (1961).

- Fritz, James S., Janet E. Abbink and Marilee A. Payne, Naphthyl Azoxime S as a Complexometric Indicator. *Anal. Chem.* 33, 1381-1383 (1961).
- Fritz, J. S. and B. B. Garralda, Cation Exchange Separation of Metal Ions with Hydrobromic Acid. *Anal. Chem.* 34, 102-106 (1962).
- Fritz, J. S. and T. A. Palmer, Ion Exchange Separations Using Sulfo-salicylic Acid. *Talanta* 9, 393-397 (1962).
- Garfinkel, H. M. and F. R. Duke, Complex Ions in Fused Salts. Effect of Solvent Cation. *J. Phys. Chem.* 65, 1629-1630 (1961).
- Gerstein, B. C., F. J. Jelinek and F. H. Spedding, Correlation between Heat Capacity Anomaly in Tb and Magnetic Transition in Tb_2O_3 . *Phys. Rev. Letters* 8, 425 (1962).
- Hansen, Robert S., Diffusion and the Kinetics of Adsorption of Aliphatic Acids and Alcohols at the Water-Air Interface. *J. Colloid Sci.* 16, 549-560 (1961).
- Hansen, Robert S., Thermodynamics of Interfaces between Condensed Phases. *J. Phys. Chem.* 66, 410-415 (1962).
- James, D. B., J. E. Powell and F. H. Spedding, Cation Exchange Elution Sequences. I. Divalent and Rare-Earth Cations with EDTA, HEDTA and Citrate. *J. Inorg. Nucl. Chem.* 19, 133-141 (1961).
- Kamada, H. and V. A. Fassel, Emission Spectrometric Determination of the Gaseous Elements in Metals - VII. Nitrogen in Steels. *Spectrochim. Acta* 17, 121-126 (1961).
- Kivel, J. and A. F. Voigt, Gamma Radiolysis of Carbon-14 Labeled Isobutane. *Intern. J. Appl. Rad. Iso.* 10, 181-190 (1961).
- Kolat, R. S. and J. E. Powell, Acetate Complexes of the Rare-Earth and Several Transition Metal Ions. *Inorg. Chem.* 1, 293 (1962).
- Kopecky, K. R., D. Nonhebel, Gene Morris and George S. Hammond, Preparation of Dipivaloyl-methane. *J. Org. Chem.* 27, 1036-1037 (1962).
- Lang, C. E. and A. F. Voigt, Recoil Reactions of Carbon-11 in n-Hexane and Cyclohexane. *J. Phys. Chem.* 65, 1542-1546 (1961).
- Lunden, Arnold, Transport Numbers in Pure Fused Zinc Chloride. *J. Electrochem. Soc.* 109, 260-267 (1962).
- Mackey, J. L. and J. E. Powell, Determination of the Rare-Earth-HEDTA Stability Constants with the Mercury Electrode. *Inorg. Chem.* 1, 418-421 (1962).

- Mackey, J. L., J. E. Powell and F. H. Spedding, A Calorimetric Study of the Reaction of Rare-Earth Ions with EDTA in Aqueous Solution. *J. Am. Chem. Soc.* 84, 2047-2050 (1962).
- Mackey, J. L., M. A. Hiller and J. E. Powell, Rare-Earth Chelate Stability Constants of Some Aminopoly Carboxylic Acids. *J. Phys. Chem.* 66, 311-314 (1962).
- Marple, Leland W. and J. S. Fritz, Potentiometric Studies of the Titration of Weak Acids with Tetrabutyl Ammonium Hydroxides. *Anal. Chem.* 34, 796-800 (1962).
- Martin, D. S., Jr. and R. J. Adams, Trans-Dichlorodiammineplatinum(II). Acid Hydrolysis and the Isotopic Exchange of the Chloride Ligands. *Advances in the Chemistry of the Coordination Compounds*, 579-589 (1961).
- Mee, J. E. and J. D. Corbett, Titrimetric Determination of Gallium and of Gallium in the Presence of Aluminum. *Chemist-Analyst* 50, 74-76 (1961).
- Myklebust, R. L. and A. H. Daane, The Yttrium-Manganese System. *Trans. Met. Soc. AIME* 224, 354-357 (1962).
- Powell, J. E., The Separation of Lithium Isotopes by Ion Exchange. *J. Inorg. Nucl. Chem.* 24, 183-186 (1962).
- Ryan, T. D. and R. E. Rundle, The Crystal Structure of Ethylenediamine Tribromoplatinum ($C_2N_2H_8$)PtBr₃. *J. Am. Chem. Soc.* 83, 2814-2816 (1961).
- Saalfeld, F. E. and H. J. Svec, The Mass Spectrum of Stannane. *J. Inorg. Nucl. Chem.* 18, 98-102 (1961).
- Sutula, C. L. and L. S. Bartell, Structure and Molecular Orientation in Multimolecular Films of Long-Chain n-Hydrocarbon Derivatives. *J. Phys. Chem.* 66, 1010-1014 (1962).
- Tracy, J. W., N. W. Gregory, E. C. Lingafelter, J. D. Dunitz, H. C. Mez, R. E. Rundle, C. Scherlinger, H. L. Yakel, Jr. and M. K. Wilkinson, The Crystal Structure of Chromium(II) Chloride. *Acta Cryst.* 14, 927-929 (1961).
- Wolf, Edward D., Transport Numbers in Pure Fused Cesium Chloride. *J. Electrochem. Soc.* 108, 811-812 (1961).

IS-500

ANNUAL SUMMARY RESEARCH REPORT IN ENGINEERING

by

AMES LABORATORY ENGINEERING STAFF

F. H. Spedding, Director, L. E. Burkhart, G. Burnet, R. W. Fahien,
R. W. Fisher, G. Murphy, E. H. Olson, M. Smutz and D. R. Wilder

IS-500

ANNUAL SUMMARY RESEARCH REPORT IN ENGINEERING

For the period July 1, 1961 - June 30, 1962

This report is prepared from material
submitted by the group leaders
of this Laboratory

Previous research reports in this series are:

ISC-35	ISC-393
ISC-41	ISC-420
ISC-56	ISC-449
ISC-69	ISC-483
ISC-74	ISC-504
ISC-76	ISC-529
ISC-79	ISC-573
ISC-113	ISC-605
ISC-130	ISC-642
ISC-133	ISC-710
ISC-137	ISC-760
ISC-171	ISC-836
ISC-193	ISC-904
ISC-220	ISC-978
ISC-247	ISC-1051
ISC-274	ISC-1118
ISC-298	IS-16
ISC-320	IS-190
ISC-336	IS-348

CONTENTS

ENGINEERING

	<u>Chemical Engineering</u>	Page
1.	An Infrared Study of the TBP-HNO ₃ -H ₂ O Extraction System (M. Smutz).....	1
2.	Infrared Spectra Studies of Various Solutes in Organic Solvents (M. Smutz).....	2
3.	Separation of the Rare Earths by Solvent Extraction with Tri-butyl Phosphate (M. Smutz).....	4
4.	Fused Salt-Molten Metal Extractor Studies (L. Burkhart).....	5
5.	Extraction from Single Droplets during Drop Formation and Collapse (L. Burkhart).....	7
6.	Nuclear Magnetic Resonance Flowmeter (L. Burkhart).....	7
7.	Control of Nucleate Boiling Heat Transfer Equipment (G. Burnet)	8
8.	Corrosion Inhibition for the Lead-Bismuth Eutectic (G. Burnet) .	9
9.	Separation of Liquid Metals by Flash Distillation (G. Burnet)...	10
10.	Predicting Entrainment from a Bubble-Cap Tray (G. Burnet)...	12
11.	Turbulent Mass Transport in Liquids-Tube Flow (R. Fahien)...	12
12.	Turbulent Mass Transport in Liquid Systems-Packed Tubes (R. Fahien).....	14
13.	Momentum Transport in Packed Tubes (R. Fahien).....	15
14.	Turbulent Mass Transport in Gas Streams-Tube Flow (R. Fahien).....	15
15.	Quantum Effects in Calculation of Transmission Coefficients (R. Fahien).....	16
16.	Two-Phase Disperser Extractor (E. Olson).....	16
17.	Separation of Thorium and U-233 (E. Olson).....	18
18.	Growth of Single Crystals (E. Olson and M. Smutz).....	20
	18.1 Zinc.....	20
	18.2 Bismuth.....	20
	<u>Nuclear Engineering</u>	
1.	Slurry Program (G. Murphy).....	22
2.	Engineering Properties of Materials (G. Murphy)	23
	<u>Mechanical Engineering</u>	
1.	Electrical Resistivity Studies (R. Fisher)	24
	1.1 Thorium-Magnesium Eutectic.....	24
	1.2 Uranium-5 Wt% Chromium Alloy.....	25

Ceramic Engineering

1.	Self-Diffusion of Y_2O_3 (D. R. Wilder).....	28
2.	Emissivity of Refractory Oxides (D. R. Wilder).....	29
3.	Refractory Protective Coatings for Yttrium (D. R. Wilder).....	30
4.	Rare-Earth Oxide Applications in Ceramic Systems (D. R. Wilder).....	30
5.	Sintering Mechanism of the Refractory Oxides (D. R. Wilder)...	30
6.	Heat Capacity of Refractory Ceramics (D. R. Wilder).....	31

List of Reports and Publications

1.	Reports for Cooperating Laboratories	33
2.	Publications	33

CHEMICAL ENGINEERING

1. AN INFRARED STUDY OF THE TBP-HNO₃-H₂O EXTRACTION SYSTEM (M. Smutz* and P. Kinney)

A detailed infrared study on the systems TBP (tributyl phosphate), HNO₃, TBP-HNO₃, TBP-HNO₃-CCl₄, and TBP-HNO₃-H₂O coupled with phase distribution data support the following conclusions concerning the molecular interactions in the TBP-HNO₃-H₂O solvent-extraction system:

1. A strong TBP-HNO₃ complex forms by hydrogen bonding at the P=O site of the TBP. This conclusion is consistent with the phase distribution data and is established by the spectral changes observed. Such changes are the frequency shifts from 3480 to 2620 cm⁻¹ for the OH stretching mode of HNO₃, 1686 to 1653 cm⁻¹ for the NO₂ stretching mode, from 889 to 939 cm⁻¹ for the NO¹ stretching mode, and from 1283 to 1215 cm⁻¹ for the P=O stretching mode of TBP in the TBP-HNO₃-CCl₄ system. Parallel shifts were noted in the TBP-HNO₃ and TBP-HNO₃-H₂O systems. Bands due to the complexed acid could be easily identified by comparison with the spectra of the pure constituents and by their intensity variation with HNO₃/TBP ratio.

2. The excess HNO₃ past a 1/1 HNO₃/TBP ratio exists in solution by a mechanism of solubility of HNO₃ in the strong TBP-HNO₃ complex. Possible structures involving further complexing of acid with the TBP-HNO₃ complex at the ether linkages, at the P=O site, or at the HNO₃ oxygens are eliminated by the infrared results. The characteristic

*First name listed indicates group leader in charge of work.

absorption bands of the TBP-HNO₃ complex are unchanged in frequency or intensity by further addition of HNO₃ other than changes shown to be due to non-specific interactions or a "dielectric effect". The spectra of the excess acid is equivalent to the spectra of free HNO₃ or to a free HNO₃-H₂O solution depending on the system.

3. The phase distribution data indicate that two mechanisms are important in the extraction of water. The first mechanism is the formation of a weak TBP-H₂O complex with free TBP; the second mechanism is that of simple solubility of H₂O in the strong TBP-HNO₃-free HNO₃ solution. The infrared results of the system TBP-H₂O and TBP-HNO₃-H₂O are consistent with this interpretation. The net effect of these two mechanisms is that the initial displacement of H₂O from the weak TBP-H₂O complex by HNO₃ causes a decrease in the water content of the organic phase. However, the increasing solubility of H₂O in the strong TBP-HNO₃-free HNO₃ solution causes the water content to rise after going through a broad, non-zero minimum in the region of a 1/1, HNO₃/TBP mole ratio.

2. INFRARED SPECTRA STUDIES OF VARIOUS SOLUTES IN ORGANIC SOLVENTS

(M. Smutz and E. Nadig)

An extensive infrared spectra investigation of various solutes in various organic solvents was made. Most of the work involved tributyl phosphate and tri-n-octyl phosphine oxide as solvents. Band assignments were made for all the spectra.

The addition of a solute to these solvents causes a shift of the P→O stretch band to lower frequencies. This indicates the attachment

of the solute to the phosphoryl oxygen. In all cases, the existence of a single complex was indicated.

In tributyl phosphate, no indication of an attachment of the solute to the oxygen of the P-O-C bond is given. The P-O-C stretch remains at the same frequency on the addition of the solute.

The infrared spectra of the various nitrates in tributyl phosphate and tri-n-octyl phosphine oxide indicate that they are of the following structure: $M \leftarrow O-N \begin{array}{c} \diagup O \\ \diagdown O \end{array}$.

For each solvent, an essentially linear relation was obtained between $P \rightarrow O$ stretch frequency shift and the ionic potential (charge of cation/ionic radius of cation) of the solute. It would be expected that the higher the ionic potential of the solute the stronger the bond formed between it and the solvent. From theoretical considerations the shift is interpreted as indicative of the strength of the complex formed, possibly quantitatively. The correlation of $P \rightarrow O$ shift and ionic potential is consistent with these viewpoints.

For each solvent, an essentially linear relation was obtained between $P \rightarrow O$ stretch frequency shift and the amount of "covalence" of a nitrate as measured by the frequency difference $\gamma_4 - \gamma_1$. Although the assignment of an amount of "covalence" to a nitrate based on the frequency difference $\gamma_4 - \gamma_1$ may not be justified, the correlation of $P \rightarrow O$ stretch frequency shift with $\gamma_4 - \gamma_1$ is consistent with the fact that covalent solutes are extracted better than ionic solutes.

For tributyl phosphate an essentially linear relation exists between $P \rightarrow O$ stretch frequency shift and grams of extractable species per 100 grams of complex with two exceptions: ferric chloride and ferric nitrate. Grams of extractable species per 100 grams of complex can be represented

as $m_1/m_1 + m_2(100)$, where m_1 = molecular weight of the solute and m_2 = the number of tributyl phosphate molecules attached to the metal multiplied by the molecular weight of tributyl phosphate. This relationship represents a reasonably reliable means of estimating the number of tributyl phosphate molecules in a complex.

3. SEPARATION OF THE RARE EARTHS BY SOLVENT EXTRACTION WITH TRIBUTYL PHOSPHATE (M. Smutz and B. Sharp)

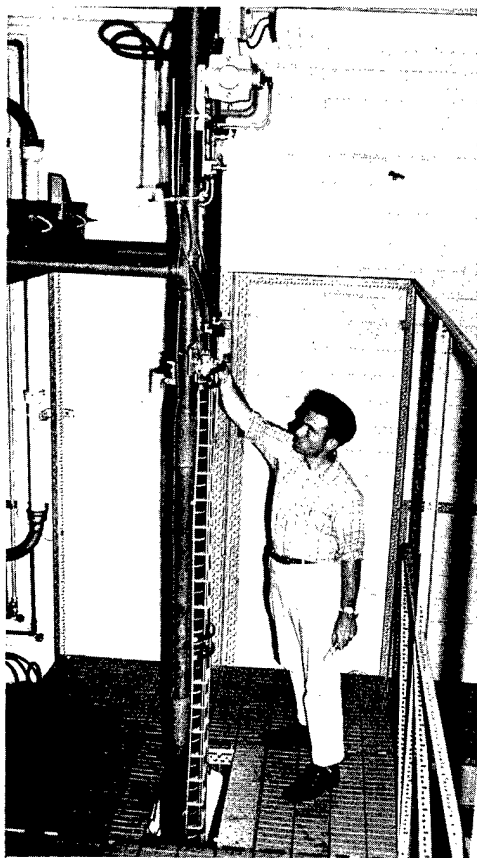


Fig. 1. Pulse extraction column.

An 80-plate pulse extraction column 3 in. in diameter was designed, erected and tested. Runs were made with the system kerosene and water and the system sodium nitrate-nitric acid-water-tributyl phosphate to estimate the range of operating conditions possible with the extractor. A test run made with rare-earth nitrate as feed indicated that no diluent will be required when tributyl phosphate is used as the solvent. At

this time it is not possible to indicate the number of theoretical stages obtainable with this system.

As yet, it has not been possible to develop a method of predicting solvent extraction equilibria for the general system of rare-earth nitrates-nitric acid-tributyl phosphate. Such relationships have been worked out with a few systems containing three solutes although the correlations are empirical. We anticipate developing a general correlation from a better understanding of several simple systems.

4. FUSED SALT-MOLTEN METAL EXTRACTOR STUDIES (L. Burkhart and R. Felt)

Initial tests with a mercury-water system have been completed on a low temperature fused salt-molten metal extraction unit shown in Fig. 2. Metal drops of remarkably uniform size can be produced by the rotating cups which collect and redisperse the discontinuous metal by forcing it through holes at the periphery of the cups. Since the column is made of glass and is surrounded by a hot-air bath encased in thermopane glass, the drop size can be measured photographically. Another method which has been developed, however, is to immerse a sampling probe covered with a sticky material into the top of the column, remove those drops which stick to the probe, and measure them directly. This sampling technique permits accurate measurement of both interfacial area and interstage concentration. An additional sampling port draws metal samples from each rotating cup into a sampler located inside the central rotating shaft.

The unusual sampling techniques developed can be used to provide detailed information on dynamic conditions in a fused salt-molten metal extractor. Equilibrium data have been completed on the $(\text{Na}, \text{K}, \text{Li})\text{NO}_3$ -Ca-Hg system which will be used next in the extractor.

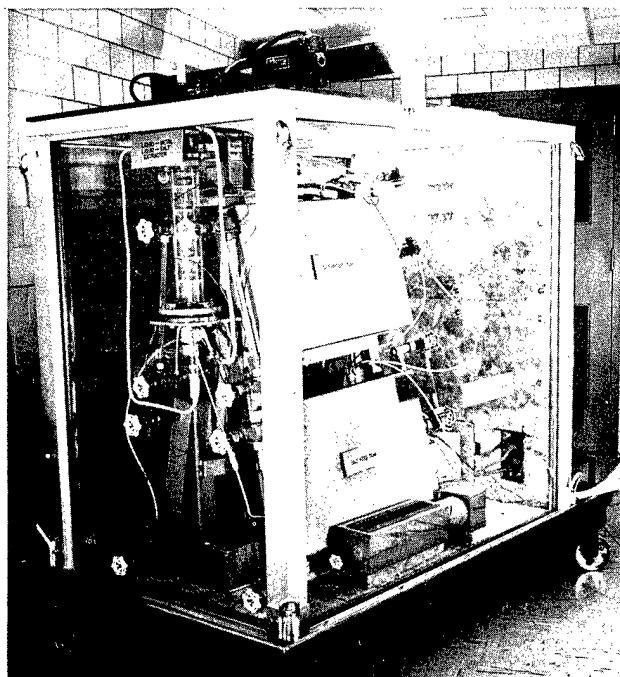


Fig. 2. Fused salt - molten metal extractor.

A summary of earlier work on the fused salt-molten metal extractor was published in an article entitled "A Fused Salt-Molten Metal Extractor" by P. R. Josephson and L. E. Burkhart in Trans. Am. Nuc. Soc. 4, 352 (1961).

Abstract--A multistage, counter-current extractor was developed and tested for use with fused salt-molten metal systems. The extractor was a modified disc and doughnut type constructed of type 316 stainless steel. Metal phase entered the top distributor, an inverted cone with holes at the base of a peripheral rim. When the cup was rotated, metal droplets flowed through the holes, down through the continuous salt phase, and were directed into the next distributor by a conical baffle. The extractor had three mechanical stages. For the system (KCl-ZnCl) - (Cd) - (Bi), stage efficiencies up to 37% were obtained.

5. EXTRACTION FROM SINGLE DROPLETS DURING DROP FORMATION AND COLLAPSE (L. Burkhart and J. Golden)

Mass transfer rates from large single drops are being studied as a function of time of formation and collapse of the drop. Previous results have been somewhat doubtful because the changes in mass transfer rates measured have been of the same magnitude as the experimental error involved. Equipment was designed to form and collapse drops at pre-determined rates. Initial results have shown that changes in mass transfer rates greater than the experimental error can be achieved for the system mineral oil-propionic acid-water with drops of 1.0-5.0 ml in volume and drop formation times of 10-30 sec. Automatic control devices to be added to the unit will permit accurate measurement of smaller formation and collapse times. The basic importance of the work lies in a study of mass transfer across a changing interfacial area.

6. NUCLEAR MAGNETIC RESONANCE FLOWMETER (L. Burkhart and D. Arnold)

A new type of flowmeter has been designed which operates on the principle of nuclear magnetic resonance. The unit measures the change of absorption amplitude of a nuclear magnetic resonance signal when flow occurs. The system is designed initially to handle flow rate measurement of fused salts but should be useful for measuring flow rates of other corrosive materials.

In a preliminary experiment, an aqueous solution of manganese chloride was allowed to flow through an NMR unit. Two effects of flow were observed:

- 1) If the repetition of double pulse groups is at a shorter interval than T_1 , an echo pulse was observed whose amplitude was increased to a maximum

by flow; 2) If the double pulse repetition rate is longer than T_1 the maximum echo pulse amplitude was observed with a reduction of amplitude as flow started.

Each one of these phenomena might be used to measure flow rate independently. In the first case, the volume flow rate $h = V_e/t_m$, where V_e is the volume of fluid within the effective area of the receiving coil, and t_m is the minimum time interval between double pulse groups (less than T_1) at which the maximum amplitude echo is observed. A complete flow meter system has been designed and is being constructed.

7. CONTROL OF NUCLEATE BOILING HEAT TRANSFER EQUIPMENT (G. Burnet and B. Breen)

Boiling is important in many material processing operations and in some nuclear reactors. Large heat fluxes can be obtained where nucleate boiling exists. However, due to hydrodynamic limitations there is a maximum nucleate boiling heat flux, and a corresponding temperature difference. Film boiling develops at higher temperature differences and a large drop in heat flux results.

The purpose of this project is to explore a method of determining continuously the approach to peak heat flux by measuring the change in slope of the boiling curve (ΔT vs heat flux). The continuity of this change in slope is presently being studied from both the experimental and theoretical viewpoints. An experimental boiling apparatus has been built and several boiling tube and thermocouple designs tested. The electronic and passive electrical networks to be used in differentiating the heat flux signal have been designed.

8. CORROSION INHIBITION FOR THE LEAD-BISMUTH EUTECTIC (G. Burnet and S. Stachura)

It has been confirmed that Zr in concentrations as low as 50 ppm is effective in controlling corrosion when the lead-bismuth eutectic is contained in low alloy steel (2 1/4% Cr - 1% Mo). Inhibition results from the formation of a film of zirconium nitride on the surface of the steel. A thermal convection loop (Fig. 3) has been in operation for 7,280 hr at temperatures from 300-700°C. Frequent spectrographic analysis of the circulating eutectic has failed to show the presence of corrosion products.

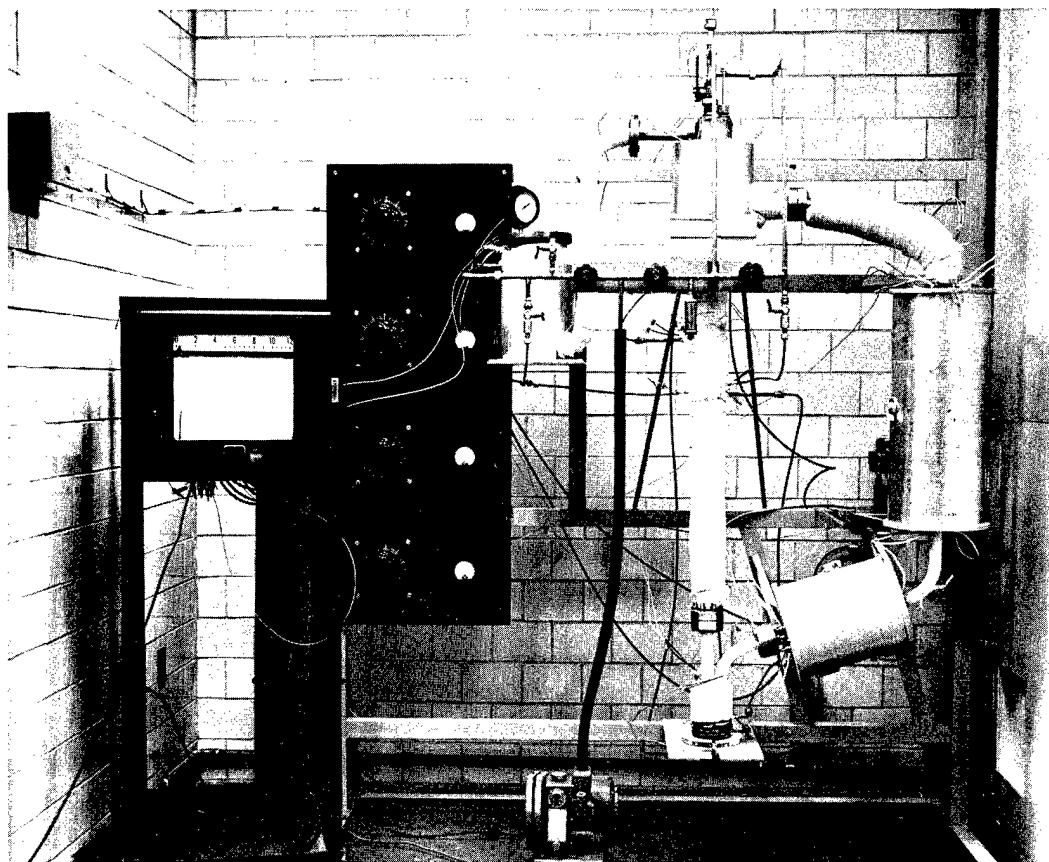


Fig. 3. Thermal convection loop used for corrosion studies.

A report (IS-316) entitled "The Lead-Bismuth Eutectic" by S. J. Stachura and G. Burnet was distributed.

Abstract--This paper is a review of the information available on the liquid lead-bismuth eutectic. It includes a compilation of physical, thermodynamic and nuclear properties and a discussion of corrosion inhibition and handling of the eutectic with particular reference to the work which has been done at the Ames Laboratory in these areas.

A paper entitled "The Lead-Bismuth Eutectic as a Heat Transfer Medium" by S. J. Stachura and G. Burnet has been submitted for presentation at the Annual Meeting of the American Institute of Chemical Engineers, Chicago, December, 1962.

Abstract--Information available on the heat transfer properties of the lead-bismuth eutectic are reviewed and compared to those of other high-temperature heat transfer media. New work reported deals with corrosion, corrosion inhibition and handling of the eutectic in heat transfer systems.

9. SEPARATION OF LIQUID METALS BY FLASH DISTILLATION (G. Burnet and D. Westerheide)

A flash distillation chamber with integral condenser has been constructed and is now being installed in a forced convection loop which will circulate to the chamber a superheated liquid metal mixture. The Pb-Bi eutectic will serve as the non-volatile component, with cadmium as the volatile. A polarographic method for the analysis of Cd in the presence of Pb and Bi has been developed.

Components of the forced convection loop (type 446 stainless steel), are shown in Fig. 4, and were tested during a 5,300 hr run. Corrosion at the walls was not severe but fractures of the stress corrosion type

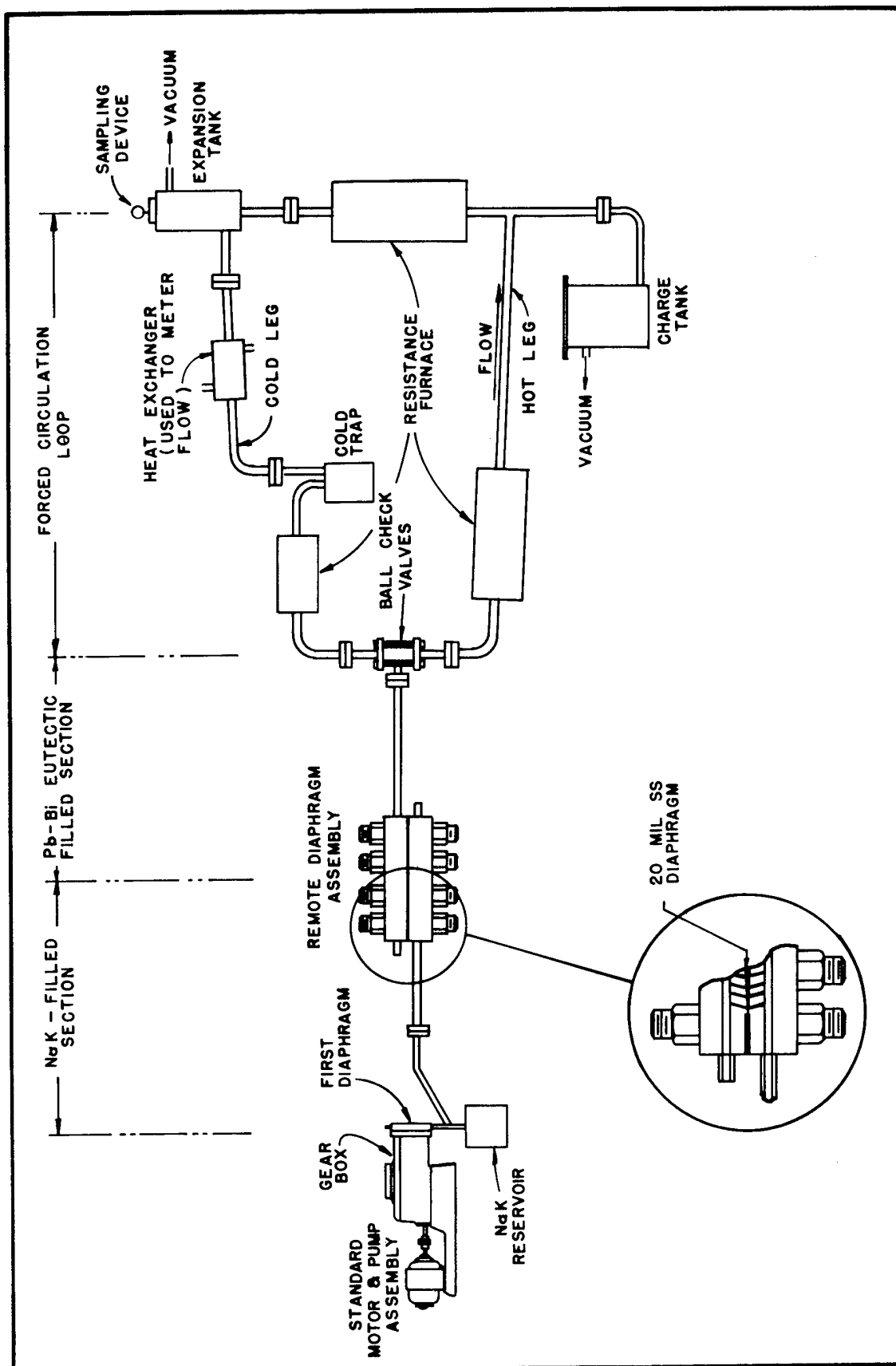


Fig. 4. Forced convection loop used for corrosion and loop component design studies.

were encountered. The satisfactory use of a diaphragm pump in the loop represented a new application for this type of pump.

A paper entitled "A Diaphragm Pump for Liquid Metal Service" by D. E. Westerheide, J. C. Clifford and G. Burnet has been submitted for publication in Nuclear Science and Engineering.

Abstract--The construction and operation of a diaphragm pump for liquid metal service is described. Centrifugal and electromagnetic liquid metal pumps are briefly reviewed. From the results of a 5300-hr test of the diaphragm pump, it is concluded that a diaphragm pump is well suited to the pumping of liquid metals at low flow rate where pulsating flow can be tolerated.

10. PREDICTING ENTRAINMENT FROM A BUBBLE-CAP TRAY (G. Burnet and G. Quentin)

Entrainment rate was studied as a function of vapor properties, velocity, density and viscosity, and tray spacing to develop an improved parameter for correlation of entrainment. A parameter, compounded from three separate vapor groups, was developed which provided an excellent linear correlation of entrainment rate for the four tray spacings investigated. When extended to data of other investigators, the correlation gave fair to excellent results. Further work to confirm the validity of the correlation is required.

11. TURBULENT MASS TRANSPORT IN LIQUIDS-TUBE FLOW (R. Fahien and A. Konopik)

An analytical solution has been obtained for the partial differential equation describing the radial, angular, and axial turbulent diffusion of a tracer issuing from two side injector sources into a stream flowing through a tube. In this solution, the nine off-diagonal components of the eddy diffusivity tensor were neglected while the diagonal components

and the velocity were assumed independent of radial position. Results were obtained for various relative values of the diffusivities. These results indicate that angular diffusion can have a significant effect in determining the concentration profiles in process systems. Experimental apparatus has been designed for measuring these concentration profiles. A mathematical method has been proposed for numerically solving the partial differential equation to yield values of the nine components of the diffusivity tensor as a function of position in the tube. These results are to be compared with alternate turbulent diffusion models based on the interaction of velocity and concentration fluctuations.

A detailed report which covers this work (IS-419-thesis) entitled "Turbulent Mass Transfer in Liquid Streams" by R. C. Seagrave and R. W. Fahien was distributed.

Abstract--The total mass transfer diffusivity for turbulent pipe flow has been represented by a second order tensor with two significant components, the radial mass diffusivity and the axial mass diffusivity. These components have been determined as functions of radial position for three Reynolds numbers in the low turbulent range by making a study of the transient diffusion of a dye solution from a point source into water in turbulent pipe flow. Concentration data were obtained as a function of position and time. These data were combined with the results of a steady state experiment to compute the diffusivities from a second order linear partial differential equation. Two solution methods were used: a graphical derivative evaluation procedure, and a method which applies the LaPlace transform in both time and axial distance. Both methods produced two simultaneous ordinary differential equations which could be numerically integrated to produce the diffusivities.

Both the radial and axial diffusivity were found to vary with radial position. The variation of the radial component qualitatively resembles

the variation of eddy viscosity in the same system. The axial component was appreciable only in the central or core region of the stream. The average values of both components were found to increase linearly with Reynolds number. The diffusivities could be correlated as functions of position and Reynolds number by expressions which accounted for the effects of the velocity, the velocity gradient, and the boundary layer.

The ratio of axial diffusion to bulk flow was found to increase slightly with Reynolds number through the range studied. Eddy diffusion was about one hundred thousand times greater than molecular diffusion. Neglecting the contribution of axial diffusion produces smaller calculated values of the radial diffusivity.

The variation of the Peclet and Schmidt numbers in the system was similar. Both quantities decreased with increasing Reynolds number in the range. Although a rough analogy between mass and momentum transport existed, the diffusivities were generally not equal. The Schmidt number varied from a value less than one to a value greater than one across the tube radius.

It was found that the position Peclet numbers for both mass and momentum varied similarly with position Reynolds numbers. Both quantities increased near the wall, and approached values given by correlations which have been previously proposed for momentum quantities.

12. TURBULENT MASS TRANSPORT IN LIQUID SYSTEMS-PACKED TUBES (R. Fahien and W. Beckwith)

Representative calculations have been carried out to determine the conditions under which the effects of axial diffusion in packed columns are important with respect to radial diffusion. Similar calculations have indicated that one-dimensional models in which radial diffusion is described in terms of equivalent axial dispersion are subject to severe limitations and require drastic assumptions not met in practice.

Experimental work has been directed toward measurement of the fine structure of radial concentrations variations. Because of the low molecular diffusivity of liquids, extreme variations in concentration have been found to occur in liquid systems at low flow rates. These will be analyzed from the standpoint of obtaining average effects.

13. MOMENTUM TRANSPORT IN PACKED TUBES (R. Fahien and J. Frandolig)

An experimental method has been developed for obtaining information on pore geometry, fractional free area, and transfer surface for cylindrical tubes packed with materials of various shapes. A generalized model for predicting velocity profiles, average velocities and momentum loss in cross sections of arbitrary shape has been developed. An over-all macroscopic momentum balance has been written to describe form drag, friction drag, kinetic energy and their effects for arbitrary shapes. These results will be used in conjunction with a Monte Carlo calculation to compute the total pressure drop in beds of varying size and shape of packing.

14. TURBULENT MASS TRANSPORT IN GAS STREAMS-TUBE FLOW (R. Fahien and A. Bekelman)

A method is being developed for the measurement of carbon dioxide samples in an air stream by spark gap emission spectroscopy. This will permit the continuous measurement of concentration as a function of position within gaseous streams. From this information the eddy diffusivity tensor can be determined as a function of position.

15. QUANTUM EFFECTS IN CALCULATION OF TRANSMISSION COEFFICIENTS

(R. Fahien and R. Lantz)

The fraction of collisions in reaction can be calculated from quantum mechanics. This fraction is the energy distribution weighted with a transmission coefficient integrated over the energy range.

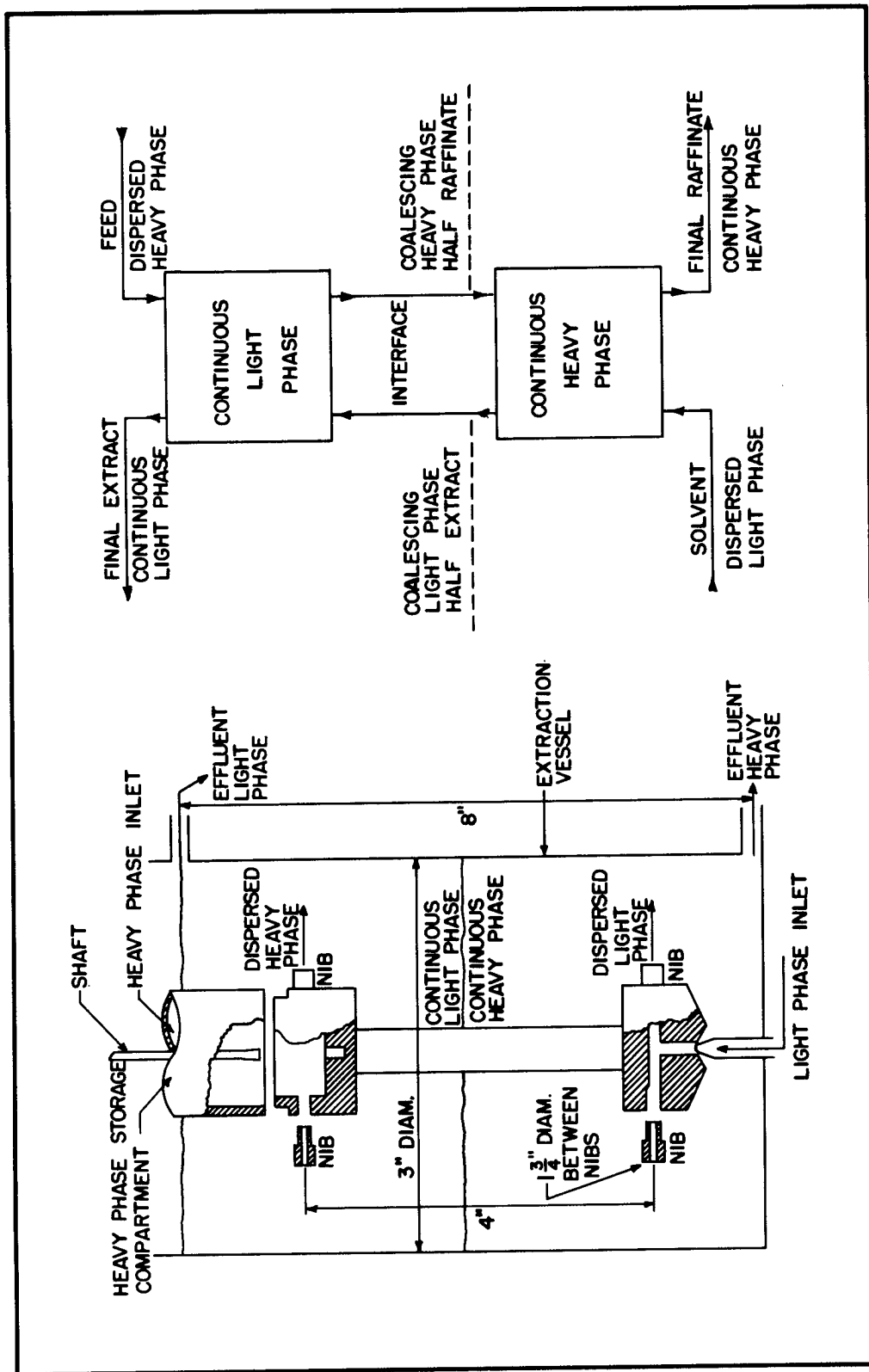
The purpose of this project is to provide a quantum mechanics basis for collision theory. Results will be compared to classical collision theory based on reaction rate kinetics.

A method has been developed for the numerical solution of the Schroedinger equation in order to calculate transmission coefficients as a function of energy for conditions in which quantum effects are important.

16. TWO-PHASE DISPERSER EXTRACTOR (E. Olson)

The two-phase disperser (TPD) extractor is a modified mixer-settler type in which the light and heavy phases are simultaneously dispersed in each other by the centrifugal motion of the dispersing unit. It is similar in operation to a combination of two ordinary mixer-settler stages within the same vessel. Figure 5a is a cut-away section view of the TPD; Fig. 5b is a process flow diagram showing the continuous light and heavy phases.

The TPD was found to be an efficient, highly compact extractor. At 100% extraction efficiency two equilibrium extraction stages would be the maximum attainable. For the system methyl isobutyl ketone-acetic acid-water system 1.3 to 1.8 equilibrium extraction stages were obtained depending on the operating conditions used. Similar efficiencies



a. Vertical section

b. Flow design

Fig. 5. The TPD extractor.

were obtained with the systems carbon tetrachloride-propionic acid-water and octyl alcohol-acetic acid-water. Extraction efficiency increased significantly with increased combined phase flow rate; the reverse is true in many other extractors. Extraction efficiency was lower for low solvent to feed (L/H) flow rate ratios, increasing and leveling off at the high L/H ratios. Speed of rotation had little effect on extraction efficiency above 500 rpm, provided all the liquids entered the system through the disperser nibs.

Disperser nib hole size affected both the extraction efficiency and total flow of the combined phases through the unit. Smaller diameter holes resulted in higher efficiencies but substantially lowered the pumping rate.

The solute concentration was relatively uniform throughout a particular continuous or dispersed phase. Interface level was found to have little effect on extractor efficiency provided the interface was maintained between the two sets of dispersing nibs.

The compactness and high extraction efficiency make possible application of the TPD to processes where space is at a premium or in which costly solvents or process materials are involved. Interface and flow rate control between units are problems requiring further investigation for multi-unit operation.

17. SEPARATION OF THORIUM AND U-233 (E. Olson)

This project is concerned with the development and testing of equipment, and determining the operating conditions required to separate fissionable U²³³ from the thorium in thorium blanket materials in

breeder reactors. The process currently being studied is a magnesium dissolution of thorium followed by separation of the Mg-35 wt% Th eutectic from the insoluble uranium. Investigations during this period have been on the time required for dissolution of thorium by magnesium, and corrosion testing to find suitable materials for containing the eutectic.

Thorium dissolution runs using molten magnesium to form the low melting Mg-35 wt% Th eutectic were made in 3-in. -diameter graphite crucibles in a system pressurized to 10 psig with purified argon. Three hundred grams of 99.9% purity thorium turnings approximately 0.08 in. thick by 0.1 in. wide, hydraulically pressed into a briquet 2 7/8 in. in diameter by 2 1/2 in. long were placed in the graphite crucible. The required amount of magnesium was then added and the system was heated to the corrosion test temperature. A vaned stirrer was used to facilitate the mixing and thorium dissolution. Samples of the magnesium phase were taken periodically and analyzed for thorium to determine when the thorium was completely dissolved. A summary of the results is shown in Table I.

Table I

Results of Magnesium-Thorium Dissolution Runs

Temp. °C	Stirrer Speed RPM	Dissolution Time (Min.)	Stirrer Material	Corrosion
750	200	90 - 120	Stainless Steel	Severe
750	400	20 - 30	Tantalum	None
900	400	5 - 10	Tantalum	None

Durichlor (a high silicon cast iron), Croloy (a high chromium stainless steel) and low carbon steel were corrosion tested in the eutectic

for 250 hr at 750°C. Corrosion of low carbon steel was found to be excessive; an initial wall thickness was reduced from 0.110 in. to 0.075 in. Corrosion was uniform with no deep pits or cracks noted. Durichlor and Croloy appeared to be quite corrosion resistant, from dimensional measurements and microscopic examination.

18. GROWTH OF SINGLE CRYSTALS (E. Olson, M. Smutz, R. Slonaker and I. Peterson)

18.1 Zinc

During this period the assembly of the large Bridgman-type crystal growing unit shown in Fig. 6, was completed and tested. The results are reported in IS-459, "Large Bridgman-Type Unit for Preparing Large and Small Diameter Single Crystals" by Robert E. Slonaker, Jr., Morton Smutz and Edwin H. Olson.

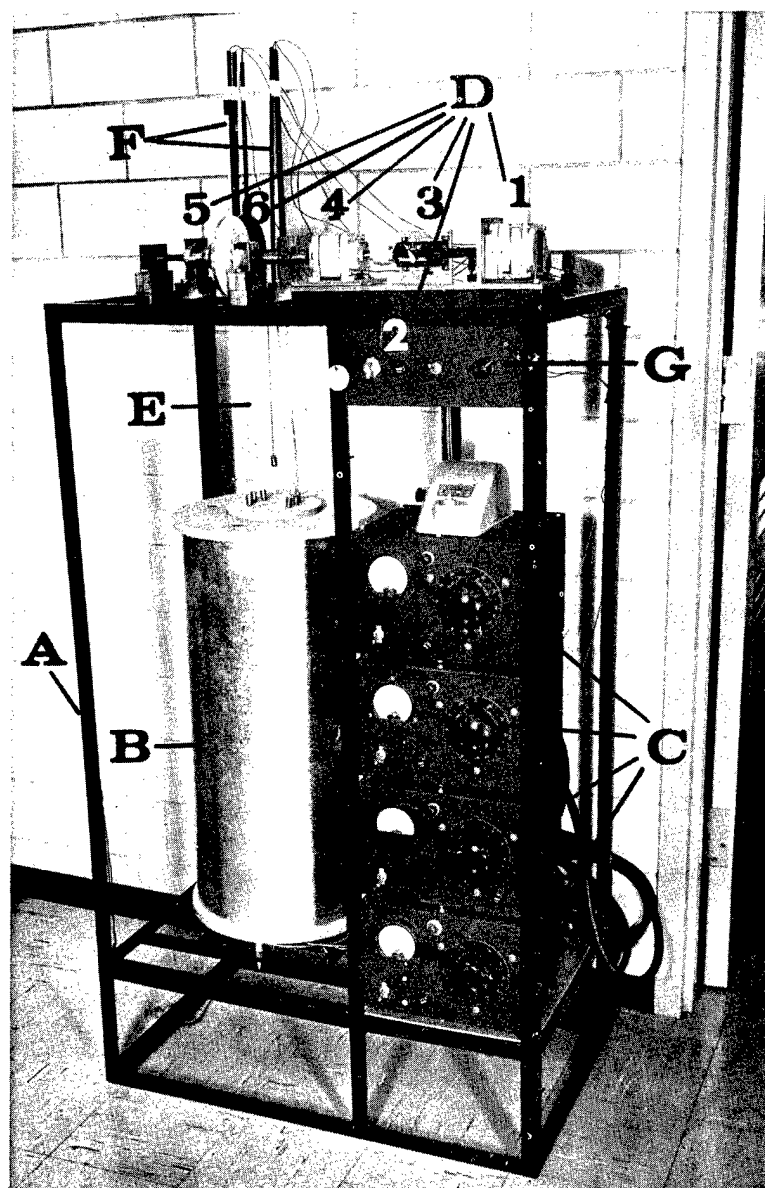
Abstract--The design and performance of a large, Bridgman-type single crystal growing unit is presented. Dimensioned drawings and photographs of the crystallizing crucibles, furnace and crystallizing crucible assemblies are included.

Preliminary tests were made with zinc of 99.99+ percent purity. It was demonstrated that single crystals of zinc 2 1/4 inches in diameter by 7 1/4 inches in length could be grown in graphite crucibles having 50 degree conical nucleating tips. It was also possible to grow seven single crystals 3/8-inch in diameter by 7 3/8 inches in length, simultaneously, employing the same operating conditions.

The unit is apparently adaptable to growing single crystals of many other materials that melt below 900°C, the temperature limit of the furnaces.

18.2 Bismuth

Bismuth single crystals 3 1/4 in. in length tapering from 0.6 in. in diameter at the top to 0.5 in. at the bottom and terminating in a



- | | |
|-----------------------------------|---------------------------------------|
| A . Angle iron frame | D. <u>Sample lowering assembly</u> |
| B . Furnace assembly | 1 - Motor |
| C . Powerstats | 2 - Motor control switches |
| E . Thermocouple wires | 3 - Variable speed changer |
| F . Thermocouple wire guide tubes | 4 - Speed reducer |
| G . Thermocouple selector switch | 5 - Sample lowering pulley |
| | 6 - Calibrated pulley (sample travel) |

Fig. 6. Large Bridgman-type crystallizing unit.

50 degree conical tip were grown by use of an alundum powder, soft mold technique.

Specific resistivity (ρ) measurements over a 1 1/2 in. length of each crystal were made. The ρ values ranged from a minimum of 111.06×10^{-6} ohm-cm for a crystal with an angle (θ) of 83 degrees between the "c" axis (111 axis of rhombohedral bismuth) and the sample axis to a maximum of 146.48×10^{-6} ohm-cm for a θ of 35 degrees. By plotting ρ vs θ for each of the 16 single crystals grown, it was found that ρ could be related to θ by the following equation:

$$\rho_{\theta} = \rho_{\parallel} \cos^2 \theta + \rho_{\perp} \sin^2 \theta .$$

By curve fitting, the parameters ρ_{\parallel} (ρ at $\theta = 0$ degrees) and ρ_{\perp} (ρ at $\theta = 90$ degrees) were found to be 163.03×10^{-6} ohm-cm and 112.01×10^{-6} ohm-cm, respectively.

Annealing the crystals was found to have no significant effect on resistivity.

NUCLEAR ENGINEERING

1. SLURRY PROGRAM (G. Murphy and R. Hendrickson)

The purpose of this project is to investigate the lift force developed on a spherical particle which is moving through a fluid medium. It has direct application to the behavior of a slurry, such as that in a slurry reactor, and is a part of the program of predicting conditions under which coring occurs in vertical flow of a slurry.

Extensive observations have been taken on the conditions leading to lateral movement of a particle which is moving longitudinally through a

tube. By inclining the tube, the lift acting on the particle may be evaluated. The magnitude of the lift has been correlated with significant parameters such as particle and tube size, particle and fluid densities, particle velocity, fluid viscosity, and surface condition of particle. Test results correlate within a few percent and a general equation is being developed from the data. Five dimensionless parameters are involved.

2. ENGINEERING PROPERTIES OF MATERIALS (G. Murphy, D. Sasscer and K. Pedersen)

The evaluation of the high temperature tensile properties of materials has continued with work on uranium and zirconium.

Specific numerical data have been obtained for yield strength, tensile strength, modulus of elasticity, percentage elongation and endurance limit at temperatures up to 750°C for uranium, sponge source zirconium and crystal bar zirconium. A report on uranium (IS-400) entitled "Effects of Temperature on Mechanical Properties of Normal Uranium Dingot" by Knud Pederson and Glenn Murphy was distributed.

The study of tensile creep has been devoted primarily to an evaluation of the activation energy for creep of aluminum and uranium. Extensive effort has been involved in developing and improving the strain indicating equipment and in reducing the temperature gradient along the test specimen. Preliminary specimens of bismuth have also been used, since studies of the effect of neutron irradiation on the creep of bismuth can be made in conjunction with the reactor of the Department of Nuclear Engineering.

Flexural creep testing of uranium has continued with the objective of predicting flexural creep characteristics with tensile creep behavior.

A cement has been found that will permit strain gages to remain active up to strains of 20,000 microinches. Analysis is being conducted concurrently with the experimental phase of the study.

MECHANICAL ENGINEERING

1. ELECTRICAL RESISTIVITY STUDIES (R. Fisher, D. Provow, D. Bluhm and R. Cash)

1.1 Thorium-Magnesium Eutectic

The electrical resistivity properties of polycrystalline 39 wt% thorium-magnesium eutectic were determined for the solid from room temperature to its melting point (589°C) and as a liquid from its melting point to 900°C. Figure 7 shows the electrical circuit which utilizes rapid, successive measurement of resistivity by reversing the direction of the current through the sample and minimizes the error caused by Seebeck effects.

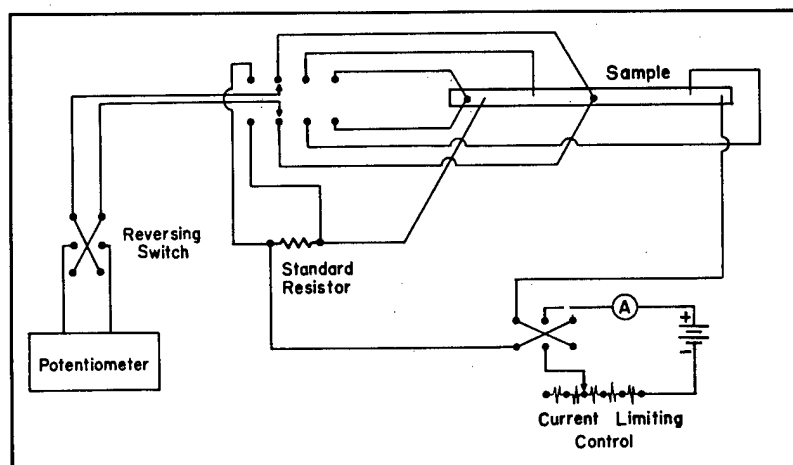


Fig. 7. Potentiometric circuit for measuring resistance.

Since magnesium and thorium react readily with most container materials at or above the melting point of the eutectic, tantalum tubing was used as the container after first determining its electrical resistivity for the temperatures and vacuum conditions employed. It was found that even in a

vacuum of 10^{-5} mm mercury at temperatures of 800-1000°C tantalum absorbs oxygen, resulting in a change in its electrical resistivity. The oxygen content on the original tantalum tubing was 150 ppm. After four runs in vacuum it contained 740 ppm oxygen. This change was taken into account in calculating the resistivity of the eutectic.

The resistivity values in one direction were averaged with those obtained by reversing the current. Resistivity data for the tantalum-clad solid bar fell within the range of experimental error when compared to data taken with the unclad solid bar.

The electrical resistivity curve is shown in Fig. 8. It is noted that the resistivity of the molten eutectic decreases as the temperature increases, similar to that reported for molten magnesium.

A detailed report (IS-437) by D. M. Provow and R. W. Fisher covering this work was distributed.

1.2 Uranium-5 Wt% Chromium Alloy

The electrical resistivity of the uranium 5 wt%-chromium alloy was determined using the same techniques and equipment employed for determining the resistivity of the thorium-magnesium eutectic.

Particular attention was given to pinpointing the temperature at the transitional changes. The rate at which the alloy was heated was reduced to 10°C per hour. Figure 9 shows the alpha to beta transition temperature to be $653^{\circ}\text{C} \pm 2^{\circ}$ and the beta to gamma transition to occur at $756^{\circ}\text{C} \pm 2^{\circ}$. These results are within the experimental error of values reported by Argonne National Laboratory for uranium metal.

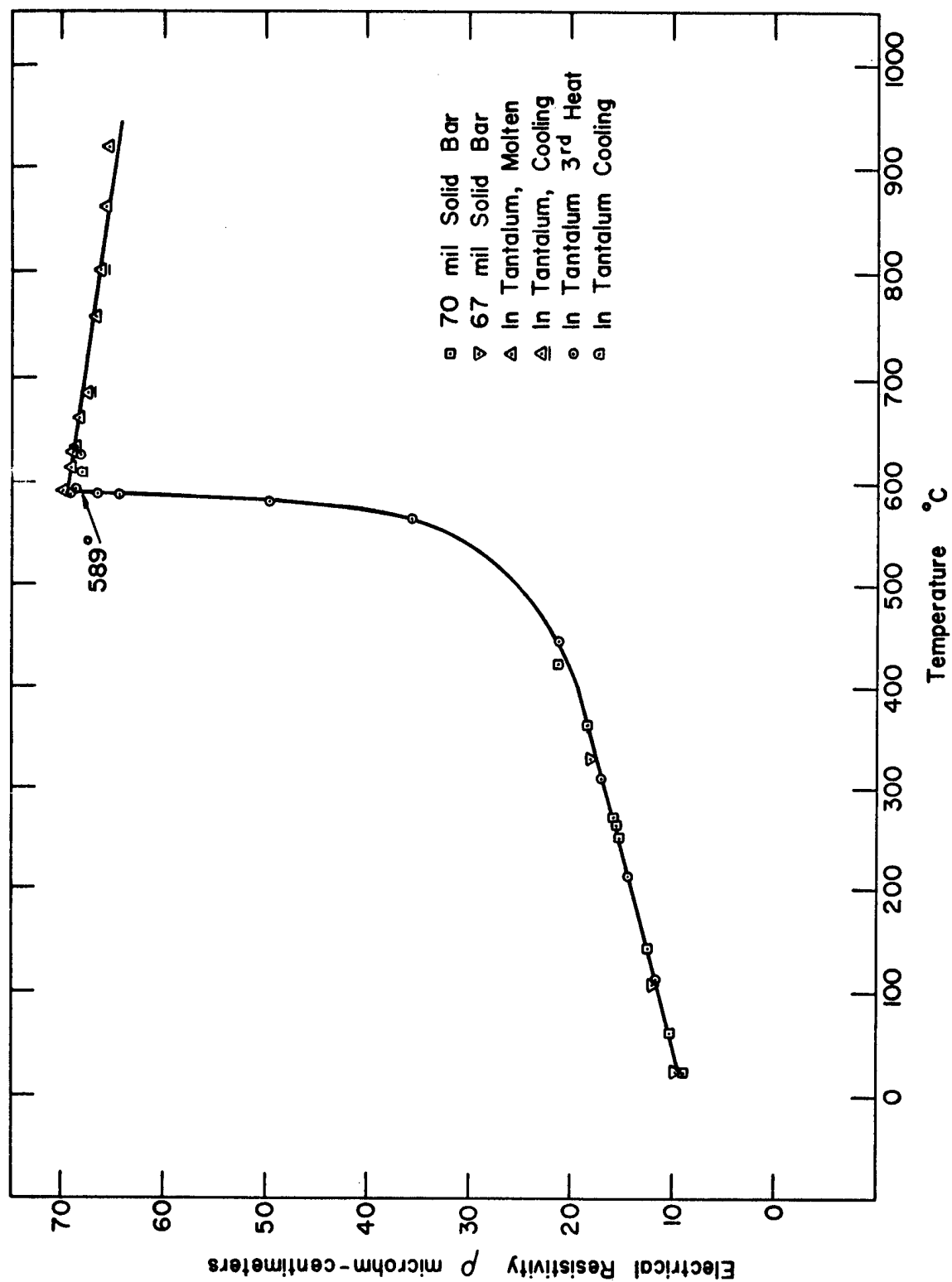


Fig. 8. Electrical resistivity of 39 wt% thorium-magnesium eutectic.

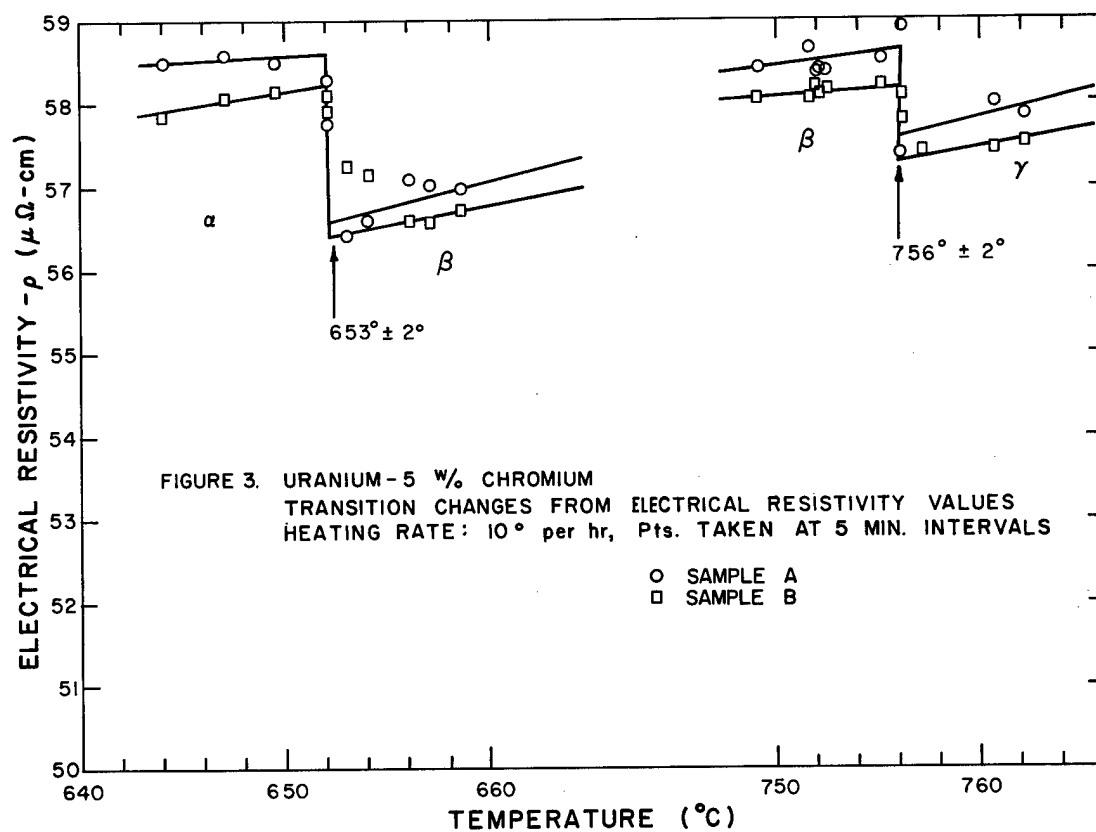


Fig. 9. Uranium - 5 wt% chromium
Transition changes from electrical resistivity values
Heating rate: 10° per hr, pts. taken at 5 min. intervals.

These data also confirm the transition temperature as reported in Report ISC-1020. Figure 9 shows the electrical resistivity values, however, to be higher. This discrepancy may be due to a difference in composition of the uranium-chromium alloy. Photomicrographs show this alloy to be near the eutectic point. By comparing these photomicrographs with those from M.I.T., the 5 wt% alloy was found to be on the chromium-rich side. Chemical analyses had shown the alloy to be 5.02% chromium.

CERAMIC ENGINEERING

1. SELF-DIFFUSION OF Y_2O_3 (D. R. Wilder and M. Berard)

Y_2O_3 has considerable potential as a refractory component in a nuclear reactor and as an additive for fuels. An investigation is nearing completion concerning the diffusion rate of yttrium in yttrium oxide over the temperature range in which sintering occurs, i.e., 1400-1700°C.

Polycrystalline specimens having widely varying porosities are being employed. Preliminary results indicate a diffusion coefficient varying with temperature, according to the following relation:

$$D = 2.41 \times 10^{-4} \exp(-43.990/RT) \frac{\text{cm}^2}{\text{sec}} .$$

A bibliography (IS-448) entitled "Diffusion in Ceramic Systems; A Selected Bibliography" by Michael F. Berard, has been distributed.

Abstract--This bibliography and set of tables are the result of an effort to bring together much of the literature pertaining to diffusion in ceramic systems. Primary classification is by the type of diffusion system, i.e., oxides, silicates and glasses, or borides, carbides and graphite. Subclassification in each case is by the diffusion species.

Whenever possible, the data have been presented in tabular form according to the Arrhenius temperature dependence equation:

$$D = D_o \exp(-Q/RT)$$

where the frequency factor, D_o , is given in square centimeters per second, and the activation energy, Q , is given in kilogram-calories per mole. In some cases only the diffusion coefficient, D , for a given centigrade temperature is tabulated.

An alphabetical author index keyed to the bibliography is included.

2. EMISSIVITY OF REFRACTORY OXIDES (D. R. Wilder and W. McMahon)

Measurements are being made on spectral and total emissivities as a function of temperature using an arc-image furnace as the heat source.

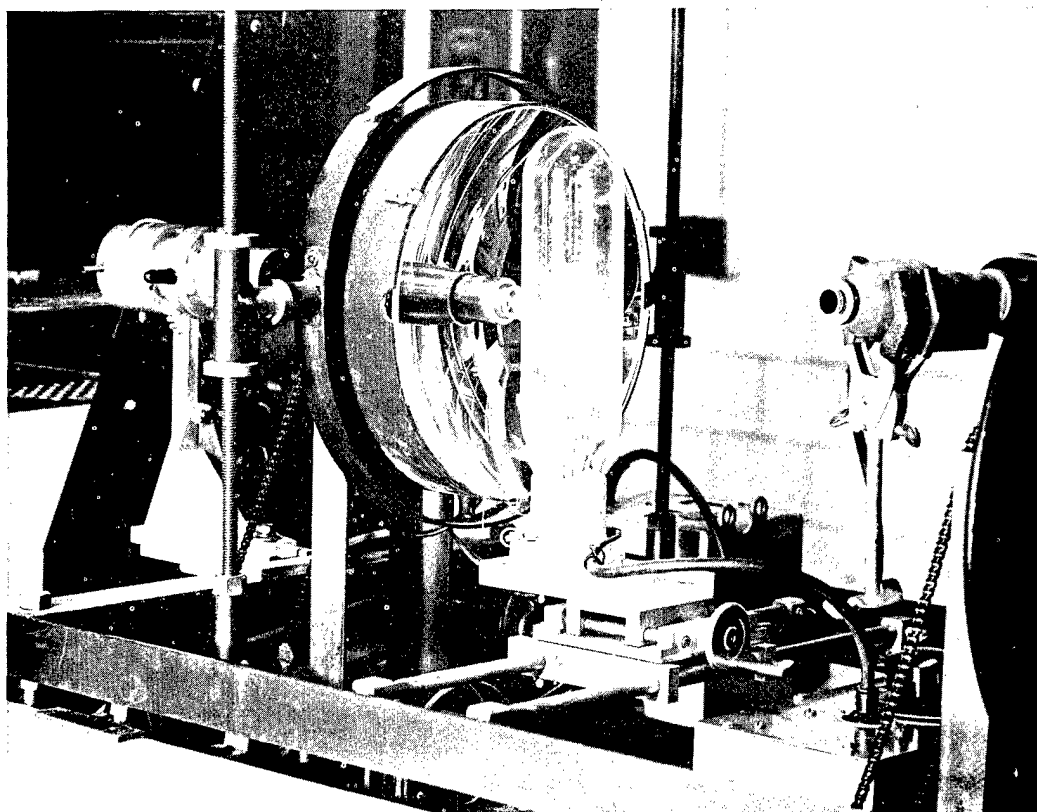


Fig. 10. Furnace for determining emissivities of refractory oxides.
Calibration lamp in specimen position.

Preliminary measurements were made with a system of rotating shutters to separate the radiation reflected from a sample and the energy emitted by the same sample. It was observed that these two types of radiation were of sufficiently divergent wavelengths that a separation was readily achieved without the use of shutters. By proper choice of photocell to observe the emittance, a clean separation of these two radiations is readily attained.

3. REFRACTORY PROTECTIVE COATINGS FOR YTTRIUM (D. R. Wilder and D. Wirkus)

Refractory, oxidation resistant coatings are being developed for use on yttrium metal.

Conventional silicate glasses have been prepared and used with good success for this application. Vanadium pentoxide-aluminum oxide mixtures have been found to develop good crystalline coatings which provide excellent oxidation resistance for many hours at 800°C. Various combinations of these oxides and others have been evaluated.

4. RARE-EARTH OXIDE APPLICATIONS IN CERAMIC SYSTEMS (D. R. Wilder and M. Berard)

A report (IS-447) entitled "The Discovery and Development of the Lanthanon Rare Earths" by Michael F. Berard has been accepted for publication in Ceramic Age.

Abstract--A brief history is given of the discovery and separation of the lanthanon rare earths. The invention of the Welsbach incandescent gas mantle in 1884 and the advent of the Manhattan Project in the early 1940's were responsible for the research that eventually changed the role of these elements from chemical curiosities to important and useful components of the modern materials picture. Present-day applications of these elements in the ceramic industries are listed with special emphasis on reactor uses.

5. SINTERING MECHANISM OF THE REFRACTORY OXIDES (D. R. Wilder and M. Marlowe)

A report (IS-460) entitled "Progress in Sintering" by D. R. Wilder has been submitted for publication in the Journal of the Electrochemical Society.

Abstract--Sintering is broadly defined as all aspects of the adhesion, densification, shrinkage, and consolidation which accompanies the reduction in surface energy of a powder compact which occurs upon application of heat and/or pressure. The process of sintering is then further divided into the initiation, material transport, and grain growth-recrystallization stages. A general review is made of each of these stages, noting typical work which has contributed to progress in each area involved.

6. HEAT CAPACITY OF REFRACTORY CERAMICS (D. R. Wilder and W. McMahon)

An investigation of the heat capacities of refractory oxides and other ceramic materials is being pursued. An arc-image furnace is employed as the source of energy, and the thermal decay of the specimen which has been heated is observed with a photocell and/or thermocouple. From knowledge of the specimen shape, fundamental laws of radiation, and the specimen's emissivity, the heat capacity can be determined. A decay curve for Al_2O_3 is shown in Fig. 11. Heat capacities of other refractory materials are being measured in a similar manner.

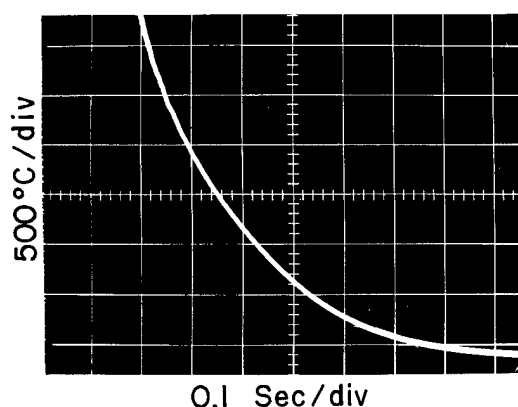


Fig. 11. Temperature decay by radiation of Al_2O_3 after arc-image heating.

LIST OF REPORTS AND PUBLICATIONS

1. REPORTS FOR COOPERATING LABORATORIES

- IS-221 Watson, J. and D. R. Wilder, Role of Niobium Pentoxide, Vanadium Pentoxide and Titanium Dioxide in the Grain Growth and Sintering of Uranium Dioxide.
- IS-316 Stachura, Stanley J. and George Burnet, The Lead-Bismuth Eutectic.
- IS-348 Ames Laboratory Staff, Annual Summary Research Report in Engineering for July 1, 1960 - June 30, 1961.
- IS-400 Pedersen, Knud and Glenn Murphy, Effects of Temperature on Mechanical Properties of Normal Uranium Dioxide.
- IS-419 Seagrave, R. C. and R. W. Fahien, Turbulent Mass Transfer in Liquid Streams.
- IS-420 Josephson, P. R., Jr., Development of a Countercurrent, Multistage, Fused Salt-Molten Metal Extractor.
- IS-437 Provow, D. M. and R. W. Fisher, The Electrical Resistivity of Molten and Solid Thorium-Magnesium Eutectic.
- IS-448 Berard, Michael F., Diffusion in Ceramic Systems; A Selected Bibliography.
- IS-501 Walker, John Craig, E. H. Olson and L. E. Burkhart, Preparation of Sodium Ethyl-sulfate.

2. PUBLICATIONS

- Calderwood, F. W., D. R. Wilder and H. A. Wilhelm, The Jolt-Pack Fabrication of Special Ceramic Ware. Iowa Acad. Sci. 68, 202-221 (1961).
- Clifford, J. C. and George Burnet, Use of Flanged Joints in Liquid-Metal Service. Chem. Eng. 179-180 (1961).
- Josephson, P. R. and L. E. Burkhart, A Countercurrent, Multistage, Fused Salt-Molten Metal Extractor. Trans. Am. Nucl. Soc. 4, 352 (1961).
- Wirkus, C. D. and D. R. Wilder, Uranium-Bearing Glasses in the Silicate and Phosphate Systems. J. Nuclear Materials 5, 140-146 (1962).

A vertical dashed line consisting of 20 short, thick black horizontal bars spaced evenly along the left margin of the page.

METALLURGY

DIVISION

M-i

IS-500

ANNUAL SUMMARY RESEARCH REPORT IN METALLURGY

by

AMES LABORATORY METALLURGY STAFF

52101

F. H. Spedding, Director, H. A. Wilhelm, O. N. Carlson, P. Chiotti,
W. L. Larsen, R. E. McCarley, D. T. Peterson and J. F. Smith

IS-500

ANNUAL SUMMARY RESEARCH REPORT IN METALLURGY

For the period July 1, 1961 - June 30, 1962

This report is prepared from material
submitted by the group leaders
of this Laboratory

Previous research reports in this series are:

ISC-35	ISC-396
ISC-41	ISC-423
ISC-56	ISC-453
ISC-69	ISC-485
ISC-74	ISC-506
ISC-76	ISC-531
ISC-79	ISC-575
ISC-113	ISC-607
ISC-130	ISC-644
ISC-133	ISC-708
ISC-137	ISC-759
ISC-171	ISC-835
ISC-193	ISC-903
ISC-220	ISC-977
ISC-248	ISC-1050
ISC-290	IS-17
ISC-300	IS-193
ISC-323	IS-351
ISC-339	

IS-500

CONTENTS

METALLURGY

	Page
1. Metal Preparation and Purification Studies.....	1
1.1 Vanadium	1
1.1.1 Iodide Refining (O. N. Carlson).....	1
1.1.2 Vanadium Iodides (R. E. McCarley).....	2
1.1.3 Deoxidation and Decarburization of Vanadium (O. N. Carlson).....	4
1.2 Niobium (Columbium).....	6
1.2.1 Preparation of <u>High Purity</u> Niobium (H. A. Wilhelm).....	6
1.2.2 Purification of Niobium by <u>Iodide Refining</u> (R. E. McCarley).....	7
1.2.3 Calcium Deoxidation of Niobium (D. T. Peterson).....	9
1.3 Thorium	9
1.3.1 Purification by Electron-Beam Melting (D. T. Peterson).....	9
1.3.2 Preparation of Thorium Tetrachloride (D. T. Peterson).....	11
1.3.3 Preparation by Magnesium Reduction (D. T. Peterson).....	13
1.4 Yttrium Metal (O. N. Carlson)	14
1.4.1 Purification of Yttrium Metal by <u>Electron Beam</u> <u>Melting</u>	14
1.4.2 Purification of YF_3 - $CaCl_2$ Salt Mixture.....	15
1.5 Chromium (O. N. Carlson).....	15
1.5.1 Preparation of <u>High Purity</u> Chromium Metal by Vacuum Sublimation.....	15
1.5.2 Zone Refining of Chromium Metal.....	17
1.5.3 Purification of Chromium Using a Special Diffusion Technique.....	18
1.6 Solid State Electrolysis Refining of Tungsten (O. N. Carlson).....	18
2. Phase Equilibria and Thermodynamic Properties of Alloys	19
2.1 Thallium-Indium <u>Phase Diagram</u> as a Function of Compo- sition, Temperature and Pressure (J. F. Smith)	19
2.2 Phase Diagram and Thermodynamic Properties of the Yttrium-Zinc System (P. Chiotti).....	22
2.3 Thermodynamic Properties of Binary Magnesium Alloys from Magnesium Vapor Pressure Measurements (J. F. Smith).....	30
2.3.1 Magnesium-Zirconium System.....	30
2.3.2 Thorium-Magnesium System.....	31

	Page
2. 4 Uranium-Rhenium Alloy System (W. L. Larsen).....	32
2. 5 Determination of the Oxygen Solubility Limits in the Niobium-Zirconium-Oxygen Ternary System (W. L. Larsen).....	34
2. 6 Thorium-Molybdenum System (W. L. Larsen).....	34
2. 7 Thorium-Vanadium System (W. L. Larsen).....	35
2. 8 Distribution of Solutes between Liquid Lead and Zinc (D. T. Peterson).....	35
2. 9 Yttrium-Oxygen System (O. N. Carlson).....	36
2. 10 Ternary Metal-Carbon-Hydrogen Phase Systems (D. T. Peterson).....	38
2. 11 Strontium-Strontium Hydride System (D. T. Peterson).....	39
2. 12 Zirconium-Bismuth Alloy Studies (H. A. Wilhelm).....	39
2. 13 Zirconium-Cobalt Alloy Investigation (W. L. Larsen).....	40
2. 14 Yttrium-Magnesium Alloy Studies (O. N. Carlson).....	41
2. 15 Chromium-Nickel Phase Studies (O. N. Carlson).....	44
2. 16 Niobium-Tin Alloy System (H. A. Wilhelm).....	45
2. 17 Nb ₃ Sn - Nb ₃ Al Alloy System (H. A. Wilhelm).....	46
2. 18 Calorimetric Determination of the Enthalpies of Formation of Some Intermetallic Compounds (J. F. Smith).....	46
2. 19 Phase Diagram and Electrical Resistivity of Thorium- Carbon Alloys (P. Chiotti).....	46
2. 20 Zirconium-Niobium-Titanium Alloy Studies (H. A. Wilhelm).....	47
2. 21 Aluminum-Tantalum Alloy Studies (H. A. Wilhelm).....	48
3. Mechanical Properties of Metals and Alloys.....	48
3. 1 Effect of Oxygen on Mechanical Properties of Niobium (H. A. Wilhelm).....	48
3. 2 Mechanical Properties of Thorium (D. T. Peterson).....	49
3. 3 Work Hardening of Thorium (W. L. Larsen).....	50
3. 4 Mechanical Forming of Yttrium (O. N. Carlson).....	51
3. 5 Ductility of Chromium and Chromium-Base Alloys (O. N. Carlson).....	52
3. 5. 1 Properties of Chromium Single Crystals.....	52
3. 5. 2 Effect of Nitrogen on Mechanical Properties of Chromium.....	53
3. 5. 3 Effect of Alloy Additions on Brittle-Ductile Transi- tion of Chromium.....	55
3. 5. 4 Forming of Chromium and Chromium-Base Alloys (O. N. Carlson).....	58
3. 6 Plastic Properties of Vanadium (O. N. Carlson).....	59
4. Solid State Investigations.....	59
4. 1 Magnetic Susceptibility Measurements.....	59
4. 1. 1 Vanadium-Carbon System (J. F. Smith).....	59
4. 1. 2 Magnetic Susceptibilities of the Halides of the Second and Third Period Transition Elements and of Their Organic Complexes (J. F. Smith).....	60
4. 1. 3 Miscellaneous Magnetic Susceptibility Measure- ments (J. F. Smith).....	60

	Page
4.2 Anisotropic Thermal Expansion of Indium (J. F. Smith)....	61
4.3 Measurement of Elastic Constants of Single Crystals	61
4.3.1 Thallium (J. F. Smith)	61
4.3.2 Chromium (J. F. Smith)	66
4.4 Crystal Structures	67
4.4.1 Strontium-Tin (J. F. Smith)	67
4.4.2 Yttrium-Magnesium (J. F. Smith)	67
5. Separation Studies	67
5.1 Liquid-Liquid Extraction (H. A. Wilhelm)	67
5.2 Pyrometallurgical Separations	68
5.2.1 Oxidation States of Thorium Chloride in a KCl- LiCl/Zinc System (P. Chiotti)	68
5.2.2 Reaction of Uranium and Thorium Carbides in a KCl-LiCl/Zinc System (P. Chiotti)	69
5.2.3 Separation of Uranium from Thorium by Oxidation with ZnCl_2 in a KCl-LiCl/Zinc System (P. Chiotti) ..	71
5.2.4 Reaction of Hydrogen with Solutes in Metals (P. Chiotti)	73
5.2.5. Extraction of Rare Earths from Mg-40 wt% Th Solutions (P. Chiotti)	75
6. Other Investigations	77
6.1 Internal Friction in Thorium Hydride (D. T. Peterson)	77
6.2 Metallography (D. T. Peterson)	78
6.3 Vapor Pressure of Calcium over Solutions of Calcium in Liquid Calcium Chloride (D. T. Peterson)	78
6.4 Transport Reactions of the Vanadium(III) Halides (R. E. McCarley)	78
6.5 Vapor Pressures and Dissociation Pressures of Vanadium Bromides	79
6.5.1 Dissociation and Disproportionation Equilibria of Vanadium(III) Bromide and the Formation of Vanadium(IV) Bromide (R. E. McCarley)	79
6.5.2 The Vapor Pressures of VCl_2 , VBr_2 , VCl_3 and VBr_3 by the Knudsen Effusion Method (R. E. McCarley)	80
6.6 Molybdenum Halides	81
6.6.1 The Preparation and Properties of Molybdenum(IV) Bromide (R. E. McCarley)	81
6.6.2 Vaporization Equilibria of Molybdenum(III) Bromide (R. E. McCarley)	82
6.6.3 Preparation and Properties of Molybdenum(IV) Chloride (R. E. McCarley)	82
6.7 Niobium Halides	83
6.7.1 Reactions of Niobium(V) Halides with Pyridine (R. E. McCarley)	83
6.7.2 Reactions and Properties of the Niobium(IV) Halides (R. E. McCarley)	84
6.8 Air Oxidation of Yttrium Metal (O. N. Carlson)	86
6.9 Extrusion of Thorium-Magnesium Alloy (D. T. Peterson) ..	89

	Page
6.10 Tantalum Halides (R. E. McCarley).....	89
6.11 Tungsten Halides (R. E. McCarley).....	91
6.12 Investigation of the Oxidation of Niobium (W. L. Larsen)...	92
6.13 Co-Reduction of Nb_2O_5 and UO_2 with Carbon to Produce a 20 wt% U, Nb Alloy (H. A. Wilhelm).....	93
6.14 Deformation Behavior of Niobium and Tantalum (H. A. Wilhelm) <i>Cb, Ta</i>	94

List of Reports and Publications

1. Reports for Cooperating Laboratories	97
2. Publications	97

METALLURGY

1. METAL PREPARATION AND PURIFICATION STUDIES

1.1 Vanadium

1.1.1 Iodide Refining (O. N. Carlson,^{*} C. V. Owen and L. S. Todd)

Approximately 20 lb of crystal bar vanadium was prepared by the iodide refining process utilizing a retort with a capacity of about 4 lb per batch. The problem of shorting out of the filament which was previously encountered was overcome by the use of Lucalox insulators in the system. This material, which is Al_2O_3 fused at a high temperature and pressure, is capable of withstanding the temperatures employed in this process without undergoing decomposition or loss of insulating properties.

The reduction of V_2O_5 and V_2O_3 with Mg and Al was studied. The purpose of this work was to produce a cheap form of vanadium which could be incorporated as feed material in the iodide refining process. The reduction of V_2O_5 with magnesium was successfully ignited by external heating; however, the reaction could not be contained in the steel bomb casing as penetration of the ceramic liners was encountered for various materials that were tried. The reduction of V_2O_3 and a mixture of V_2O_5 and V_2O_3 with aluminum likewise was unsuccessful. There appeared to be some reaction at ignition, but no metal was formed. Metallic buttons were produced from the reduction of V_2O_5 employing a stoichiometric amount of aluminum. The metal was analyzed

^{*}First name listed indicates group leader in charge of work.

and found to contain 92 wt% vanadium and 2.5 wt% aluminum. Other reductions made with a 5 wt% deficiency of aluminum were found to contain 94 wt% vanadium and 2 wt% aluminum. Transparent inclusions in the microstructure have been tentatively identified as Al_2O_3 which should not be transferred during iodide refining. This has yet to be confirmed by experiment, however.

1.1.2 Vanadium Iodides (R. E. McCarley and K. O. Berry)

An investigation of the vanadium iodides was initiated during this period. The major objectives of this study will be to identify and characterize the condensed phases in the vanadium-iodine system and to determine the modes and thermodynamics of vaporization of the vanadium iodides. Methods similar to those used in the study of the vaporization equilibria of the vanadium bromides (see Sec. 6.5 of this report) will be extended to this work. It is anticipated that this work will provide information which is necessary for an interpretation of the processes important in the iodide purification of vanadium metal.

Several reactions between vanadium and iodine were performed during this period using the following technique. Vanadium metal and iodine were sealed in opposite ends of an evacuated Pyrex tube. The tube was subsequently heated under a controlled temperature gradient which was varied from 350 - 500°C at the vanadium metal to 120 - 180°C at the iodine. Under these conditions iodine reacted with the metal to form a volatile vanadium iodide which migrated down the tube to a region of lower temperature and formed a crystalline deposit. It was found in all cases

that the iodide deposited in an area of the tube where the temperature was between 190 and 250°C. Lustrous, black lamellar crystals up to 10 mm on the side were formed by this process.

Analytical data on the crystals formed in these reactions showed that a non-stoichiometric iodide is formed under the conditions outlined above. While additional work needs to be done, the average composition of the crystals was found to be $\text{VI}_{2.12 \pm 0.02}$. The temperature of the metal during the reaction had no effect on this composition, but some variation of composition with the iodine pressure in the tube was indicated.

X-ray diffraction patterns of the $\text{VI}_{2.12}$ were indexed on the basis of a hexagonal structure of the CdI_2 type. The lattice parameters given by Klemm and Grimm¹ for pure VI_2 also appear to be appropriate for $\text{VI}_{2.12}$, although our x-ray data and calculations have not been refined so that final lattice parameters can be reported.

On heating crystals of $\text{VI}_{2.12}$ at 600°C, elemental iodine was evolved and the stoichiometric iodide VI_2 was obtained. Anal. Calcd. for VI_2 : V, 16.7; I, 83.3. Found: V, 16.7; I, 83.4. This material gave an x-ray diffraction pattern which also was indexed on the hexagonal structure but the lattice constants did not agree with those given by Klemm and Grimm for pure VI_2 . From this preliminary work it appears that the diffraction data reported by the previous workers for VI_2 was more likely data for an iodide of composition near $\text{VI}_{2.12}$.

Further work will be directed towards establishment of the temperature-pressure-composition diagram for VI_2 , the identification of important vapor

¹W. Klemm and L. Grimm, Z. anorg. u. allgem. Chem. 249, 198 (1941).

species in the vaporization of vanadium iodides and measurement of the vaporization equilibria.

1.1.3 Deoxidation and Decarburization of Vanadium (O. N. Carlson, C. V. Owen, R. W. Thompson and F. A. Schmidt)

Several methods were tried in an attempt to further decrease the oxygen and carbon content of iodide vanadium. Deoxidation by treatment with calcium vapors was continued. A six-day treatment at 1100°C has been shown to give a consistent decrease in the oxygen content from 150 - 300 ppm in the iodide metal to 10 - 25 ppm. In one experiment a specimen containing 35 ppm oxygen was found to contain a non-detectable amount of oxygen (less than 5 ppm) after the calcium treatment. Several rods have been treated in this manner and fabricated into sheet or tensile specimens.

Electron beam melting was also investigated as a possible method for purifying vanadium. Samples of iodide and bomb-reduced vanadium were analyzed before and after beam melting and the results from several runs have been compiled in Table I.

Table I
Effect of Electron Beam Melting on Vanadium Metal

Run No.	Specimen History	O	H	Fe	C	N
1	Before EB melting	370	13	1300	195	115
	After EB melting	115	3	260	290	354
2	Before EB melting	340	12	--	2850	< 5
	After EB melting	40	5	--	3100	< 5
3	Before EB melting	221	15	--	115	35
	After EB melting	113	9	--	245	39
4	Before EB melting	1480	18	1150	750	240
	After EB melting	310	20	180	630	480

Approximately one-third of the sample was lost during melting due to volatilization which is at least partially responsible for the increased carbon content of the metal. The data show clearly that oxygen, hydrogen and iron are removed during the melting process and suggests the possibility of removing carbon by distillation of vanadium. One experiment was performed in an attempt to remove carbon by distillation in an electron beam furnace. The vaporized metal was deposited on a 2-mil vanadium sheet containing 400 ppm carbon. Analysis of the combined substrate and condensate showed only 200 ppm carbon present whereas the carbon content of the vanadium residue after distillation was 4200 ppm.

A specimen was held in a molten zinc bath for five days at 600°C in an attempt to decarburize vanadium. The carbon and oxygen contents of the metal were unaltered by this treatment while the nitrogen content increased from 65 - 200 ppm.

A solid state electrolysis technique was also applied to vanadium with some success. In one experiment a dc current was passed through a vanadium rod at 1400°C for 24 hr under a dynamic vacuum. Another run was made at 1450°C for 100 hr under 5 psi positive pressure of argon. The results of these experiments (shown in Table II) indicate that oxygen and nitrogen are depleted at the anode end and concentrated at the cathode. This is complicated however, by the simultaneous loss of oxygen by volatilization when the experiment is run under vacuum. Carbon does not appear to migrate toward either electrode although the results may be somewhat inconclusive.

Table II
Purification of Vanadium by Solid State Electrolysis

Impurity	Original Bar	Cathode End	Center	Anode End	Experimental Conditions
Oxygen	345	210	50	130	In vacuo at 1400°C for 24 hr
Carbon	140	120	100	120	In vacuo at 1400°C for 24 hr
Nitrogen	6	15	4	2	In vacuo at 1400°C for 24 hr
Oxygen	210	375	250	135	Under 5 psi argon at 1450°C for 100 hr
Carbon	140	160	160	275	Under 5 psi argon at 1450°C for 100 hr
Nitrogen	220	395	365	17	Under 5 psi argon at 1450°C for 100 hr

Purification of vanadium by zone refining is also being studied and a molten zone has recently been passed along a vanadium rod using high frequency induction heating. Results are still pending.

1.2 Niobium (Columbium)

1.2.1 Preparation of High Purity Niobium (H. A. Wilhelm, T. G. Ellis and F. A. Schmidt)

High purity niobium metal has been produced by electron beam melting niobium that had been prepared by aluminothermic reduction of niobium pentoxide (Nb_2O_5). Although the "as reduced" niobium metal contained at least 1/2% aluminum as well as oxygen and other contaminants, electron beam melting this metal in a high vacuum produced niobium that was spectroscopically pure and had Brinell hardness numbers of 30 - 50.

The samples prepared to date have been relatively small, 10 - 50 grams. In order to prepare spectroscopically pure metal a relatively long holding

time, ~30 min, was required in the low power electron beam melter employed. It may be desirable to perform an intermediate vacuum consumable arc melting step in the process in order to reduce the contaminant concentration somewhat before the final electron beam melting step.

1.2.2 Purification of Niobium by Iodide Refining (R. E. McCarley and W. Tadlock)

An important aspect of the iodide method for purification of niobium is the effect of temperature of the feed metal on the growth rate of the crystal bar niobium. Earlier studies had shown that this growth rate attained maxima at 450°C and ~750°C with a minimum at the intermediate temperature of 550°C. In order to gain some insight into the mechanism responsible for the behavior of the growth rate some experiments designed to identify the niobium iodides formed in the reactions were performed.

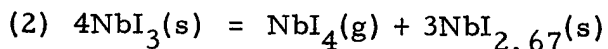
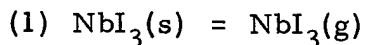
Reactions between niobium and iodine were performed at temperatures between 350 and 700°C, and iodine pressures between 0.3 and 10 mm Hg. Table III lists the I:Nb ratios obtained at the various temperatures and pressures.

Table III
Results of Niobium-Iodine Reactions

Temp. °C	I:Nb Ratios at the Indicated Iodine Pressure			
	0.3 mm	1 mm	10 mm	1000 mm
350	3.85	3.47	3.21	
450		3.52	3.29	
550	3.04	3.49	3.68	
600		3.92	4.00	3.23
700		3.57	3.61	

X-ray diffraction powder patterns of the products of these reactions showed that NbI_5 was not an important product at low iodine pressures, since lines attributable to NbI_5 were generally absent from the powder patterns. All of the products did appear to contain both NbI_4 and NbI_3 and lines corresponding to both substances were found in the powder patterns. The analytical results given in Table III thus reflect the relative proportions of NbI_4 and NbI_3 in the product. These data indicate that at temperatures near the minimum of the growth-rate curve (550 - 600°C) in the iodide purification process $\text{NbI}_4(\text{g})$ is the principal species responsible for transport of the metal. At the higher temperatures $\text{NbI}_4(\text{g})$ must be formed by decomposition of $\text{NbI}_{2.67}$, or by reaction of the latter solid with iodine vapor, since solid NbI_4 is not stable above 503°C.¹ At 700°C, where the I:Nb ratio returned to lower values, some direct vaporization of the only stable subhalide, $\text{NbI}_{2.67}$, must also take place; how $\text{NbI}_{2.67}$ may vaporize is open to question.

Below 550°C an anomaly in the I:Nb ratios occurs; this ratio decreased with increasing iodine pressure in the reaction. No explanation for this behavior can be given at the present time. However, the decrease in the I:Nb ratio (increase in proportion of NbI_3 volatilized) with decreasing temperature below 550°C can be accounted for in terms of the reactions (1) and (2).



¹P. X. Seabaugh, Ph.D. Thesis, Iowa State University, 1961.

If reaction (2) becomes relatively less important at the lower temperatures, then vaporization by (1) should be more important and a decrease of the I:Nb ratio in the products would be observed. Some quantitative data on the vaporization equilibria of the niobium iodides is needed in order to make a more rigorous interpretation.

1.2.3 Calcium Deoxidation of Niobium (D. T. Peterson)

A study of the deoxidation of niobium by the alkaline earth metals was started. Specimens of niobium with various oxygen levels were equilibrated with the individual alkaline earth metals at 1200°C. Samples have been submitted for oxygen determination and a new set of specimen are being equilibrated at 1100°C.

1.3 Thorium

1.3.1 Purification by Electron-Beam Melting (D. T. Peterson, F. A. Schmidt and W. E. Krupp)

A study was made to determine what effect electron-beam melting has on the impurity content and hardness of thorium metal. Samples of arc-cast thorium containing various amounts of oxygen, iron, carbon, nitrogen and hydrogen were melted in a 9 kw electron-beam furnace and evaluated. The significant analytical data and hardness values for these samples before and after electron-beam melting are shown in Table IV. As can be seen from the table, substantial decreases in oxygen and hydrogen content and hardness were obtained by the electron-beam melting. In most cases, a decrease in the iron content was also observed. No consistent change was noted in the carbon or nitrogen content.

Table IV
Effect of Electron-Beam Melting on Impurity Content
and Hardness of Thorium Metal

Sample No.		Analytical Data in PPM			Hardness
		O*	Fe	H	DPH
1	Arc-melted	7660	347	10	70
	EB-melted	75	44	2	33
2	Arc-melted	7660	347	10	70
	EB-melted	48	12	2	35
3	Arc-melted	4800	414	5	67
	EB-melted	140	10	2	51
4	Arc-melted	700	51	5	75
	EB-melted	200	9	1	59
5	Arc-melted	500	12	3	71
	EB-melted	125	2	1	55
6	Arc-melted	470	42	4	70
	EB-melted	172	44	2	56
7	Arc-melted	470	42	4	70
	EB-melted	172	14	2	53
8	Arc-melted	375	18	5	43
	EB-melted	115	5	2	35
9	Arc-melted	85	7	3	54
	EB-melted	50	8	1	50

*Analysis by vacuum fusion.

The effect of electron-beam melting on the impurity content of thorium metal is further illustrated by comparing the microstructures of the arc-melted and beam-melted metal. The arc-melted specimen in Fig. 1 contains 4800 ppm oxygen which appears as the dark snow-flake pattern. This specimen electron-beam melted, shown in Fig. 2, contains 140 ppm oxygen.

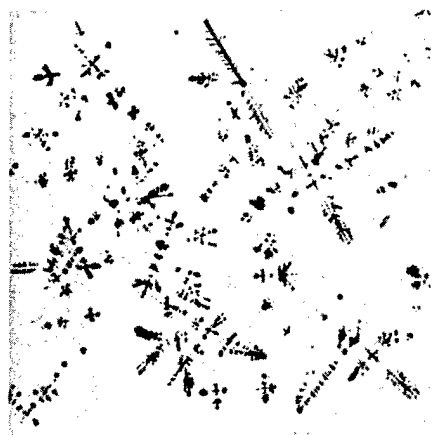


Fig. 1. Arc-melted thorium metal. Mechanically polished. Magnification 250X

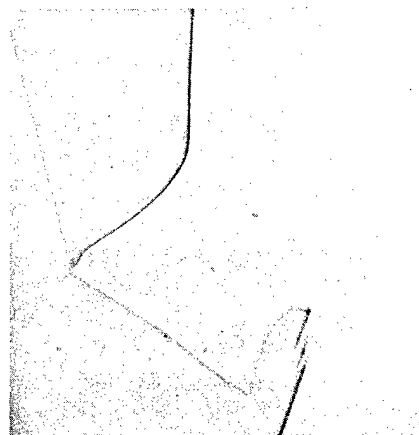


Fig. 2. Beam-melted thorium metal. Electropolished with HClO_4 . Magnification 250X

1.3.2 Preparation of Thorium Tetrachloride (D. T. Peterson, F. A. Schmidt and W. E. Krupp)

Various chlorinating agents were employed in an effort to prepare anhydrous ThCl_4 from ThO_2 . The chlorinating agents studied were: carbon and chlorine, sulphur and chlorine, phosgene gas, and ammonium chloride and chlorine. It became apparent that an important factor in the effectiveness of the preparations was the temperature of calcination of the oxide. As a result of this observation, the reactions were studied using both a high-fired and low-fired form of ThO_2 . The high-fired, less reactive form of ThO_2 was prepared by thermally decomposing $\text{Th}(\text{C}_2\text{O}_4)_2 \cdot x\text{H}_2\text{O}$ at 900°C . The low-fired, reactive form of ThO_2 was prepared by heating the hydrated oxalate at 300°C . The optimum temperatures at which maximum yields of ThCl_4 were obtained for each chlorinating

agent were determined for both types of ThO_2 . These temperatures and corresponding yields are shown in Table V. Several kilograms of ThCl_4

Table V

Optimum Temperatures and Yields Obtained Using Various
Chlorinating Agents on ThO_2

Chlorinating Agents	Optimum Reaction Temp. °C	Average Percent Yield of ThCl_4	
		Low-Fired ThO_2	High-Fired ThO_2
$\text{C} + \text{Cl}_2$	600	96	60
$\text{S} + \text{Cl}_2$	400	82	40
COCl_2	600	94	32
$\text{NH}_4\text{Cl} + \text{Cl}_2$	250	92	--

were prepared from ThO_2 using carbon and chlorine as the chlorinating agents. This method was chosen due to the high yields obtained, ease in handling, and low cost of the reactants. The ThCl_4 was prepared by blending the low-fired form of ThO_2 with graphite powder in a 1:2 molar ratio and heating the mixture in a chlorine gas stream at 600°C for 4 hr. Thorium tetrachloride obtained in this manner was in crystalline form and contained occluded graphite particles.

The ThCl_4 was purified by multiple sublimation under a reduced pressure. The sublimations were made at 750°C under 25 mm of mercury pressure over a period of 24 hr in order to reduce entrainment of unreacted ThO_2 and carbon. In the second and third sublimations, the ThCl_4 vapors were passed through thorium metal turnings prior to condensation in order to remove various metallic chlorides present as impurities. The purified chloride was white in color and contained less than 100 ppm of carbon.

1.3.3 Preparation by Magnesium Reduction (D. T. Peterson, F. A. Schmidt and W. E. Krupp)

Thorium metal was prepared from the high purity ThCl_4 by a magnesium intermediate alloy process. The ThCl_4 was mixed with an amount of magnesium sufficient to both reduce the ThCl_4 and to form a Th-20 wt% Mg alloy. The reduction was made by heating the mixture to 965°C for one hour in a tantalum metal crucible under an inert gas atmosphere. After cooling to room temperature the MgCl_2 slag was removed from the alloy. All transfer operations were done in an inert gas glove box in order to minimize contamination by atmospheric moisture. The alloy was crushed and heated in vacuo to remove the magnesium and any remaining slag. A stepwise heating cycle was used during the magnesium removal step in order to prevent melting of the alloy. The alloy was heated at temperatures of 350 , 550 and 750°C for 2 hr. The temperature was then raised to 920°C for 24 hr which insured complete magnesium removal. The thorium sponge was consolidated by non-consumable arc-melting. The arc-melted metal was purified by electron-beam melting as described in Sec. 1.3.1 of this report. A representative chemical analysis of thorium metal prepared in this manner is shown in Table VI.

Table VI

Analysis of Thorium Metal Prepared by the
Magnesium Intermediate Alloy Process

Impurity	Analysis in PPM
C	20 - 50
N	40 - 60
O	50 -150*
H	1*

Table VI (Continued)

Impurity	Analysis in PPM
Al	<30
Cr	<20
Fe	10 - 40
Mg	<20
Mn	<20
Ni	<20
Si	<50

*Determined by vacuum fusion.

1.4 Yttrium Metal (O. N. Carlson, J. A. Haefling and F. A. Schmidt)

1.4.1 Purification of Yttrium Metal by Electron Beam Melting

The purification of yttrium metal prepared by the magnesium intermediate alloy process was studied using electron beam melting. The analysis of the metal before and after electron beam melting is shown in Table VII. From these data it is apparent that carbon, nitrogen and oxygen are not removed during the melting step but hydrogen, fluorine, chromium, iron and silicon contents of yttrium are substantially lowered by electron beam melting.

Table VII

Purification of Yttrium Metal by Electron Beam Melting

Element	Analysis in PPM	
	Before	After
C	130	135
N	12	35
O	650	650
H	135	10
F	105	25
Cr	165	20
Fe	210	105
Si	trace	faint trace

1.4.2 Purification of $\text{YF}_3\text{-CaCl}_2$ Salt Mixture

The principal purpose of this study was to decrease the iron and nickel content of the $\text{YF}_3\text{-CaCl}_2$ salt mixture used in the preparation of a Y-24 wt% Mg alloy. This alloy is further processed to yttrium metal by heating in vacuo to sublime off the magnesium.

Iron and nickel salts present as impurities in the $\text{YF}_3\text{-CaCl}_2$ mixture are reduced by zinc or a magnesium-zinc alloy thus facilitating their removal from the salt.

In three reductions where the fused salts were heated with zinc, the iron content of the yttrium metal produced was 95 ppm and the nickel content was 65 ppm.

When fused $\text{YF}_3\text{-CaCl}_2$ was contacted with a Zn-15 wt% Mg alloy before the reduction step the resulting yttrium contained 60 ppm iron and 10 ppm nickel. Yttrium prepared from untreated $\text{YF}_3\text{-CaCl}_2$ usually contains about 250 ppm iron and 125 ppm nickel.

1.5 Chromium (O. N. Carlson, L. Sherwood and F. A. Schmidt)

1.5.1 Preparation of High Purity Chromium Metal by Vacuum Sublimation

During the period of this report several methods of sublimation were used in an effort to further purify iodide chromium metal. The chromium used in this work was obtained from the Chromalloy Corporation.

In one of these methods chromium metal was placed in a tantalum crucible and heated in an induction furnace to 1600°C . A temperature gradient was maintained in the crucible by means of a baffle so that fractions of the sublimate were collected in different regions of the vessel. The sublimation was carried out either under a dynamic vacuum or by evacuating and sealing the tantalum crucible. This latter method,

consisting of the use of a static vacuum, was designed to eliminate contamination from the external vacuum system.

Another method used to sublime chromium utilized an electron beam for the heat source. The chromium metal was placed in a tungsten vessel which was heated in an electron beam furnace to 1600°C under a pressure of 0.003 microns of mercury. The chromium was volatilized out of the crucible and directed onto a tantalum plate where it was condensed. A comparison of the analysis of the chromium before and after sublimation and of the residue is given in Table VIII. While the results are somewhat inconclusive the following observations can be made. There is a slight increase in nitrogen during sublimation under a dynamic vacuum but no change in nitrogen content resulting from either of the other procedures. There appears to be some decrease in the carbon content in both the condensate and residue after sublimation although the scatter in analytical results makes this interpretation somewhat uncertain. These experiments indicate that purification by a distillation technique is not particularly applicable to chromium.

Table VIII
Results of Sublimation Experiments on Chromium

Method of Sublimation	Analysis of Cr Before Sublimation (ppm)		Analysis of Cr After Sublimation (ppm)	
	C	N	C	N
<u>Static Vacuum (sealed)</u> Run #1	68	15	Residue	76
			1st Fract.	96
			2nd Fract.	68
				15
Run #2	140	7	Residue	36
			1st Fract.	60
			2nd Fract.	97
				8

Table VIII (Continued)

Method of Sublimation	Analysis of Cr Before Sublimation (ppm)		Analysis of Cr After Sublimation (ppm)		
	C	N		C	N
<u>Dynamic Vacuum</u>					
Run #1	242	8	Residue	73	27
			1st Fract.	65	<10
			2nd Fract.	47	15
Run #2	182	<5	Residue	55	< 8
			1st Fract.	87	21
			2nd Fract.	59	20
<u>Electron Beam Heated</u>					
Run #1	155	45	Residue	42	25
			Condensate	104	34
Run #2	116	37	Residue	141	61
			Condensate	39	47
Run #3	43	9	Residue	--	--
			Condensate	53	8
Run #4	93	<9	Residue	--	--
			Condensate	70	6
Run #5	35	25	Residue	--	--
			Condensate	86	10
Run #6 Cr-10 wt% Nb	45	7	Residue	--	--
			Condensate	54	3

1.5.2 Zone Refining of Chromium Metal

Due to the high vapor pressure of chromium metal at its melting point, several attempts were made to zone refine chromium by restraining the vapor within a sealed rhenium tube. Rods of iodide chromium measuring 1/4 in. in diameter and 6 in. long were sealed in a rhenium tube and an effort was made to pass a zone along the composite using a 2 kw electron beam as the heating source. At 1850°C, which was considered to be the melting temperature of chromium, alloying between

the chromium and rhenium appeared to take place and melting through the rhenium jacket was repeatedly encountered.

1.5.3 Purification of Chromium Using a Special Diffusion Technique

Experiments were conducted designed to purify iodide chromium by the diffusion of impurities toward regions of high dislocation density within a specimen. A layer of high dislocation concentration was induced at the specimen surface by either cold working or quenching. The specimen was then annealed at 450°C for 120 hr to promote diffusion of impurity atoms from the core to the surface. After annealing, the specimen was electropolished in concentrated H_3PO_4 to remove the surface layer supposedly containing a higher concentration of impurities. Both polycrystalline and single crystal specimens in sizes ranging from 1/4 in.-thick rectangular bars to 0.010 in.-thick slices were treated. The extent of purification was determined by comparing the residual resistivity ratios and chemical analyses of the untreated and treated specimens.

The results thus far obtained indicate no purification has been realized by this type of refining procedure although sporadic increases in the resistivity ratio have been observed.

1.6 Solid State Electrolysis Refining of Tungsten (O. N. Carlson and K. E. Solie)

A number of solid state electrolysis runs were carried out on tungsten in an effort to purify this metal by migration of impurities along the bar under the driving force of a potential gradient. A current of approximately 300 amps was passed through a tungsten rod heating the specimen to about 2200°C. An inert gas pressure of 0.001 mm

of Hg was maintained in the system. Analytical data obtained from a representative run are shown in Table IX.

Table IX
Chemical Analysis of Tungsten Rod Before and After
Solid State Electrolysis Treatment

Section of Rod	Mo	PPM Impurity			
		Fe	O	N	C
Original W rod	20	10	40	85	35
Cathode end	15	18	30	35	75
Center	20	18	55	30	80
Anode end	15	8	40	45	30

The above data would indicate that no discernible migration of impurities has taken place as a result of the passage of the current through the bar.

2. PHASE EQUILIBRIA AND THERMODYNAMIC PROPERTIES OF ALLOYS

2.1 Thallium-Indium Phase Diagram as a Function of Composition, Temperature and Pressure (J. F. Smith and R. W. Meyerhoff)

The thallium-indium phase diagram was determined from ambient pressure to 5.5 kbars. The diagram was constructed primarily from electrical resistivity data obtained as a function of composition, temperature and pressure. Electrical resistivity data was supplemented with x-ray data to determine the phase diagram at ambient pressure. The isobaric sections of the thallium-rich region of the phase diagram are shown in Fig. 3. The isobaric sections for 1 bar and 5 kbars are based upon direct measurements while the isobaric sections for 30 and 40 kbars are based on extrapolation of the observed pressure dependence

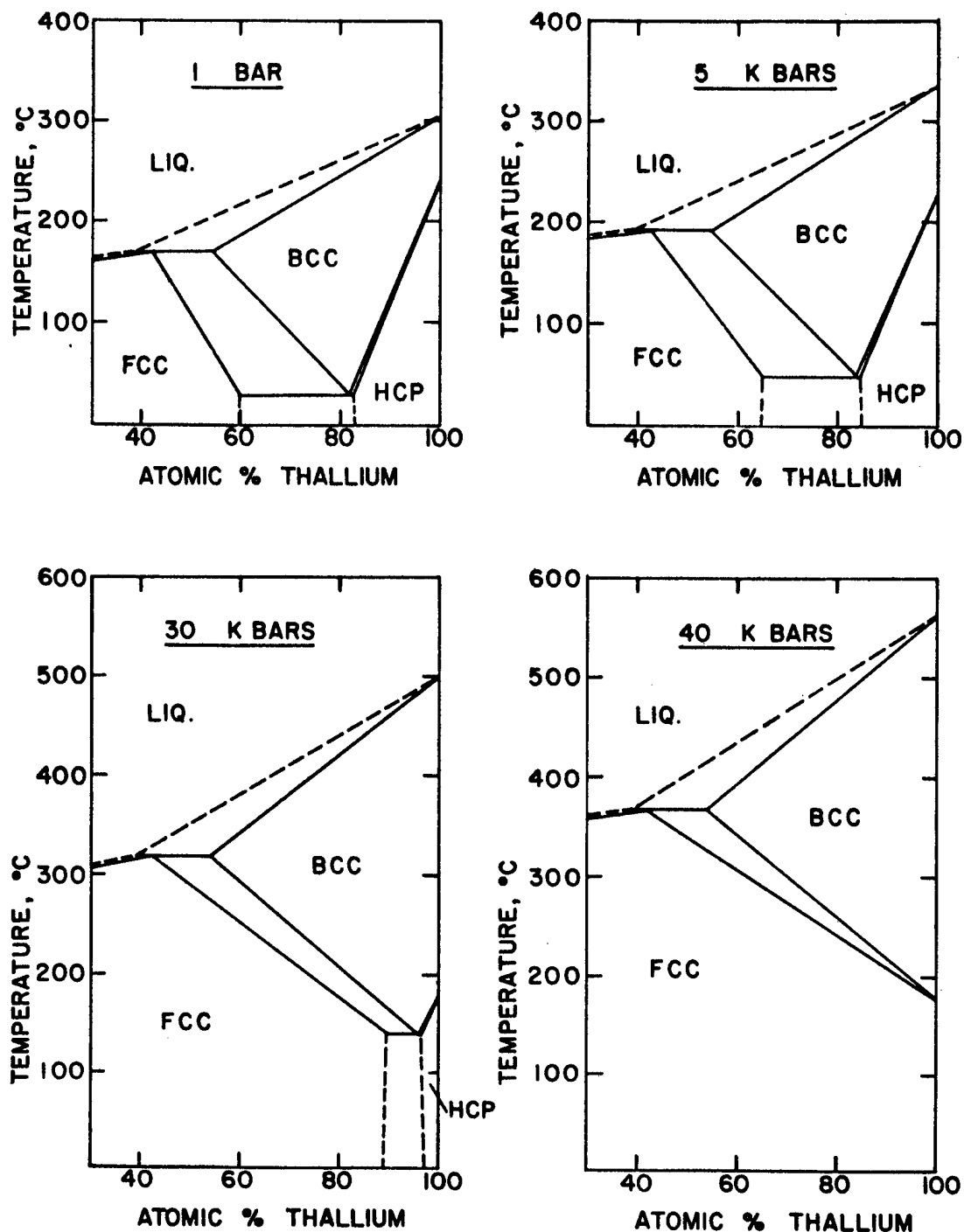


Fig. 3. Isobaric sections of the thallium-rich region of the proposed thallium-indium phase diagram. The sections shown for atmospheric pressure and 5 kbars are based on experimental results while the sections shown for 30 and 40 kbars were obtained by extrapolation of the observed pressure dependence.

of the various phase boundaries. Extrapolation over such a wide pressure range can be justified by the excellent agreement between the position of the triple point in pure thallium which is indicated by the extrapolation and the position indicated by previous experimental measurements¹ on pure thallium.

The mean temperature of the hexagonal close packed-body-centered cubic transition of thallium as a function of pressure and indium concentration can be approximated by the following equation:

$$T_{\text{hcp-bcc}} = 234 - (1.2 \times 10^{-3}) N_2 - (2.03 + 17.1 N_2) P$$

where $T_{\text{hcp-bcc}}$ is in °C, N_2 is the mole fraction of indium, and P is the pressure in kbars. The eutectoid temperature and the peritectic temperature as functions of pressure can be represented by the following equations:

$$T_E = 30 + 3.68 P,$$

$$T_P = 171.5 + 4.9 P,$$

again with temperature in °C and pressure in kbars. Thus as pressure increases the eutectoid temperature increases while the hexagonal close packed - body-centered cubic transition temperature decreases with a concomitant decrease of the solubility of indium in hexagonal close packed thallium. Extrapolation to higher pressures indicates a triple point in

¹P. W. Bridgman, Phys. Rev. 48 (1935).

pure thallium between hexagonal close packed, body-centered cubic, and a high-pressure phase at 162°C and 35.8 kbars. The high-pressure phase of pure thallium is continuous with the face-centered cubic - phase which occurs in the indium-thallium system at ambient pressure between 40 and 77 at. % indium so that the data indicate that the high-pressure allotrope of thallium is face-centered cubic. Thus thallium is shown to exhibit all three of the crystal structures which are common in elemental metals.

2.2 Phase Diagram and Thermodynamic Properties of the Yttrium-Zinc System

(P. Chiotti, J. T. Mason and K. J. Gill)

Work on the yttrium-zinc system has been completed. Alloys were prepared from Bunker-Hill slab zinc, 99.99% pure, and Ames Laboratory yttrium. The yttrium was in the form of sponge and arc-melted buttons. The arc-melted buttons gave the following analysis in parts per million; C-129, N-12, O-307, Fe-209, Ni-126, Mg-13, Ca<10, F-105 and Ti<50. Some of the early work was done with yttrium which contained about 5000 ppm of titanium as the major impurity. The results obtained for yttrium-rich alloys prepared from the lower purity yttrium were discarded.

Tantalum crucibles were used as containers in alloy preparation, thermal analysis and vapor pressure measurements. Procedures employed in preparing the alloys and the dew-point method for measuring zinc vapor pressures over the alloys have been described in previous reports and in the published literature.¹

¹P. Chiotti and K. J. Gill, "Phase Diagram and Thermodynamic Properties of the Thorium-Zinc System", Trans. AIME 221, 573 (1961).

The revised phase diagram based primarily on thermal and metallographic data is presented in Fig. 4. The microstructures of furnace cooled alloys indicate that the range of composition of the compounds formed is very small. An appreciable range of solubility for the YZn compound is indicated from the results of thermal analyses for temperatures near the eutectic temperature, 875°C , as shown in Fig. 4. The compound YZn_2 undergoes an allotropic transformation at 750°C for compositions between YZn and YZn_2 . In this composition range the transformation is isothermal, gives a weak thermal arrest which is reproducible to $\pm 10^{\circ}\text{C}$, and the YZn_2 phase has a coarsely twinned structure. Alloys of approximately the stoichiometric composition of YZn_2 and in the two phase YZn_2 - YZn_3 region do not give a thermal arrest at 750°C and the YZn_2 phase has a fine acicular microstructure. Electrical resistivity measurements confirm the existence of a transformation in the YZn_2 compound and show that in this composition range the transformation occurs over a wide temperature range on both heating and cooling. On cooling the transformation begins at temperatures well below 750°C and is accompanied by loud clicks and sudden increases in electrical resistivity. On heating no sonic activity was detected, the resistance-temperature curve shows an increase in resistance up to about 300°C and then a gradual decrease in resistance to about 750°C followed by an increase in resistance with a further increase in temperature. This transformation behavior is rather surprising in view of the limited composition range for the YZn_2 phase. Further work is being done in an attempt to understand the character and mechanism of this transformation.

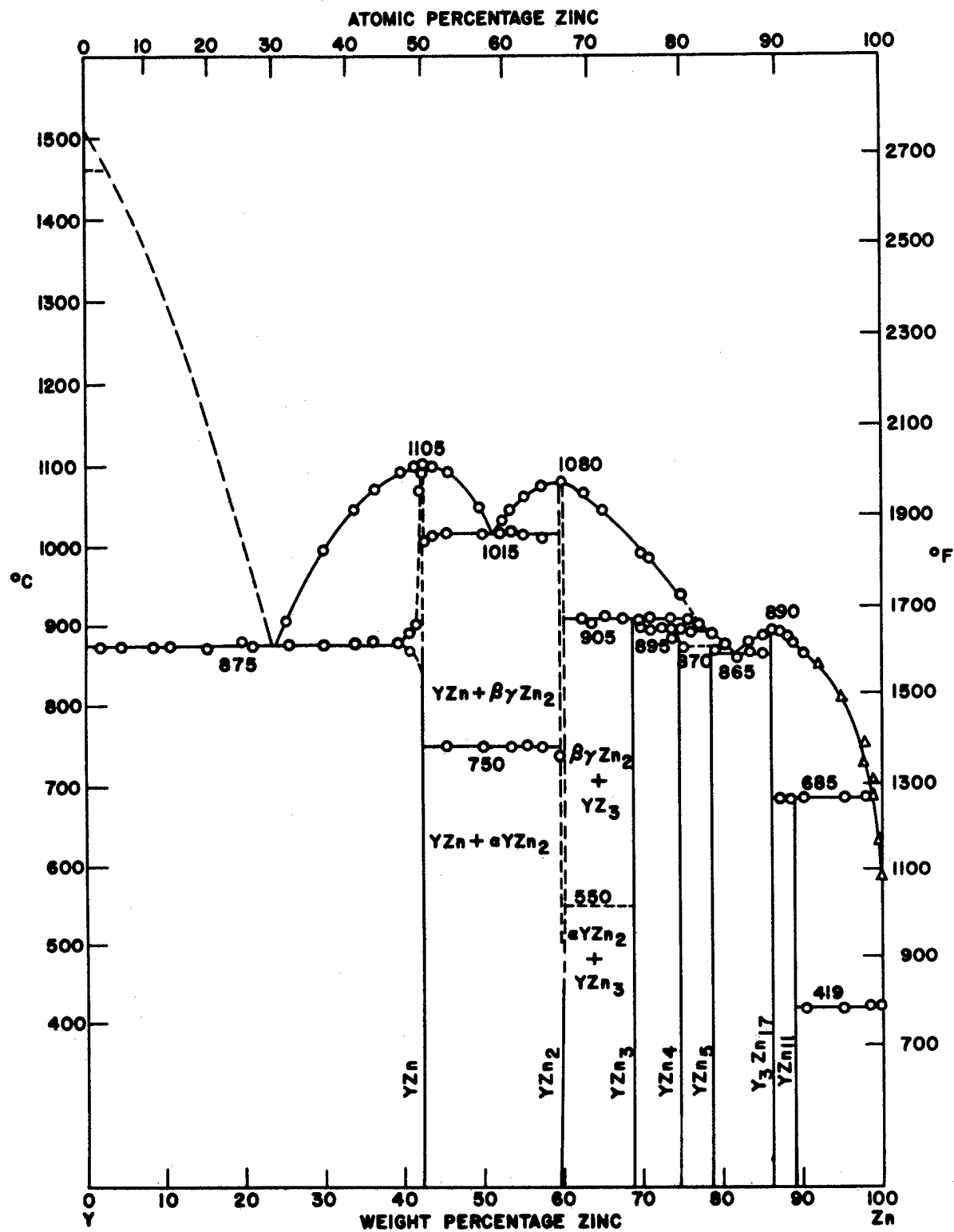


Fig. 4. Phase Diagram for the Yttrium-Zinc System under Constrained Vapor Conditions

Three compounds, YZn , YZn_2 and Y_2Zn_{17} , melt congruently at 1105, 1080 and 890°C respectively. Four compounds with stoichiometric formulas YZn_3 , YZn_4 , YZn_5 and YZn_{11} undergo peritectic reactions at 905, 895, 870 and 685°C respectively. The three eutectics shown in Fig. 4 have the following eutectic temperatures and zinc contents; 875°C-23.2 wt% Zn, 1015°C-51 wt% Zn, and 865°C-82 wt% Zn. The solubility of yttrium in liquid zinc, indicated by triangular points in Fig. 4, for the temperature range 495 - 850°C was determined in an earlier investigation, see USAEC Report No. IS-193, p. 89. These data are consistent with the thermal analyses data of the present work. The solid solubility of zinc in yttrium is small but has not been definitely determined.

The results of zinc vapor pressure measurements are summarized in Table X. Plots of $\log P$ vs $1/T$ were fitted to a straight line by a least squares treatment. The data for alloys in the YZn - YZn_2 region showed a definite change in slope at 750°C, 1023°K, the transformation temperature in the YZn_2 phase. Consequently the vapor pressure data for alloys in this region was fitted to two straight lines. No definite change in slope was detectable for the vapor pressure data in the YZn_2 - YZn_3 region, presumably due to the high degree of supercooling or martensitic character of the YZn_2 transformation in this composition region.

The standard free energy of vaporization and vapor pressure of pure liquid zinc in the temperature range 692.7 - 1181°K may be represented by the relations

Table X

Zinc Vapor Pressure as a Function of Temperature
for Yttrium-Zinc Alloys

$$\text{Log}_{10} P_{\text{atm}} = a/T + b$$

Equilibrium Phases	a	σa^*	b	σb^*	Temp. Range °K
Y-YZn	-11,510	69	7.02	0.07	905-1145
YZn- α YZn ₂	- 9,640	104	6.71	0.11	815-1020
YZn- β YZn ₂	- 9,100	92	6.19	0.10	1020-1190
β YZn ₂ -YZn ₃	- 8,110	27	6.30	0.03	735-1170
YZn ₃ -YZn ₄	- 7,670	14	6.01	0.02	840-1100
YZn ₄ -YZn ₅	- 8,190	40	6.78	0.04	865-1110
YZn ₅ -Y ₂ Zn ₁₇	- 7,800	52	6.47	0.06	830-1115
Y ₂ Zn ₁₇ -YZn ₁₁	- 6,800	29	5.87	0.04	720- 960

* σa and σb are the standard deviations for the constants a and b respectively.

$$\Delta F^\circ = 30,547 + 5.826T \log T - 43.766T \quad (1a)$$

and

$$\log_{10} P_{\text{atm}} = \frac{-6,678}{T} - 1.274 \log T + 9.568, \quad (1b)$$

respectively. For the sublimation of pure solid zinc, 298 - 692.7°K, the corresponding relations are

$$\Delta F^\circ = 31,400 + 0.875T \log T + 1.2 \times 10^{-3} T^2 - 31.757T \quad (2a)$$

and

$$\log_{10} P_{\text{atm}} = \frac{-6,865}{T} - 0.1913 \log T - 0.262 \times 10^{-3} T + 6.943. \quad (2b)$$

The vapor pressures of zinc over the alloys were calculated from the dewpoint temperatures and Eq. (1b). A few measurements for which the dewpoint temperatures were below the melting point of pure zinc required the use of Eq. (2b). The relations for the vapor pressure given

in Table X are based on vapor pressures determined from these two equations, (1b) and (2b). From these data it is possible to derive relations for the standard free energy, enthalpy and entropy of formation of the various intermetallic compounds formed. In these calculations it is assumed that the compounds are line compounds, negligible composition range, and that the heat of vaporization or sublimation of zinc from the alloys is a constant as determined from the linear relations for $\log P$ vs $1/T$ plots as given in Table X. If heat capacity data for the alloys or intermetallic compounds were available the latter assumption would not be necessary.

Assuming only random errors in the zinc vapor pressures for the alloys the probable error in $\log P$ may be calculated from the relation

$$P(\log p) = \left[\sigma_b^2 + \frac{\sigma_a^2}{T} \left(\frac{1}{T} - \frac{2}{T_{\text{ave.}}} \right) \right]^{1/2} (0.675) \quad (3)$$

where σ_b and σ_a are the standard deviations in the intercept and slope, respectively, of the $\log p$ vs $1/T$ relations in Table X, and $T_{\text{ave.}}$ is obtained from the average $1/T$ for the measurements. The probable error in $\log P$ is a minimum at $(1/T)_{\text{ave.}}$. The probable error in ΔF° per mole of zinc vaporized is given by the relation

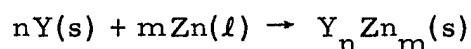
$$P_{\Delta F^\circ} = 2.303 RT P(\log p). \quad (4)$$

For a further discussion of the preceding relations see reference 1 of this section.

Derived relations for the standard free energy of formation of the various yttrium-zinc compounds for temperatures above 692.7°K are given in Table XI. Relations for ΔH° and ΔS° may be derived from the

Table XI

Relations for the Standard Free Energy of Formation of Y-Zn Compounds

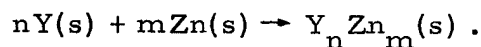


Compound	Equation
YZn	$\Delta F^\circ = -22,090 + 5.826T \log T - 11.657T$
αYZn_2	$\Delta F^\circ = -35,630 + 11.65T \log T - 24.73T$
βYZn_2	$\Delta F^\circ = -33,170 + 11.65T \log T - 27.13T$
YZn_3	$\Delta F^\circ = -39,710 + 17.48T \log T - 42.07T$
YZn_4	$\Delta F^\circ = -44,260 + 23.30T \log T - 58.36T$
YZn_5	$\Delta F^\circ = -51,160 + 29.13T \log T - 71.13T$
Y_2Zn_{17}	$\Delta F^\circ = -138,250 + 99.04T \log T - 241.31T$
YZn_{11}	$\Delta F^\circ = -70,560 + 64.09T \log T - 162.92T$

equation for ΔF° from the relations

$$\frac{d\Delta F^\circ/T}{d(1/T)} = \Delta H^\circ, \text{ and } \frac{d\Delta F^\circ}{dT} = -\Delta S^\circ.$$

If it is assumed that the log *P* equations for the alloys can be extrapolated to room temperature then appropriate combination of these relations with Eq. (2a) will yield the room temperature standard free energy of formation of the compounds. The reactions in this case involve solid zinc,



The 298°K values for the thermodynamic quantities given in Table XII were calculated in this way. The calculated values for the temperatures of 773, 973 and 1173°K were obtained from the relations given in Table XI.

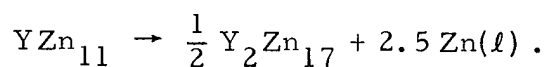
Table XII

Calculated Values for the Standard Free Energy, Enthalpy and Entropy
of Formation of Y-Zn Compounds

Compound	Temp. °K	$-\Delta F^\circ$ cal/mole	ΔH° cal/mole	$-\Delta S^\circ$ cal/mole °K
YZn	298	20,380	21,460	3.61
	773	18,090	24,050	7.70
	973	16,490	24,550	8.28
	1173	14,790	25,060	8.75
YZn ₂ α	298	32,630	34,370	5.81
	773	28,730	39,540	14.0
	973	25,820	40,560	15.2
	1173	23,040	39,110	13.7
YZn ₂ β	298	36,700	37,810	3.74
	773	33,210	45,580	16.0
	973	29,830	47,100	17.8
	1173	26,130	48,610	19.2
YZn ₃	298	40,920	41,730	2.72
	773	37,340	52,080	19.1
	973	33,290	54,110	21.4
	1173	28,810	56,130	23.3
YZn ₄	298	46,440	47,990	5.22
	773	41,110	60,930	25.6
	973	35,670	63,460	28.6
	1173	29,720	66,000	30.9
YZn ₅	298	122,050	127,500	18.3
	773	103,670	171,510	87.8
	973	85,090	180,110	97.7
	1173	64,730	188,710	105.7
Y ₂ Zn ₁₇	298	62,100	63,600	5.04
	773	53,430	92,080	50.0
	973	42,760	97,640	56.4
	1173	30,940	103,210	61.6

In the temperature range of 773 - 1173°K the free energy data are probably within one to two percent of the true values with the higher uncertainty being associated with the free energy of formation

of Y_2Zn_{17} and YZn_{11} . The free energy of formation of compounds with higher zinc content is determined from their dissociation pressure and the free energy of the compound of next lower zinc content and consequently the errors are accumulative. An indication of the magnitude of the error involved in the individual equilibrations can be obtained from the reaction.



At the peritectic decomposition temperature 685°C (958°K) ΔF° for the reaction should be small,

$$\Delta F^\circ = -2.5 RT \ln\left(\frac{p}{p^\circ}\right)_{\text{Zn}}.$$

The zinc liquid in equilibrium with YZn_{11} and Y_2Zn_{17} at 958°K is 99 at.% zinc. If the activity of zinc is taken to be 0.99 (Raoult's law) then ΔF° for the above reaction should be +53 calories. From the free energy relations in Table XI the calculated value is +316 calories. The agreement is fairly good.

The enthalpy data are estimated to be within 5% of their true values. Once heat capacity data are available for the compounds refinement of these data can be made.

2.3 Thermodynamic Properties of Binary Magnesium Alloys from Magnesium Vapor Pressure Measurements (J. F. Smith and D. B. Novotny).

2.3.1 Magnesium-Zirconium System

Taschow and Sauerwald¹ have reported the existence of a compound in the magnesium-zirconium system. Attempts to prepare alloys

¹H. J. Taschow and F. Sauerwald, *Zeitschrift für anorganische and allgemeine Chemie* 307, 123 (1961).

containing this compound have failed. A variety of techniques were tried, and these included powder metallurgical techniques as well as the sealing of magnesium in a zirconium pressure vessel to allow reaction at very high temperature. In no case was there an indication of the occurrence of an intermediate phase. Only when magnesium and zirconium were in contact with MgO was there indication of some reaction. X-ray diffraction patterns of this latter material show a limited and incomplete correspondence with the diffraction lines reported by Taschow and Sauerwald. On this basis it seems probable that there is no intermediate phase in the magnesium-zirconium binary system but rather that the reported phase belongs to the magnesium-zirconium-oxygen ternary system. This is supported by the work of DeLuca et al.¹ In view of the negative alloying results, no measurements of magnesium vapor pressures were attempted and work on this system will be discontinued.

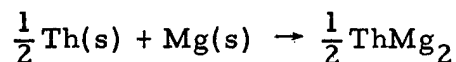
2.3.2 Thorium-Magnesium System

Thorium-rich alloys of thorium and magnesium have been prepared by reduction of ThCl_4 with excess magnesium. X-ray diffraction patterns indicate that the alloys are two phase, containing thorium and the cubic Laves phase, ThMg_2 . Vapor pressures of magnesium over these alloys have been measured by the Knudsen effusion method and may be represented by the equation:

$$\log P \text{ (mm Hg)} = - \frac{(9080 \pm 240)}{T} + (10.28 \pm 0.32) .$$

¹L. S. DeLuca, H. T. Sumison, and D. D. Van Horn, "Magnesium-Zirconium Diffusion Studies", U. S. Atomic Energy Commission Report No. KAPL-1746 (1957).

This vapor pressure relationship may be combined with that for pure magnesium to yield for the reaction



the relationship,

$$\Delta F^\circ = -(7.0 \pm 1.8) + (7.3 \pm 2.3) \times 10^{-3}T \text{ kcal},$$

wherein activity variation due to limited solubility of magnesium in thorium has been neglected and the ΔC_p for the reaction has been approximated as zero.

2.4 Uranium-Rhenium Alloy System (W. L. Larsen, R. J. Jackson and D. E. Williams)

Recent work has shown that the previously reported uranium-rich phase of questionable stability and composition is indeed a stable phase and has a composition near U_2Re . This phase forms sluggishly via a peritectoid reaction at temperatures below 750°C . Experiments to determine the structure and solubility limits of this phase are in progress and will probably require several months for completion due to the slow reaction rates at the temperatures involved. Results to date support the revised phase diagram presented in Fig. 5.

The phase diagram is of the double eutectic type with the intermediate phase having the composition URe_2 . This phase exhibits allotropy at 180° and melts congruently at 2200°C . The phase, URe_2 , reacts sluggishly with the uranium solid solutions below 750°C to form the peritectoid compound U_2Re . Eutectic reactions occur at 1104 and 2105°C at respective compositions of 10.5 and 65.5 wt\% Re . Eutectoid reactions occur at 643 and 681°C at compositions of 1.4 and 6 wt\% Re ,

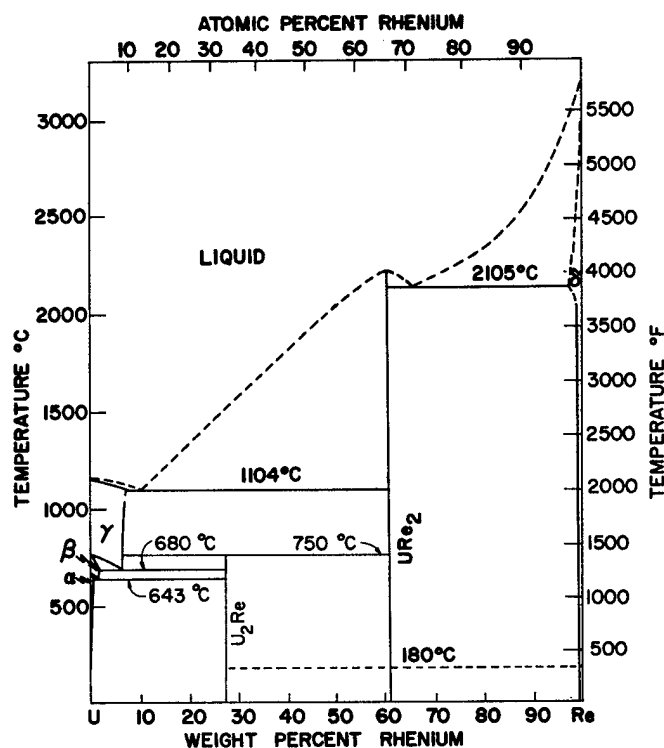


Fig. 5. The Uranium-Rhenium Phase Diagram

respectively. The maximum solubility of rhenium in alpha uranium is about 0.4 wt% at 643°C and in beta uranium is 1.9 wt% at 681°C. The solubility of rhenium in gamma uranium is 6 wt% at 681°C and increases to about 7 wt% at 975°C. The solubility of uranium in rhenium is 0.6 wt% at room temperature with little variation up to 2000°C.

Alloys of beta and gamma uranium containing more than about 1.2 and 7 wt% Re, respectively, can be readily supercooled to room temperature. Rapid cooling of gamma alloys containing less than about 6 wt% Re resulted in a direct gamma to alpha transformation giving rise to a supersaturated alpha phase (α') having a banded microstructure. Evidence was found for the existence of two transition states, one involving the gamma phase decomposition and the other the beta to alpha transformation.

2.5 Determination of the Oxygen Solubility Limits in the Niobium-Zirconium-Oxygen Ternary System (W. L. Larsen and V. C. Marcotte)

Alloys have been prepared by arc melting Nb, Zr and Nb₂O₅ under helium. Oxygen and zirconium have been added to niobium in amounts up to 1 at.% and 25 at.%, respectively. As-cast alloys contained β Zr-Nb solid solution and ZrO₂. These alloys recrystallize at about 1400°C with little solution of ZrO₂.

Work has been concentrated on achieving homogeneous alloys by prolonged heat treatment. Alloys in both wire and massive forms heated at 1800 and 1900°C show considerable surface depletion of oxygen. There is also some metal deposition on cold parts of the furnace with Nb and Zr being deposited in approximately equal amounts.

At present no oxides other than ZrO₂ have been positively identified but precipitates of various morphologies have been observed. Future work will continue to be directed toward achieving homogeneous equilibrated alloys. When the services become available, electron microprobe and electron microscopy studies will be made.

2.6 Thorium-Molybdenum System (W. L. Larsen, O. D. McMasters and P. E. Palmer)

This investigation has been completed and a manuscript entitled "The Thorium-Molybdenum Phase Diagram", by the above authors, has been accepted for publication in the Journal of Nuclear Materials.

Abstract--The phase diagram of the thorium-molybdenum alloy system has been determined to be of the eutectic type with a eutectoid reaction associated with the thorium alpha-beta transformation. X-ray, thermal, electrical resistance and metallographic methods have established the eutectic point at $1380 \pm 10^\circ\text{C}$ and $7.0 \pm 0.5 \text{ wt\% molybdenum}$. A

eutectoid reaction is proposed at $1358 \pm 5^\circ\text{C}$ and less than 0.1 wt% molybdenum. No solubility of thorium in molybdenum was detected at 1325°C .

2.7 Thorium-Vanadium System (W. L. Larsen, P. E. Palmer and O. D. McMasters)

Work on this system has been completed and a paper based on the results has been published in the Trans. Am. Soc. Metals 55, No. 2, 301-306 (1962).

Abstract--The phase diagram of the thorium-vanadium system was determined by thermal, electrical resistance, x-ray and metallographic methods. The diagram is simple eutectic in form with a eutectoid reaction associated with the thorium α - β transformation. The eutectic point was established at $1435 \pm 10^\circ\text{C}$ and 5.0 ± 0.5 wt% vanadium. The eutectoid reaction occurs at $1345 \pm 10^\circ\text{C}$ and less than 0.1 wt% vanadium. The solubility of vanadium in thorium is less than 0.4 wt% at the eutectic temperature. The solubility of thorium in vanadium was determined to be less than 0.4 wt% at 1390°C .

2.8 Distribution of Solutes between Liquid Lead and Zinc (D. T. Peterson and R. Kontrimas)

The distribution coefficients of gold, manganese, copper, iron, nickel and cobalt in this system have been determined. The distribution coefficient, the ratio of the mole fraction of solute in the zinc phase to that in the lead phase, for manganese is given by the expression $\log K_d = -2.13 + 4,402/T$. The distribution coefficient for copper is given by the expression $\log K_d = -2.22 + 3,900/T$. The distribution coefficient for gold was the only one which appeared to vary with concentration. The coefficient at 0.0084 mole fraction gold in the zinc phase is given by the expression $\log K_d = -2.13 + 4,402/T$. The distribution coefficients

for iron, cobalt and nickel were so large that, even with approximately one weight percent of any of these elements in the zinc phase, the concentration in the lead phase was below one ppm and could not be detected. The distribution coefficients of cadmium, indium and antimony are being investigated but the data are not complete.

2.9 Yttrium-Oxygen System (O. N. Carlson, R. C. Tucker and E. D. Gibson)

Studies have been made on yttrium-oxygen alloys to determine the solid solubility of oxygen in yttrium, the solidus boundary and the nature of the yttrium allotropic transformation in this system. These studies have been carried out by quenching and microscopic examination, melting point determinations, diffusion couple experiments and x-ray methods.

The solvus boundary in the yttrium-oxygen system has been determined between 600 and 1200°C by annealing, quenching and microscopic examination of a series of alloys. Results of these experiments indicate the primary solid solubility to increase from less than 0.1 wt% O at 600°C to 3.75 wt% O at 1200°C. No irregularities or discontinuities in the curve were encountered in this temperature range. Extension of the solubility data to higher temperatures awaits equipment for annealing in this temperature range.

A diffusion couple consisting of an yttrium cylinder coated with a thin layer of yttrium oxide was annealed at 675°C for 24 hr in an effort to confirm the solubility data by an independent method. Oxygen analyses were run on annular increments machined from this cylinder. The results of this experiment indicate a solubility of oxygen in yttrium between 0.3 and 0.4 wt% O at 675°C which is in quite good agreement with the

interpolated solubility curve as determined from the quenching data. Further use of diffusion couple experiments is contemplated to obtain additional solubility data and diffusion coefficients for oxygen in yttrium.

A high temperature x-ray camera has been set up and calibrated for use in determining the limits of primary solid solubility. The sample temperature was calibrated against a silver standard.

A portion of the solidus in the Y-O system has been determined on alloys containing up to 5 wt% O employing an optical pyrometer melting bar technique. At least three independent measurements were taken on each alloy listed in Table XIII. The estimated accuracy of each melting

Table XIII

Melting Points of Yttrium-Oxygen Alloys

Alloy Composition, wt% O		Melting Temp. °C
0.05	Analyzed	1520
0.82	"	1533
1.2	"	1546
1.7	"	1565
2.7	Nominal	1581
3.0	"	1603
3.3	"	1606
3.9	"	1602
4.2	"	1639
4.5	"	1678
4.8	"	1674
5.1	"	1660

point is $\pm 5^\circ\text{C}$. From these data it appears that the melting point of yttrium is raised by the addition of oxygen to the metal, indicative of a peritectic-type reaction. The peritectic horizontal temperature has been estimated at 1605°C and the peritectic composition between 3 and 3.9 wt% O. There is some evidence to indicate that the melting point

of alloys containing more than 5 wt% O is decreasing, possibly due to a eutectic reaction at the higher oxygen concentrations. The existence of this peritectic could account for the discrepancy between these and previous solidus data.

2.10 Ternary Metal-Carbon-Hydrogen Phase Systems (D. T. Peterson and J. Rexer)

The investigation of metal-carbon-hydrogen systems has established the existence of the new ternary phases $\text{LaC} \cdot \text{LaH}_x$, $\text{YC} \cdot \text{YH}_x$ and $\text{VC} \cdot \text{VH}_x$. These ternary compounds all have structures in which the metal atoms are arranged on a hexagonal closest packed lattice. The approximate stoichiometry and the lattice constants of the ternary compounds which have been discovered to date are shown in Table XIV. The enthalpies

Table XIV

Lattice Constants of Ternary Metal-Carbon-Hydrogen Compounds

Compound	$A_o (\text{\AA})$	$C_o (\text{\AA})$	C/A
$\text{TiC} \cdot \text{TiH}_x$	3.083	5.042	1.635
$\text{ZrC} \cdot \text{ZrH}_x$	3.347	5.492	1.640
$\text{HfC} \cdot \text{HfH}_x$	3.291	5.385	1.635
$\text{ThC} \cdot \text{ThH}_x$	3.816	6.302	1.652
$\text{YC} \cdot \text{YH}_x$	3.732	5.960	1.597
$\text{LaC} \cdot \text{LaH}_x$	4.041	6.554	1.622
$\text{VC} \cdot \text{VH}_{0.46}$	2.899	4.600	1.587

of formation of the thorium, hafnium, zirconium and titanium ternary compounds from gaseous hydrogen, the metal and the carbide are -48.4, -45.2, -48.8 and -43.7 kcal per mole of hydrogen.

respectively. This phase of the study is completed and is being prepared for publication.

2.11 Strontium-Strontium Hydride System (D. T. Peterson and R. Colburn)

The investigation of the Sr-SrH₂ phase system has been nearly completed. There is an extensive solid solubility of hydrogen in strontium metal. The solidus rises smoothly from the melting point of strontium at 768°C to a peritectic at 880°C and 38 mole % strontium hydride. There is a phase transition in strontium hydride in equilibrium with strontium metal at 855°C. The phase transition at 557°C in strontium is raised by the addition of hydrogen to a peritectoid at 620°C. The solid solubility of strontium hydride in strontium decreases from the 14 mole % strontium hydride at peritectoid to 2.5 mole % at 210°C. No evidence has been found by thermal analysis or by x-ray diffraction of the transition which has been reported at 230°C in pure strontium. X-ray diffraction studies indicate that the strontium phase is face-centered cubic both above and below this temperature and no evidence for a hexagonal intermediate phase similar to that in the calcium-calcium hydride system has been found.

2.12 Zirconium-Bismuth Alloy Studies (H. A. Wilhelm and C. B. Hamilton)

In this alloy system there appear to be four intermetallic compounds of compositions approximating ZrBi₂, ZrBi, Zr₃Bi₂, and Zr₂Bi. Only the ZrBi₂ has been reported by other investigators. The ZrBi compound is peritectic, decomposing at 1300 ± 10°C. The compound assumed to be Zr₃Bi₂ has a melting point of 1491 ± 15°C. The Zr₂Bi compound is peritectic with a decomposition temperature of 1337 ± 15°C. One eutectic is found at 1285 ± 15°C at about 75 at.% zirconium.

The compounds found in this alloy system exhibit various degrees of instability in the presence of moisture; the ZrBi compound is especially reactive.

2.13 Zirconium-Cobalt Alloy Investigation (W. L. Larsen, W. H. Pechin and D. E. Williams)

The investigation of the zirconium-cobalt system has continued. The results to date are plotted as the partial phase diagram shown in Fig. 6. This is an extension and revision of the data previously reported (USAEC Report IS-193).

While the liquidus lines have not been determined with precision, the eutectic points and the melting points of congruently melting compounds are as shown.

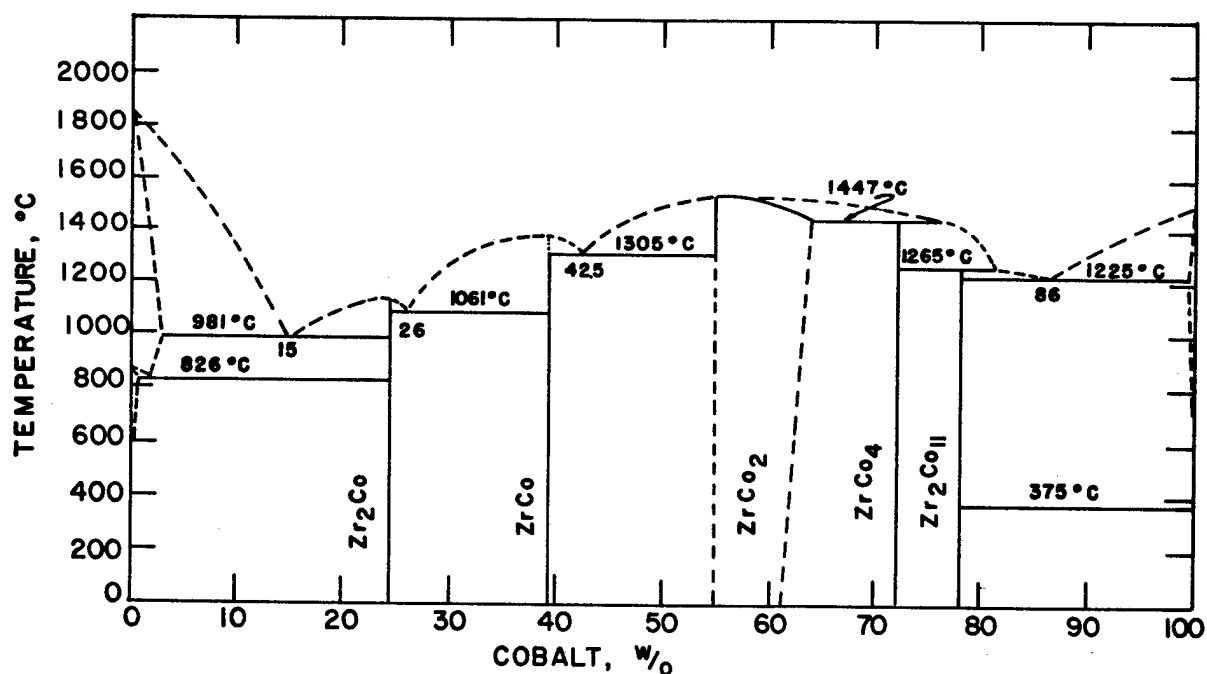


Fig. 6. The Zirconium-Cobalt Phase Diagram

At the solidus temperature the ZrCo_2 phase has a range of solubility extending from 55 to 62 wt% Co. The lattice parameter varies from 6.960Å for 55 wt% Co to 6.878Å for 62 wt% Co.

Zirconium dissolves less than 3 wt% Co and cobalt dissolves less than 0.5 wt% Zr.

Future work will be directed to determining more precisely these terminal solubilities, the eutectoid compositions of the reactions associated with the allotropic transformations of the component metals, and the solubility limits of the ZrCo_2 phase.

2.14 Yttrium-Magnesium Alloy Studies (O. N. Carlson, L. Moore, R. C. Tucker and E. D. Gibson)

The preparation of yttrium-magnesium alloys containing 0.5 to 5 wt% Mg for use in the determination of the solid solubility of magnesium in yttrium has been undertaken and the transformation characteristics of the eutectoid alloy (composition ~10 wt% Mg) have been investigated.

Several methods for preparing yttrium-magnesium alloys containing small amounts of magnesium were tried. Initially, attempts were made to prepare the alloys by co-melting the component metals in sealed tantalum crucibles. This method proved unsatisfactory due to excessive tantalum pick-up in the alloys. Powder metallurgy techniques were also tried by annealing compacts prepared from yttrium and magnesium powders. This technique was also eliminated as a method for alloy preparation since non-porous alloys could not be formed and yttrium powder of high purity was difficult to prepare. Recently a method whereby yttrium rod or sheet is infused with magnesium

vapor in a sealed tantalum crucible has been employed with some success. Results of these experiments indicate that a continuous layer of the compound YMg is formed on the surface of the metal at temperatures below 775°C. It should thus be possible through diffusion-type studies to obtain solid solubility data and also data concerning the diffusion coefficient for magnesium in yttrium.

The transformation characteristics of the Y-10 wt% Mg alloy have been investigated by hardness measurements and microscopic and x-ray examination of structures resulting from isothermal transformation of the alloy at temperatures below 775°C.

Two techniques have been used to heat treat the alloy specimens. In the initial stage of this investigation an interrupted quench from the solution treatment temperature (850°C) into a molten lead bath at 400, 500, 600 or 700°C for from 10 sec to 10 min was employed. Later, it was shown that quenching all specimens to room temperature from 850°C and then aging for various times at temperatures from 200 to 650°C gave more consistent results making possible a better evaluation of the effect of the transformed structure on the properties of the alloy.

Results of these experiments on the isothermal transformation of the eutectoid alloy have shown that the hardness of the alloy is increased by this aging process. A curve of aging time vs hardness for a series aged at 400°C is shown in Fig. 7. The effect of the aging time at various temperatures shows an "over aging" effect occurring at the higher temperatures with prolonged annealing times (see Fig. 8). The microstructures of the alloy specimens show that precipitation of the

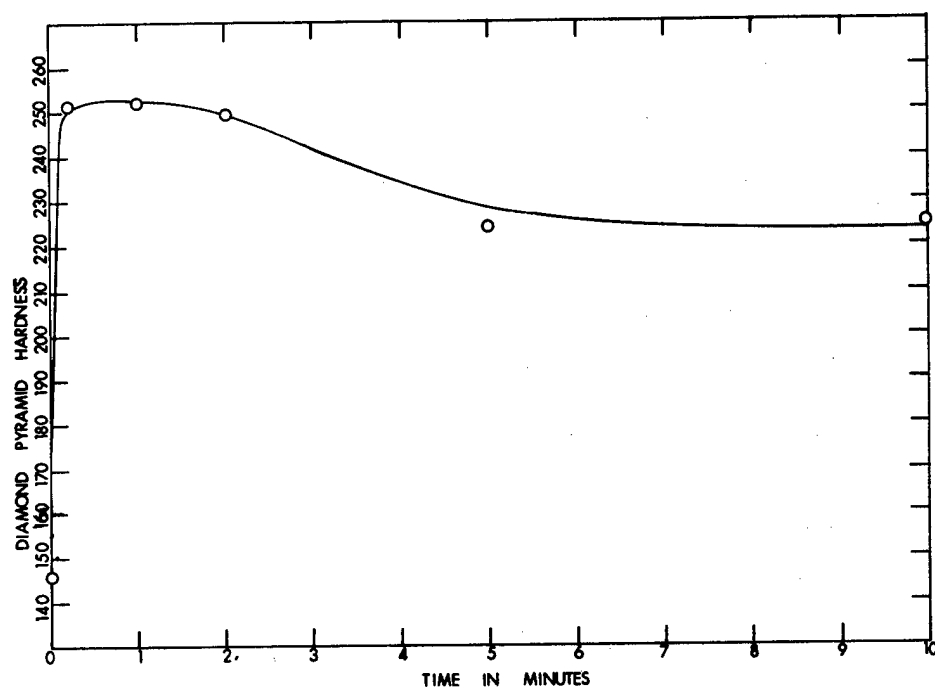


Fig. 7. Effect of Time of Aging at 400°C on Hardness of Y-10 wt% Mg Alloy

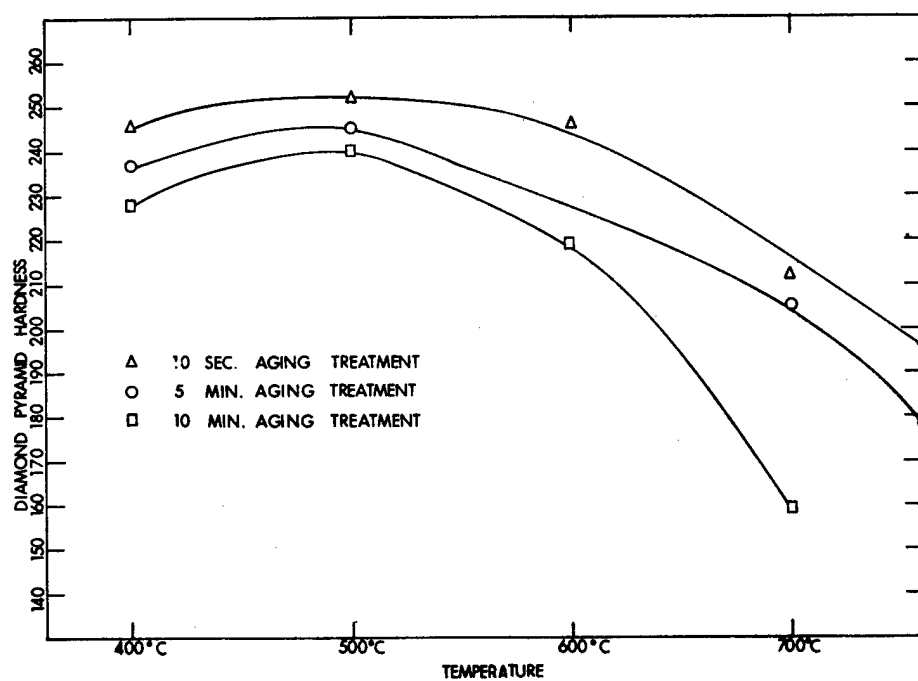


Fig. 8. Hardness vs Temperature Curves for Different Aging Times for Y-10 wt% Mg Alloy

transformed product begins at the grain boundaries and at later stages intergranular precipitation is encountered. Electron micrographs of the transformed regions show no substructure present in this phase. X-ray patterns taken of the alloy in various heat-treated conditions show that quenching retains the high temperature, body-centered cubic phase, and the transformed structure consists of a simple cubic phase and one tentatively identified as the hexagonal form of yttrium. The partially transformed alloy, aged at 400°C, contains all three crystal-line forms.

2.15 Chromium-Nickel Phase Studies (O. N. Carlson, D. W. Bare and E. D. Gibson)

A study of chromium-nickel and chromium-nickel-molybdenum alloys by melting point determinations, thermal analyses and x-ray techniques is being made in an effort to confirm or refute the postulated high temperature allotropic transformation in chromium.¹ Attempts are also being made to develop a method to determine (with a high degree of precision) the disputed melting point of chromium metal.

Five binary Cr-Ni alloys and three ternary Cr-Ni-Mo alloys were prepared for use in seeking evidence for the high temperature allotope of chromium. Nickel and molybdenum have been reported to stabilize the high temperature form of chromium. Thermal analyses run on all five binary Cr-Ni alloys have shown no thermal arrests up to 1340°C. Melting points were taken on these alloys and the results are in agreement with published data on the Cr-Ni system.

A high-temperature x-ray camera has recently been set up for examination of the Cr-Ni alloys in an effort to identify the phases present at elevated temperatures.

¹D. S. Bloom and N. J. Grant, "Chromium-Nickel Phase Diagram", Trans. AIME 194, 1009 (1951).

Considerable attention has been given to an accurate measurement of the melting point of unalloyed iodide chromium. Several attempts were made to determine the melting point by a conventional optical pyrometer technique but absorption by chromium vapor in the optical sight path or other difficulties have led to wide scatter in this data. Alternative methods for determining the melting point of chromium designed to eliminate errors introduced by metallic vapors are now being developed.

2.16 Niobium-Tin Alloy System (H. A. Wilhelm and T. G. Ellis)

A proposed constitutional diagram was developed from equilibrium data obtained for the niobium-tin binary alloy system. The data were gathered by photomicrographic, chemical and x-ray techniques. The equilibrium solubility of niobium in liquid tin varied from approximately 250 - 2000 ppm at 580 and 1000°C, respectively. The equilibrium solubility of tin in niobium varied from approximately 2.5 wt% tin to 3 wt% tin at 550 and 1000°C. Two previously unreported intermetallic compounds, Nb_2Sn_3 and Nb_3Sn_2 , in addition to Nb_3Sn were found in the system. Nb_3Sn , previously reported,¹ decomposed peritectically into niobium and liquid tin at $2125 \pm 25^\circ\text{C}$. Nb_3Sn_2 decomposed into Nb_3Sn and liquid tin at $915 \pm 5^\circ\text{C}$. Nb_2Sn_3 , the assumed but unverified composition for the most tin-rich compound, decomposed into Nb_3Sn_2 and liquid tin at $820 \pm 3^\circ\text{C}$. The stoichiometry of this most tin-rich compound was based on a chemical analysis. However, crystallographic evidence indicates a strong possibility that this compound may be NbSn_2 .

¹B. T. Matthias, T. H. Geballe, S. Geller and E. Corenzwit, Phys. Rev. 95, 1435 (1954).

The assumed Nb_2Sn_3 has a D_{2h}^{24} -Fddd structure with lattice parameters of $5.72 \pm 0.04 \text{ \AA}$, $10.03 \pm 0.06 \text{ \AA}$ and $19.06 \pm 0.06 \text{ \AA}$. Nb_3Sn_2 has a body-centered orthorhombic crystal structure with lattice parameters of $5.637 \pm 0.001 \text{ \AA}$, $9.204 \pm 0.003 \text{ \AA}$ and $16.667 \pm 0.003 \text{ \AA}$. The number of possible space groups for Nb_3Sn_2 has been reduced to four, D_2^8 -I222, D_2^9 - $2_12_12_1$, D_{2h}^{25} =Immm and C_{2v}^{20} -Imm.

2.17 Nb_3Sn - Nb_3Al Alloy System (H. A. Wilhelm and T. G. Ellis)

The intermetallic compounds Nb_3Sn and Nb_3Al were found to be completely miscible in the solid state. All of the alloys between these compounds were simple cubic (Cr_3O type). Their lattice constants followed Vegard's rule except in the vicinity of mole ratios of 1:3 and 3:1. At these mole ratios the lattice constants deviated to values larger than predicted by Vegard's rule.

Alloying Nb_3Sn with Nb_3Al appears to raise the zero field superconducting transformation temperature of Nb_3Sn slightly.

2.18 Calorimetric Determination of the Enthalpies of Formation of Some Inter-metallic Compounds (J. F. Smith and J. E. Davison)

Because of the inherent limitations on precision in the determination of small heats of formation by combustion calorimetry, measurements by this method have been discontinued. Instead, a differential solution calorimeter has been designed and constructed. Test runs are now in progress on this solution calorimeter.

2.19 Phase Diagram and Electrical Resistivity of Thorium-Carbon Alloys (P. Chiotti and F. Korbitz)

Some of the phase fields in the thorium-carbon system have not been definitely established. Previous work has indicated a complete

series of solid solutions exists at high temperatures ranging from pure thorium to ThC_2 . Carbon occupies the octahedral interstitial sites in the face-centered lattice of thorium. Once all the octahedral sites are filled with carbon atoms the composition corresponds to that for ThC . As more carbon is added C_2 groups can form and as long as these remain randomly oriented at the octahedral sites the basic structure can remain face-centered cubic and a continuous one-phase region is possible. The purpose of the present investigation is to measure the temperature dependence of the electrical resistance of thorium-carbon alloys and to establish the phase fields, transformation temperature of ThC_2 (which must exist if a complete series of solid solutions exists at high temperatures) and other features of this system.

Present efforts have been directed toward the preparation of dense alloys in a form suitable for resistance measurements. Arc-melting and diffusion techniques are being investigated. Once resistance data on dense or void free alloys are available, resistivity-composition plots can be helpful in establishing the phase boundaries.

2.20 Zirconium-Niobium-Titanium Alloy Studies (H. A. Wilhelm and K. M. Wolf)

Microstructures of slowly cooled alloys indicate a rather extensive one-phase area in this ternary system for room temperature. However, sluggishness of the beta to alpha transformation might contribute to this condition. The one phase represented by this area is assumed to be the body-centered cubic structure common to all three pure components at certain temperatures.

Most of the ternary alloy compositions in the assumed one-phase area hot worked with difficulty. This behavior possibly indicates good high

temperature strength. Since these alloys fall in the superconductivity realm some are being tested for such properties as well as for corrosion resistance.

2.21 Aluminum-Tantalum Alloy Studies (H. A. Wilhelm and J. H. Witte)

Powder metallurgy techniques were found best for the preparation of these alloys, with the major problems in their preparation being aluminum loss by vaporization and reaction with the container material during the heating cycle, especially at temperatures above 1500°C. Two compounds that are believed to be peritectic in nature exist in the system. These are TaAl_3 (tetragonal) and Ta_2Al (tetragonal). X-ray data show both compounds exhibit solid solubility. Incipient meltings of the stoichiometric compounds were observed for TaAl_3 at $1500 \pm 50^\circ\text{C}$ and for Ta_2Al at $2100 \pm 50^\circ\text{C}$.

3. MECHANICAL PROPERTIES OF METALS AND ALLOYS

3.1 Effect of Oxygen on Mechanical Properties of Niobium (H. A. Wilhelm and E. P. Neubauer)

A detailed report of this investigation is being prepared for distribution as USAEC Report No. IS-503. Series of samples of niobium containing oxygen in amounts up to 2400 ppm were tested for tensile properties over the temperature range from room temperature to 500°C. Hardness values were obtained on the series only at room temperature.

Oxygen additions increased both the yield and tensile strengths at all temperatures investigated. A maximum in the tensile stress-temperature relationship (Fig. 9) appeared at about 225°C for compositions studied that were 500 ppm or greater in oxygen; this maximum was more pronounced for the higher oxygen contents.

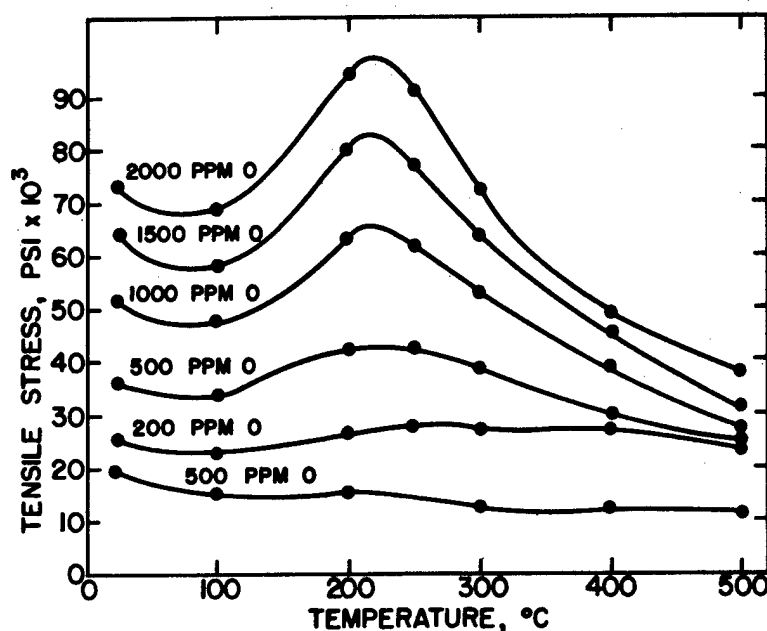


Fig. 9. Tensile Stress-Temperature Relationships for Niobium. Maximum at about 225°C Associated with Oxygen Content

3.2 Mechanical Properties of Thorium (D. T. Peterson and J. D. Young)

The creep deformation of thorium metal is being investigated in the temperature range from -100 - $+200^{\circ}\text{C}$. The relationships between the creep rate and the stress, strain and temperature will be determined. Creep at room temperature has been observed at a stress of 10,000 psi although the 0.2% offset strength of metal of similar purity at normal tensile testing rates is greater than 20,000 psi. The behavior of thorium in creep parallels its behavior in normal tensile testing in that the creep rate increases after a plastic strain corresponding to the upper yield point and then decreases following a strain corresponding to the lower yield point. An apparatus has been designed and constructed for making creep tests at constant temperatures over the temperature range of interest in this investigation.

3.3 Work Hardening of Thorium (W. L. Larsen and D. E. Williams)

The investigation of the variation of the hardness of thorium with the degree of cold work has been completed.

It has been found that the hardness of thorium increases rapidly up to about 10% reduction, increases very slowly thereafter up to about 80% reduction, and increases a bit more rapidly beyond 80% reduction. This behavior is represented by the Vickers Hardness Number data previously reported.¹ The variation of Vickers hardness with percent cold work is independent of whether the thorium is rolled or swaged. The Rockwell-E (R_E) hardness measured on rolled samples shows the same dependence upon cold work with the exception of the slight tailing upward near 90% reduction, observed in Vickers tests, which may only be a reflection of the greater sensitivity of the Vickers test to surface hardening.

Rockwell-E hardness measurements on cylindrical swaged samples show a drop in hardness beyond about 50% reduction as reported by Lowenstein.² However, the application of a correction factor necessary for cylindrical samples³ brings this curve into coincidence with the R_E curve for flat rolled samples.

It is concluded that the apparent conflict in previously reported data is due to the use of an inappropriate hardness scale, that thorium does not

¹"Annual Summary Research Report in Metallurgy", USAEC Rept. IS-351, p. 53 (December 1961).

²P. Lowenstein, "Technical Progress Report for the Period April 1952 through September 1952", MIT-1102 (1952).

³W. E. Ingerson, "Rockwell Hardness of Cylindrical Specimens", Proc. ASTM 39, 1281-1291 (1939).

soften with progressive cold work, and that the earlier data of Hamby¹ are essentially correct.

3.4 Mechanical Forming of Yttrium (O. N. Carlson and C. V. Owen)

The fabrication of high purity yttrium metal by rolling, swaging and extrusion was investigated during this period. Experiments were conducted to determine the contamination of yttrium by different cladding materials during the production of high purity sheet from arc-cast ingots. The rolling temperature, speed and the reduction per pass were held constant for all experiments. Ingots encapsulated in titanium, copper, 1010 steel and tantalum, were rolled at 550°C into a thin plate and the jacket removed by mechanical or chemical procedures. Analysis of the yttrium before and after rolling showed appreciable contamination by all cladding materials except titanium. Further work with the titanium-clad ingots showed that high purity yttrium can be fabricated into sheets at 600°C without any detectable contamination. Swaging was also carried out under these same conditions.

The extrusion of yttrium into solid rods and small diameter tubing has been achieved using the newly installed 700 ton extrusion press. The extrusion ratio was maintained at a constant value of 15 to 1 while the temperature, force and speed were varied independently. Some billets were jacketed before extrusion while others were extruded in the unclad condition.

For the unclad billets, the optimum conditions for extrusion were found to be an extrusion speed of 3 in./sec and a force of 200 tons at

¹D. E. Hamby, "Interim Report on Metallurgy of Thorium and Thorium Alloys", ORNL-1090 (1951).

450°C. Billets jacketed in copper extruded satisfactorily at a temperature of 675°C at a speed of 0.5 in./sec with a force of 100 tons; however, appreciable contamination of the yttrium with copper was encountered necessitating the use of a thin titanium barrier between the copper jacket and the ingot. Successful extrusion of these ingots was accomplished at 750°C. Upon removal of the cladding material the surface of the yttrium rod was seen to be somewhat irregular but otherwise of generally good condition.

Yttrium tubing, 3/4 in. O.D. and 0.060 in. in wall thickness, was fabricated by extrusion. An unclad billet was extruded into tubing at 575°C and two billets clad in the titanium-copper jacket were successfully formed at 750°C. Further work on improving the surface condition of the unclad billet by proper selection of a die lubricant is in progress. This method offers considerable promise of producing a tube free of flaws and surface defects while having the necessary dimensions required in the hot loop experiments.

3.5 Ductility of Chromium and Chromium-Base Alloys (O. N. Carlson, D. W. Bare, L. Sherwood, K. E. Solie and F. A. Schmidt)

3.5.1 Properties of Chromium Single Crystals

Several chromium single crystals were prepared by a high temperature grain growth technique for use in ductility studies. The single crystals were grown by induction heating of arc-melted specimens in a sealed crucible at 1700°C for 7 - 21 hr. Rhenium crucibles were used in the earlier work but contamination of the rhenium by chromium vapors was found to shorten the crucible lifetime of this material making it brittle and difficult to weld. Crucibles made from the ductile Mo-50 wt% Re

alloy are more inert toward chromium at 1700°C and this alloy was successfully used in all subsequent runs.

Attempts were made to grow single crystals of chromium for use as tensile test specimens. Although no single crystals were grown several bi- and tri-crystal specimens were obtained. When tested in tension at room temperature they exhibited remarkable ductility undergoing greater than 95% reduction in area and 40 - 65% total elongation.

3.5.2 Effect of Nitrogen on Mechanical Properties of Chromium

During this report period a study was initiated on the effect of nitrogen on the mechanical properties of iodide chromium. As a part of this investigation the effects of prior working and heat treatment were studied and the variations in the tensile properties of polycrystalline iodide chromium with temperature and strain rate were investigated.

Rods of chromium prepared by swaging at 750°C were fabricated into tensile specimens. These were vacuum annealed for one hour at temperatures of 300 - 800°C, all below the recrystallization temperature of this material, and then tested in tension. From the data in Table XV it is apparent that working enhances the room temperature ductility of chromium but that annealing of the worked metal has a detrimental effect upon the tensile properties of the metal, particularly the ductility parameters.

The tensile strength vs temperature curve for unalloyed chromium exhibits a strain aging peak in the range of 300 - 400°C for tests carried out at a strain rate of 0.013 min^{-1} . Additional evidence for strain-aging in this region is a minimum in the strain rate sensitivity between 250 - 500°C and a return of the yield point following aging at 350°C.

Table XV

Tensile Properties of Annealed Chromium at Room Temperature

Prior Treatment	Yield Strength psi	Total Elongation, %	Total Elongation, %	Reduction in Area, %
As swaged	75,400	4	17.6	75.9
300°C anneal	73,700	11.2	26.4	33.2
350°C anneal	72,600	2.2	2.2	2.9
400°C anneal	74,100	0	1.4	0
500°C anneal	72,800	0	0.4	0
800°C anneal	58,000	0	0	0

Tests run at a higher strain rate, 0.13 min^{-1} , indicate the presence of two maxima in the tensile strength-temperature curve, a small, broad peak at 510°C and a large one at 665°C . This investigation will determine if either of these peaks is due to nitrogen and what effect nitrogen has on the strength and ductility of iodide chromium.

The role of nitrogen in the strain age hardening of chromium is also being investigated. In addition to bringing about a return of the yield point, aging a chromium specimen at 350°C after straining results in an increase in the flow curve. This phenomenon is referred to as strain age hardening and has been previously observed in iron.¹ The explanation that has been offered for this phenomenon is the precipitation of impurities at dislocation sites to form a second phase which produces precipitation hardening. Evidence for this precipitation in chromium is now being sought.

The brittle-ductile transition temperature of chromium has been reported to be sensitive to the nitrogen content of the metal. Grant and

¹B. B. Hundy, "The Strain Age Hardening of Mild Steel", Metallurgica 53, 195, p. 203.

Abrahamson¹ reported that electrolytic chromium containing 80 ppm N exhibits a transition temperature of 300 - 350°F while metal containing 150 ppm N has a transition temperature of 1000 - 1050°F. Hardness measurements were taken on a series of iodide specimens containing additions of 50, 100, 150 and 200 ppm N (see Table XVI) and bend test specimens were prepared for use in studying the influence of nitrogen on the bend transition temperature. These tests are now in progress.

Table XVI

Hardness vs Nitrogen Content of Iodide Chromium

DPH Hardness Numbers	Nominal Nitrogen Addition to Iodide Chromium (ppm)
117	0
140	50
139	100
154	150
163	200

3.5.3 Effect of Alloy Additions on Brittle-Ductile Transition of Chromium

An investigation of the effect of alloying on the ductility of iodide chromium was undertaken in an effort to improve the mechanical properties of chromium and to elucidate the phenomenon of the brittle-ductile transition. The bend transition temperature was determined as a function of alloy composition for a large number of binary additions.

The alloys were prepared by arc melting and bend specimens 1 in. by 1/4 in. by 0.045 in. were cut directly from the arc casting or in a few cases from sheet prepared by rolling at 750°C. The specimens were electropolished to a final thickness of 0.40 in. using concentrated H_3PO_4 as the electrolyte.

¹N. J. Grant and E. P. Abrahamson, Chromium-Base Alloys, U. S. Patent No. 3,008,854 (November 1961).

The transition temperatures were determined from bend tests performed at a constant deflection rate of 0.04 in./min on a three-point loading apparatus.

Three different lots of iodide chromium obtained from the Chromalloy Corporation were used as the base metal. Brittle-ductile transition temperatures and analytical data for the unalloyed chromium are presented in Table XVII.

Table XVII

Transition Temperature and Analytical Data
for Different Lots of Iodide Chromium

Lot No.	Condition	B-D Transition Temp. °C	Impurity Content, ppm				
			C	Fe	N	O	H
556	As-arc-melted	-45±5°	60	28	20	8	1
550	As-arc-melted	-42±5°	50	55	30	3	1
542	As-arc-melted	-40±5°	140	33	7	4	1
542	As-rolled	-30±5°	140	33	7	4	1

As can be seen from the table there is little difference in the transition temperature in spite of a considerable variation in carbon and nitrogen content. Furthermore the as-rolled specimen has a brittle-ductile transition temperature which is only 10° higher than the same material in the arc cast condition.

Chromium-base alloys containing 0.1 to 3.0 wt% of the binary addition were prepared and the transition temperature of these alloys was determined. The results are presented in Table XVIII in order of decreasing brittle-ductile transition temperature.

Table XVIII

Brittle-Ductile Transition Temperatures of Chromium-Base Binary Alloys

wt% Alloying Element	B-D Transition Temp. °C	wt% Alloying Element	B-D Transition Temp. °C
3.0-Cu	>200	0.5-Pd	15
1.5-Cu	> 82	0.1-Pd	-60
0.5-Cu	-20	0.5-Ta	-55
1.5-Sn	> 95	0.5-Rh	-60
3.0-Sn	> 25	0.1-Rh	-75
0.5-Sn	> 25	0.1-Ir	> -40
0.1-Sn	-25	1.5-Ir	-50
0.5-Gd	70	0.5-Ir	-87
3.0-Gd	55	0.1-Os	-85
1.5-Gd	50	0.5-Mo	-65
0.5-Dy	60	3.0-Ru	> -60
1.5-Dy	50	3.0-Mn	-22
3.0-Dy	40	3.0-Re	-35
3.0-Nd	35	*1.5-Re	-67
1.5-Nd	25	*0.5-Re	-67
0.5-Nd	10	*0.1-Re	-105
1.5-Pr	35	*3.0-Ag	-55
3.0-Pr	20	*1.5-Ag	-70
3.0-Th	> 25	*0.5-Ag	-70
1.5-Th	> 25	0.1-Ag	-55
0.5-Th	> 25	0.5-Ru	-75
0.1-Hf	> 25	1.5-Ru	-85
*3.0-Y	5	0.1-Ru	-85
*1.5-Y	5	3.0-Au	> 25
*0.5-Y	5	1.5-Au	> 25
3.0-V	25	0.5-Au	> 25
1.5-V	15	0.1-Au	-82
0.5-V	-15	0.5-Pt	> -30
2.0-V	-20	0.05-Pt	-75
1.0-V	-25	0.1-Pt	-125
3.0-Al	> 25		
1.5-Al	> -20		
0.5-Al	-35		

* Tested on specimens prepared from sheet fabricated by rolling at 750°C.

Alloy additions of Re, Ag, Au, Pt, Pd, Ir, Os, Ru, Mo, Ta and Rh were found to depress the transition temperature whereas the other elements either raise it or have no appreciable effect in the composition range investigated.

In general, the ductility increases with decreasing percentage of the alloying element, however, the reverse is true in the case of the rare-earth metals. One empirical correlation that has been noted from these data is the tendency of those elements having atomic volumes slightly larger than that of chromium to reduce the brittle-ductile transition temperature of iodide chromium.

3.5.4 Forming of Chromium and Chromium-Base Alloys (O. N. Carlson and C. V. Owen)

The fabrication of unalloyed iodide chromium and chromium containing up to 200 ppm of nitrogen was investigated. Specimens were first encapsulated in a mild steel jacket and swaged at 750°C allowing adequate time between each pass for the bar to reach the required temperature. This equilibration time was found to be critical, because specimens held for shorter periods of time developed surface folds and radial cracks. The same temperature conditions were employed in the rolling experiments. Unalloyed chromium and specimens containing 50 ppm nitrogen were rolled at the same temperature without difficulty but those containing higher concentrations of nitrogen developed large transverse cracks early in the rolling process. Stainless steel was substituted for the mild steel jacket on these alloys and the rolling temperature was raised to 800-850°C. This resulted in chromium sheet of excellent quality.

3.6 Plastic Properties of Vanadium (O. N. Carlson and R. W. Thompson)

Work has been initiated on the effect of nitrogen on the mechanical properties of vanadium. Tensile specimens have been prepared for determining the role of nitrogen in strain aging and its effect on the ductility of iodide vanadium.

4. SOLID STATE INVESTIGATIONS

4.1 Magnetic Susceptibility Measurements

4.1.1 Vanadium-Carbon System (J. F. Smith and J. D. Greiner)

The compounds V_2C and VC both exist over a range of composition on the vanadium-rich side of their respective stoichiometries. The solid solubilities are based upon defect structures. Because of the extensive solid solubilities there exists the possibility that composition inhomogeneities might occur in test specimens. To test for this possibility, magnetic susceptibilities were measured directly on arc-melted samples. These samples were subsequently given a prolonged annealing treatment to induce homogenization and again measured. No significant susceptibility changes were found after the annealing treatment.

It is difficult to prepare either compound at stoichiometry. A sample of the hexagonal phase at $VC_{0.48}$ and of the cubic phase $VC_{0.98}$ were prepared and measured over the temperature range 78 - 300°K. Both samples were found to exhibit a weak, temperature independent paramagnetism of the Pauli type. The numerical value for $VC_{0.48}$ is near 210 e.m.u. per mole of vanadium while $VC_{0.98}$ is near 30 e.m.u. per mole of vanadium.

It was also observed that hydrogen addition lowered the susceptibility of V_2C .

4.1.2 Magnetic Susceptibilities of the Halides of the Second and Third Period Transition Elements and of Their Organic Complexes (J. F. Smith, J. D. Greiner and R. E. McCarley)

The following salts were found to be diamagnetic with little or no temperature dependence: TaBr_4 , TaBr_3 , TaI_3 , WBr_3 , WBr_4 , WBr_5 and NbI_3 . Weak paramagnetism without pronounced temperature dependence was found in MoBr_3 and MoBr_4 . Thus there is no indication in these compounds of the presence of unpaired electrons which behave as independent dipoles.

However, the complexes $\text{TaCl}_4 \cdot 2\text{pyridine}$, $\text{TaBr}_4 \cdot 2\text{pyridine}$, $\text{MoBr}_4 \cdot 2\text{pyridine}$ and the compound K_2NbCl_6 were all found to exhibit strongly temperature dependent paramagnetism of the Curie-Weiss type. The indicated magnetic moments for the tantalum complexes are less than one-half the 'spin only' value for Ta(IV).

4.1.3 Miscellaneous Magnetic Susceptibility Measurements (J. F. Smith and J. D. Greiner)

The tetragonal sodium tungsten bronze, $\text{Na}_{0.1}\text{WO}_3$, was measured in powder form. Within experimental precision the measured susceptibility was the same as that of pure WO_3 . This is in marked contrast to the susceptibility behavior of the cubic sodium tungsten bronzes.¹

The following carbides have also been measured:

NbC (299°K)	-0.12	$\times 10^{-6}$	e.m.u./gram
NbC (111°K)	-0.13	"	"
$\text{NbC}_{0.75}$ (300°K)	+0.20	"	"
$\text{TaC}_{<0.75}$ (298°K)	-0.07	"	"

¹J. D. Greiner, H. R. Shanks and D. C. Wallace, J. Chem. Phys. 36, 772 (1962).

4.2 Anisotropic Thermal Expansion of Indium (J. F. Smith and V. L. Schneider)

Measurements of the anisotropic thermal expansion of three commercial grades of indium and of a number of dilute alloys of tin, thallium, cadmium, or lead in indium have confirmed that the anisotropy is highly sensitive to the degree of purity of indium. The volume coefficient of expansion is considerably less sensitive but not independent of purity.

The measurements were made by means of x-ray diffraction with a modified Norelco diffractometer. Indium is tetragonal, and the thermal expansion parallel to the c-axis was determined from the shift in position with temperature of the (004) peak while the expansion perpendicular to the c-axis was determined from the (310) peak. A change in the diffraction angle of 0.01° could be detected. Thus the variation of the lattice parameters from sample to sample is not particularly significant, but the variation of the lattice parameter within a given sample at constant mounting geometry is quite significant. The experimental results are shown in Figs. 10 through 13.

4.3 Measurement of Elastic Constants of Single Crystals

4.3.1 Thallium (J. F. Smith and R. Ferris)

Below 230°C thallium crystallizes with a hexagonal closest packed crystal structure whose elastic behavior is specified by five independent elastic constants. Four of these five constants have been determined from $4.2 - 300^\circ\text{K}$ by the ultrasonic pulse-echo technique. The fifth constant has been measured at 4.2°K and 78°K and measurements over the remaining temperature range will soon be completed.

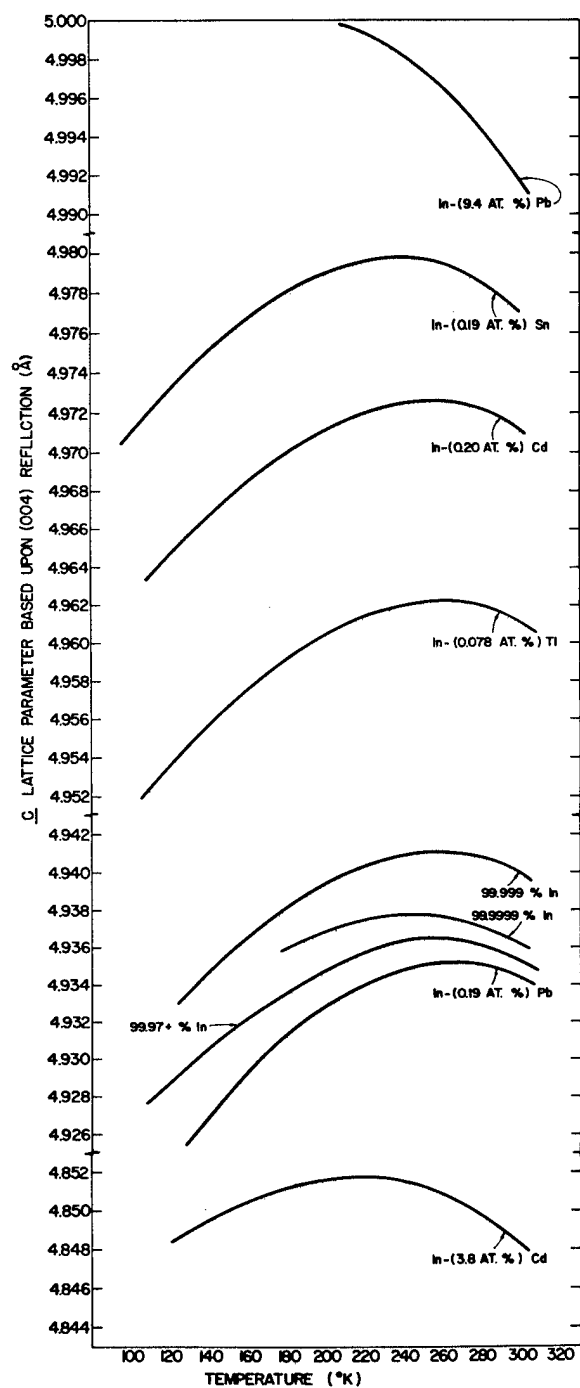


Fig. 10. a_c Lattice Parameter of Indium and Indium Alloys vs Temperature

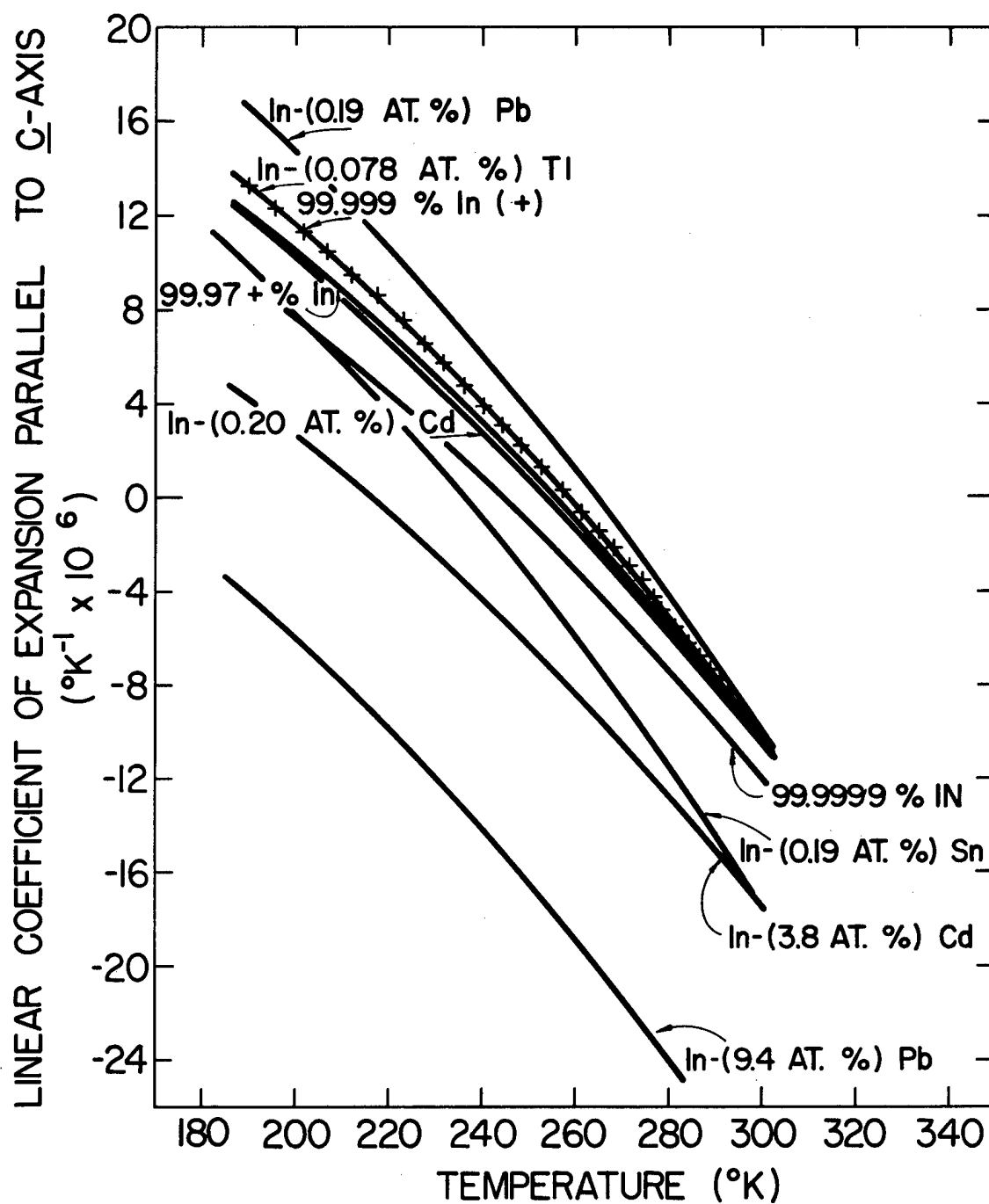


Fig. 11. Linear Coefficient of Thermal Expansion Parallel to the C-Axis vs Temperature for Indium and Indium Alloys

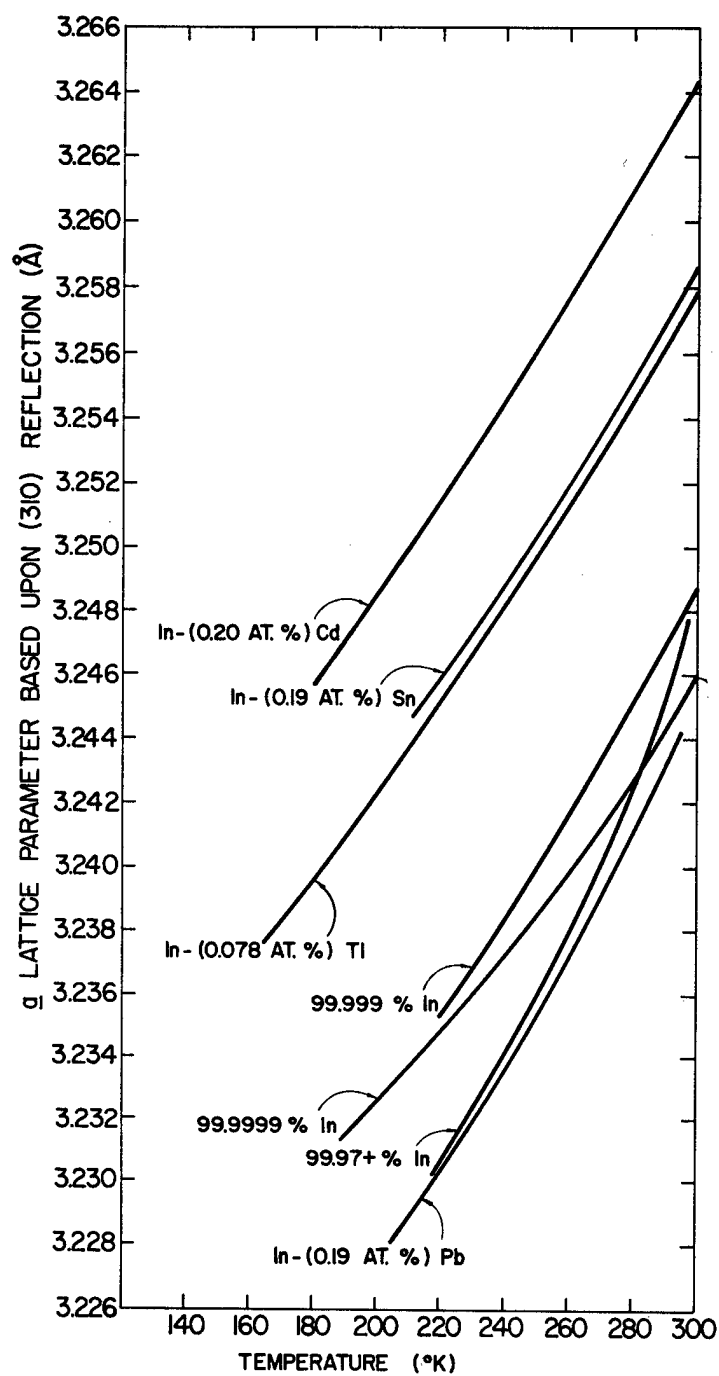


Fig. 12. A Lattice Parameter of Indium and Indium Alloys vs Temperature

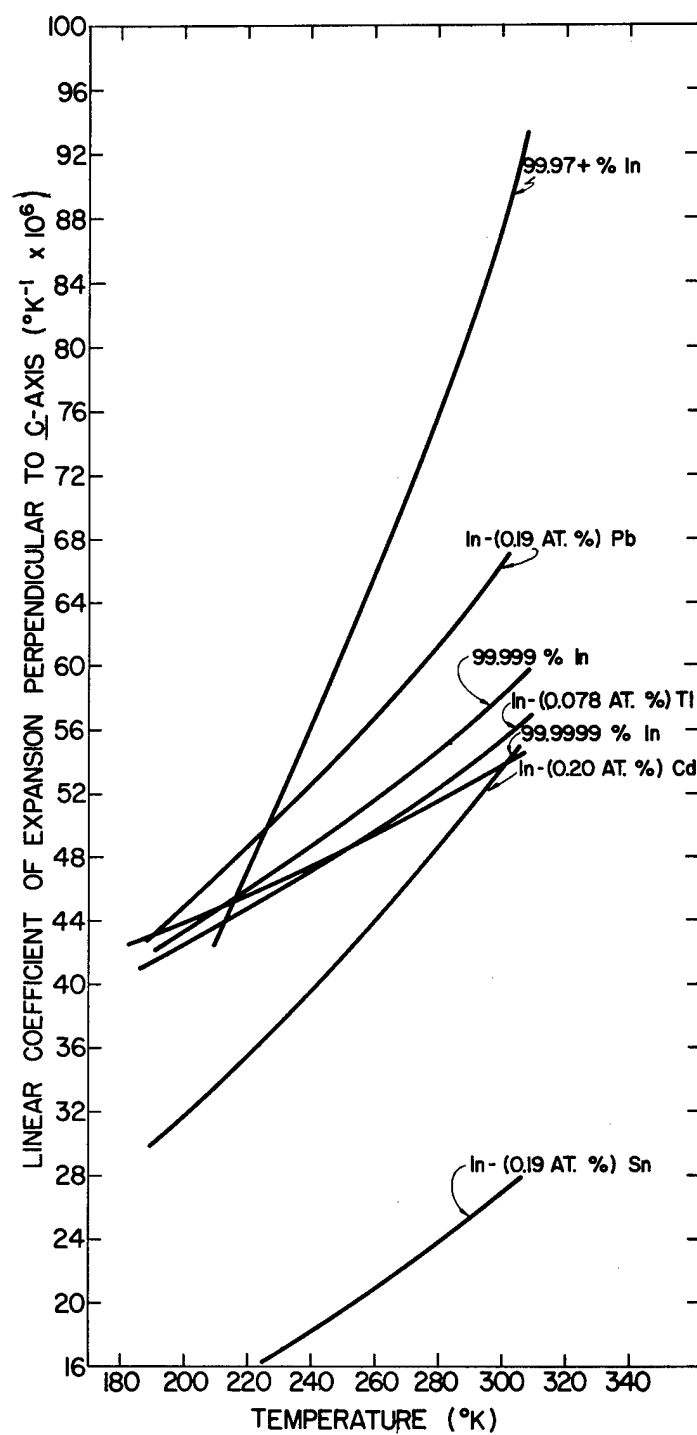


Fig. 13. Linear Coefficient of Thermal Expansion Perpendicular to the C-Axis vs Temperature for Indium and Indium Alloys

4.3.2 Chromium (J. F. Smith, Ali Sumer and D. M. Bailey)

An apparatus has been constructed for the measurement of thermal diffuse x-ray spectra of large single crystals from which the single crystalline elastic constants may be determined. This apparatus is currently in the process of testing and some preliminary values for the elastic constants of chromium have been obtained. The elastic constants of chromium have also been measured by the ultrasonic pulse-echo technique. The two sets of data for chromium may be compared:

<u>Diffuse x-ray</u>	<u>Ultrasonic pulse-echo</u>
$C_{11} = 25.9 \times 10^{11} \text{ d/cm}^2$	$C_{11} = 34.2 \times 10^{11} \text{ d/cm}^2$
$C_{12} = 10.3 \quad " \quad "$	$C_{12} = 6.70 \quad " \quad "$
$C_{44} = 11.3 \quad " \quad "$	$C_{44} = 9.98 \quad " \quad "$

There is no question but that the ultrasonic values are more reliable and reproducible. The interesting feature of the comparison is that the constants of chromium differ in the same manner as vanadium with C_{11} (x-ray) being lower than C_{11} (ultrasound) and C_{12} (x-ray) being lower than C_{11} (ultrasound) and C_{12} (x-ray) and C_{44} (x-ray) both being greater than the respective C_{12} (ultrasound) and C_{44} (ultrasound). The vanadium values are:

<u>Diffuse x-ray</u> ¹	<u>Ultrasonic pulse-echo</u> ²
$C_{11} = 19.6 \times 10^{11} \text{ d/cm}^2$	$C_{11} = 22.8 \times 10^{11} \text{ d/cm}^2$
$C_{12} = 13.5 \quad " \quad "$	$C_{12} = 11.9 \quad " \quad "$
$C_{44} = 6.7 \quad " \quad "$	$C_{44} = 4.26 \quad " \quad "$

¹E. Sandor and W.A. Wooster, Acta Cryst 12, 332 (1959).

²G. Alers, Phys. Rev. 119, 1532 (1960).

Whether this trend is fortuitous or whether there is a systematic and significant difference between x-ray and ultrasonic elastic constants remains to be determined.

4.4 Crystal Structures

4.4.1 Strontium-Tin (J. F. Smith and D. Hansen)

An investigation of the compounds which form between alkaline earth metals and Group IVB metals is in progress. A single crystal of a strontium-tin compound (believed to be SrSn_4) has been isolated and examined by x-ray diffraction. The crystal is monoclinic with $a_0 = 12.17\text{\AA}$, $b_0 = 4.06\text{\AA}$, $c_0 = 5.16\text{\AA}$ and $\beta = 104.3^\circ$. The symmetry of Weissenberg and precession patterns is consistent with space group Cm, C2 or C2/m. Intensity data have been accumulated, and an attempt to determine the atomic positions will be made.

4.4.2 Yttrium-Magnesium (J. F. Smith and D. M. Bailey)

Work on the delta-phase and epsilon-phase in yttrium-magnesium system was interrupted but has been resumed. The structure of the delta-phase ($\sim\text{Y}_2\text{Mg}_5$) is still not proved, but the projection normal to c-axis has been refined and the phase seems to be either a nonstoichiometric C_{14} Laves phase or a very closely related structure. The compound exists over a range of composition between 42 wt% and 46 wt% magnesium.

5. SEPARATION STUDIES

5.1 Liquid-Liquid Extraction (H. A. Wilhelm and T. L. Young)

An investigation is underway directed toward a study of liquid-liquid extraction techniques as a means for separating cesium and rubidium. These metals usually have associated with them considerable amounts of

the other alkali metals. Much of the work to date has dealt with the concentration of cesium and rubidium from lithium, sodium and especially potassium. At present it appears that treatment of a solid potassium-rubidium-cesium concentrate from lithium production can yield a starting material for the liquid-liquid extraction studies.

5.2 Pyrometallurgical Separations

5.2.1 Oxidation States of Thorium Chloride in a KCl-LiCl/Zinc System

(P. Chiotti and C. Dock)

Previous work (USAEC Report IS-351) on the oxidation of thorium with ZnCl_2 in a KCl-LiCl/zinc system showed that 1.5 moles of ZnCl_2 were required to transfer one mole of thorium from the zinc to the salt phase. Likewise 1.5 moles of magnesium were required to transfer one mole of thorium from the salt to the zinc phase. These results indicate that the valence of thorium as chloride in the salt is three. The possibility of mixed valence states, such as Th^{+2} and Th^{+4} , cannot be excluded on the basis of the above observations. The existence of both ThCl_2 and ThCl_3 have been reported in the literature.^{1,2} An attempt is being made to establish more precisely the valence states of thorium in the salt for the oxidation-reduction processes described above.

Attempts to prepare a pure lower valent thorium chloride have thus far been unsuccessful. A mixture of 16.3 grams of anhydrous ZnCl_2 and 20.0 grams of thorium powder were equilibrated in a sealed tantalum

¹M. V. Smirnov and L. D. Yushina, "Equilibrium Potentials of Thorium in Chloride Melts", Izvest. Akad. Nauk. S.S.S.R., Othel Khim Nauk 2, 251-258 (1959).

²E. H. Hayek, T. Rehner and A. Frank, "Halogenide des Zwei- und dreiwertigen Thoriums", Monatsh 82, 575 (1951).

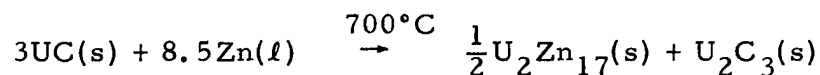
crucible at 700 - 730°C for 24 hr and rapidly cooled. The product was an orange colored salt which analysed 65.12 wt% thorium. X-ray diffraction analyses showed only the pattern for ThCl_4 . A similar experiment with 4.40 grams of thorium and 15.48 grams of ThCl_4 gave a purple salt with a Cl/Th atom ratio of 3.8. Experiments in which KCl-LiCl eutectic was used as a solvent gave Cl/Th ratios of 3.5 - 4.0 for the thorium halide in the salt. All of the salts prepared evolved hydrogen when dissolved in water. Fused salt polarography and other techniques which may be helpful in establishing the valence of thorium in these salts are being considered.

5.2.2 Reaction of Uranium and Thorium Carbides in a KCl-LiCl/Zinc System

(P. Chiotti and W. C. Robinson)

Both uranium and thorium carbides have been considered as reactor fuels. Reaction of these carbides in a KCl-LiCl/zinc system is considered of potential interest in the reprocessing of carbide fuels.

Further work has been done on the reaction of UC with zinc. From a consideration of presently available thermodynamic data (see Table XIX) the free energy change for the reaction



is negative by at least -6.0 kcal. In view of the low solubility of these compounds in liquid zinc the reaction should go to completion if kinetic factors are favorable. In estimating the free energy change for the reaction the free energy of formation of U_2C_3 was assumed to be the sum of the free energies of formation of UC and UC_2 . Reaction of liquid

Table XIX

Standard Free Energy Data in kcal/mole

Compound	Temp. °C			Reference
	500	700	900	
UC ₂	- 28.9	- 28.8	- 28.4	*
UC	- 20.7	- 20.7	- 20.3	*
UCl ₃	-173.5	-163.4	-153.7	*
ZnCl ₂	- 73.9	- 69.3	---	+
U ₂ Zn ₁₇	- 54	- 38	- 19.6	†

* M. H. Rand and O. Kubaschewski, "The Thermochemical Properties of Uranium Compounds", Report AERE-R3487, Chemistry Division, Atomic Energy Research Establishment, Harwell, Berkshire, England, 1960.

† W. J. Hamer, M. S. Malmberg and Bernard Rubin, J. Electrochem. Soc. 103, 8-16 (1956).

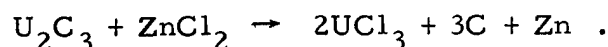
† P. Chiotti and G. R. Kilp, Trans. AIME 218, 41-46 (1960).

zinc with the higher uranium carbides to form U₂Zn₁₇ and carbon does not appear to be favorable.

Equilibrations of UC powder with liquid zinc in sealed tantalum containers at 550°C give reaction products which show the presence of at least three phases, zinc, a carbide phase and an intermetallic compound. X-ray diffraction analyses indicate the phases present are zinc, U₂Zn₁₇ and U₂C₃. The large number of lines in this diffraction pattern makes an unambiguous interpretation difficult. Similar equilibrations with finely divided carbon, uranium chips and zinc give similar diffraction patterns which indicate U₂C₃ is the carbide phase formed. Separation

of the carbide phase by dissolution of the matrix material with dilute nitric or concentrated sodium hydroxide solutions should permit a more definite determination of the carbide phase formed.

Equilibrations of UC and UC₂ in a KCl-LiCl-ZnCl₂/zinc system at 700°C have been made. The equilibrium reaction is presumably



Some data are available for the activity of UCl₃ and ZnCl₂ in KCl-LiCl eutectic from which an estimate of the standard free energy for the above reaction can be made. Effects of particle size of the initial UC and equilibration time on the equilibrium constant are being investigated. Results thus far obtained indicate that the free energy of formation of U₂C₃ is in the range of -65 to -75 kcal/mole. Further work is in progress.

5.2.3 Separation of Uranium from Thorium by Oxidation with ZnCl₂ in a KCl-LiCl/Zinc System (P. Chiotti and W. C. Robinson)

The separation of uranium from thorium in thorium-rich alloys is of interest in the reprocessing of thorium-uranium fuel. Previous work has shown that in a KCl-LiCl/zinc system containing uranium and thorium as minor components, the uranium and thorium can be transferred from the zinc-rich alloy to the salt by the addition of ZnCl₂ or reduced from the salt phase by the addition of magnesium. Results indicated that it may be possible to achieve a fair degree of separation of uranium from thorium. In these equilibrations the initial components, uranium and thorium, in a ratio of U/Th of about 1.4 on a weight basis, were added to the system. On oxidation at 500°C by the controlled addition of ZnCl₂

to the system the ratio of uranium to thorium transferred to the salt phase remained essentially constant, 1.3 - 1.5. The effect of large variations in the U/Th ratio of the added components was not investigated.

The solubility of thorium or uranium in zinc is very small at 500°C. In the binary systems the solubility of thorium is 0.022 wt% and the solubility of uranium is 0.033 wt%. The solubility of uranium and thorium in zinc for ternary U-Th-Zn alloys is not known but the combined uranium and thorium in solution in the zinc-rich liquid may be assumed to be small. If the ternary zinc-rich alloy consists of three phases, two solid compounds and zinc-rich liquid, then at constant temperature and pressure the phase rule requires that at equilibrium the composition of each phase remains constant as one or more of the components is added or removed, or until one of the phases disappears. Such a three phase alloy in contact with KCl-LiCl salt would give a constant ratio of U/Th transferred to the salt on the addition of ZnCl_2 until one of the phases disappears. If the above idealized conditions hold, negligible solubility of uranium in $\text{Th}_2\text{Zn}_{17}$, then calculations show that at 500°C about 90% of the uranium in a Th-1.0 wt% U alloy could be transferred to the salt phase and the U/Th ratio in the salt maintained at about 1.0. This possibility and the effect of varying the U/Th ratio of the added components are being investigated.

An arc-melted thorium-uranium alloy containing 2.0 wt% uranium was reacted with zinc to produce a slurry of intermetallic compound or compounds in a zinc-rich liquid and equilibrated at 500°C with KCl-LiCl salt containing enough ZnCl_2 to oxidize a total of 3.5% of the combined

thorium and uranium. A similar experiment was conducted with the uranium and thorium added as unalloyed pure components. The final U/Th ratio in the salt was found to be 0.09 and 0.07 respectively, or much less than the calculated value given above. Other equilibrations have been made which show that the U/Th ratio in the salt increases with the U/Th ratio of the added components. This trend is reasonable if the uranium exists in solid solution in the $\text{Th}_2\text{Zn}_{17}$ or some other ternary Th-U-Zn compound. Other equilibrations are being analyzed and results of these experiments will be presented in the next report.

5.2.4 Reaction of Hydrogen with Solutes in Metals (P. Chiotti and R. W. Curtis)

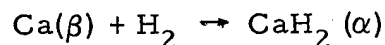
Measurement of the hydrogen dissociation pressure of calcium hydride, CaH_{2-x} , has been completed. The final results are presented below. A least square fit to the data obtained in the temperature range 600 - 780°C gives

$$\log P_{\text{H}_2, \text{ atm}} = -9610/T + 7.346 .$$

The standard deviation in the slope and intercept were calculated to be 134 and 0.146 respectively. In the temperature range of 780 - 900°C the data show a significant change in slope which is to be expected on the basis of the Ca- CaH_2 phase diagram determined by Peterson and Fattore, see USAEC Report IS-351, pp. 105 and 29. Their phase diagram indicates that a peritectic horizontal occurs at 780°C due to a transformation in CaH_2 . The best straight line through the 780 - 900°C data which intersects the line represented by the above equation at 780°C is represented by the relation

$$\log P_{\text{H}_2, \text{ atm}} = -8890/T + 6.66 .$$

The standard free energy change for the reaction



in the temperature range 440 - 780°C may be represented by the relation

$$\Delta F^\circ = -42,278 + 31.52T,$$

and for the same reaction with alpha calcium, 298 - 440°C, by the relation

$$\Delta F^\circ = -41,410 + 24.78T + 1.93T \log T.$$

Values calculated from these relations are given in Table XX.

Table XX

Standard Free Energy, Enthalpy and Entropy of Formation for CaH_2			
Temp. °C	$-\Delta F^\circ$ cal/mole	$-\Delta H^\circ$ cal/mole	$-\Delta S^\circ$ cal/mole °C
25	32,610	41,650	30.4
400	21,060	41,975	31.1
500	17,910	42,280	31.5
600	14,760	42,280	31.5
700	11,610	42,280	31.5

From the measured equilibrium hydrogen pressure for the reaction



and the above data for CaH_2 the thermodynamic properties for CaMg_2 may be calculated. Experimental details and the equilibrium hydrogen pressures obtained are being summarized for publication and will not be presented here. The calculated thermodynamic properties for CaMg_2 are summarized in Table XXI.

Table XXI

Standard Free Energy, Enthalpy and Entropy of Formation for CaMg_2			
Temp. °C	$-\Delta F^\circ$ cal/mole	$-\Delta H^\circ$ cal/mole	$-\Delta S^\circ$ cal/mole °C
25	9,045	9,980	3.16
300	8,090	10,220	3.70
400	7,720	10,300	3.84
450	7,530	10,620	4.28
500	7,315	10,620	4.28

5.2.5 Extraction of Rare Earths from Mg-40 wt% Th Solutions (P. Chiotti and J. Klepfer)

Rare earths can be extracted from Mg-40 wt% Th with KCl-LiCl eutectic containing 15 wt% MgCl_2 . The distribution coefficients for yttrium, cerium and neodymium are small. These components can be reduced from the salt phase by scrubbing it with Zn-3 wt% Mg alloy. The data obtained suggest the possibility of obtaining effective extraction of these components from the Mg-40 wt% Th solution by a cyclic process in which the KCl-LiCl- MgCl_2 salt is equilibrated with Mg-Th solution, separated and scrubbed with Zn-3 wt% Mg and then returned to the Mg-Th solution and the cycle repeated. Data thus far obtained on the distribution of various components between Mg-40 wt% Th and Zn-3 wt% Mg with the salt are presented in Tables XXII and XXIII, respectively. These data were obtained from small scale equilibrations with approximately equal weights, 20 grams each, of salt and metal phases. Tantalum containers were used in each case. Larger scale experiments have been

Table XXII

Distribution of Various Components between Mg-40 wt% Th
and KCl-LiCl-15 wt% MgCl_2

Component	Temp. °C	$\frac{\text{wt\% in Salt}}{\text{wt\% in Metal Solution}}$
Y	700	----
	600	7.5 ± 0.8
Ce	700	2.5 ± 0.1
Nd	700	10.5
	600	2.4
Sm	700	>500
	600	>500
Th	700	$(2.0 \pm 0.3) \times 10^{-3}$
	600	$(1.8 \pm 0.5) \times 10^{-3}$
Pa	700	2.3×10^{-3}
	650	0.8×10^{-3}

Table XXIII

Distribution Coefficients for Various Components between
Zn-3 wt% Mg and KCl-LiCl-15 wt% MgCl_2

Component	Temp. °C	$\frac{\text{wt\% in Salt}}{\text{wt\% in Metal}}$
Y	700	3.0×10^{-1}
	600	1.9×10^{-1}
Ce	700	5.3×10^{-2}
	600	3.5×10^{-2}
Nd	700	2.1×10^{-2}
	600	3.8×10^{-2}
Sm	700	23.5
	600	16.0
Th	700	$\sim 5.0 \times 10^{-4}$
	600	$\sim 5.0 \times 10^{-4}$

designed in which the Mg-Th solution and Zn-3 wt% Mg solution held in separate tantalum containers make mutual contact with the salt phase. The transfer of the individual components as well as mixed components from the Mg-Th to the Zn-Mg solutions is being investigated.

6. OTHER INVESTIGATIONS

6.1 Internal Friction in Thorium Hydride (D. T. Peterson and C. C. Hammerberg)

A torsional pendulum device for measuring internal friction was constructed to study internal friction phenomena in thorium hydride. The specimens were 0.040 in. by 6 in. cylindrical specimens which were prepared by allowing hydrogen gas to react with a thorium metal wire. Specimens prepared at temperatures below 700°C always had a longitudinal crack the full length of the wire. Specimens prepared at 900°C were solid and free from cracks. The microstructure of the specimens prepared at 900°C was entirely different from that of the specimens prepared at 700°C. The high temperature specimens had large equiaxed and heavily twinned grains while the low temperature specimens had small grains, free from twins and with a strong texture. The specimens prepared at 900°C had only one internal friction peak. This was at about 510°C. No measurements could be made on specimens prepared at 700°C because of the extensive cracks. A thermal analysis was made on a specimen of thorium hydride and a strong arrest was found at 840°C. This was interpreted as being due to a phase transition in thorium hydride. This phase transition is probably responsible for the difference in the microstructures of the low and high temperature specimens.

6.2 Metallography (D. T. Peterson and E. N. Hopkins)

The installation of the RCA EMU-3 electron microscope was completed and the microscope placed in operation. The development program of the Metallography Service Section resulted in the preparation of two reports which were presented at the AEC Metallography Group Meeting at Hanford, Washington. The titles of these reports are "The Application of Wax Laps to Vibratory Polishers" and "Thirty-five Millimeter Color Photomicrography" by E. N. Hopkins and D. T. Peterson. Work is underway to improve methods for the metallographic preparation of the rare-earth metals and on a study to find optimum polishing conditions for vibratory polishers.

6.3 Vapor Pressure of Calcium over Solutions of Calcium in Liquid Calcium Chloride (D. T. Peterson and D. V. Rigney)

A Knudsen effusion apparatus for measuring vapor pressures was designed and constructed. This apparatus uses an analytical microbalance to measure the rate of weight loss from the effusion cell. The vapor pressure of pure calcium has been measured and measurements of the vapor pressure of calcium over solutions of calcium in liquid calcium chloride have been started. From the concentration dependence of this vapor pressure, information can be obtained about the nature of the solution of an alkaline earth metal in its molten halide salt.

6.4 Transport Reactions of the Vanadium(III) Halides (R. E. McCarley, J. W. Roddy and K. O. Berry)

During this period the study of the reactions of bromide and iodine with VCl_2 , VBr_2 , VCl_3 and VBr_3 was completed. The manuscript

covering this work has been prepared and will be submitted to Inorganic Chemistry for publication.

Abstract--The reactions of VCl_2 , VCl_3 , and mixtures of VCl_3 and VBr_3 with bromine vapor at $350 - 450^\circ\text{C}$ led to vaporization of the halides and deposition of mixed halides of vanadium(III) at lower temperatures. A study of solid solution formation in the system $\text{VCl}_3\text{-VBr}_3$ indicated the two components were miscible in the solid state, and that the mixed halide VCl_2Br should be regarded as such a solid solution. The pure compounds VCl_3 and VBr_3 , the mixed halides VCl_2Br and VBr_2I , and all compositions in the system $\text{VCl}_3\text{-VBr}_3$ were hexagonal solids with the BiI_3 -layer structure; the lattice constants for these compounds are given. Vaporization of VBr_2 in iodine vapor at $350 - 400^\circ$ resulted in the transport and deposition of VBr_2I , but the analogous reaction between VCl_2 and iodine yielded only a deposit of VCl_2 . Formation of vanadium(IV) mixed halides containing iodine have been postulated to account for the vaporization at these temperatures.

6.5 Vapor Pressures and Dissociation Pressures of Vanadium Bromides

6.5.1 Dissociation and Disproportionation Equilibria of Vanadium(III) Bromide and the Formation of Vanadium(IV) Bromide (R. E. McCarley and J. W. Roddy)

This work has been completed and is described in a paper which will be submitted for publication in Journal of Physical Chemistry.

Abstract--The equilibria (1) $\text{VBr}_3(\text{s}) = \text{VBr}_2(\text{s}) + \frac{1}{2}\text{Br}_2(\text{g})$ and (2) $2\text{VBr}_3(\text{s}) = \text{VBr}_2(\text{s}) + \text{VBr}_4(\text{g})$ were studied over the range $644 - 805^\circ\text{K}$ by transpiration in helium. The expressions $\log P_{\text{mm}}(\text{Br}_2(\text{g})) = -5070/T + 5.02$ and $\log P_{\text{mm}}(\text{VBr}_4(\text{g})) = -8240/T + 8.47$ were derived from the measurements for (1) and (2), respectively; for (1) $\Delta H^\circ = 23.1 \pm 0.9 \text{ kcal/mole}$ and $\Delta S^\circ = 9.8 \pm 0.4 \text{ e.u.}$, while for (2) $\Delta H^\circ = 37.7 \pm 1.3 \text{ kcal/mole}$ and $\Delta S^\circ = 25.5 \pm 0.8 \text{ e.u.}$ Both transpiration in bromine vapor and static pressure measurements using a glass diaphragm gauge showed that $\text{VBr}_3(\text{s})$

vaporized as $\text{VBr}_4(\text{g})$ in the presence of bromine according to (3)
 $\text{VBr}_3(\text{s}) + \frac{1}{2}\text{Br}_2(\text{g}) = \text{VBr}_4(\text{g})$. Data from the transpiration and diaphragm
 gauge measurements were in excellent agreement; the transpiration
 measurements gave for (3) $\log K_p(\text{atm}^{\frac{1}{2}}) = -3455/T + 5.22$ and $\Delta F^\circ =$
 $15.80 \times 10^3 - 23.8T$ for $T = 515\text{--}585^\circ\text{K}$.

Solid VBr_4 was isolated by condensation of the vapor at -78°C ,
 and was found to be stable at -45°C . At higher temperatures the
 solid decomposed to $\text{VBr}_3(\text{s})$ and bromine.

6.5.2 The Vapor Pressures of VCl_2 , VBr_2 , VCl_3 and VBr_3 by the Knudsen Effusion Method (R. E. McCarley and J. W. Roddy)

During the work on the transport of the vanadium(III) halides (see
 Sec. 6.4 of this report) a knowledge of the vapor pressure of the solid
 compounds was needed in order to estimate the relative importance of
 vaporization by sublimation and by formation of vanadium(IV) halide
 vapor species. The Knudsen effusion method was chosen for these
 measurements since the pressures were found to be from 10^{-5} to 10^{-2} mm
 at the temperatures of interest.

The results of this investigation are complete and a paper which is
 now in preparation will be submitted to Journal of Physical Chemistry.
 A summary of the results follows.

The vapor pressures of VCl_2 , VBr_2 , VCl_3 and VBr_3 have been
 measured by the Knudsen effusion method using Pyrex and Vicor effusion
 cells. The equations $\log P_{\text{mm}} = -9804/T + 8.713$ and $\log P_{\text{mm}} = -10460/T +$
 9.081 were obtained for the vapor pressures of crystalline VCl_2 and VBr_2 ,
 respectively, over the range $750 - 950^\circ\text{K}$. From these expressions were
 derived the standard heats and entropies of vaporization, respectively,
 44.8 kcal and 26.6 e.u. for VCl_2 and 47.8 kcal and 28.3 e.u. for VBr_2 .

During the measurements on VCl_3 and VBr_3 decomposition and disproportionation of the samples occurred simultaneously with the simple vaporization. However, because the product of each of these processes was collected separately during an experiment, the vapor pressure due to sublimation was obtained without difficulty. Results of the measurements were $\log P_{\text{mm}} = -9777/T + 11.20$, $\Delta H^\circ = 44.7$ kcal and $\Delta S^\circ = 38.0$ e.u. for vaporization of VCl_3 over the range 625 - 740°K. For VBr_3 , $\log P_{\text{mm}} = -9470/T + 11.12$, $\Delta H^\circ = 43.3$ kcal and $\Delta S^\circ = 37.7$ e.u. were obtained over the range 590 - 700°K. All of the calculations are based on the assumption that the halides vaporized as the gaseous monomer.

6.6 Molybdenum Halides

6.6.1 The Preparation and Properties of Molybdenum(IV) Bromide (R. E. McCarley and P. J. H. Carnell)

A paper bearing the above title, by P. J. H. Carnell and R. E. McCarley, has been submitted for publication in Inorganic Chemistry.

Abstract--The preparation of pure molybdenum(IV) bromide was accomplished conveniently by the reaction between molybdenum(III) bromide and liquid bromine at ~55°C. Molybdenum(IV) bromide was found to be soluble in liquid bromine, and this property was utilized to separate and purify the molybdenum(IV) bromide. The solution of MoBr_4 in bromine was a poor electrical conductor. No evidence was found for the formation of MoBr_4 from MoBr_3 and bromine vapor at 2-4 atm and temperatures from 180 - 400°C. However, MoBr_4 was completely decomposed at 110 - 130°C, in vacuo, with formation of MoBr_3 and bromine.

6.6.2 Vaporization Equilibria of Molybdenum(III) Bromide (R. E. McCarley and W. Tadlock)

Preliminary observations have indicated that the vaporization of MoBr_3 is not a simple process, but that dissociation with formation of bromine and MoBr_2 , and disproportionation may accompany the sublimation process. In order to confirm the formation of MoBr_4 as a vapor species above $\text{MoBr}_3(\text{s})$ experiments to determine the equilibrium pressures in the $\text{MoBr}_3(\text{s})\text{-Br}_2(\text{g})$ reaction have been initiated. The pressures will be measured with a glass diaphragm gauge in a manner analogous to that used for the study of the $\text{VBr}_3\text{-Br}_2$ reaction. Owing to experimental difficulties with the diaphragm gauge no results were obtained during this period.

6.6.3 Preparation and Properties of Molybdenum(IV) Chloride (R. E. McCarley and D. Anthes)

Attempts to prepare MoCl_4 by reaction of MoCl_5 with molybdenum metal have led only to formation of MoCl_3 . The reactions were performed under conditions similar to those used for preparation of the tetrahalides of niobium and tantalum, i. e. in a sealed tube under a controlled temperature gradient. There is some evidence that MoCl_4 is formed in the vapor phase in the reaction with the metal. The vapor then migrates down the tube to a lower temperature where it deposits MoCl_3 by disproportionation either in the gas phase, or after condensation of solid MoCl_4 . At the temperatures used in the reactions, MoCl_3 is not expected to exhibit a vapor pressure sufficiently large to account for its location in the tube after deposition.

This work will be continued with some new approaches to the preparation of MoCl_4 , and with a study of the physical and chemical properties of the solid.

6.7 Niobium Halides

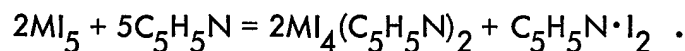
6.7.1 Reactions of Niobium(V) Halides with Pyridine (R. E. McCarley and B. G. Hughes)

This work has been completed, and the results were combined with some of those from work on the reactions of the niobium(IV) and tantalum(V) halides for a paper presented at the American Chemical Society meeting in Washington, D.C., March, 1962. This paper has been submitted for publication in a book combining all of the papers presented before the Symposium on Homogeneous Catalysis and the Reactions of Coordinated Ligands at the Washington meeting. An abstract of the paper entitled "Reduction of the Niobium(V) and Tantalum(V) Halides by Pyridine, Derivatives of Niobium(IV) and Tantalum(IV)", by R. E. McCarley, B. G. Hughes, J. C. Boatman and B. A. Torp, is given below.

Abstract--The reaction of pyridine and niobium(V) bromide was found to proceed by oxidation-reduction to yield a derivative of niobium(IV), $\text{NbBr}_4(\text{C}_5\text{H}_5\text{N})_2$. This product was identical to that given by the reaction of pyridine and niobium(IV) bromide at room temperature. The oxidation of pyridine by niobium(V) bromide led to the production of 1-(4-pyridyl)-pyridinium bromide (I) and pyridinium bromide. Identification of I was accomplished by comparison of the ultraviolet spectra in acidic and basic solutions with those of known salts of I. Niobium(V) chloride also was reduced by pyridine in a manner similar to the reduction of the bromide, but a different reaction stoichiometry was obtained. Tantalum(V) chloride

and bromide were not reduced in pyridine but afforded the adducts $\text{TaCl}_5(\text{C}_5\text{H}_5\text{N})$ and $\text{TaBr}_5(\text{C}_5\text{H}_5\text{N})$.

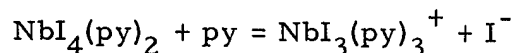
In contrast to the mode of the reduction of NbBr_5 and NbCl_5 , both NbI_5 and TaI_5 appeared to undergo dissociation in pyridine according to



The compound $\text{NbI}_4(\text{C}_5\text{H}_5\text{N})_2$ was prepared also by the reaction of NbI_4 and pyridine.

6.7.2 Reactions and Properties of the Niobium(IV) Halides (R. E. McCarley and B. A. Torp)

During this period the conductances of solutions of the niobium(IV) halide-pyridine adducts in pyridine were determined. The chloride and bromide complexes proved to be non-conductors in pyridine but solutions of the iodide complex were weakly conducting. Slight ionization of the tetraiododi(pyridine) niobium(IV) in the solutions thus was indicated. Observations on the optical spectrum given by the iodide complex in pyridine also indicated that more than one species existed in the solutions. In an effort to eliminate impurities from consideration special efforts to purify both solvent pyridine and the NbI_4 were made, but no change in the results from those given above was obtained. Slight ionization of the type



is a possible explanation of this behavior.

Molar extinction coefficients for the absorption maxima in the spectra¹ of $\text{NbX}_4 \cdot 2\text{py}$ ($\text{X} = \text{Cl}, \text{Br}, \text{I}$) dissolved in pyridine were determined and

¹For the details of these spectra see IS-351, Sec. 6.7.2.

found to be in the range 300 - 1000 liters mole⁻¹cm⁻¹ for all of the complexes. These values are much larger than those usually observed for d-d electronic transitions in octahedral complexes. More normal extinction coefficients for such transitions have values in the range 10-100. Because of the observed, unusually large extinction coefficients there is considerable doubt about the correctness of the energy levels previously assigned to the transitions. For the reasons cited above charge transfer absorption can no longer be excluded from consideration. Additional information on the complexes must be obtained before the final assignments can be made.

Further x-ray diffraction studies on NbBr₄ have revealed that it is orthorhombic with unit cell dimensions $a = 8.60$, $b = 9.31$ and $c = 7.19$ Å. Rough lattice parameters were obtained from single crystal rotation and Weissenberg photographs, but because of twinning of the crystals and consequent streaking of the diffraction spots on the films a more accurate estimation was not possible. The lattice constants given above were obtained by adjusting the rough constants so that good agreement resulted between the calculated and observed reflections on the powder pattern. There are four molecules in the unit cell; the calculated density is 4.79 gram/cc, while a density of 4.65 ± 0.1 gram/cc was observed experimentally. Further work on the structure of NbBr₄ and the related compounds TaBr₄, MoBr₄ and WBr₄ will be undertaken if suitable crystals can be obtained.

In a phase study of the system NbCl₄-KCl Korshunov and Safonov¹ reported the congruently melting compound K₂NbCl₆. Because of the

¹B. G. Korshunov and V. V. Safonov, Zhur. Neorg. Khim 6, 753 (1961).

more symmetrical ligand configuration about the Nb(IV) in the ion NbCl_6^- this compound was prepared in order to measure and compare its susceptibility with that of other niobium(IV) compounds prepared in this work.

The K_2NbCl_6 was prepared by heating a stoichiometric mixture of KCl and NbCl_4 to 790°C (the reported melting point of K_2NbCl_6 was 782°C). On cooling the reaction tube a ruby red, crystalline product was obtained. X-ray diffraction patterns of the powdered solid were indexed on a face-centered cubic cell of dimensions $a = 9.98 \text{ \AA}$. Information on the magnetic susceptibility of this compound is given in Sec. 4.1.2 of this report.

6.8 Air Oxidation of Yttrium Metal (O. N. Carlson, J. A. Haeffling and F. A. Schmidt)

Air oxidation studies of high purity yttrium metal were continued and the temperature range was extended to 1400°C . The samples were heated at various temperatures until a definite oxidation rate was established. A plot of the weight gain vs time of oxidation at temperatures of $500 - 1400^\circ\text{C}$ is shown in Fig. 14. When yttrium metal begins to oxidize a black adherent coating is first formed on the surface. This coating, believed to be a solution of yttrium in yttrium oxide, was found to form at an increasing rate at the higher temperatures. At 900°C and above, the black coating gradually transforms into the white oxide form, after which the oxidation process proceeds quite rapidly. The sample heated in air at 950°C underwent no further weight gain after 100 hr although at that time it was less than 10% oxidized. However in a previous experiment the same metal heated under identical conditions was completely

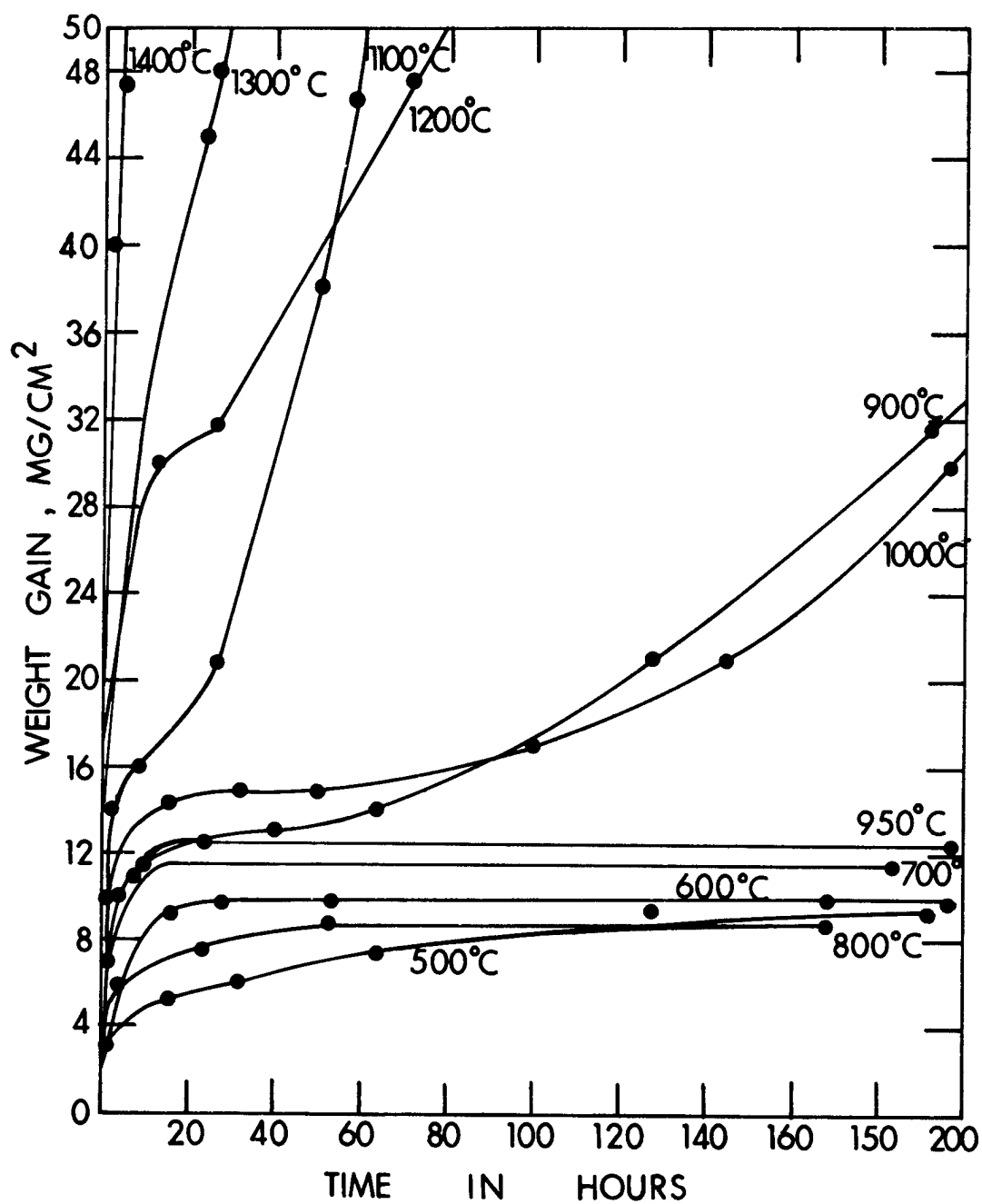


Fig. 14. Weight Gain vs Time of Oxidation of Yttrium Metal
for Temperatures of 500 to 1400°C

oxidized after 120 hr. This inconsistent behavior is believed to be associated with the instability of the black coating in this temperature region.

An experiment was performed that throws some light on the identity of the black corrosion product. A Y_2O_3 wafer was melted in an electron beam furnace. A considerable fraction of the oxide underwent thermal decomposition and was volatilized off leaving behind a black residue. This material was identified by x-ray and chemical analysis as Y_2O_3 and was observed to turn white upon heating in air at $1000^\circ C$. From these and other observations the black phase is considered to be an oxygen deficient form of Y_2O_3 .

Chemical analyses were made of the metal under the surface of the oxide coatings. The amount of oxygen in the metal varied from 0.24 wt% for samples which were oxidized at $500^\circ C$ to 2.65 wt% for samples oxidized at $1200^\circ C$. These same specimens were found to contain less than 500 ppm each of hydrogen and nitrogen regardless of the temperature of oxidation.

X-ray studies were made on yttrium test specimens containing 100 - 1200 ppm fluorine. These studies indicated that fluorine has no observable effect on the lattice parameter of yttrium.

A comparison of the oxidation rates of arc-melted and electron-beam melted yttrium revealed that electron-beam melted yttrium has twice as high an oxidation rate at $900^\circ C$ as in the arc-melted condition. The electron-beam melted yttrium was found to contain slightly more carbon, nitrogen, oxygen and nickel but lesser amounts of iron, chromium, fluorine and hydrogen. Previous oxidation tests showed that carbon, nitrogen, oxygen, iron and nickel do not affect the oxidation rate of

yttrium and that fluorine has a detrimental effect. Thus it appeared that small amounts of either hydrogen or chromium were responsible for the lower oxidation rate of arc-melted yttrium. In order to substantiate this conclusion, several alloys were prepared in an arc furnace to produce samples containing a range of compositions of hydrogen and chromium. It was found that at hydrogen concentrations of 10 to 140 ppm there was no observable difference in the oxidation rate of yttrium but that chromium in amounts up to 85 ppm retards the oxidation rate slightly. No further change in the oxidation rate was noted in samples containing additional amounts, however.

6.9 Extrusion of Thorium-Magnesium Alloy (D. T. Peterson and C. V. Owen)

The fabrication of a Mg-35 wt% Th alloy into rods by extrusion was studied because of the interest in this alloy as a possible molten reactor fuel. Because of the difficulties encountered in casting this alloy into solid rods of 3/4-in. diameter, the applicability of extrusion was investigated. A billet suitable for extrusion was cast in an induction furnace. This alloy was successfully extruded at 500°C with an extrusion ratio of 7 to 1 and a speed of 0.3 in./sec. No cladding was required and the surface quality of the rod was very good.

6.10 Tantalum Halides (R. E. McCarley and J. C. Boatman)

Conditions have been established for the preparation of TaBr_4 by reaction of TaBr_5 with tantalum metal. Using a sealed tube in a controlled temperature gradient it was found that a reaction temperature of at least 600°C at the metal was necessary for reduction of TaBr_5 to occur at a significant rate. In the reactions reported below the

temperature of the metal was held constant at 630°C. The temperature at the opposite end of the tube controlled the vapor pressure of the TaBr_5 in the reaction, and also determined the products of the reaction. When the temperature of the cool end of the tube was maintained at 330°C or less, a crystalline deposit of pure TaBr_4 was obtained near the cool end. At temperatures above 330°C, a green powdery deposit having the composition $\text{TaBr}_{2.5}$ was obtained. Further heating of $\text{TaBr}_{2.5}$ in vacuo at 700°C resulted in decomposition of the sample with loss of TaBr_5 and formation of TaBr_2 as a nonvolatile residue. Anal. Calcd. for TaBr_2 : Ta, 53.10; Br, 46.90. Found: Ta, 53.20; Br, 46.70; Br/Ta, 1.98. Calcd. for TaBr_4 : Ta, 36.15; Br, 63.85. Found: Ta, 35.90; Br, 63.50; Br/Ta, 4.03. A sample of TaBr_4 heated in vacuo first began to decompose at 220 - 250°C with evolution of TaBr_5 .

An x-ray powder pattern of TaBr_4 was indexed on the basis of an orthorhombic unit cell of the dimensions $a = 8.58$, $b = 9.30$ and $c = 7.21$ Å; it is isomorphous with NbBr_4 , and is diamagnetic.

Several unsuccessful attempts were made to prepare TaI_4 by a procedure similar to that used for preparation of the bromide. Reactions at 1 to 2 atm of TaI_5 and a metal temperature of 630° yielded only TaI_3 . Anal. Calcd. for TaI_3 : Ta, 32.20; I, 67.80. Found: Ta, 32.40; I, 67.50; I/Ta, 2.98. Magnetic susceptibility measurements showed TaI_3 to be diamagnetic. The crystalline TaI_3 produced in this way is not isomorphous with NbI_3 ,¹ although the latter is also diamagnetic.

Reactions of TaCl_4 and TaBr_4 with pyridine were performed by a procedure previously described for the reactions of the corresponding

¹L. F. Dahl and P. W. Seabaugh, University of Wisconsin, Madison, Wis., private communication, 1962.

niobium(IV) halides. The product in each case was the di-pyridine adduct of the halide: $\text{TaCl}_4(\text{C}_5\text{H}_5\text{N})_2$ and $\text{TaBr}_4(\text{C}_5\text{H}_5\text{N})_2$. Anal.
Calcd. for $\text{TaCl}_4(\text{C}_5\text{H}_5\text{N})_2$: Ta, 37.60; Cl, 29.55; $\text{C}_5\text{H}_5\text{N}$, 32.90.
Found: Ta, 37.22; Cl, 29.17; $\text{C}_5\text{H}_5\text{N}$, 32.71. Calcd. for $\text{TaBr}_4(\text{C}_5\text{H}_5\text{N})_2$:
Ta 27.50; Br, 48.60; $\text{C}_5\text{H}_5\text{N}$, 24.00. Found: Ta, 27.40; Br, 48.30;
 $\text{C}_5\text{H}_5\text{N}$, 23.80.

X-ray powder patterns of the two compounds were practically identical with those of the corresponding niobium compounds. There is little doubt that the two sets of compounds are isomorphous. Magnetic susceptibility measurements were made also; they are reported in another section of this report (Sec. 4.1.2).

It is clear that most of the compounds of tantalum in lower oxidation states reported here are strikingly similar to the analogous compounds of niobium and also bear some resemblance to those of molybdenum and tungsten, where the molybdenum and tungsten compounds have been available for comparison. However, the tantalum compounds are much more difficult to prepare than those of niobium. Several of the compounds reported here were prepared in quantities of 1 gram or less because of the experimental difficulties. For more complete characterization of the lower halides in particular, better methods of preparation need to be developed.

6.11 Tungsten Halides (R. E. McCarley and T. M. Brown)

A communication entitled "Tungsten Tribromide and Tungsten Tetra-bromide" has been accepted for publication in The Journal of the American Chemical Society. This paper is a brief note which describes methods for

the preparation of the new compounds WBr_3 and WBr_4 and some preliminary observations on their properties. This work is significant since WBr_3 apparently is the only known example of a binary compound of tungsten(III). A more complete study of WBr_3 thus may provide a better understanding of the chemistry of tungsten in this rarely observed oxidation state.

Tungsten(IV) bromide was prepared in a sealed tube reaction of the type described in Sec. 6.10 for the preparation of TaBr_4 . From x-ray diffraction data for the substances it appears that NbBr_4 , TaBr_4 , MoBr_4 and WBr_4 are isomorphous. The structure of these compounds is of considerable interest because of their unusual magnetic properties; the latter indicate some direct metal-metal bonding between nearest neighboring metal atoms in the solids. Additional work on the structure determination will be undertaken if suitable single crystals of one or more of the materials listed above can be obtained.

6.12 Investigation of the Oxidation of Niobium (W. L. Larsen and J. H. Doyle)

At atmospheric pressures niobium oxidizes in dry air and in oxygen approximately five times as fast at 575°C as at 625°C . This rate reversal is being investigated by x-ray and metallographic means.

All samples oxidized between 500 and 750°C show the presence of lower oxides¹ at the metal surface. Those oxides formed below 575°C are in the form of needles penetrating the metal while above 625°C a very thin continuous oxide layer is formed having no needles. Between 575 and 625°C both types of lower oxide form on the metal surface. The continuous layer appears to be NbO while the needles have a different, but as yet unidentified, composition.

¹Oxides with an O/Nb atomic ratio <2.5 .

Additional metallographic, structural, and kinetic data are being obtained in an effort to provide a mechanistic interpretation of the rate reversal phenomenon.

6.13 Co-Reduction of Nb_2O_5 and UO_2 with Carbon to Produce a 20 wt% U, Nb Alloy (H. A. Wilhelm and J. H. Elwell)

An investigation of the process variables necessary to produce a uniform 20 wt% U-Nb alloy was undertaken. The process is based on an initial vacuum reduction of the mixed oxides by carbon. Graphite was chosen since this form of carbon permits the sintering charge to be consolidated by cold pressing without use of a binder. The effect of graphite particle size on reaction rate was studied in a qualitative manner using grade no. 38 graphite which had been circulated through a colloid mill. A small improvement in reaction rate was observed for the milled material.

Data on CO gas-evolution with temperature were obtained for the reaction to form the 20 wt% U-Nb alloy. A typical curve from plots of these data shows maxima at about 1500 and 1750°C. Work is in progress to determine the phases present at temperatures selected from the gas evolution curve. Debye-Scherrer x-ray analysis methods are employed in this determination. At 1500°C niobium carbide is present in all samples.

Techniques of melting the sintered cylindrical samples were studied. Repeated non-consumable arc melting resulted in segregation and vaporization of uranium. The alloy formed by arc melting contained <500 ppm carbon; carbide and oxide appeared in the microstructure. Electron beam melting further reduced the uranium and oxygen content but did not appreciably change the carbon content.

Calculation of the carbon required for each charge is complicated by carbon introduced from the graphite heater during sintering at high temperatures in the particular furnace employed. The magnitude of the carbon added was investigated using niobium strip samples heated under process conditions. The amount of graphite in the reduction charge was then adjusted for a particular time-temperature program.

It had been found by other investigators that any melting process for forming niobium-rich alloys in the 20 wt% uranium range resulted in loss of uranium and microsegregation of the uranium in the solid solution. It appears that a 20 wt% U-Nb alloy prepared by reacting a mixture of oxides with carbon in a vacuum at temperatures up to the solidus line of the niobium-uranium phase diagram will have essentially all of the uranium distributed homogeneously in niobium solid solution. This uniform distribution of uranium in niobium could be an important feature in design and fabrication of enriched uranium fuel elements.

6.14 Deformation Behavior of Niobium and Tantalum (H. A. Wilhelm and D. S. Cowgill)

The purpose of this investigation which has recently been initiated is to compare the deformation behaviors of niobium and tantalum in the temperature range of the ductile-to-brittle transformation for niobium metal. The comparison is expected to provide information toward understanding the fundamental nature of the ductile-to-brittle transformation phenomena.

Techniques have been established and equipment prepared for cleaning, electropolishing and photo-gridding tensile specimens preparatory to tensile testing, and for replication of fracture surfaces for electron microscopic examination after testing. The behavior of photo-grid material at

M-95

-196°C is being evaluated, and the low temperature tensile testing chamber is being constructed.

LIST OF REPORTS AND PUBLICATIONS

1. REPORTS FOR COOPERATING LABORATORIES

- IS-118 Bernstein, B. T. and J. F. Smith, A Calculation of the Elastic Constants of Yttrium and the Rare-Earth Metals.
- IS-131 Ray, A. E. and J. F. Smith, A Test for Electron Transfer in the Intermetallic Compound, V_4Al_{23} .
- IS-262 Williams, D. E. and H. L. Levingston, Arc Melting in the Tungsten Electrode Furnace.
- IS-351 Ames Laboratory Staff, Annual Summary Research Report in Metallurgy for July 1, 1960 - June 30, 1961.
- IS-374 Haefling, J. A., F. A. Schmidt and O. N. Carlson, A Study of Several Metals as Reductants for Yttrium Metal.
- IS-440 Smith, J. F., Determination of Thermodynamic Functions for the Formation of Binary Intermetallic Phases from Vapor Pressure Measurements.
- IS-503 Neubauer, Edwin Paul and H. A. Wilhelm, Effect of Oxygen on Mechanical Properties of Niobium.
- IS-505 Meyerhoff, Robert Wagner and J. F. Smith, The Thallium-Indium Phase Diagram as a Function of Composition, Temperature and Pressure.

2. PUBLICATIONS

- Bailey, D. M. and J. F. Smith, A Note on the Structure of Zr_2Co . Acta Cryst. 14, 1084 (1961).
- Bradford, S. A. and O. N. Carlson, Effect of Oxygen on the Lattice Constant, Hardness and Ductility of Vanadium. Trans. Am. Soc. Metals 55, 169-178 (1962).
- Carlson, O. N. and F. A. Schmidt, Metallothermic Preparation of Yttrium Metal "The Rare Earths" (John Wiley and Sons, Inc., New York, 1961), p. 118.
- Carlson, O. N. and F. A. Schmidt, Preparation of the Rare-Earth Fluorides, "The Rare Earths" (John Wiley and Sons, Inc., New York, 1961), p. 77.
- Hamilton, C. B. and H. A. Wilhelm, The Preparation of Tantalum Metal by the Carbon Reduction of Tantalum Pentoxide. Iowa Acad. Sci. 68, 189-201 (1961).

- Kirkpatrick, M. E., D. M. Bailey and J. F. Smith, The Structures of NiZr_2 , NiZr and Their Hafnium Analogs. *Acta Cryst.* 15, 252-255 (1962).
- Kirkpatrick, M. E. and W. L. Larsen, Phase Relationships in the Nickel-Zirconium and Nickel-Hafnium Alloy Systems. *Trans. Am. Soc. Metals* 54, 580-590 (1961).
- McMasters, O. D. and W. L. Larsen, Phase Equilibria in the Thorium-Tantalum System. *J. Less-Common Metals* 3, 312-320 (1961).
- Meyerhoff, R. W. and J. F. Smith, Anisotropic Thermal Expansion of Single Crystals of Thallium, Yttrium, Beryllium and Zinc at Low Temperatures. *J. Appl. Phys.* 33, 219-224 (1962).
- Palmer, P. E., O. D. McMasters and W. L. Larsen, Thorium-Vanadium Phase Diagram. *Trans. Am. Soc. Metals* 55, 301-306 (1962).
- Peterson, David T., Thermodynamics and Kinetics of the Deoxidation of Thorium by Calcium. *Trans. Met. Soc. AIME* 221, 924-926 (1961).
- Peterson, D. T. and V. G. Fattore, Calcium-Calcium Hydride Phase System. *J. Phys. Chem.* 65, 2062-2064 (1961).
- Peterson, D. T. and V. G. Fattore, Determination of Hydrogen in Calcium by Vacuum Fusion. *Anal. Chem.* 34, 579-580 (1962).
- Peterson, D. T. and J. Rexer, The Composition of ThH_2 and Diffusion of Hydrogen in ThH_2 . *J. Less-Common Metals* 4, 92-97 (1962).
- Williams, D. E., R. J. Jackson and W. L. Larsen, The Tantalum-Zirconium Alloy System. *Trans. Met. Soc. AIME* 224, 751 (1962).

PHYSICS
DIVISION

IS-500

ANNUAL SUMMARY RESEARCH REPORT IN PHYSICS

by

AMES LABORATORY PHYSICS STAFF

F. H. Spedding, Director, R. G. Barnes, N. Bernardes, B. C. Carlson,
B. C. Cook, G. C. Danielson, R. Fuchs, R. H. Good, Jr., C. L. Hammer,
E. N. Hatch, D. E. Hudson, E. Iloff, J. M. Keller, A. J. Kromminga,
S. Legvold, D. W. Lynch, A. Mackintosh, M. G. Stewart,
C. A. Swenson, T. A. Weber, and D. J. Zaffarano

IS-500

ANNUAL SUMMARY RESEARCH REPORT IN PHYSICS

For the period July 1, 1961 - June 30, 1962

This report is prepared from material
submitted by the group leaders
of this Laboratory

Previous research reports in this series are:

ISC-35	ISC-395
ISC-41	ISC-422
ISC-56	ISC-451
ISC-69	ISC-508
ISC-74	ISC-533
ISC-76	ISC-577
ISC-79	ISC-608
ISC-113	ISC-645
ISC-130	ISC-707
ISC-133	ISC-758
ISC-137	ISC-833
ISC-171	ISC-901
ISC-193	ISC-975
ISC-220	ISC-1048
ISC-246	ISC-1115
ISC-283	IS-14
ISC-301	IS-191
ISC-338	IS-349

IS-500

CONTENTS

PHYSICSNuclear Physics, Theoretical Reports

	Page
1. Inelastic Scattering of Protons by Nuclei (A. J. Kromminga)....	1
2. The Many-Boson Problem (A. J. Kromminga).....	1
3. High-Energy Potential Scattering (B. C. Carlson).....	2
4. Hypergeometric Functions (B. C. Carlson).....	2
5. Elliptic Integrals of the Second Kind (B. C. Carlson).....	3
6. Pair Production Calculations (C. L. Hammer).....	3
7. Angular Distribution of Photoelectrons (T. A. Weber).....	4
8. Time Dependent Perturbation Theory (C. L. Hammer).....	4
9. Coulomb Wave Functions (C. L. Hammer).....	5
10. Quantized Theory for Particles with Mass (C. L. Hammer and R. H. Good).....	5
11. Equations of Motion for a Polarized Particle (R. H. Good).....	6
12. Basic Theory of the Electron (R. H. Good).....	7
12.1 Uniqueness of the Electron Polarization Operator.....	7
12.2 Tensor Operator for Electron Polarization.....	7
12.3 Relation between the Foldy-Wouthuysen and Lorentz Transformations.....	8
13. Connection between Displacement Operators and Integrals of Motion for Photons (R. H. Good).....	8
14. Beam Extraction Studies for Accelerators (C. L. Hammer).....	9

Nuclear Physics, Synchrotron Group

1. Large Angle Pair Production (C. L. Hammer).....	10
2. Photonuclear Reactions (M. G. Stewart).....	10
3. The $O^{16}(\gamma, n)O^{15}$ Cross Section (B. C. Cook).....	10
4. Nuclear Photo-Particle Production (E. L. Iloff).....	11
5. Least Structure Solution to Photonuclear Yield Functions (B. C. Cook).....	14

Nuclear Spectroscopy

1. Internal Conversion Coefficients (E. N. Hatch).....	18
2. Beta-Decay Energy Systematics (E. N. Hatch).....	19
3. Positron Lifetimes in Metals (M. G. Stewart).....	19

Solid State Theoretical Reports

	Page
1. Quadrupole Precession (R. H. Good)	22
2. Transport Properties of Cubic Sodium Tungsten Bronzes (R. Fuchs).....	22
3. Dielectric Constant of Ionic Crystals (R. Fuchs).....	23
4. Properties of Solids at Low Temperatures (N. Bernardes).....	24
4.1 Solid and Liquid He ³	24
4.2 Bulk Properties.....	25
5. Contribution of Anharmonic Forces to the Specific Heat of Solids (J. M. Keller)	25
6. Dependence of Electrical Resistivity of Rare-Earth Metals on Relative Magnetization (J. M. Keller).....	25

Solid State Experimental Results

1. Semiconducting Compounds (G. C. Danielson).....	26
1.1 Seebeck Effect in Mg ₂ Si Single Crystals	26
1.2 Elastic Constants of Mg ₂ Si.....	27
2. Thermal Properties of Solids above 300°K (G. C. Danielson)...	27
2.1 Dynamic Methods for Determining Thermal Conductivity .	27
2.2 Thermal Diffusivity Measurements on a Finite Disk.....	28
2.3 Thermal Diffusivity of Armco Iron.....	28
2.4 Thermal Diffusivity of Zirconium.....	29
2.5 Specific Heat of Armco Iron.....	29
2.6 Specific Heat of Zirconium.....	29
3. Tungsten Bronzes (G. C. Danielson).....	29
4. Preparation of Single Crystals (G. C. Danielson)	30
5. Color Centers in Alkali Halides (D. W. Lynch)	31
5.1 Color Centers in CsBr.....	31
5.2 V ₂ and V ₃ Centers in Alkali Halides.....	32
6. Optical Properties of Cubic Sodium Tungsten Bronzes (D. W. Lynch and G. C. Danielson)	33
7. Optical Properties of Semiconductors (D. W. Lynch).....	34
7.1 Index of Refraction and Reflectivity of Mg ₂ Si, Mg ₂ Ge and Mg ₂ Sn.....	34
7.2 Photoconductivity in Mg ₂ Si and Mg ₂ Ge.....	35
8. Experimental Determination of the Electronic Structure of Metals (A. R. Mackintosh)	35
8.1 Ultrasonic Attenuation in Lead.....	35
8.2 Cyclotron Resonance in Lead at 36 kmcs.....	36
8.3 Positron Annihilation in Solids (A. R. Mackintosh and D. J. Zaffarano).....	36
8.4 Electronic Structure of Rare-Earth Metals (A. R. Mackintosh).....	37
8.5 Magnetic Ordering and the Electronic Structure of Rare-Earth Metals	38
9. Transport Properties of Dilute Rare-Earth Alloys (A. R. Mackintosh).....	38

10.	Superconductivity of Lanthanum Alloys (A. R. Mackintosh, C. A. Swenson and F. H. Spedding).....	38
11.	Thermoelectric Power in Chromium and Vanadium (A. R. Mackintosh).....	39
12.	The de Haas-van Alphen Effect (A. V. Gold)	39
12.1	The de Haas-van Alphen Effect and the Band Structure of Lead.....	39
12.2	The de Haas-van Alphen Effect in Transition Metals	41
13.	Conduction Processes in Diamond (D. E. Hudson)	41
14.	Cohesion of Intermetallic Compounds (D. E. Hudson)	42
15.	Growing Large Crystals (S. Legvold).....	42
16.	Magnetic Phenomena in Crystals (S. Legvold).....	43
16.1	Electrical and Magnetic Properties of Holmium Single Crystals.....	43
17.	Magnetostriction (S. Legvold)	44
18.	Superconductivity (C. A. Swenson).....	44
18.1	Niobium	44
18.2	Tin.....	45
18.3	Critical Field of Superconductors.....	45
19.	High Pressure Studies (C. A. Swenson).....	46
19.1	Cesium.....	46
19.2	Xenon	46
19.3	Mercury.....	47
20.	Heat Capacity of Solid He ³ (C. A. Swenson).....	47
21.	Nuclear Magnetic Resonance Studies (R. G. Barnes).....	48
21.1	Nuclear Magnetic Resonance in Chromium Metal.....	48
21.2	Nuclear Magnetic Resonance and Knight Shift in Solid Indium.....	49
21.3	Nuclear Magnetic Resonance in Ytterbium Metal	51
21.4	Nuclear Magnetic Resonance of V ⁵¹ in Vanadium Carbides.....	53
21.5	Nuclear Quadrupole Resonance and Bonding in Solid Layer Type Metal Halides	55
21.6	Nuclear Magnetic Resonance of Cl ³⁵ in Paramagnetic FeCl ₂	55
22.	Electron Paramagnetic Resonance Studies of Impurity Centers in Crystals (R. G. Barnes).....	57
22.1	Co ²⁺ Ion in Single-Crystal Titanium Oxide (Rutile)	57
22.2	V ⁴⁺ Ion in Single-Crystal Titanium Oxide (Rutile)	59
22.3	Reduced TiO ₂ (Ti ³⁺ Ion in Single-Crystal Rutile) (R. G. Barnes).....	60

List of Reports and Publications

1.	Reports for Cooperating Laboratories	65
2.	Publications	65

PHYSICS

NUCLEAR PHYSICS, THEORETICAL REPORTS

1. INELASTIC SCATTERING OF PROTONS BY NUCLEI (A. J. Kromminga^{*})

A paper entitled "A Simple Direct Reaction Model of Proton Inelastic Scattering", by A. J. Kromminga and I. E. McCarthy,¹ was published in Nucl. Phys. 31, 678-688 (1962).

Abstract--The model of McCarthy and Pursey for angular distributions in direct nuclear reactions is extended to the case of proton inelastic scattering, a reaction whose angular distributions at medium energies are unintelligible from the point of view of the plane-wave Born approximation. The model is closely analogous to the plane-wave model in that it does not require a partial-wave expansion of the optical-model wave functions. The distortion is included by simple but realistic generalizations of the optical-model wave functions. The present work includes a parameter representing the focus in the wave functions which is seen to account for the shapes of the angular distributions for the (p,p') reaction on carbon-12 at medium energies. It is shown how intuition gained from the present simple theory can lead to useful knowledge about nuclei.

2. THE MANY-BOSON PROBLEM (A. J. Kromminga²)

A paper entitled "Perturbation Theory of Many-Boson Systems", by A. J. Kromminga and M. Bolsterli, Physics Dept., Univ. of Minnesota, was submitted for publication in The Physical Review.

^{*}First name listed indicates group leader in charge of work.

¹Department of Physics, University of Adelaide, Australia.

²Some of this work was performed before Dr. Kromminga joined the Ames Laboratory.

Abstract--A noncanonical transformation of the Boson creation and annihilation operators is performed in order to obtain a Hamiltonian which can be treated by the standard methods of field-theoretic perturbation theory. The standard results¹ (with a slight modification) are rederived by this technique.

3. HIGH-ENERGY POTENTIAL SCATTERING (B. C. Carlson)

A paper entitled "Theory of High-Energy Potential Scattering", by P. J. Lynch and B. C. Carlson, will be published in J. Math. Phys. 3, 440-450 (1962).

Abstract--The exact amplitude for scattering of a Schrödinger or Dirac particle by a static potential is rewritten in a two-potential form by splitting the potential into two parts, one of which contributes only to exactly forward scattering. Replacement of the exact wave function by a modified plane wave gives a high-energy approximation that is shown to be equivalent to the Saxon-Schiff approximation in the Schrödinger case. Corrections to the approximation are obtained in principle from a simplified series expansion of the exact wave function having the modified plane wave as leading term. The approximate amplitude reduces at small scattering angles to a well-known result; at large angles, it reduces to Schiff's stationary-phase approximation in the Dirac case but not, as shown by the example of a Gaussian potential, in the Schrödinger case.

4. HYPERGEOMETRIC FUNCTIONS (B. C. Carlson)

The elliptic integrals encountered in an earlier study of the nuclear liquid-drop model with high angular momentum have stimulated an investigation of a hypergeometric function of n variables known as Lauricella's function F_D . It includes as special cases the Gauss hypergeometric function

¹S. T. Belyaev, J. Exp. Theoret. Phys. (U.S.S.R.) 34, 417 (1958); Soviet Phys. JETP 7, 289 (1958).

and Appell's function F_1 . A new approach to the theory of this function has been found by introducing homogeneous variables, with the result that the Euler transformations, the differential equations, and the relations between contiguous functions are greatly simplified. Among the byproducts of this investigation are a new representation of F_1 as the integral of a Gauss hypergeometric function and the evaluation of an integral over the surface of a sphere which shows the relation of the incomplete elliptic integrals to the geometry of the ellipsoid.

5. ELLIPTIC INTEGRALS OF THE SECOND KIND (B. C. Carlson)

The study of hypergeometric functions described in the preceding item has shown that the well-known linear transformations of the elliptic integrals F and E are special cases of the Euler transformations of Appell's function F_1 . This identification suggests that Legendre's standard elliptic integral of the second kind, $E(\phi, k)$, is a less advantageous choice than

$$G(\phi, k) = \sin^2 \phi E(\phi, k) + \cos^2 \phi F(\phi, k) + \sin \phi \cos \phi (1 - k^2 \sin^2 \phi)^{\frac{1}{2}}.$$

The five linear transformations that carry $F(\phi, k)$ into a multiple of itself also carry $G(\phi, k)$, but not $E(\phi, k)$, into a multiple of itself. The surface area of a general ellipsoid, which plays an important part in the nuclear liquid-drop model with angular momentum, has a simple expression in terms of $G(\phi, k)$.

6. PAIR PRODUCTION CALCULATIONS (C. L. Hammer)

A paper entitled "Z Correction to the Bethe-Maximon Pair Production Cross Section", by David S. Moroi and C. L. Hammer, was submitted for publication in The Physical Review.

Abstract--The first order correction in αZ to the Bethe-Maximon pair production cross section is calculated for the case where the incident photon and one of the electrons has an energy much greater than mc^2 . Comparison of these calculations to the experimental data of Plimpton and Hammer shows an improvement in agreement between theory and experiment of approximately a factor of $1 + (\alpha Z 4\pi/15)$ for low positron kinetic energies. However, for positron kinetic energies of the order of 1 Mev, no improvement is obtained.

7. ANGULAR DISTRIBUTION OF PHOTOELECTRONS (T. A. Weber)

A paper entitled "Angular Distribution of Relativistic Atomic K-Shell Photoelectrons", by T. A. Weber and C. J. Mullin,¹ was published in Phys. Rev. 126, 615 (1962).

Abstract--Using the high energy limit of the exact Coulomb wave function for the outgoing electron, the differential cross section, correct to three orders in αZ , is calculated for the K-shell photoeffect. An analytic expression, exact in αZ , is obtained for the differential cross section for the special case in which the electron emerges in the forward direction.

8. TIME DEPENDENT PERTURBATION THEORY (C. L. Hammer)

A paper with the above title, by T. A. Weber and C. L. Hammer, was submitted for publication in The Physical Review.

Abstract--Standard treatments² of time dependent perturbation theory use detailed and sometimes spurious arguments to surmount various mathematical difficulties which appear. Needless to say, this obscures the physics involved in the problem.

¹Department of Physics, University of Notre Dame, Notre Dame, Indiana.

²See, for example, L. I. Schiff, "Quantum Mechanics", 2nd Ed., McGraw-Hill Book Company, New York.

In our present treatment, we consider a time dependent perturbation which in various limits of a parameter gives the sudden and the adiabatic approximation. Thus, both approximations are contained in one formulation. Further, we find that in connection with the sudden approximation for discrete energy levels, one must consider transitions to final perturbed states and not to unperturbed states as is done in standard treatments. Thus the theory becomes physically transparent. We are also treating the cases of wave packets and the problem of damping phenomena.

9. COULOMB WAVE FUNCTIONS (C. L. Hammer)

A paper, "Coulomb Wave Functions", by D. Fradkin, T. Weber and C. L. Hammer, was submitted for publication in The Physical Review.

Abstract--In order to make improved calculations of Coulomb scattering, bremsstrahlung, and pair production, the scattering solutions of the Dirac equation containing a Coulomb potential have been studied. These solutions behave asymptotically at large distances like a distorted plane wave plus an outgoing (ingoing) spherical wave. The exact solution has been given as an infinite series by Darwin,¹ and recently has been reorganized by Johnson and Deck.²

The result of Johnson and Deck has been re-derived in an alternate fashion, and the differential relations satisfied by the three functions has been obtained. By letting $(\alpha Z)^2 \rightarrow 0$, the Sommerfeld-Maue approximation is obtained directly from the differential equations. Other schemes of approximation, particularly those suitable for a range of Z , have been studied.

10. QUANTIZED THEORY FOR PARTICLES WITH MASS (C. L. Hammer and R. H. Good, Jr.)

Hammer and Good^{3,4} have constructed a relativistic c-number theory describing particles with arbitrary spin and zero mass. The quantization

¹See, for example, Akhiezer and Berestetsky, Quantum Electrodynamics, AEC-tr-2876 (Part I).

²W. R. Johnson and R. T. Deck, to be published.

³C. L. Hammer and R. H. Good, Jr., Phys. Rev. 108, 882 (1957).

⁴Ibid. 111, 342 (1958).

of this theory gives a connection between the spin and the statistics of the particles. It is of interest to extend these ideas to a general theory for all spins and arbitrary rest mass. The particles of mass m and spin s are described by symmetric spinors of rank $2s$. These spinors have $2s + 1$ independent components and consequently can describe the polarization degrees of freedom of a spin s particle. Since there are two independent kinds of symmetric spinor, upper-undotted and lower-dotted, the antiparticle as well as the particle can be described. To construct the spinors one starts with the spin one-half functions, the lower-dotted and upper-undotted rank one spinors, expanded as a Fourier integral of plane-wave solutions of the Dirac-Hamiltonian and of the polarization operator.¹ From an examination of the transformation properties of the components of the Fourier integral under continuous Lorentz transformations one finds the correct way to combine the components to form symmetric spinors of higher rank. The construction of these spinors depends only on the notion of the spin of a particle in its rest system and Lorentz covariance. It is expected that these notions alone will lead to the connection between spin and the statistics.

11. EQUATIONS OF MOTION FOR A POLARIZED PARTICLE (R. H. Good, Jr.)

A paper with the title "Classical Equations of Motion for a Polarized Particle in an Electromagnetic Field", by R. H. Good, Jr., was published in Phys. Rev. 125, 2112-2115 (1962).

¹D. M. Fradkin and R. H. Good, Jr., Rev. Mod. Phys. 33, 343 (1961).

Abstract--This paper gives the classical relativistic equations of motion for a particle with intrinsic angular momentum in an external electromagnetic field, including the effects of first-order field gradients. The system considered especially is a nucleus in its ground state. The preferred value of the electric quadrupole moment Q is found to be $-(2I-1)\mu(\hbar/mc)$ where I is the spin and μ the magnetic moment of the particle.

12. BASIC THEORY OF THE ELECTRON (R. H. Good, Jr.)

12.1 Uniqueness of the Electron Polarization Operator

A paper with the above title, by M. E. Rose¹ and R. H. Good, Jr., was published in Il Nuovo Cimento 22, 565-568 (1961).

Abstract--The most general three-vector polarization operator, that commutes with the Hamiltonian and has the algebra of spin one-half, is constructed for a free Dirac particle. The non-uniqueness inherent in this operator may be resolved by imposing either of the following two conditions: (1) The operator should be well-defined in the rest system. (2) It should correspond to the space part of a four-vector operator evaluated in the rest system. In either case the operator obtained is the Foldy-Wouthuysen transform of $\beta\sigma$.

12.2 Tensor Operator for Electron Polarization

A paper with the above title, by D. M. Fradkin and R. H. Good, Jr., was published in Il Nuovo Cimento 22, 643-649 (1961).

Abstract--In this paper it is shown that the polarization of a free Dirac particle can be treated in a covariant way in terms of an antisymmetric second-rank tensor operator which commutes with the Hamiltonian. The operator has the interpretation that in the rest system of the particle the space-space part is the spin and the space-time part is zero. In the

¹Department of Physics, University of Virginia, Charlottesville, Virginia.

quantized theory the second-rank tensor description of the polarization is a more appropriate notion than the four-vector description. The converse holds for the Foldy-Wouthuysen mean spin.

12.3 Relation between Foldy-Wouthuysen and Lorentz Transformations

A paper with the above title, by R. H. Good, Jr. and M. E. Rose, has been published in Il Nuovo Cimento 24, 864 (1962).

Abstract--It is shown that, in the Dirac theory of a free electron, the Foldy-Wouthuysen transformation corresponds to the Lorentz transformation from the laboratory to the rest system of the electron, together with a factor which preserves the norm of the wave function. This consideration resolves the ambiguity in the Foldy-Wouthuysen transformation. Also it is shown that covariantly-defined Lorentz-tensor operators may be interpreted as Lorentz transforms of matrix operators from the rest to the laboratory system.

13. CONNECTION BETWEEN DISPLACEMENT OPERATORS AND INTEGRALS OF MOTION FOR PHOTONS (R. H. Good, Jr.)

The above paper, by R. H. Good, Jr., has appeared in Il Nuovo Cimento 24, 713 (1962).

Abstract--In this paper it is shown that the energy, momentum, and angular momentum in the electromagnetic field may be written as a certain double integral involving the fields and the displacement operators of the corresponding transformations. The quantity that corresponds to the identity transformation is found to be the excess of right-hand over left-hand polarized photons. It is shown that the uncertainty principle applies for a photon packet provided that energy-weighted averages of position and momentum are used.

14. BEAM EXTRACTION STUDIES FOR ACCELERATORS (C. L. Hammer)

The electron beam from the Iowa State University Synchrotron has been successfully extracted using the resonant methods described by Hammer, Bureau and Laslett^{1,2,3,4} to cause the beam to enter a magnetic shunt. Detailed computer studies using the exact synchrotron and shunt fields completely verify the observed behavior of the extracted beam. The predicted extraction efficiency is expected to be greater than 60%, depending upon the actual phase space distribution of the beam, with a predicted radial and vertical phase space area of less than one centimeter milli-rad. Measurements are now in progress which will attempt to verify these predictions.

In addition to these studies, preliminary calculations have been made for resonant extraction of the electron beam from the M.U.R.A. 50 Mev F.F.A.G. synchrotron. Computer studies using the exact guide field for several different perturbations designed to use the $\nu_x = 4.5$ resonance show no large induced vertical oscillations. Thus, little or no coupling seems to exist between the radial and vertical betatron oscillations during the extraction process. Furthermore, the large radial growth superimposed upon the scalloped equilibrium orbit can be made to occur at one azimuthal position in the accelerator. Although further study is needed, this method of extraction appears to be very promising for the F.F.A.G. type accelerators.

¹C. L. Hammer and A. J. Bureau, Rev. Sci. Instr. 26, 594 (1955).

²Ibid. 26, 598 (1955).

³C. L. Hammer and L. J. Laslett, 2nd Intern. Conf. Peaceful Uses Atomic Energy, Geneva 30, 151 (1958).

⁴C. L. Hammer and L. Jackson Laslett, Rev. Sci. Instr. 32, 144 (1961).

NUCLEAR PHYSICS, SYNCHROTRON GROUP

1. LARGE ANGLE PAIR PRODUCTION (C. L. Hammer)

A paper with the above title, by J. D. Plimpton and C. L. Hammer, was submitted for publication in The Physical Review.

Abstract--The energy spectrum of positrons emitted from gold and tin targets at 90° with respect to the incident x-ray beam of the Iowa State University Synchrotron has been measured for positron energies between 0.1 and 1.4 Mev. A discrepancy of more than an order of magnitude is found between the experimental results and the theory as represented by calculations to lowest order in αZ .

2. PHOTONUCLEAR REACTIONS (M. G. Stewart)

A paper, "The Photoproton Reaction in Be^9 ", by F. M. Clikeman, A. J. Bureau and M. G. Stewart, was published in Phys. Rev. 126, 1822 (1962).

Abstract--The reaction $\text{Be}^9(\gamma, p)\text{Li}^8$ was measured from threshold (16.89 Mev) up to 57 Mev using the bremsstrahlung beam from the Iowa State University electron synchrotron. The data were taken in energy steps of ~ 0.050 Mev for the first several Mev and in energy steps of ~ 1.0 Mev for the remainder of the yield curve. A number of small resonances near threshold were observed. The giant resonance cross section reaches a peak value of 2.64 ± 0.30 mb at an energy of 23 Mev, and it possesses a large high energy tail. The integrated cross section to 56.8 Mev is 41.4 ± 4.6 Mev-mb.

3. THE $\text{O}^{16}(\gamma, n)\text{O}^{15}$ CROSS SECTION (B. C. Cook)

A photonuclear yield function for the $\text{O}^{16}(\gamma, n)\text{O}^{15}$ reaction has been obtained by the detection of the radioactivity of O^{15} . Measurements were made in 0.5 Mev energy intervals from the reaction threshold of 15.5 Mev

to 64.5 Mev. A minimum of three measurements of the O^{15} yield was made at each energy. From the reproducibility of the data we deduce an accuracy of 0.5% at all energies above 26 Mev. The yield function was analyzed using the "Least Structure" method in one Mev intervals for the cross section. The resulting cross section curve is shown in Fig. 1 where the two curves obtained by using one Mev intervals are superimposed. The agreement between the two curves is excellent for all energies below 44 Mev, but is poor at higher energies. Four peaks at 17, 20.4, 23 and 24.5 Mev were found at lower energies. These agree closely with the work of other investigators and with the theory of O^{16} . Four levels predicted by Elliot and Flowers are shown as arrows in Fig. 1. Additional structure is seen at higher energies but only the peaks at 33 and 41 Mev which occur in both independent curves are statistically significant. Measurement of the yield curve has been repeated to confirm the existence of structure at 33 and 41 Mev and to resolve the discrepancies at higher energy. A cross section analysis for this latter data is now well underway. We plan to extend the measurements to higher energies and to investigate further the remaining reasons for fluctuations in the data to improve accuracy.

4. NUCLEAR PHOTO-PARTICLE PRODUCTION (E. L. Illoff)

A measurement has been made of the relative numbers of deuterons to protons produced by the irradiation of a cobalt target with 45 Mev maximum energy bremsstrahlung. The technique used is described in detail in our previous work on the ratio of the yields of photodeuterons

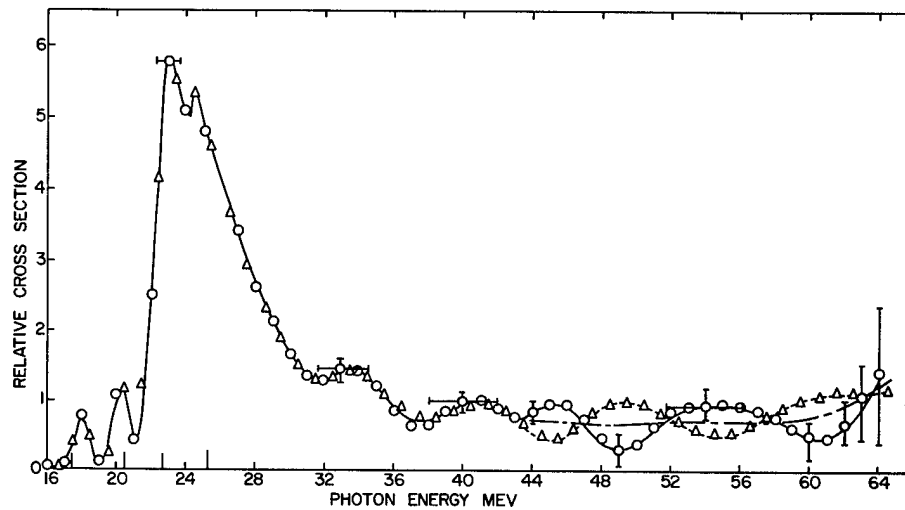


Fig. 1. The $O^{16}(\gamma, n)O^{15}$ Cross Section

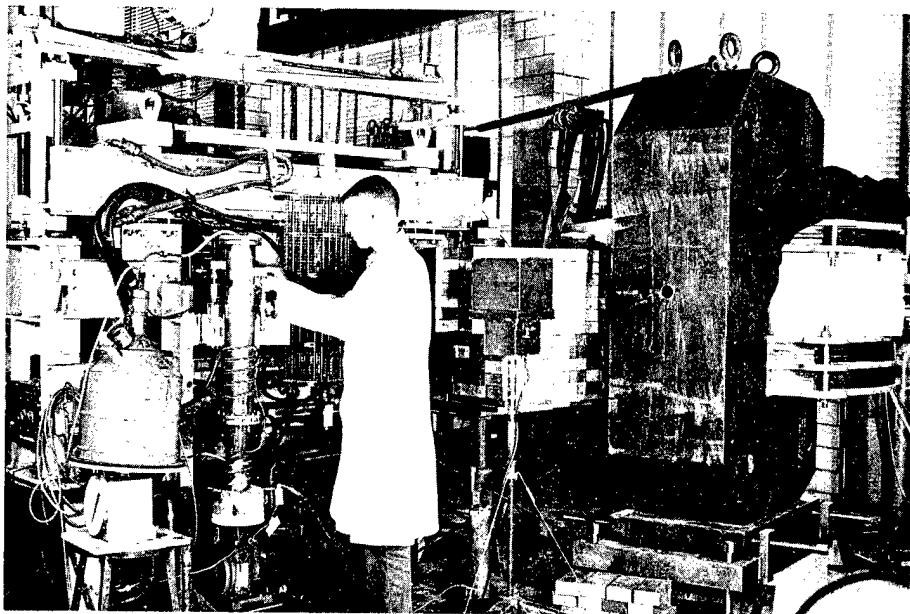


Fig. 2. Experimental Set-up Involving 70 Mev
ISU Synchrotron

to photoprotons for copper.¹ The charged particles from the target pass through a magnetic field and are detected in nuclear emulsion plates. The positions and angles of entrance of the detected particles and their ranges in nuclear emulsion are used to retrace their paths back to the target and identify them.

The experimental technique has been improved considerably. The vacuum chamber containing the target and plates is kept at a constant relative humidity of about 50% to prevent shrinkage and destruction of the emulsions due to a long exposure period in vacuum. The long exposure time makes possible the use of a target of about one-fourth the thickness of that used previously and thus allows particles of lower energies to be observed. The mass resolution was greatly improved and background was much reduced by the use of a tapered collimator. These improvements allow the accurate identification of individual particles. About 25 deuterons have been identified in the cobalt experiment. Within the statistics there is little variation in the deuteron to proton yield ratio with energy of the particle produced. Particles from 2 to 15 Mev are included in the measurement. There appears to be an increase in the ratio as the angle of the outgoing particle increases within the angular interval included in the measurements, that is from 20 to 90°.

The mean value we find for the deuteron to proton ratio for cobalt including all the particles identified is

$$\frac{Y(\gamma, d)}{Y(\gamma, p)} = 0.02 \pm 0.005 .$$

¹G. P. Ho and Edwin L. Iloff, Nucl. Phys. 27, 234 (1961).

This result for cobalt, as was our earlier result for copper, is about an order of magnitude lower than the results of the older work done by less reliable methods. The ratio we find is much too large to be explained by an evaporation model. Recent careful theoretical work by Madsen and Henley¹ proposes that two processes are largely responsible for photodeuteron production. Their calculations for direct production include the "pick-up" process and they show that this results in a much smaller contribution than has been suggested by earlier investigators. Our experimental ratio for cobalt is in agreement with the calculations of Madsen and Henley for the direct process and compound nucleus formation combined, or for compound nucleus formation alone. Our result seems too large to be accounted for by the direct process alone.

5. LEAST STRUCTURE SOLUTION TO PHOTONUCLEAR YIELD FUNCTIONS (B. C. Cook)

Most photonuclear cross sections have been obtained by unfolding photonuclear yield functions. The cross sections, σ , obtained by unfolding without smoothing the yield functions, oscillate drastically as a function of photon energy. This effect is particularly pronounced in the energy region above the giant resonance energy. However, if the yield function is smoothed using graphical or analytical methods, one obtains physically acceptable solutions to the yield functions. Since the amount of smoothing required is quite subjective, no general agreement among workers in photonuclear physics about smoothing has been possible.

¹V. A. Madsen and E. M. Henley (to be published).

A new method,¹ called "Least Structure Solution to Photonuclear Yield Functions", has been developed to solve yield functions for cross sections. An auxiliary function S of the σ 's called the Structure is defined. One possible form for S that has been tried is as follows:

$$S_2 = \sum_{i=2}^{N+1} (\sigma_{i+1} - 2\sigma_i + \sigma_{i-1})^2 \quad (1)$$

Other S functions have also been tried and it is found that the solutions for σ do not change drastically for other definitions of S . A set of σ_i 's is considered to be a solution to the bremsstrahlung equation

$$\tilde{N} \cdot \vec{\sigma} = \vec{Y} \quad (2)$$

provided

$$\sum_i w_i (\bar{y}_i - y_i)^2 = \chi^2 \pm \Delta\chi^2 \quad (3)$$

where

\vec{Y} = measured yield function

\tilde{N} = bremsstrahlung matrix

χ^2 = expectation value of χ^2 determined by the
accuracy of the yield function \vec{y}

$\Delta\chi^2$ = expectation value of the probable error of χ^2

w_i = weighting function of the i th yield value .

A solution $\vec{\sigma}$ is now sought to minimize the structure S (Eq. 1) yet satisfy the bremsstrahlung Eq. (2) in the sense of Eq. (3). The result is given in Eq. (4).

¹ A similar method for the solution of integral equations has been proposed. See "A Technique for the Numerical Solution of Certain Integral Equations of the First Kind", by David L. Phillips, Argonne National Laboratory, Applied Mathematics Division, Technical Memorandum No. 19 (internal).

$$(\underset{\sim}{N} + \lambda \underset{\sim}{N}^{-1} \cdot \underset{\sim}{S}) \cdot \vec{\sigma} = \vec{Y} \quad (4)$$

where

λ = Lagrangian multiplier introduced into the
variational problem

$\underset{\sim}{N}^{-1}$ = the inverse of the transpose of $\underset{\sim}{N}$

$\underset{\sim}{S}$ = a smoothing matrix determined by the structure
function S .

Equation (4) has N equations in N unknowns σ_i and one additional unknown λ . However, Eq. (3) must also be satisfied. Thus λ can be calculated as a function of χ^2 .

A program has been written in FORTRAN for the IBM-704 computer to solve the equations of "Least Structure". Many test problems using simulated and actual photonuclear yield functions have been analyzed using this program. The results of one of these tests is shown in Fig. 3a. A hypothetical cross section curve was generated from two Gaussians. This cross section was then converted into a yield by folding in the bremsstrahlung spectrum. An error of one percent distributed as a Gaussian error function was introduced into the yield at each energy. The resulting yield function was solved by Least Structure for a cross section. This solution as well as the assumed cross section is shown in Fig. 3b. The presence of the higher energy peak is clearly established. Without smoothing, no evidence could be found for this higher energy peak. Ten such functions were generated and all exhibit the second peak so that we are confident that one percent data is sufficiently accurate to establish structure above the giant resonance if the integrated cross

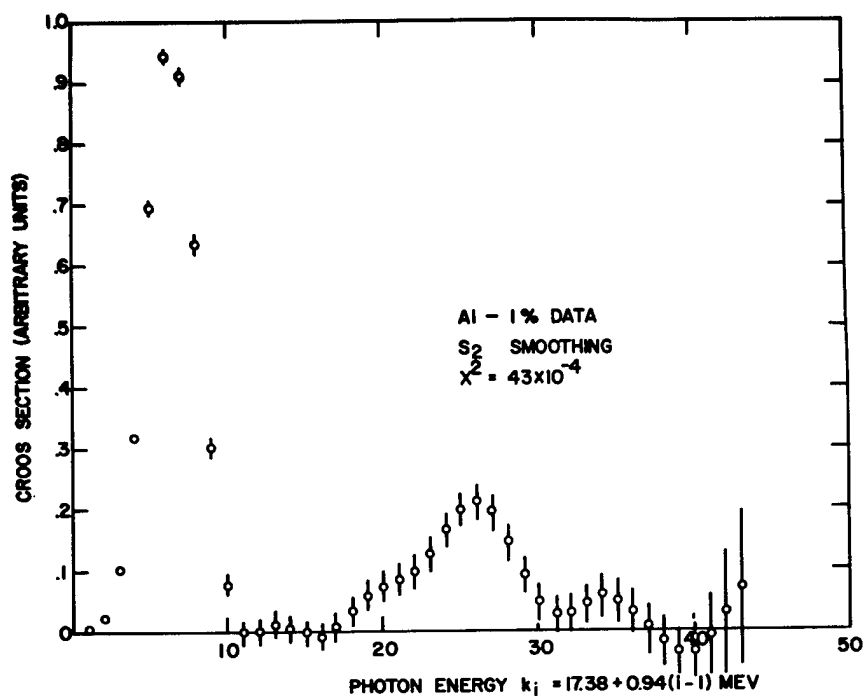


Fig. 3a. Assumed Cross Section

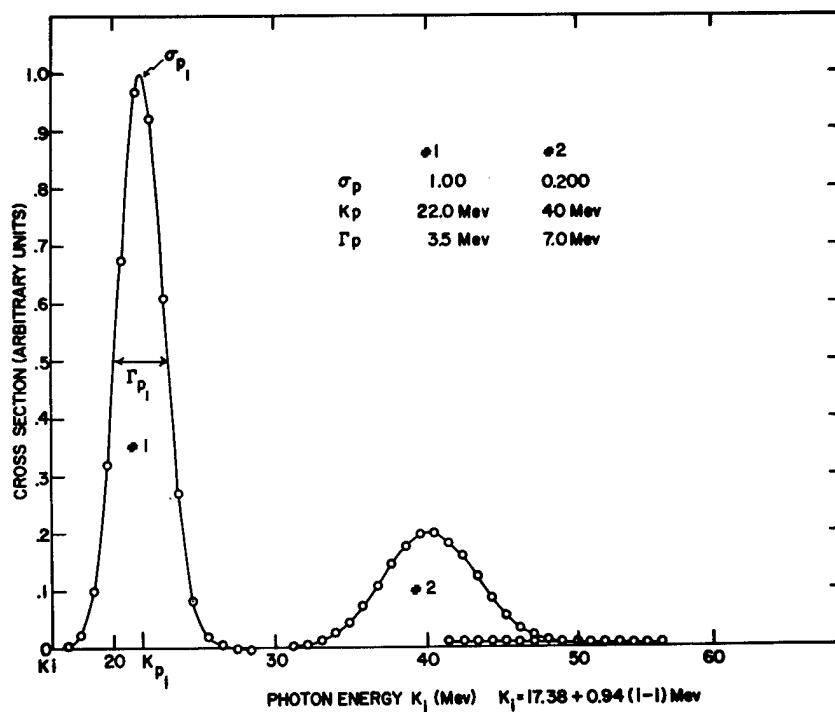


Fig. 3b. "Least Structure" Solution of Field Curve Calculated from Assumed Cross Section

section is 20% of the cross section in the giant resonance. The error at each point and the resolution (full width at one-half maximum) at a few representative energies are also indicated. Other cross section curves, differing errors for the same cross section, alternative definitions of structure, and solutions for other than optimum X^2 , i.e., undersmoothing and oversmoothing, have been tried. These many trials have proved the utility of the method for the analysis of photonuclear yield functions. A report of the work was given as a paper delivered at the April 1962 meeting of the American Physical Society.

NUCLEAR SPECTROSCOPY

1. INTERNAL CONVERSION COEFFICIENTS (E. N. Hatch)

A paper entitled "Internal Conversion Coefficients of the $2^+ - 0^+$, E2 Transitions in Even-Even Sm^{152}_{90} and Gd^{152}_{88} ", by D. C. Lu and G. Schupp, has been submitted to The Physical Review.

Abstract--To investigate the deviation of the internal conversion coefficients of E2 transitions from theoretical computations and their possible dependence on nuclear deformation, the total internal conversion coefficient of the 121.8-keV $2^+ - 0^+$ transition in ellipsoidal Sm^{152}_{90} was measured to be 1.135 ± 0.010 with a high accuracy coincidence-sum method. The K-shell to total internal conversion ratio was determined to be 0.590 ± 0.003 with a β -ray spectrometer. The K-, L- and M-shell internal conversion coefficients were deduced as: $\alpha_K = 0.670 \pm 0.008$, $\alpha_{L1} = 0.070 \pm 0.003$, $\alpha_{L2} = 0.155 \pm 0.005$, $\alpha_{L3} = 0.151 \pm 0.006$, $\alpha_{M1} = 0.011 \pm 0.001$, $\alpha_{M2} = 0.037 \pm 0.003$, and $\alpha_{M3} = 0.036 \pm 0.005$. The α_K of the 344-keV $2^+ - 0^+$ transition in near spherical Gd^{152}_{88} was measured to be $(2.87 \pm 0.06) \times 10^{-2}$ by β -conversion electron coincidence method using two β -ray spectrometers end to end. The K-shell to total internal conversion ratio was determined to be 0.786 ± 0.004 . The K electron to total electron capture ratio, from Eu^{152} to the 1.53-MeV state in Sm^{152} was also measured to be 0.79 ± 0.02 .

2. BETA-DECAY ENERGY SYSTEMATICS (E. N. Hatch)

A paper entitled "Nuclear Beta-Decay Energy Systematics Including Excited States", by F. Everling, has been accepted for publication in Nuclear Physics.

Abstract--A survey of experimental beta-decay energies involving ground states and excited states in the mass region $A = 40$ to 150 is presented in examples. The data have been compared with the hypothesis that straight lines are an approximation to the order of 30 Kev in portions of the smooth, often bent Way and Wood trends and the corresponding constant neutron trends, which turned out to look similar, as expected. An attempt was only made to correlate states with the same spin and parity which seemed to belong to the same subshell. At the mass difference, Cd-In, this permits the interpolation of $\text{Cd}^{111} - \text{In}^{111} = (-0.82 \pm 0.03)$ Mev, calculated from experimental data to be -1.24 ± 0.21 . In Y^{93} , however, the hypothesis requires a $\frac{9}{2}^+$ ground state in contrast to the experimental ($\frac{1}{2}^-$). Furthermore, the Pd^{99} (2.0 ± 0.1) Mev β^+ -ray must be assumed to lead to the Rh^{99} ground state. Two quadrangle-patterns can then be drawn in the range $A = 91$ to 101 for Y-Zr, Nb-Mo, Tc-Ru, and Rh-Pd, being five-fold overdetermined. Each consists of 12 beta-decay energies interconnected by seven straight lines. Twenty consequences concerning decay energies, excitation energies, and spins are given as possibilities to check the hypothesis for this mass range. Its validity would mean that also the level distances, e.g. between the $\frac{1}{2}^-$ and $\frac{9}{2}^+$ states in Y, Nb, Tc, and Rh for $N = 50, 52, 54$, and 56 each, vary almost linearly for isotopes and isotones, and that the subshell structure is not obscured by configuration mixing. A required $\frac{9}{2}^+$ level in Y^{89} at (1.50 ± 0.03) Mev would explain the deviation from the allowed shape observed in the $\text{Zr}^{89} \beta^+$ -spectrum.

3. POSITRON LIFETIMES IN METALS (M. G. Stewart)

A transistorized time-to-pulse-height circuit has been designed and tested, and it is being used to measure positron lifetimes in metals. By

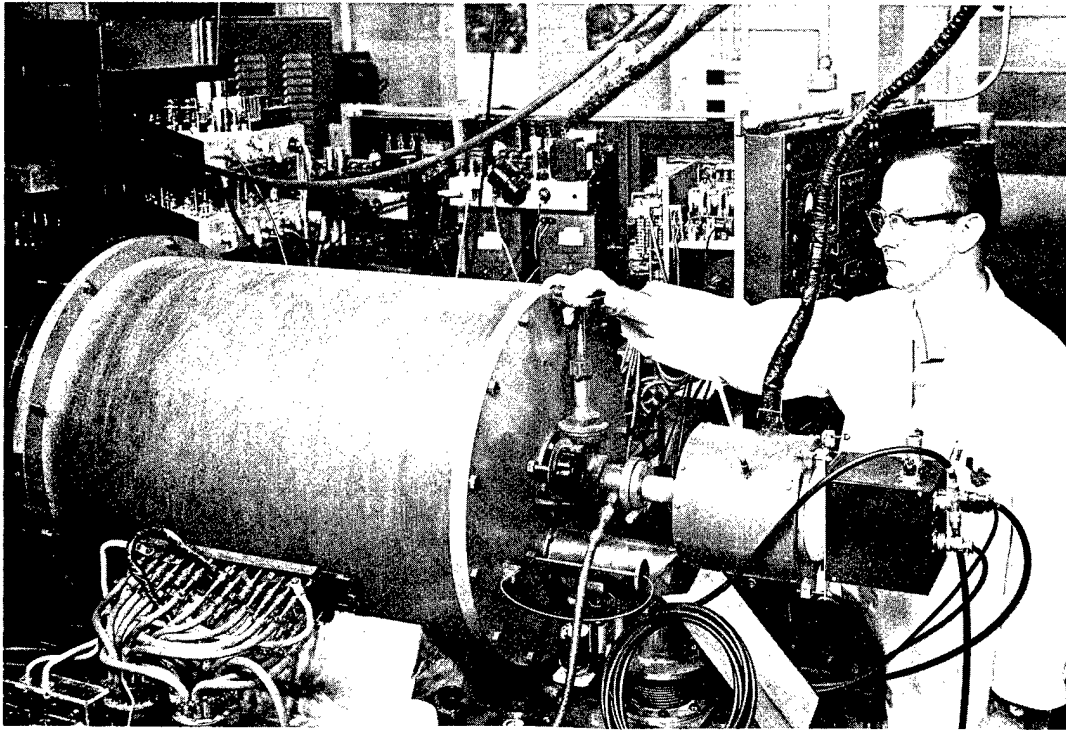


Fig. 4. β -ray Spectrometer

using a cycling system in which the unknown lifetime is compared to a standard (such as the positron lifetime in aluminum) a difference measurement can be made with an accuracy on the order of 3×10^{-12} sec. When measuring the absolute lifetime the accuracy is somewhat poorer, since the radiation from the prompt source generally has a different energy distribution. Figure 5 shows a typical time distribution for a prompt source (Co^{60}) and for positrons in aluminum. Two lifetimes are apparent; a fast component with a mean life of 2.11×10^{-10} sec, and a slower component with a mean life of 3.81×10^{-10} sec. The relative intensities are about 94% and 6% respectively. The measured centroid shift of 2.25×10^{-10} sec agrees with that calculated from the two slopes. The result of many runs gives an average centroid shift of 2.10×10^{-10} sec,

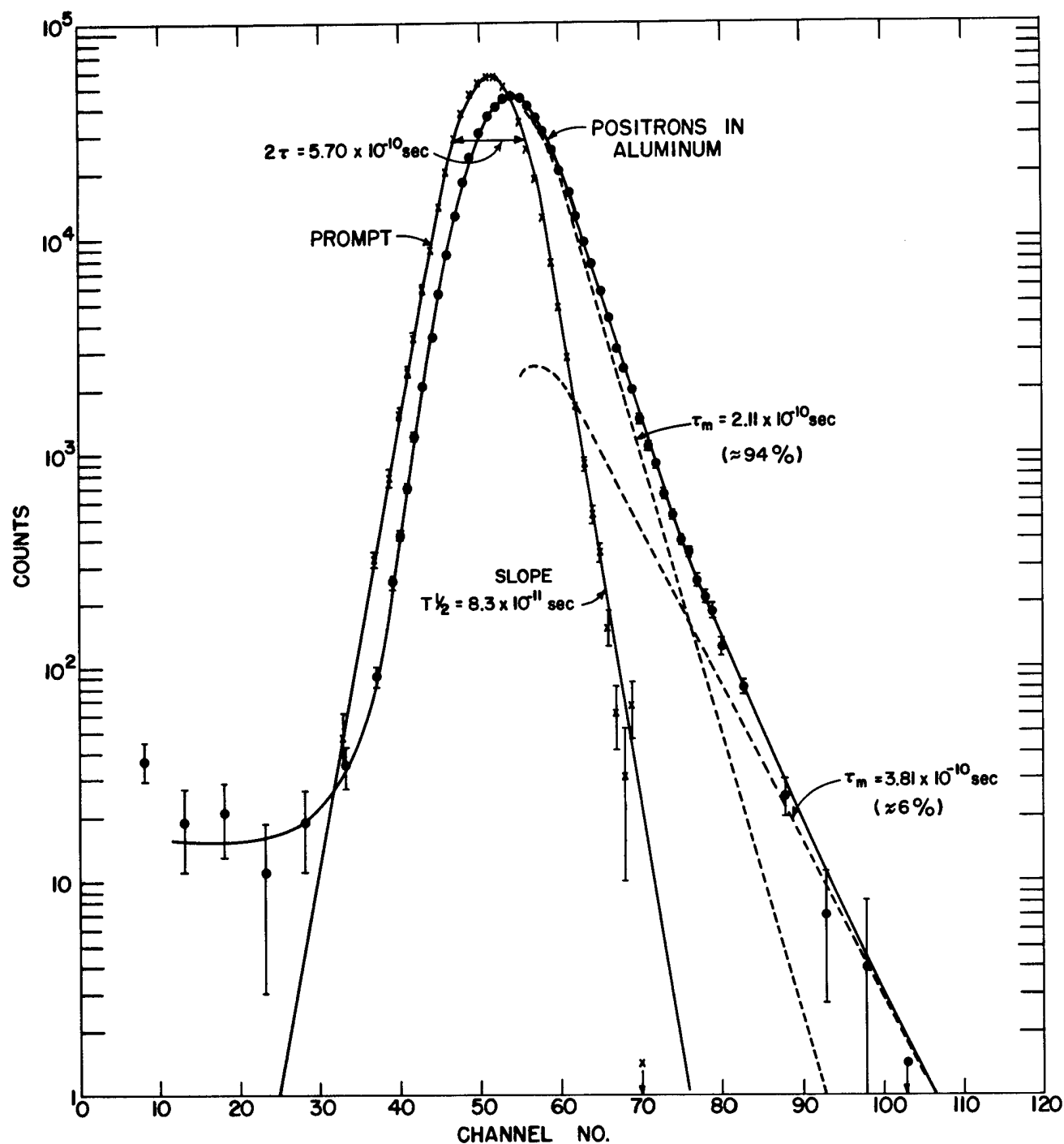


Fig. 5. Typical Time Distribution for Prompt Source (Co^{60}) and for Positrons in Aluminum

which corresponds to a fast component $T_m = (1.97 \pm 0.15) \times 10^{-10}$.

These values are in good agreement with those of Bell and Torgesen.¹

A measurement of the positron lifetime in molybdenum compared to that in aluminum gives a centroid shift of $-(0.50 \pm .02) \times 10^{-10}$ sec.

SOLID STATE THEORETICAL REPORTS

1. QUADRUPOLE PRECESSION (R. H. Good, Jr.)

A paper entitled "Discussion of Quadrupole Precession", by J. C. Raich and R. H. Good, Jr., has been submitted for publication in the American Journal of Physics.

Abstract--The purpose of this paper is to provide the classical picture of an electric quadrupole moving in an external magnetostatic field. Details about the classical orbits are given and the classical precession frequencies are shown to be related to the quantum mechanical dipole transition frequencies.

2. TRANSPORT PROPERTIES OF CUBIC SODIUM TUNGSTEN BRONZES (R. Fuchs)

Many properties of the sodium tungsten bronzes (Na_xWO_3) can be explained by assuming that the electrons introduced with the sodium tend to remain localized on the sodium atoms. The cubic sodium lattice forms a three-dimensional conducting network; if sodium atoms are missing from certain sites, the electrical conduction is blocked at these points. Band theory is inapplicable if sodium atoms are missing ($x < 1$) since it does not allow the electron charge density to be reduced at the sodium vacancies.

For a starting approximation 3p wave functions localized on the sodium atom are used. This model implies that the density of states

¹R. E. Bell and M. H. Torgesen, Can. J. Phys. 38, 652 (1960).

$N_x(E)$ is proportional to x : $N_x(E) = xN_1(E)$. The Fermi energy is therefore independent of x . Properties depending on the density of states, such as the electronic specific heat and paramagnetic susceptibility, are proportional to x . At high temperatures the electrical resistivity is due to scattering by lattice vibrations. We assume that at each sodium atom the electrons are scattered randomly into those directions where other sodium atoms are present. The electrical conductivity is proportional to the diffusion constant in a cubic network with junctions missing at random. The calculated dependence of the conductivity on x is in good agreement with experiment. The theory of the low-temperature conductivity is not yet complete. This model is consistent with the observed dependence of the Seebeck coefficient on x .

3. DIELECTRIC CONSTANT OF IONIC CRYSTALS (R. Fuchs)

The temperature coefficient at constant volume of the static dielectric constant of ionic crystals is due to the nonlinear dependence of the polarization on ionic displacement and the anharmonic terms in the expansion of the lattice energy as a function of the positions of the ions. The anharmonic terms have been estimated from the Born-Mayer repulsive potential between nearest neighbors; the magnitude of the nonlinear polarization can be found from the overlap of the nearest neighbors. Calculated values of the temperature coefficient for alkali halides of the NaCl type are in good agreement with experiment. We have obtained an expression for the temperature coefficient in terms of the static and high frequency dielectric constants, ionic masses and radii, and average frequencies of optical and acoustical lattice vibrations. This expression

implies that the temperature coefficient, which is positive for alkali halides with a small dielectric constant, remains positive and increases in magnitude as the dielectric constant increases. This result is in disagreement with the experimental observation that the temperature coefficient of ionic crystals with a high dielectric constant is negative. In these materials it may be essential to take account of the details of the crystal structure and the non-central forces between atoms.

4. PROPERTIES OF SOLIDS AT LOW TEMPERATURES (N. Bernardes)

4.1 Solid and Liquid He³

Research on the properties of solid and liquid He³ has continued. An analysis of the relative stability of the body-centered cubic phase and the hexagonal close packed fails to explain why the cubic phase is found (experimentally) to be the most stable one at 0°K. Nevertheless, an analysis of the transition data from the Los Alamos Scientific Laboratory (Mills and Grilly), the specific heat data of Swenson and Heltemes,¹ and the thermal conductivity of Fairbank and Walker² has shown important relations between the entropies of the two phases. This analysis was the subject of a publication by N. Bernardes in Phys. Rev. Letters 8, 164 (1962).

A long and extensive review of the properties of solid and liquid He³ has been written in collaboration with D. F. Brewer (Oxford University, England), and has appeared in Revs. Mod. Phys. 34, 143 (1962). Part of this work is also covered in report IS-285 by N. Bernardes.

¹This Laboratory.

²Yale University, New Haven, Connecticut.

4.2 Bulk Properties

A theoretical investigation of the influence of zero point nuclear motion on the bulk properties of solids (density and compressibility) has been carried out, and will be the subject of a forthcoming publication. The results show that quantum mechanical corrections to the density and compressibility can be simply expressed in terms of $k\theta/BV$, where k is Boltzmann's constant, θ the Debye temperature, B the bulk modulus and V the molar volume.

5. CONTRIBUTION OF ANHARMONIC FORCES TO THE SPECIFIC HEAT OF SOLIDS

(J. M. Keller)

A paper with the above title, by Duane C. Wallace and J. M. Keller, has appeared in Phys. Rev. 126, 1275 (1962).

Abstract--At temperatures appreciably above the Debye temperature, anharmonic parts of the lattice potential of a crystal make a contribution to the specific heat at constant volume that is nearly linear with the temperature, but of uncertain sign. Calculations on bcc and fcc crystals with a single atom per unit cell, based on central Lennard-Jones forces, show that the net effect is one of specific heat decreasing as temperature increases. The complicated sums involved can be simplified by use of a matrix inverse to the harmonic dynamical matrix, or by neglecting the dependence of phonon frequency on polarization. The latter method is used here. Forces between nearest and next-nearest neighbors are considered, and phonon dispersion is included approximately.

6. DEPENDENCE OF ELECTRICAL RESISTIVITY OF RARE-EARTH METALS ON RELATIVE MAGNETIZATION (J. M. Keller)

A study was made of some measurements on electrical resistivity and magnetization of rare-earth metals performed by members of Dr. Legvold's

group. If it is assumed that the resistance is made up of the sum of a non-magnetic part and a part due to magnetic disordering, it appears that the magnetic part is well represented by

$$\rho_{\text{mag}} = A(1 - \xi^\eta)$$

where A and η are constants, and ξ is the ratio of magnetization to saturation magnetization. The value for η is within experimental error 4.0 for Gd and for ferromagnetic Dy, 4.3 for Tb and 4.8 for Dy in the antiferromagnetic region. This is an improved form of the equation proposed by Birss and Dey¹ to represent their own measurements on gadolinium.

SOLID STATE EXPERIMENTAL RESULTS

1. SEMICONDUCTING COMPOUNDS (G. C. Danielson)

1.1 Seebeck Effect in Mg_2Si Single Crystals

A paper with the above title, by M. W. Heller and G. C. Danielson, has been published in J. Phys. Chem. Solids **23**, 601-610 (1962).

Abstract--The Seebeck coefficients (thermoelectric powers), resistivities, and Hall coefficients of Mg_2Si single crystals have been measured from 7°K to 1000°K. At low temperatures, the magnitude of the Seebeck coefficient showed a pronounced maximum which is interpreted in terms of the phonon drag effect. Both n-type and p-type crystals exhibited this effect. The magnitude of the phonon contribution to the Seebeck coefficient was found to be proportional to $T^{-3.0}$ at temperatures above the boundary scattering range. In the intrinsic temperature range (650°K to 1000°K), the Seebeck coefficients of the n-type samples were proportional to $1/T$ and implied a ratio of electron to hole mobility of about 3.5. The density-of-states effective mass parameters were calculated both from data in the extrinsic temperature range (200°K to 300°K) and from data in the intrinsic temperature range. Consistent results of

¹R. R. Birss and S. K. Dey, Proc. Roy. Soc. (London) A263, 473 (1961).

$m_n = 0.5 m_o$ and $m_p = 2m_o$ were obtained if it were assumed that optical mode scattering predominated in the pure n-type samples above 200°K, but that optical mode scattering and ionized impurity scattering were comparable in the doped p-type samples between 200°K and 300°K.

1.2 Elastic Constants of Mg_2Si

The elastic constants of Mg_2Si single crystals have been determined from measurements of sound velocities in the 110 and 111 directions. The measurements were made by means of a resonance technique from 80 - 300°K.

The elastic constants at 300°K, as determined from the five different sound velocities and the x-ray density of 2.00 gram/cm³, are the following:

$$C_{11} = (12.12 \pm 0.12) \times 10^{11} \frac{\text{dyne}}{\text{cm}^2}, \quad C_{12} = (2.20 \pm 0.09) \times 10^{11} \frac{\text{dyne}}{\text{cm}^2},$$

$$\text{and } C_{44} = (4.65 \pm 0.08) \times 10^{11} \frac{\text{dyne}}{\text{cm}^2}.$$

The relative magnitudes of these elastic constants indicate that non-central forces between nearest neighbors are appreciable. It seems probable that the binding in this semiconducting compound is largely covalent.

2. THERMAL PROPERTIES OF SOLIDS ABOVE 300°K (G. C. Danielson)

2.1 Dynamic Methods for Determining Thermal Conductivity

A paper with the above title, by P. H. Sidles and G. C. Danielson, was published. (Conference on Thermal Conductivity Methods. October 26-28, 1961, Battelle Memorial Institute, pp. 229-239).

Abstract--The quantities which enter into a steady state thermal conductivity measurement and those which enter into a dynamic thermal diffusivity measurement are compared. It is concluded that the dynamic or thermal

diffusivity approach becomes clearly superior in accuracy at high temperatures. Three methods for measuring thermal diffusivity are discussed in some detail and the results for Armco iron are compared with those obtained from a steady state thermal conductivity method.

2.2 Thermal Diffusivity Measurements on a Finite Disk

A report (IS-492) with the above title by, Paul Maycock and G. C. Danielson, is being distributed.

Abstract--A new technique has been developed for measuring the thermal diffusivity of finite disk-shaped samples. The radial heat flow equation was solved by the method of finite differences. An axial heater was turned on and the temperatures at three radial positions were measured as functions of time. The procedure determined the boundary conditions necessary for the solution of the heat flow equation. By assuming various values of the thermal diffusivity, we obtained the solution at the middle thermocouple. The value which gave the best agreement between the computed solution at the middle thermocouple and the experimental curve obtained at the midpoint was considered to be the best value for the diffusivity. A FORTRAN program which calculates the diffusivity from the experimental data was developed and an IBM-704 computer was used to process the data. Data on Armco iron show that the method is capable of giving correct values for thermal diffusivity.

2.3 Thermal Diffusivity of Armco Iron

Thermal diffusivity measurements have been made on a "round-robin" sample of Armco iron furnished by Battelle Memorial Institute. Measurements have been made from room temperature to 1000°C by means of a finite-rod method. Preliminary measurements have also been made by a recently developed radial method at room temperature. Both methods gave a room temperature value of $0.20 \text{ cm}^2/\text{sec}$. The Curie temperature was found to be between 762 and 773°C and the alpha-beta transition between 904 and 914°C.

2.4 Thermal Diffusivity of Zirconium

The thermal diffusivity of alpha-zirconium has been measured from room temperature to 750°C. The thermal diffusivity at 750°C was found to be $0.09 \text{ cm}^2/\text{sec}$.

2.5 Specific Heat of Armco Iron

Data were taken on two samples prepared from the Battelle "round-robin" lot of Armco iron. Resistivity data, taken over the temperature range 25 - 1020°C, indicated a Curie temperature of 765°C and an alpha-gamma transition temperature of slightly above 900°C. The resistivity at 25°C was 10.9 ohm-cm. Specific heat data (by a pulse heating technique) were also taken over the alpha-phase region. At 25°C the specific heat was 6.03 cal/mole-°C and rose to 19.7 cal/mole-°C at the Curie temperature, which was again found to be 765°C. The heat of transition of these specimens was distributed over an appreciable temperature range, so that above 820°C the apparent specific heat was increased by the effect of the alpha-gamma transition. The specific heat curve was reproducible for the two samples.

2.6 Specific Heat of Zirconium

The specific heat curve for alpha-zirconium was extended to the alpha-gamma transition temperature of 860°C. The specific heat at 860°C was found to be 7.54 cal/mole-°C.

3. TUNGSTEN BRONZES (G. C. Danielson)

A paper, "Electrical Properties of the Tungsten Bronzes", by H. R. Shanks, P. H. Sidles, and G. C. Danielson, was accepted for publication in Inorganic Chemistry.

Abstract--The electrical resistivity of Na_xWO_3 , Li_xWO_3 , and K_xWO_3 has been measured at 300°K. The range of x values was $0.25 < x < 0.9$. All resistivities were characteristic of a metal and lie on a single curve. An extrapolation of the conductivity curve to zero conductivity indicated that the tungsten bronzes should be semi-conductors for $x < 0.25$. The resistivities that have been measured for tungsten bronzes with $x < 0.25$ showed semiconducting behavior. The resistivity of Li_xWO_3 exhibited an anomalous peak in the ρ vs T curve. The Hall coefficient of $\text{Li}_{0.37}\text{WO}_3$ indicated one free electron per alkali atom as was previously found for Na_xWO_3 . The Seebeck coefficient of Na_xWO_3 depended linearly on $x^{-2/3}$ as expected from free electron theory. The implications of these and some other data are discussed.

4. PREPARATION OF SINGLE CRYSTALS (G. C. Danielson)

Facilities have been established for growing high-purity, single crystals of metals and semiconductors employing methods which are appropriate to the various materials of interest. Single crystals of zinc and tin up to one inch in diameter and 8 in. in length have been prepared by a pulling technique. Molybdenum, tantalum, tungsten and niobium have been electron-beam zone refined. Single crystals of these metals up to 3/16 in. in diameter and 18 in. long have been obtained. A Bridgman method has been used to grow single crystals of Mg_2Si , Mg_2Ge , Mg_2Sn and Mg_2Pb . Single crystals of Li, Na and K tungsten bronze have been grown by electrolytic methods. Potassium metal has been purified by vacuum distillation and single crystals have been grown.

Ultrasonic grinding, airbrasive, acid sawing and spark cutting have been employed in shaping single crystals into research samples.

With all of these techniques, it was possible to obtain research samples which were free from mechanical strains which often cause difficulty in interpreting experimental results.



Fig. 6. Single Crystal Growing Apparatus

5. COLOR CENTERS IN ALKALI HALIDES (D. W. Lynch)

5.1 Color Centers in CsBr

A paper entitled "Color Centers in Additively Colored CsBr", by David W. Lynch, has been accepted for publication in The Physical Review.

Abstract--Color centers have been studied in CsBr single crystals additively colored with potassium or cesium. More than ten absorption bands were produced, most of which had previously been found in crystals colored by ionizing radiation. All bands produced by irradiation at or above liquid nitrogen temperature appear to arise from trapped electrons. The most prominent bands in the additively colored crystals are the F band at $642\text{ m}\mu$ (liquid nitrogen temperature) and a band at $243\text{ m}\mu$ which appears to be due to an impurity. Optically bleaching the F band at 200°K produces bands analogous to the M and R bands in other alkali halides while bleaching at liquid nitrogen temperature yields a broad band identified as the F' band. Evidence that the asymmetry of the F band arises from several excited states of the F center is presented.

5.2 V_2 and V_3 Centers in Alkali Iodides

The V_2 and V_3 bands are produced when a stoichiometric excess of iodine is introduced into an alkali iodide. They probably arise from one color center. The bands appear similar to those found in solutions of I_2 molecules. Density measurements (kindly performed for us in the laboratory of Prof. A. Smakula at M.I.T.) indicate that alkali metal vacancies are formed when the excess iodine is introduced into KI. Preliminary results of ionic conductivity measurements indicate that some of these vacancies are free to contribute to the (ionic) conductivity. Hence the V_2 and V_3 bands appear to arise from a center containing either no vacancies or one vacancy. The model proposed by Seitz has two vacancies.

V_2 and V_3 bands have been observed in KI, RbI, NaI and CsI, the latter having a different crystal structure, and the bands appear about the same, except for a wavelength shift, analogous to the shift of the bands from I_2 molecules in different solvents.

A tentative model for the center responsible for these bands is an iodine molecule formed by trapping two holes at two iodide ions next to a vacancy. The location of the vacancy with respect to the I_2 molecule has not yet been determined.

6. OPTICAL PROPERTIES OF CUBIC SODIUM TUNGSTEN BRONZES (D. W. Lynch and G. C. Danielson)

Measurements of the optical constants of cubic metallic Na_xWO_3 have been made for $0.5 < x < 0.9$ in the wavelength region 0.3 to 2.0μ . These measurements indicate that a film of WO_3 grows on the surface in air within a few minutes. Such a film (perhaps as thin as 30 \AA) can account for several previously unexplained results: the difficulty of making contacts to metallic Na_xWO_3 , the insolubility of Na_xWO_3 , and the appearance of domains on the surface under certain conditions when viewed in polarized light. Despite the presence of the film, which makes the values of the optical constants uncertain, the x -dependence of the optical constants is believed to be meaningful. There is weak interband absorption between 560 and $660 \text{ m}\mu$ with no systematic x -dependence. Free carrier absorption occurs for wavelengths longer than $700 \text{ m}\mu$. There is a sharp peak in the function $2nk(n^2+k^2)^{-2}$ vs λ , indicative of the excitation of plasma oscillations. Simple theory predicts these to occur at $\lambda_p = 246 \text{ m}\mu \cdot x^{-1/2}$ but the peaks actually are shifted to longer wavelengths and depart from the $x^{-1/2}$ dependence. Current work is directed at learning how much the WO_3 film affects the x -dependence of the plasma peaks.

7. OPTICAL PROPERTIES OF SEMICONDUCTORS (D. W. Lynch)

7.1 Index of Refraction and Reflectivity of Mg_2Si , Mg_2Ge and Mg_2Sn

Measurements of the index of refraction of the above semiconducting compounds have been made by determining the angle of minimum deviation for light refracted by a prism made of the compound. As in the case of the group IV and the III-V semiconductors the indices of refraction are between 3.5 and 4 in the part of the infrared region where the crystals are transmitting. Numerical results are given in Table I, in which the indices of refraction are given at the limits of the wavelength region of the measurements. The dispersion at long wavelengths is due to lattice vibrations, not free carriers.

Table I

	Mg_2Si	Mg_2Ge	Mg_2Sn
Index of refraction	3.762	3.761	4.15
wavelength (μ)	1.90	2.10	3.77
Index of refraction	3.613	3.690	4.06
wavelength (μ)	7.72	5.12	8.00
Wavelength (μ) of restrahl peak	35.2	46.0	49.0
Wavelength (μ) of subsidiary peak	31.0	42.0	45.0

Reflectivity measurements have been made on cleaved surfaces of Mg_2Si , Mg_2Ge and Mg_2Sn . The wavelength of restrahl reflectivity maximum for each crystal is given in Table I, as well as the wavelength of a subsidiary maximum found in each crystal. This subsidiary maximum is also characteristic of alkali halides and CaF_2 but not of the III-V

semiconductors. It probably arises from two-phonon processes. No multiple-phonon absorption peaks have been observed in preliminary transmission measurements. Because this subsidiary peak severely overlaps the principal peak, fitting the reflectivity to that expected for a damped harmonic oscillator cannot be done. The reflectivity minima on the short wavelength side of the maxima are only slightly affected by high concentrations of electrons or holes. This is consistent with the large effective masses of the carriers determined from transport measurements. The dependence of the restrahl wavelengths on the reduced masses for the $k = 0$ transverse optical mode indicates that the force constants for this mode are nearly the same in all three compounds. The fact that the restrahl spectra occur indicates that the atoms in these crystals carry at least a small amount of charge.

7.2 Photoconductivity in Mg_2Si and Mg_2Ge

Photoconductivity has been detected in Mg_2Ge and Mg_2Si at 90°K and preliminary determinations of the spectral responses have been made. The energy gaps determined from the spectral responses agree with those obtained from electrical and optical measurements. In Mg_2Ge heavily doped with Al the response has a long wavelength tail extending to wavelengths greater than 2.5μ .

8. EXPERIMENTAL DETERMINATION OF THE ELECTRONIC STRUCTURE OF METALS

(A. R. Mackintosh)

8.1 Ultrasonic Attenuation in Lead

A paper with the above title, by A. R. Mackintosh, was submitted to the Proceedings of the Royal Society, London, for publication.

Abstract--The absorption of longitudinal ultrasonic waves has been studied as a function of transverse magnetic field in pure single crystals of lead at 1.2°K. The results were found to be generally consistent with the Fermi surface of lead suggested by Gold. In particular a detailed study of the magnetoacoustic oscillations as a function of sample orientation and field direction allowed the determination of some of the dimensions of the hole surface in the second Brillouin zone and revealed a number of new electronic orbits on the multiply connected surface in the third zone. The absolute magnitude of the attenuation and its dependence on propagation direction and on magnetic field were studied and the results interpreted in terms of the general theory of ultrasonic absorption.

8.2 Cyclotron Resonance in Lead at 36 kmcs

A paper with the above title, by R. C. Young, will be submitted for publication in the Philosophical Magazine.

Abstract--This paper reports observations of Azbel-Kaner cyclotron resonance in the (100) and (211) planes of lead at 36 kmcs/sec. and 1 - 5°K. The results for the (100) plane agree with those of Khaikin and Mina. The results are interpreted in terms of Gold's model of the Fermi surface of lead. It is also shown that the open orbits observed in lead by Alekseevski and Gaidukov, and by Mackintosh, can be explained by Gold's model.

8.3 Positron Annihilation in Solids (A. R. Mackintosh and D. J. Zaffarano)

The electronic structure of solids is being investigated by observing the angular correlation of the photons from the annihilation of positrons. A study of gadolinium verified that the 4f electrons are localized at the ionic sites, and showed that the polarization of the conduction electrons in the ferromagnetic state is small. The electronic structure of liquid and solid mercury was examined and found to be apparently very similar.

8.4 Electronic Structure of Rare-Earth Metals (A. R. Mackintosh)

A paper with the above title, by A. R. Mackintosh, appeared in the Proceedings of the Second Rare-Earth Conference, Boulder, Colorado, 1961.

Abstract--The distinction between conduction electrons and localized f electrons in rare-earth metals is discussed. The phase transformation in cerium is explained in terms of the entropy difference between the two phases. The free electron Fermi surface is constructed for the trivalent rare-earth metals, and the modification due to magnetic ordering described. This effect is used to explain the effect of ordering on the transport properties of the magnetic rare-earth metals.

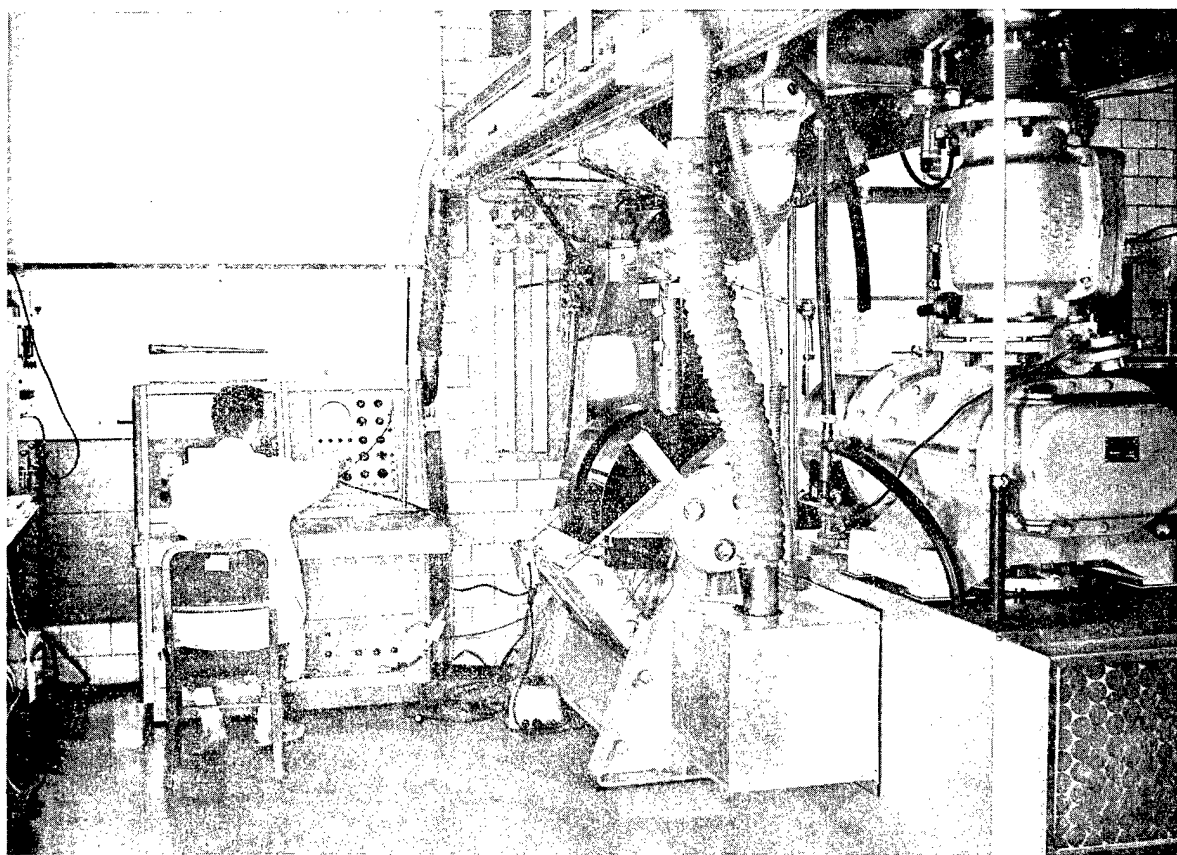


Fig. 7. Apparatus for Low Temperature Magnetic Studies

8.5 Magnetic Ordering and the Electronic Structure of Rare-Earth Metals

A paper with the above title, by A. R. Mackintosh, has been submitted to Physical Review Letters.

Abstract--The effect of magnetic ordering on the Brillouin zone structure of the conduction electrons in rare-earth metals is considered. The temperature dependence of the resistivity in erbium and terbium is interpreted, using this mechanism.

9. TRANSPORT PROPERTIES OF DILUTE RARE-EARTH ALLOYS (A. R. Mackintosh)

A study has been made of the resistivity and thermoelectric power of dilute alloys of magnetic rare-earth metals in lutetium. A paper entitled "Scattering of Conduction Electrons by Localized Moments in Metals", by A. R. Mackintosh and F. A. Smidt, Jr., has been submitted to Physical Review Letters.

Abstract--The scattering of conduction electrons from localized ionic moments in metals has been studied by observing the change in the residual resistivity of samples of pure lutetium, into which were dissolved small amounts of magnetic rare-earth metals. The results indicate that the exchange scattering of the conduction electrons is proportional to the factor $(g-1)^2 J(J+1)$ where J is the localized moment of the solute and g is the Landé factor. The magnitude of the exchange scattering is comparable with that of the direct electrostatic scattering.

10. SUPERCONDUCTIVITY OF LANTHANUM ALLOYS (A. R. Mackintosh, C. A. Swenson and F. H. Spedding)

A detailed study is being made of the variation of superconducting transition temperature with concentration in the lanthanum-lutetium and lanthanum-yttrium systems. A paper entitled "Superconductivity in

Lanthanum Alloy Systems", by A. R. Mackintosh, has been submitted to the 8th International Conference on Low Temperature Physics, for publication in the proceedings.

Abstract--It is shown that the variation of the superconducting transition temperature with concentration in the systems lanthanum-lutetium and lanthanum-yttrium is consistent with the predictions of the Bardeen-Cooper-Schrieffer theory of superconductivity. The transition temperatures for pure lutetium and yttrium are estimated by extrapolating the results for the alloys.

11. THERMOELECTRIC POWER IN CHROMIUM AND VANADIUM (A. R. Mackintosh)

The thermoelectric power of chromium and vanadium has been studied as a function of temperature from 4.2 to 350°K. In chromium the thermoelectric power was positive over the whole range, while in vanadium it changed from positive to negative at about 250°K. A clear anomaly was observed at the antiferromagnetic transition in chromium at 313°K, and a small but reproducible hysteresis occurred in vanadium at about 220°K. The latter is probably associated either with a mechanical or a magnetic transition.

12. THE DE HAAS-VAN ALPHEN EFFECT (A. V. Gold)

12.1 The de Haas-van Alphen Effect and the Band Structure of Lead

From experiments carried out earlier at 80 kG¹ it was found that the Fermi surface in Pb is qualitatively similar to that predicted by the literal free-electron model. By increasing the available magnetic field to 200 kG many new sets of oscillations have been found. These not only confirm the correctness of the existing model of the Fermi

¹A. V. Gold, Phil. Trans. A251, 85 (1958).

surface but show that it is quantitatively far closer to the free-electron model than was at first believed.

Attempts to give the shapes of the surfaces analytically in terms of a Fourier expansion of $E(\underline{k})$ did not prove fruitful. The data indicate that the sharp corners of the free-electron surfaces are not rounded-off very much in reality and one cannot obtain sufficiently rapid convergence with a Fourier series. Since experiment shows that the effective pseudo-potential must be small, one should be able to fit the the results together within the framework of an "orthogonalized-plane-wave" (OPW) calculation,¹ using a limited number of plane waves. This approach has indeed proved to be highly successful and the extensive information now at hand can be accounted for remarkably well by only two parameters, the matrix elements $V_{111} = -0.95$ ev and $V_{200} = -0.43$ ev. From these the band gaps at various points on the Brillouin zone can be calculated and are typically 1 ev, which should be compared with the Fermi energy of 9.5 ev. The influence of spin-orbit coupling on the band structure is now being studied.

While the effective masses in lead as obtained from the oscillation amplitudes are in excellent agreement with those found from the more direct cyclotron resonance experiments, they are some two or three times greater than those predicted by either the free-electron model or the OPW calculation; a detailed explanation for this discrepancy has not yet been found.

¹W. A. Harrison, Phys. Rev. 118, 1182 (1960).

12.2 The de Haas-van Alphen Effect in Transition Metals

A detailed study of tungsten and molybdenum has been started and typically four or five periods have been found at symmetry directions. These results indicated that the Fermi surface in these metals must be quite complex, but so far no convincing model has resulted.

13. CONDUCTION PROCESSES IN DIAMOND (D. E. Hudson)

A paper, "Imperfection Photoconductivity in Diamond", by J. A. Elmgren and D. E. Hudson, has been accepted for publication in The Physical Review.

Abstract--The effect of monochromatic light throughout the visible region on the rate of decay of a persistent internal field in diamond has been studied. The persistent field was generated by spatially-separated trapped electrons and holes, and was sampled by the counting rate of the polarized diamond acting as a nuclear particle counter. Under the influence of light the internal field decayed exponentially with time in a fashion characterized by an intensity-dependent decay constant. The decay constants, normalized to a common photon flux density, varied over more than four orders of magnitude in the photon energy range from 1.8 to 3.5 ev.

The results are interpreted in terms of imperfection photoconductivity arising from imperfection levels with photo-ionization energies of 2.5 ev and 3.0 ev. This photoconduction model utilizes a decay mechanism which has been overlooked in previous diamond work. An alternate conventional interpretation in terms of detrapping is also presented.

The method outlined above has provided a new and attractive way of studying the exceedingly high bulk resistivity of diamond. Recent preliminary studies on one diamond suggest that the true bulk resistivity may be greater than 5×10^{20} ohm-cm or a factor of 10^4 larger than commonly reported values.

14. COHESION OF INTERMETALLIC COMPOUNDS (D. E. Hudson)

A paper entitled "Cohesion in the Intermetallic Series Mg_2X ", by H. J. Caulfield and D. E. Hudson, is being submitted for publication in The Physical Review.

Abstract--Sublimation from the four Mg_2X compounds (Mg_2Si , Mg_2Ge , Mg_2Sn and Mg_2Pb) was studied by mass spectrometric observation of the vapor effusing from a Knudsen cell. For cases in which only one component of a solid is significantly volatile, the sublimation is governed by a direct analogue of the Clausius-Clapeyron equation. Analysis of the temperature dependence of the Mg partial pressure was used to obtain the change in partial molar enthalpy, ΔH_{Mg} during the sublimation of Mg from Mg_2X . The values of ΔH_{Mg} obtained in this work (in kcal/mole) are as follows:

Mg_2Si , 44.41 ± 0.34 at $864^\circ K$;

Mg_2Ge , 54.4 ± 1.1 at $875^\circ K$;

Mg_2Sn , 44.0 ± 1.2 at $821^\circ K$; and

Mg_2Pb , 33.6 ± 0.6 at $770^\circ K$.

From these results, and from some approximate theoretical (Wigner-Seitz) calculations, conclusions regarding bonding in the series have been obtained. The bonding in Mg_2Si , Mg_2Ge and Mg_2Sn appears to be largely covalent with a possible small ionic contribution. The compound Mg_2Pb , on the other hand, appears to have a significant amount of metallic bonding. These results are of interest in connection with the well-known anomalous conduction properties of Mg_2Pb .

15. GROWING LARGE CRYSTALS (S. Legvold)

When heliarc-melted buttons of metal are annealed in a furnace, considerable crystal growth is observed. The crystallites on the top surface of the buttons are considerably larger than on the bottom. If the buttons are now inverted, re-arc-melted and annealed a second time larger crystals than appeared previously will generally appear

because of the seeding action of the crystals remaining after the first annealing. This technique has yielded crystals of gadolinium, yttrium and dysprosium of the order of a centimeter on an edge.

16. MAGNETIC PHENOMENA IN CRYSTALS (S. Legvold)

Magnetization data on single crystals of gadolinium do not show magnetic anisotropy. This is what is expected on the basis of a half-filled 4f shell.

Similar measurements on terbium single crystals show that the "b" axis (halfway between two a-axes in the basal plane of the hexagonal close packed metal) is the easy direction of magnetization. The magnetic moments lie in the basal plane at temperatures below 231°K, the Néel point for the metal. Electrical resistivity measurements with the current along the c-axis of terbium show an interesting effect. At temperatures near and below 231°K an abnormal peak in the resistivity vs temperature curve is observed. This has now been interpreted by A. Mackintosh of this Laboratory as a manifestation of a change in the Fermi surface of terbium caused by the antiferromagnetic ordering of the magnetic moments with a periodicity along the c-axis which differs from the atomic periodicity. His prediction that the hump would disappear in a strong transverse magnetic field has been verified.

16.1 Electrical and Magnetic Properties of Holmium Single Crystals

A paper with the above title, by D. L. Strandburg, S. Legvold and F. H. Spedding, has been submitted for publication in The Physical Review.

Abstract--Magnetic moment measurements have been made on holmium single crystals (hcp) over the range 1.3 to 300°K in magnetic fields from 250 to 18,000 oe with the field applied along the c-axis, the a-axis,

and a $\langle 10\bar{1}0 \rangle$ direction. The $\langle 10\bar{1}0 \rangle$ direction is the direction of easy magnetization with an extrapolated effective moment per atom at saturation of 10.34 Bohr magnetons. Basal plane measurements showed antiferromagnetism below the Néel temperature of 132°K with basal plane anisotropy occurring below 80°K. Below the Néel point an anomalous type of transition to ferromagnetic behavior upon application of sufficient field was observed. Magnetization curves for the c-axis are linear down to 60°K, while measurements below 20°K show an initial magnetization of approximately 1.7 Bohr magnetons followed by nearly linear magnetization curves. Electrical resistivity measurements were made from 4.2 to 300°K. For the a-axis, the resistivity changes slope slightly at 20°K. A larger change in slope occurs at the Néel temperature of 132°K. For the c-axis, the resistivity changes slope slightly at 20°K, reaches a peak at 120°K, goes through a minimum at 132°K, and remains constant until approximately 150°K, after which it increases linearly with increasing temperature.

17. MAGNETOSTRICTION (S. Legvold)

The magnetostriction constants for gadolinium, determined with electrical resistance strain gages glued to single crystals, were found to be of the same order of magnitude as the constants for hexagonal cobalt.

18. SUPERCONDUCTIVITY (C. A. Swenson)

18.1 Niobium

High purity samples of niobium metal (with resistivity ratios of up to 1000) have been produced by ultra-high vacuum annealing techniques. The magnetization curves of these samples have been measured in the superconducting region, and the tentative conclusion reached that high purity niobium metal has a negative surface free energy between the normal and superconducting states.

18.2 Tin

A paper entitled "The Pressure-Effect and Thermal Expansion for Superconducting Tin", by J. E. Schirber and C. A. Swenson, will be published in the July 1 issue of The Physical Review.

Abstract--The superconducting critical field curve of white tin has been measured between 1.15° and 3.7°K at pressures up to 2800 bars using solid helium as the pressure transmitter. The results at T_c agree with previous work at this Laboratory. An analysis of the data indicates a relatively small pressure dependence of the electronic specific heat coefficient γ , and, consequently, a small electronic contribution to the thermal expansion in the normal state. The thermal expansion in the superconducting state is predicted to be large and negative, and extremely anisotropic. The deviation of the superconducting properties of tin from "simple similarity" is discussed.

18.3 Critical Field of Superconductors

A report (IS-399) entitled "An Integration of the BCS Expression for the Critical Field of Superconductors", by C. A. Swenson, was distributed.

Abstract--The BCS theoretical expressions for the temperature dependence of the energy gap and the critical field curve have been integrated to obtain $\epsilon_0(t)/\epsilon_0(0)$ vs t^2 , h^2 vs t^2 and $(h^2 - 1)/t^2$ vs t^2 .

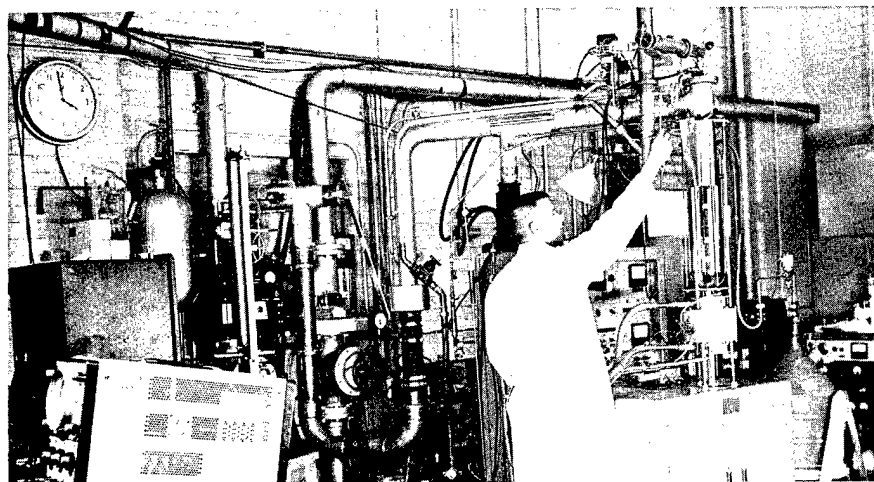


Fig. 8. Magnetic Refrigerator for Experimental Work below 1°K

A discussion of the use of these expressions in the analysis of experimental data is given.

A paper entitled "The Temperature and Pressure Dependence of Critical Field Curves", by C. A. Swenson, was published in the IBM Journal 6, 82 (1962).

Abstract--A brief discussion is given of the analysis of recent critical field measurements. In particular, a negative volume coefficient of thermal expansion is predicted for tin in the superconducting state.

19. HIGH PRESSURE STUDIES (C. A. Swenson)

19.1 Cesium

Preliminary work on the equation of state of solid cesium has been initiated in order to study the possible effects on its low temperature behavior of a room temperature high pressure electronic transition which occurs in this metal.

19.2 Xenon

An experimental equation of state has been established for solid xenon. A preliminary discussion of this work appears in a paper entitled "Pressure-Volume-Temperature Measurements on Solids", by C. A. Swenson, published in the Proceedings of a Symposium on the Physics and Chemistry of High Pressures, Third Congress of the European Federation of Chemical Engineering, London, England, June 20-29, 1962.

Abstract--The results of recent measurements on the equations of state of sodium and xenon are discussed. The experimental data for each of these are analyzed to show that the isothermal compressibility is solely a function of volume within experimental accuracy. The basic differences

between the low temperature PV relationships for sodium and xenon are shown to be easily understandable in terms of the elementary theories of these substances. The range of experimental pressures (to 20°kbars) and temperatures (20°K to the triple point) is sufficiently great so as to produce significant changes in the lattice thermal properties in each case. These changes are indicated through the use of zero pressure heat capacity data in combination with the equation of state data to calculate the volume and temperature dependence of the Debye θ . The result is quite spectacular for xenon, where a pressure of 20 kbars roughly doubles θ_D .

19.3 Mercury

A paper entitled "The Nature of the α - β Transformation in Mercury", by J. E. Schirber and C. A. Swenson, was published in Acta Met. 10, 511 (1962).

Abstract--Observations from various experiments on solidified mercury are cited which indicate that the α - β transition in mercury is martensitic in character. These indications include dependence upon shear for formation of the β phase, large hysteresis effects, apparent athermal character in the presence of sufficient shear, and a frequent appearance of stable mixed samples implying little or no growth in the presence of an abundance of nuclei. A two-step visualization of the transformation mechanism is described which emphasizes the large amount of shear which appears necessary for the formation of one phase from the other.

20. HEAT CAPACITY OF SOLID He^3 (C. A. Swenson)

Preliminary results on the measurement of the heat capacity of solid He^3 have been published (see below). The experimental methods which were used in this earlier work are being refined so that the anomalous behavior which was found may be investigated with more precision.

A paper entitled "The Specific Heat of Solid He^3 ", by E. C. Heltemes and C. A. Swenson, was published in Phys. Rev. Letters 7, 363 (1961).

Abstract--The specific heat of solid He^3 has been measured from 0.3°K to 2°K at pressures ranging from 40 to 1800 bars. The data for $\beta\text{-He}^3$ (hcp) could be represented by a Debye function, although a low temperature anomaly of unknown origin was observed. The representation of the data for $\alpha\text{-He}^3$ (bcc) required the use of both a Debye function and an Einstein function with two degrees of freedom. The volume dependences of the characteristic temperatures for each phase are given.

21. NUCLEAR MAGNETIC RESONANCE STUDIES (R. G. Barnes)

21.1 Nuclear Magnetic Resonance in Chromium Metal

A letter with the above title, by R. G. Barnes and T. P. Graham, was published in Phys. Rev. Letters 8, 248 (1962).

Abstract--The nuclear magnetic resonance of naturally abundant (9.5%) Cr^{53} has been observed in pure (crystal-bar) chromium metal at temperatures above the antiferromagnetic ordering temperature T_N of 40°C, and the Knight shift of the resonance has been measured. We have also observed the Cr^{53} resonance in chromium containing up to 3 a/o (nominal) vanadium, and have measured the Knight shift of the V^{51} resonance at 10 a/o composition intervals across the entire V - Cr system. Measurements of the V^{51} Knight shift were also made at vanadium concentrations of 0.25, 0.50, 1.5, 3.0, and 5.0 a/o. The Knight shift of the Cr^{53} resonance was measured in the range 0 - 3 a/o vanadium concentration, and except for pure chromium, the measurements were made at room temperature. In crystal-bar chromium the Cr^{53} resonance was observed only at temperatures above the Néel point of approximately 40°C. Within the experimental uncertainty, the Cr^{53} Knight shift is independent of temperature and vanadium content within the ranges investigated.

Within the composition range 0 - 3 at/o vanadium, both the V^{51} and Cr^{53} resonances are extinguished by the onset of magnetic ordering at temperatures above 77°K. In the case of pure chromium, this extinction occurs within the range 39.5 - 41.0°C, in excellent agreement with the most recent neutron diffraction studies. The magnetic ordering temperature T_N is a precipitous function of vanadium content, as indicated qualitatively by the fact that it is below 77°K at 5 at/o V. The fact that the Cr^{53} resonance is detected at temperatures above the magnetic ordering temperature of chromium, as well as the temperature independence of the Knight shift, raises the possibility that the magnetic transition is not an order-disorder type, but rather involves the onset of a local magnetic state.

Further investigation of the Cr^{53} resonance in chromium metal has been concerned with the detailed behavior of the extinction process as the antiferromagnetic state is approached. This work has been greatly facilitated by the availability (on loan from the Oak Ridge National Laboratory) of a sample of isotopically enriched chromium metal (enriched to 98.5% in the Cr^{53} isotope). Figure 9 shows the manner in which the resonance intensity decreases to zero in this sample. Qualitatively, the striking feature is the relatively large temperature range over which the resonance is extinguished. The same behavior has been observed for both the Cr^{53} and V^{51} resonances in several of the Cr-rich alloys, with the $\tanh K (T - T_N)/T$ relation ($K \approx 15$) providing a good fit to the experimental points.

21.2 Nuclear Magnetic Resonance and Knight Shift in Solid Indium

Because indium crystallizes in the face-centered tetragonal structure, the In^{115} nucleus (spin 9/2) experiences a strong nuclear quadrupole

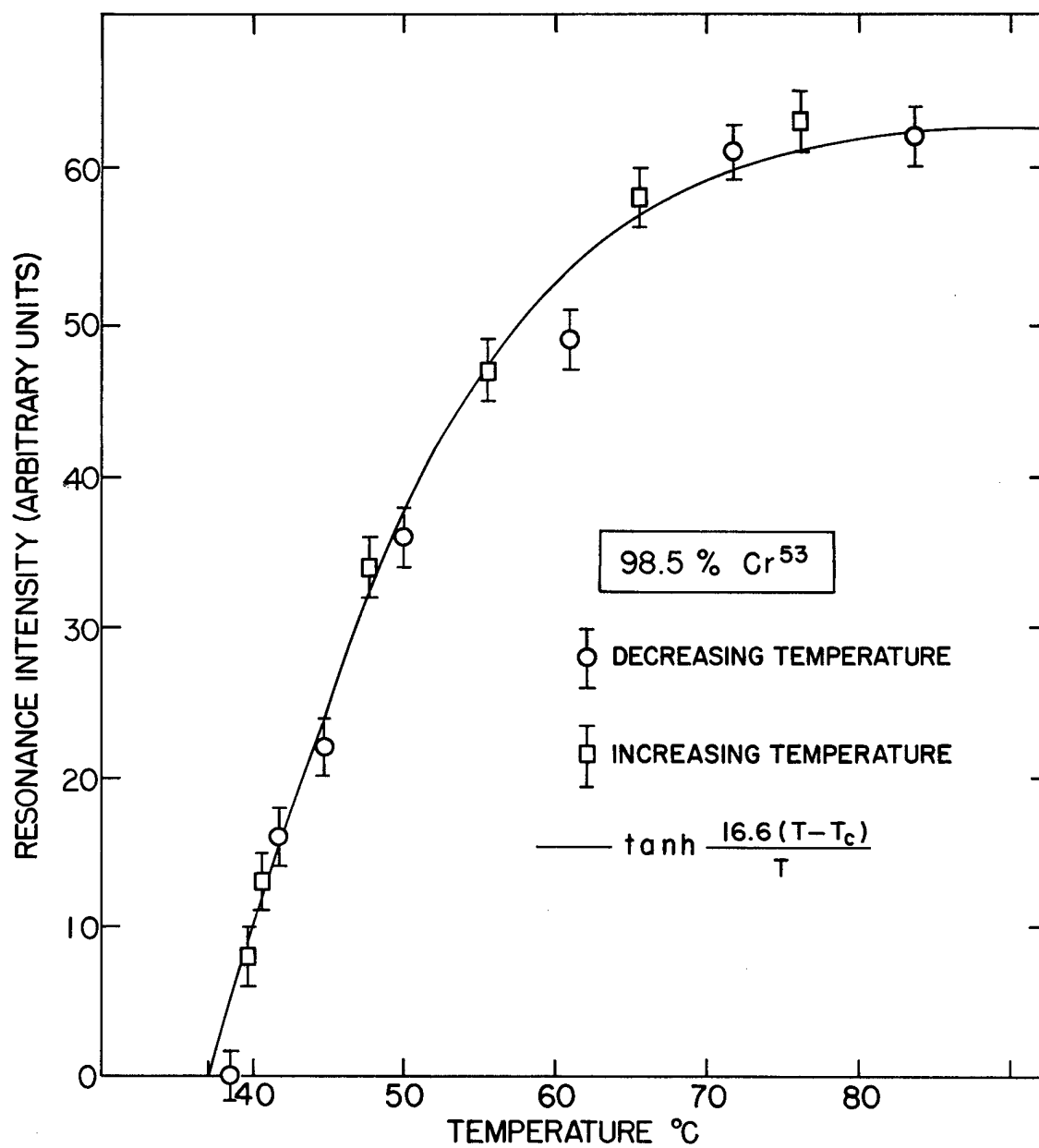


Fig. 9. Resonance Intensity as a Function of Temperature as the Néel Temperature is Approached

interaction in the solid metal. Furthermore, in a non-cubic metal, the Knight shift (conduction electron shift) of the nuclear magnetic resonance is expected to be non-isotropic. These two effects considerably complicate the nuclear magnetic resonance spectrum obtained from a polycrystalline sample. We have, however, investigated the resonance spectrum of In^{115} in polycrystalline indium in the frequency range 4 - 14 Mc/sec at room temperature, and find that the anisotropy in the Knight shift is very small, probably less than 0.02%, and that the observed spectrum can be understood in terms of the quadrupole interaction and an isotropic Knight shift.

The preliminary value which we have obtained for the isotropic Knight shift in solid indium is $0.94 \pm 0.02\%$. This value should be compared with that previously obtained for molten indium,¹ $0.794 \pm 0.002\%$. The difference between these values is the largest known, both absolutely and fractionally, for any metal thus far investigated, and strongly suggests that a considerable change in the electronic structure of indium occurs at the melting point.

21.3 Nuclear Magnetic Resonance in Ytterbium Metal

The element ytterbium (Yb) is the second-last of the rare-earth series of elements. As such, in the atomic state it lacks one 4f-electron from a closed-shell configuration. This situation is reflected in almost all salts of Yb, as well as by the Yb ion in solution, the Yb^{3+} ion being paramagnetic. Ytterbium metal is exceptional, however, in that the ion

¹W. H. Jones, T. P. Graham and R. G. Barnes, *Acta Met.* 8, 663 (1960).

is here divalent so that the metal is not paramagnetic. In addition, the metal is face-centered cubic, thereby minimizing nuclear quadrupole interaction side-effects which often hinder the observation of nuclear magnetic resonance in non-cubic metals.

Ytterbium has two nuclides of non-zero spin, each of roughly 15% abundance, Yb^{171} with spin $1/2$, and Yb^{173} with spin $5/2$. We have observed the nuclear magnetic resonance of Yb^{171} in Yb metal at room temperature, but have been unable to detect the resonance of the Yb^{173} nucleus, in spite of elaborate annealing procedures designed to reduce the effects of strains etc., on the Yb^{173} resonance. We have also made an intensive but unsuccessful search for the Yb^{171} resonance in the intermetallic YbAl_2 , in which the Yb occupies a cubic lattice site. The Al^{27} nuclear magnetic resonance in this compound has been studied previously,¹ and indicates that this compound is not paramagnetic and that Yb occurs here also as the divalent ion. This situation is not yet understood.

For Yb^{171} , the measured effective nuclear magnetic moment from the magnetic resonance experiment is $\mu = 0.490 \text{ nm}$. The most reliable prior value for this quantity is $\mu = 0.43 \pm 0.05 \text{ nm}$, based on the electron spin resonance of the Yb^{3+} ion substituted in yttrium acetate.² If the extreme of this measurement, 0.48 nm , is taken as being approximately correct for the unshifted resonance, then our measurements indicate a Knight shift on the order of 2% for Yb metal.

¹IS-349, Annual Summary Research Report in Physics, 1960-1961, Ames Laboratory Staff.

²A. H. Cooke and J. G. Park, Proc. Phys. Soc. A69, 282 (1956).

21.4 Nuclear Magnetic Resonance of V^{51} in Vanadium Carbides

The nuclear magnetic resonance of V^{51} has been investigated at room temperature in a variety of compositions in the vanadium-carbon system. In the hexagonal V_2C phase the Knight shift of the V^{51} resonance is 0.56%, not significantly different from that in pure vanadium. Within the cubic VC_x phase ($0.75 < x < 0.90$) the Knight shift changes sign, having the value +0.09% at $VC_{0.75}$ and -0.19% at $VC_{0.90}$. At the high-carbon end ($x \approx 0.92$) of the homogeneity range, a distinct first-order quadrupole satellite pattern is observed, corresponding to a quadrupole coupling of 1.50 ± 0.04 Mc/sec. In addition, the central component of the resonance exhibits a type of splitting characteristic of combined quadrupole and anisotropic shift effects.

Two factors resulting from the structural characteristics of the cubic VC_x phase are believed to contribute to the unusual features of the V^{51} resonance. In the first place, the large concentration of carbon vacancies will give rise to electric field gradients, and hence nuclear quadrupole interactions, at the positions of most vanadium nuclei. These gradients are axially symmetric for nearest-neighbor vacancies or combinations thereof, but are not axially symmetric for combinations involving vacancies in different neighboring shells. The anisotropy of the Knight shift could also result from local distortions of the conduction electron wave function caused by the vacancies. On the other hand, the fact that the Knight shift is negative appears to require the mechanism of core polarization in some form to be present. The nominal 1:1 carbides

of niobium and tantalum also exhibit negative Knight shifts for the nuclei of the metal atoms. The full 1:1 stoichiometry is much more closely approached in these compounds than in vanadium carbide, so that this effect is evidently not a property of the departure from full stoichiometry. In fact, the change in sign of the Knight shift that occurs within the cubic VC_x phase suggests strongly that this and the negative value of the shift are associated with the filling up of some set of levels within the conduction band structure.

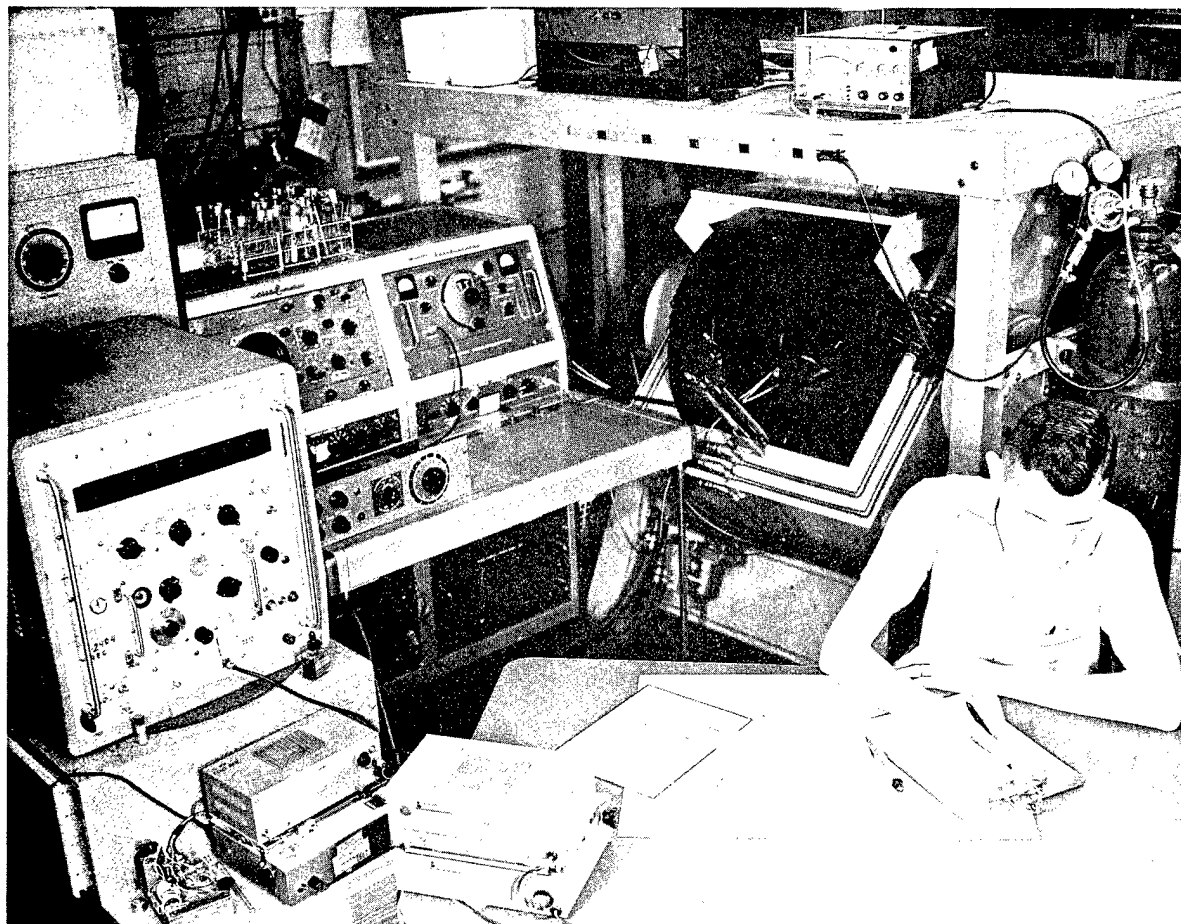


Fig. 10. Nuclear Magnetic Resonance Apparatus

21.5 Nuclear Quadrupole Resonance and Bonding in Solid Layer Type Metal Halides

A paper having the above title was submitted to the 1961 International Conference on the Chemical Physics of Non-Metallic Crystals held at Evanston, Illinois (Northwestern University), August 27 - 31, 1961. The proceedings of this conference were subsequently published in a supplementary issue of the Journal of Applied Physics, where the above paper appears as: R. G. Barnes, S. L. Segel and W. H. Jones, Jr., J. Appl. Phys. **33**, 296 (1962).

Abstract--Pure nuclear quadrupole resonance spectra have been reported for halogen nuclei in a number of metal halides crystallizing in layer structures of the CdI_2 or related types. Because of the extreme smallness of the quadrupole coupling constants, particularly in the case of the dihalides, the possible appropriateness of a purely ionic model to account for the electric field gradients has been investigated. Detailed calculations of the ion-lattice field gradient have been made for a number of compounds representing several types of infinite-layer structure. In no case is the coupling due to the ion-lattice alone sufficient to explain the observed interactions. In fact, comparison with experimental data suggests that empirical values of the antishielding factor γ_∞ about 3 - 5 times smaller than the theoretical values are appropriate to account for the ion-lattice contribution to the coupling. Covalent bonding between the metal and halogen layers involving only small departures from pure p-bond configurations at the halogens can account for the experimental results. Taking the ion-lattice gradient into account causes in general a small increase in the values of s-hybridization needed in the covalent bond model.

21.6 Nuclear Magnetic Resonance of Cl^{35} in Paramagnetic FeCl_2

The nuclear magnetic resonance spectrum of Cl^{35} has been investigated at room temperature in single and polycrystal ferrous chloride

(FeCl_2), which is one of the class of infinite-layer halides having the CdCl_2 structure. The dependence of the spectrum on magnetic field strength can be interpreted in terms of the combined effects of isotropic and anisotropic paramagnetic shifts and a nuclear quadrupole interaction.

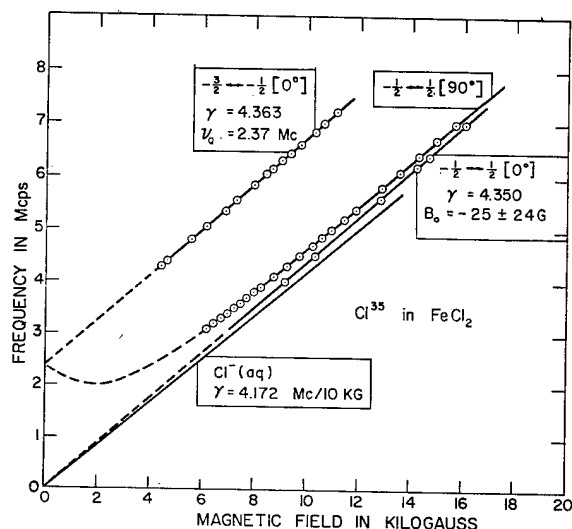


Fig. 11. Plot of experimental data (circles and solid lines) for the three transitions studied in single crystal FeCl_2 . The γ -values are in units of $\text{Mc/sec}/10^4 \text{oe}$, and the quantity B_0 is the intercept with the field axis. Dashed lines show the calculated behavior of the lines in the ranges not investigated

Figure 11 shows the resonances observed in the single crystal specimen. The quadrupole coupling is given directly by twice the zero-field intercept of the $-3/2 \leftrightarrow -1/2 (0^\circ)$ transition, and a least-squares fit to the experimental points yields $e^2 Qq/h = 4.74 \pm 0.01 \text{ Mc/sec}$. With this value of the quadrupole coupling the shift parameters were determined from the experimental shift of the $-1/2 \leftrightarrow 1/2 (0^\circ)$ and $-1/2 \leftrightarrow 1/2 (90^\circ)$ transitions from the Cl^- ion reference resonance. The values

of the various parameters are summarized in Table II.

The experimental value of $e^2 Qq/h$ should be compared with the value 0.24 Mc/sec calculated from the field gradient of the lattice of ion cores and the "empirical" antishielding factor γ_∞ for Cl^- (-10). Even if the theoretical value, $\gamma_\infty = -57$, is used, the calculated coupling constant is only one-third that observed. As in the case of other anhydrous

chlorides and bromides of the first transition series metals, the major contribution to the total field gradient appears to be due to covalent bonding.

Table II

Isotropic and anisotropic shift parameters and quadrupole coupling constant determined from the experimental data of Fig. 11. The uncertainties in k_{iso} and k_{ax} are the standard deviations for the 24 pairs of experimental values employed.

$\gamma_{eff}(\text{Mc/sec}/10^4 \text{ oe})$ and transition	k_{iso} %	k_{ax} %	$e^2 Qq/h$ (Mc/sec)
4.363 $(-3/2 \leftrightarrow -1/2)$	4.858 ± 0.124	-0.143 ± 0.062	4.74 ± 0.01
4.350 $(-1/2 \leftrightarrow -1/2)$	4.776 ± 0.138	-0.254 ± 0.069	

22. ELECTRON PARAMAGNETIC RESONANCE STUDIES OF IMPURITY CENTERS IN CRYSTALS (R. G. Barnes)

22.1 Co^{2+} Ion in Single-Crystal Titanium Oxide (Rutile)

A paper entitled "Paramagnetic Resonance of the Cobalt Ion in Rutile Single Crystal", by E. Yamaka and R. G. Barnes, was published in Phys. Rev. 125, 1568 (1962).

Abstract--The sevenfold degenerate 4F state of the free Co^{2+} ion is split into two orbital triplets and one singlet by an octahedral crystal field, one triplet lying lowest. Because of this orbital degeneracy, both the electronic spin and orbital motion contribute to the magnetic moment, so that the paramagnetic resonance spectrum of Co^{2+} is of special interest. If the spin-orbit coupling and crystal field of lower symmetry are taken into account, the twelvefold degeneracy (including the spin degeneracy) is replaced by six Kramers' doublets. Since only the lowest doublet is populated by electrons at low temperatures, the effective spin S' is taken to be $1/2$. The spectrum of Co^{2+} in single-crystal rutile is then analyzed by crystal field theory.

Table III

Values of the splitting factor g and hfs constant A for the case of Co^{2+} in TiO_2 . The decomposition into spin and orbital g -value contributions is also given, and for comparison, the corresponding values obtained by Tinkham¹ in the case of Co^{2+} in ZnF_2 are included.

	TiO ₂				ZnF ₂			
	g	g _S	g _L =kg° _L	A(10 ⁻⁴ cm ⁻¹)	g	g _S	g _L	A
x	2.19 + 0.005	2.13	0.06	(-) ^a 40 + 2	(2.6) ^a	2.33	0.22	(-43) ^a
y	5.88 + 0.02	4.67	1.21	150 + 2	6.05 + 0.01	4.42	1.63	217 + 2
z	3.75 + 0.01	3.20	0.55	26 + 1	4.1 + 0.1	3.25	0.85	(67) ^a

¹ Values enclosed in parentheses are obtained from theory.

The rutile crystal structure contains two inequivalent Ti ion positions because the distorted octahedra, which consists of the six oxygens surrounding Ti lattice sites, differ by a 90° rotation about the c-axis (z direction). This configuration causes the resonance lines to have 90° rotation period when the magnetic field is perpendicular to the c-axis, and to coincide when the field is parallel to the c-axis. The angular dependence of the Co^{2+} resonance spectrum shows that the Co^{2+} ion occupies the substitutional position in TiO_2 , just as do ions of other iron group elements.

We introduce a parameter k to take account of charge transfer when the splitting factor g and hyperfine splitting constant A are decomposed into spin and orbital parts. The values obtained for the various contributions are shown in Table III, compared with those for Co^{2+} in ZnF_2 ,¹ which has the same crystal structure as TiO_2 . Although the contribution of the higher doublets to the g and A values is neglected, and the k value is not too accurate, $k = 0.61$ from Table III is very small compared to that for other cases, e.g., Co^{2+} in MgO ($k = 0.89$). Such a large charge transfer can possibly be explained by the larger Co^{2+} ionic radius (0.78 Å) compared to the Ti^{4+} radius (0.60 Å) and by the large dielectric constant of rutile (ϵ is about 90 at 10,000 Mc/sec).

While the eight main hyperfine lines show no evidence of an associated oxygen vacancy for charge compensation, another group of weak hyperfine signals, having a different angular dependence from that of the main group, was recorded in the sample of highest cobalt concentration (the doping being 0.05%). These were so close to the main lines, however, and so weak that accurate g and A values were not obtained. It is believed that they are due to Co^{2+} combined with an oxygen vacancy.

22.2 V^{4+} Ion in Single-Crystal Titanium Oxide (Rutile)

We have observed that each of the eight hyperfine lines of V^{4+} in TiO_2 has some structure which varies with the angle between the magnetic

¹M. Tinkham, Proc. Roy. Soc. (London) A236, 549 (1956).

field and the crystal axis. If the 3d-electron of V^{4+} has its wave function spread over the nearest Ti^{4+} ion, superhyperfine structure might be expected because of the interaction between the 3d-electron and the nuclear spins of Ti^{47} and Ti^{49} . However, there are two nearest and eight next-nearest Ti^{4+} ion positions, and moreover, Ti^{47} and Ti^{49} have different nuclear spins and natural abundances ($5/2$, 7.8% and $7/2$, 5.5%, respectively), so that this structure is too complicated to calculate. Although a detailed assignment of the observed structure has not been obtained, it appears to come from the effect of the Ti nuclei.

As seen in Fig. 12 several pairs of forbidden lines $\Delta M = \pm 1$ are recorded between the main lines. The angular dependence of their intensity has the character of quadrupole coupling.¹ However, the intensity decreases monotonically within one group of hyperfine lines, whereas theory predicts that it decreases to zero from both ends of the pattern. It is of interest that these forbidden lines have a superhyperfine structure identical with that of the main hyperfine lines, as shown in Fig. 13.

22.3 Reduced TiO_2 (Ti^{3+} ion in Single-Crystal Rutile) (R. G. Barnes)

Rutile is given a blue color by heat treatment in vacuum or hydrogen gas. Hurlen² has shown the possibility that this treatment might produce the interstitial Ti^{3+} ion, because of the increase in the lattice constant. Interstitial positions, which line up along the c-axis, are divided into two magnetically inequivalent groups because they are surrounded by distorted octahedra of six oxygens, and these two groups of octahedra

¹B. Bleaney, Phil. Mag. 42, 44 (1951).

²T. Hurlen, Acta Chem. Scand. 3, 365 (1959).

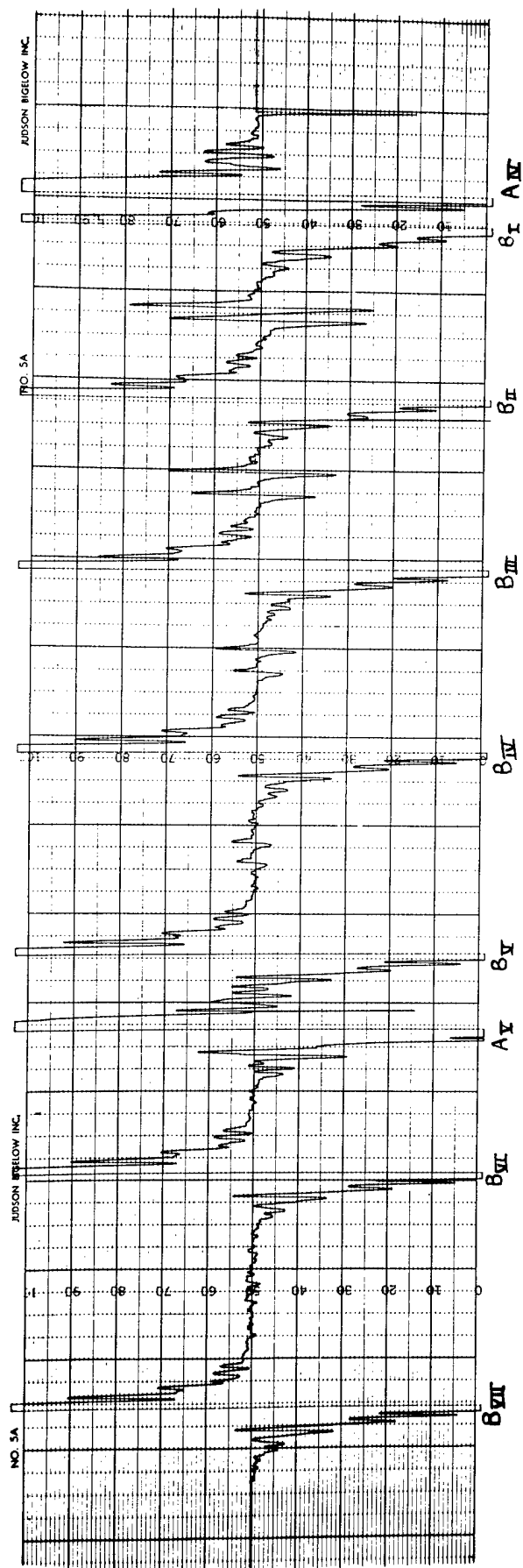


Fig. 12. The super hfs of V^{4+} in TiO_2 . H_0 is 75° away from c-axis toward $[110]$ axis. The forbidden transition lines $\Delta m = \pm 1$ are visible. The temperature is $77^\circ K$

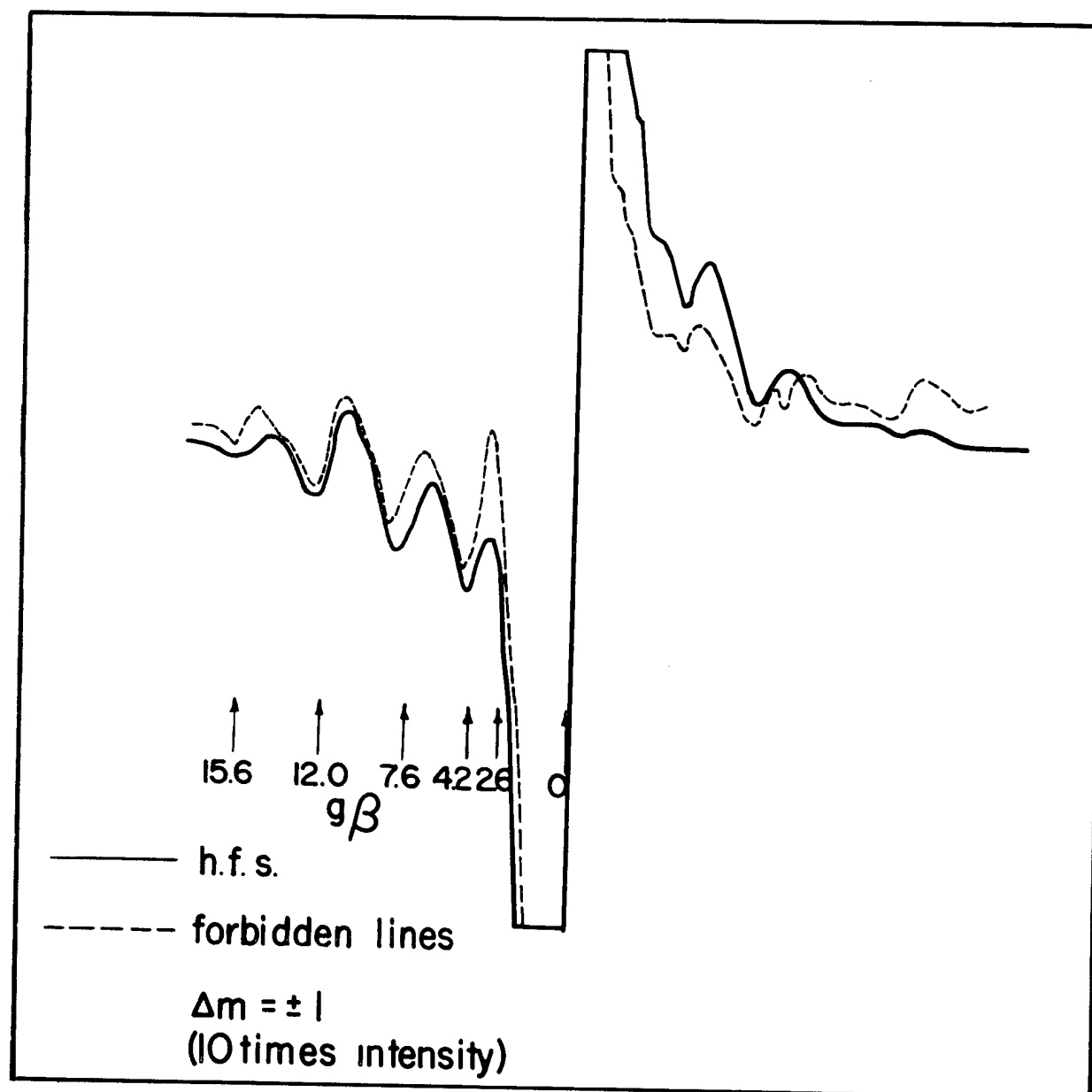


Fig. 13. The superposition of main hfs and forbidden transition of V^{+4} in TiO_2 to show the same super structure. H_0 is 75° away from C-axis toward $[110]$ axis and the temperature is $77^\circ K$

differ by approximately a 25° rotation about the c-axis as shown in Fig. 14. Furthermore, each group consists of a series of two kinds of octahedra, which differ by a 90° rotation about the c-axis. In summary, there are then four magnetically inequivalent interstitial positions in the TiO_2 structure. Four lines are divided into two groups, which differ by about 25° , and each group has a 90° rotation period when the magnetic field is normal to the c-axis. These four lines coincide in one line when the field is parallel to the c-axis.

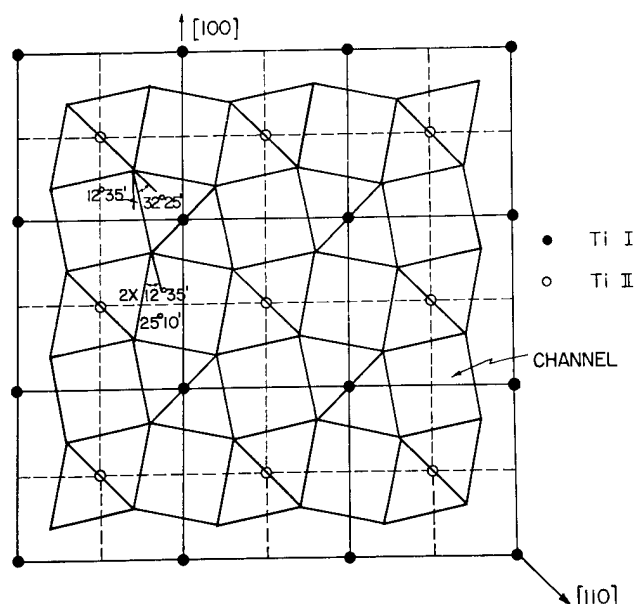


Fig. 14. The Projection of Octahedron of Rutile Structure on a Plane Perpendicular to C-axis

0.01 , $g_z = 1.939 \pm 0.001$. Comparison of these values with those of V^{4+} in TiO_2 ($g_x = 1.915$, $g_y = 1.956$, $g_z = 1.912$)¹ is interesting because both

Experiments were made at liquid helium temperature on the sample at various stages of reduction. Only one line was recorded for all orientations in the strongly reduced sample, while the signal was resolved into four lines in the general case in the slightly reduced crystal with the angular dependence following the above rules for the interstitial positions. Values obtained for g are:

$$g_x = 1.915 \pm 0.001, \quad g_y = 1.976 \pm$$

¹H. J. Gerritsen and H. R. Lewis, Phys. Rev. 119, 1010 (1960).

paramagnetic centers have one 3d-electron. The main part of their difference should arise from the difference in the octahedra which surround these centers.

Each line shows some structure, which varies with the angle between the magnetic field and the crystal axis. Only the resonance for the field along the c-axis shows a well-resolved structure, as shown in Fig. 15, because for each line with the field along the c-axis four lines arise when the field moves away from this axis, and the separation of these lines is very small. The origin of this structure has not been clarified but it is very similar to that of the hyperfine lines of V^{4+} (see Sec. 22.2).

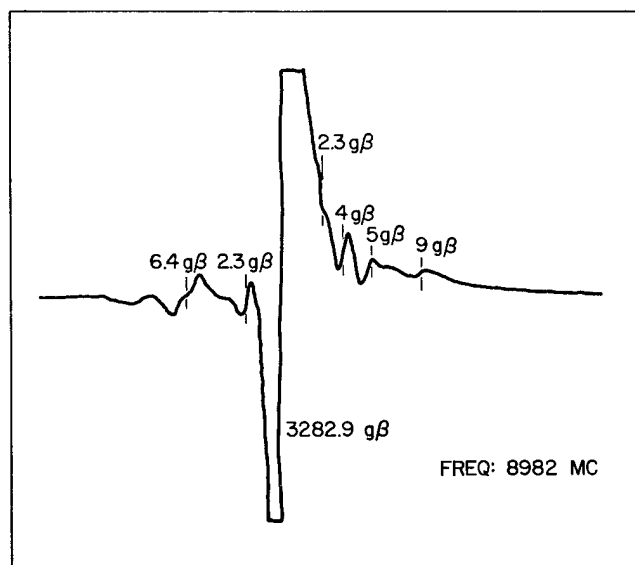


Fig. 15. Absorption of reduced TiO_2 . H_0 is parallel to the c-axis. The temperature is $4.2^\circ K$

This similarity may indicate that the structure of the resonance line in the reduced TiO_2 comes from charge transfer from the Ti^{3+} ion to the neighboring Ti^{4+} lattice ions. An objection to this interpretation is that there is no definite existence of hyperfine lines due to the Ti^{47} and Ti^{49} nuclei of the interstitial Ti^{3+} ions. However, we have observed many weak signals around the main signal, and further work is certainly required to settle this problem.

LIST OF REPORTS AND PUBLICATIONS

1. REPORTS FOR COOPERATING LABORATORIES

- IS-285 Bernardes, Newton, On the Different Crystallographic Phases of Solid Helium.
- IS-349 Ames Laboratory Staff, Annual Summary Research Report in Physics for July 1, 1960 - June 30, 1961.
- IS-399 Swenson, C. A., An Integration of the BCS Expression for the Critical Field of Superconductors.
- IS-492 Maycock, Paul D. and G. C. Danielson, Thermal Diffusivity Measurements on a Finite Disk.
- IS-506 Plimpton, J. D. and C. L. Hammer, Large Angle Pair Production.

2. PUBLICATIONS

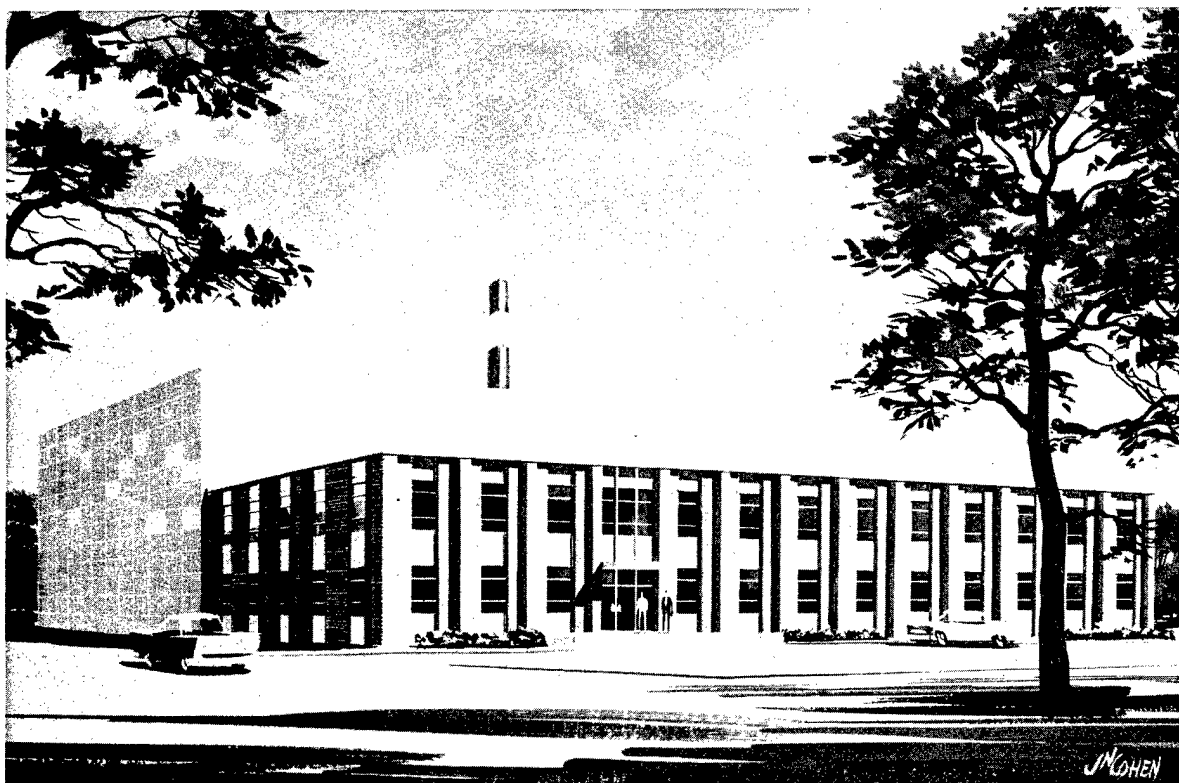
- Alstad, J. K., R. V. Colvin and S. Legvold, Single and Polycrystal Resistivity Relationships for Yttrium. *Phys. Rev.* 123, 418-419 (1961).
- Barnes, R. G., S. L. Segel and W. H. Jones, Jr., Nuclear Quadrupole Resonance and Bonding in Solid Layer Type Metal Halides. *J. Appl. Phys.* 33, 296-302 (1962).
- Bernardes, Newton, On the α - β Phase Transition of Solid He³. *Phys. Rev. Letters* 8, 164-165 (1962).
- Born, H. J., Sam Legvold and F. H. Spedding, Low Temperature Thermoelectric Power of the Rare-Earth Metals. *J. Appl. Phys.* 32, 2543-2549 (1961).
- Carlson, B. C., Some Series and Bounds for Incomplete Elliptic Integrals. *J. Math. and Phys.* 40, 125-134 (1961).
- Carlson, B. C. and Pao Lu, Charged Liquid Drop with High Angular Momentum. Rutherford Jubilee International Conf. Proceedings C2/28, 291-292 (1961).
- Ellerbeck, L. D., H. R. Shanks, P. H. Sidles and G. C. Danielson, Electrical Resistivity of Cubic Sodium Tungsten Bronze. *J. Chem. Phys.* 35, 298-302 (1961).
- Fradkin, D. M. and R. H. Good, Jr., Tensor Operator for Electron Polarization. *Il Nuovo Cimento* 22, 643-649 (1961).

- Greiner, J. D., H. R. Shanks and D. C. Wallace, The Magnetic Susceptibility of the Cubic Sodium Tungsten Bronzes. *J. Chem. Phys.* 36, 772-776 (1962).
- Heller, M. W. and G. C. Danielson, Seebeck Effect in Mg_2Si Single Crystals. *J. Phys. Chem. Solids* 23, 601-610 (1962).
- Heltemes, E. C. and C. A. Swenson, Nuclear Contribution to the Heat Capacity of Terbium Metal. *J. Chem. Phys.* 35, 1264-1265 (1961).
- Heltemes, E. C. and C. A. Swenson, Specific Heat of Solid He^3 . *Phys. Rev. Letters* 7, 363-365 (1961).
- Hinrichs, C. H. and C. A. Swenson, Superconducting Critical Field of Tantalum as a Function of Temperature and Pressure. *Phys. Rev.* 123, 1106-1114 (1961).
- Ho, Grace P. and E. L. Iloff, The Relative Deuteron/Proton Yield from 45 Mev Bremsstrahlung Irradiation of Copper. *Nucl. Phys.* 27, 234-247 (1961).
- Hultsch, R. A. and R. G. Barnes, The Pressure Dependence of Self-Diffusion in Lithium and Sodium. *Phys. Rev.* 125, 1832-1842 (1962).
- Jones, W. H., Jr., E. A. Garbaty and R. G. Barnes, Nuclear Magnetic Resonance in Metal Tungsten Bronzes. *J. Chem. Phys.* 36, 494-499 (1962).
- Keller, J. M. and D. C. Wallace, Anharmonic Contributions to Specific Heat. *Phys. Rev.* 126, 1275-1282 (1962).
- Kromminga, A. J. and I. E. McCarthy, A Simple Direct Reaction Model of Proton Inelastic Scattering. *Nucl. Phys.* 31, 678-688 (1962).
- Laslett, L. Jackson and William Lewish, Evaluation of the Zeros of Cross-Product Bessel Functions. *Mathematics of Computation* XVI (1962).
- Liu, S. H., Y. Nishina and R. H. Good, Jr., Microwave Measurement of Mobility: Analysis of Apparatus. *Rev. Sci. Instr.* 32, 784-789 (1961).
- Lynch, P. J. and B. C. Carlson, Theory of High-Energy Potential Scattering. *J. Math. Phys.* 3, 440-450 (1962).
- Moroi, D. S., Photoelectric Effect and Pair Annihilation with Large Momentum Transfer. *Phys. Rev.* 123, 167-174 (1961).
- Nelson, D. T. and S. Legvold, Adiabatic Demagnetization with Yttrium-Rare-Earth Alloys. *Phys. Rev.* 123, 80-84 (1961).

- Nishina, Y. and G. C. Danielson, Microwave Measurement of Hall Mobility: Experimental Method. *Rev. Sci. Instr.* 32, 790-793 (1961).
- Rice, M. H. and R. H. Good, Jr., Stark Effect in Hydrogen. *J. Opt. Soc. Am.* 52, 239-246 (1962).
- Schirber, J. E. and C. A. Swenson, Superconductivity of α - and β -Mercury. *Phys. Rev.* 123, 1115-1122 (1961).
- Swenson, C. A., The Temperature and Pressure Dependence of Critical Field Curves. *Proceedings of Superconductivity Conference-IBM-New York. J. Res. Dev.* 6, 82-83 (1962).
- Trulson, O. C., D. E. Hudson and F. H. Spedding, Cohesive Energies of Europium, Gadolinium, Holmium, and Erbium. *J. Chem. Phys.* 35, 1018-1026 (1961).
- Weber, T. A. and C. J. Mullin, Angular Distribution of Relativistic Atomic K-Shell Photoelectrons. *Phys. Rev.* 126, 615-619 (1962).
- Yamaka, E. and R. G. Barnes, Paramagnetic Resonance of the Cobalt Ion in Rutile Single Crystal. *Phys. Rev.* 125, 1568-1569 (1962).

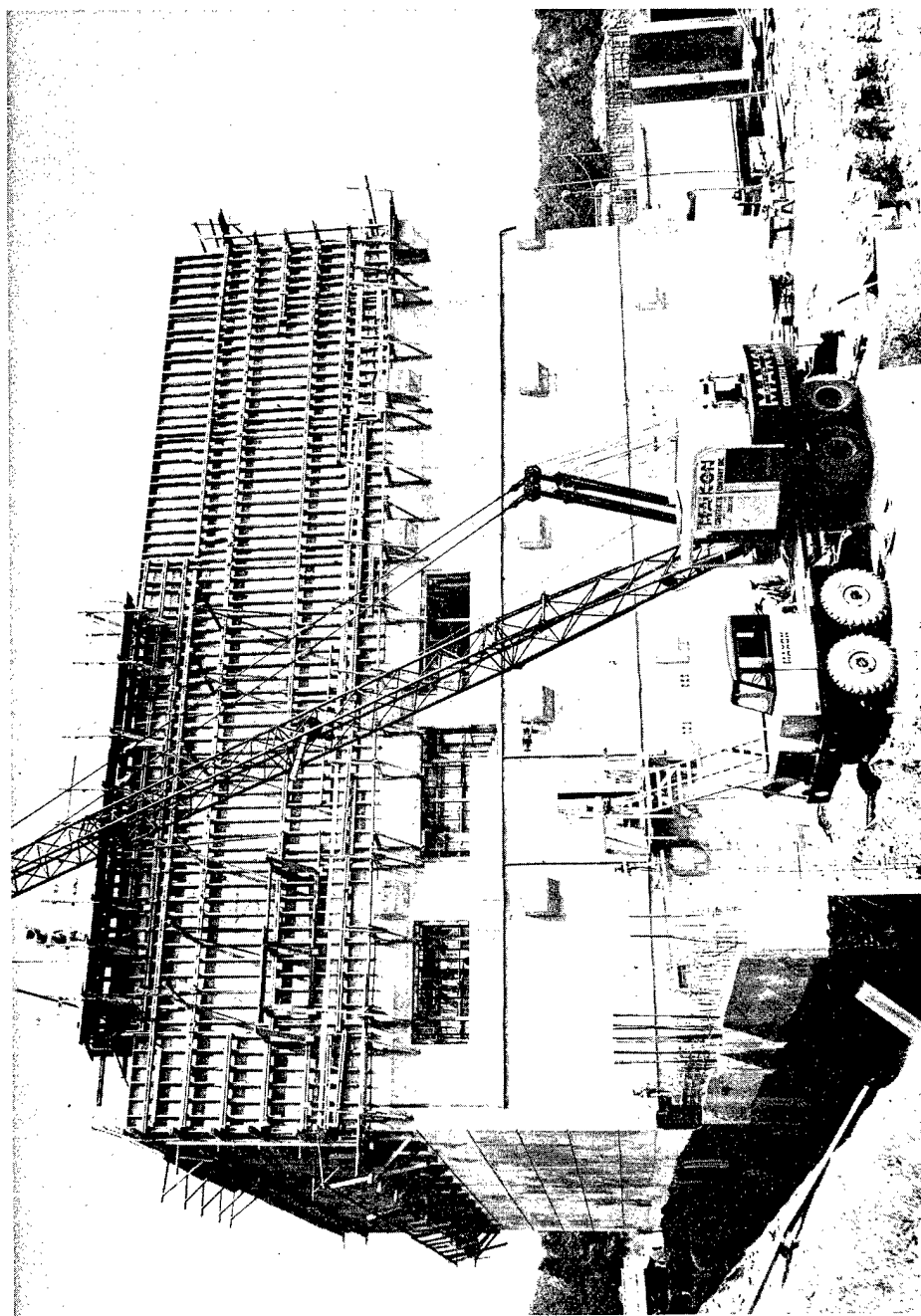
REACTOR
DIVISION

AMES LABORATORY RESEARCH REACTOR



Ames Laboratory Research Reactor Facility

Designation	-	ALRR
Power, KW(t)	-	5 megawatts
Fuel elements	-	Aluminum alloy with fully-enriched uranium-235
Moderator and coolant	-	Heavy water
Uses	-	Production of neutrons for experimental work; production of radioactive tracers
Capacity	-	Thirty-five experimental facilities, including radiation ports, beam tubes, vertical thimbles, rabbit tubes and a thermal column
Cost	-	Approximately \$4.6 million
Start-up	-	1963



Reactor Construction Progress as of July 1, 1962

APPENDICES

APPENDIX I: EDUCATIONAL SERVICES

The educational services which the Laboratory provided for the general public consisted primarily of laboratory tours, exhibits, speeches, news releases and publications.

An Open House, observing the completion of the Metals Development Building, attracted more than 6500 visitors.

Tours were conducted for 42 groups, many of which were high school science classes and science clubs.

Numerous speaking engagements with service clubs and other organizations were filled by Laboratory staff members.

A display, showing the history and some of the accomplishments of the Ames Laboratory, was prepared for the State Museum of History and Archives.

The Ames Laboratory News, a bi-monthly publication, was sent to more than 2000 high schools, colleges and laboratories, and was well received.

Many booklets and items of atomic energy information were mailed in response to requests.

"Metals Frontier", a film showing research and development in the Ames Laboratory, was used effectively for tour groups, for recruiting personnel, and showing to civic and fraternal organizations.

<u>Destination</u>	<u>Item</u>
William J. Murri Brigham Young University Provo, Utah	small sample of high purity cerium
Dr. G. M. Wolten Aerospace Corporation Los Angeles, California	60 gm hafnium oxide, specially purified
Dr. Vance L. Sailor Brookhaven National Laboratory Upton, Long Island, New York	1 single crystal holmium
Union Carbide Corporation Parma Research Center Parma, Ohio	10 gm holmium 10 gm samarium
Professor A. Smakula Massachusetts Institute of Technology Cambridge, Massachusetts	1 piece 15x15x15 mm ³ uncolored KI crystals 1 piece ~9x9x9 mm ³ colored fractured KI crystals
Mr. B. R. Watts University of Cambridge Cambridge, England	1 chromium tricrystal
D. M. Roy Pennsylvania State University University Park, Pennsylvania	small amount special samarium bifluoride
Dr. Edward S. Fisher Argonne National Laboratory Argonne, Illinois	yttrium crystals
Dr. R. M. Bozorth University of Tokyo, Azabu Minato-ku Tokyo, Japan	2 single crystals of dysprosium
IBM Research Center Yorktown, New York	1 lb pure anhydrous YF ₃